MAGNETOSTRICTION HARMONICS IN

(110) [001] SILICON - IRON

by

C.E. WHITE B.Sc.

A Thesis submitted to the C.N.A.A. for the award of the degree of Doctor of Philosophy, in partial fulfilment of the requirements for that degree.

Collaborating Establishments:

The British Steel Corporation.

The Wolfson Centre for Magnetics Technology, Cardiff.

Sponsoring Establishment:

Plymouth Polytechnic, Plymouth, Devon.

May 1982

PLYMOUTH POLYTECHNIC
LIBRARY

Accn. No.	5500076-8
Class. No.	T 538.3 WHI
Contl No.	x7001591 68

DECLARATION

I declare that this Thesis is the result of my investigations only, and is not submitted in candidature for the award of any other degrees. During the research programme I was not registered for the award of any other CNAA or University degree.

ADVANCED STUDIES

During the research programme I undertook a course of advanced studies. These included the reading of selected articles associated with the field of study. I became an Associate Member of the I.E.E., a Student Member of the Institute of Physics and joined the Magnetism Group. I attended several colloquia and meetings on subjects related to the field of study.

C. E. White

.....

Candidate

D. Maffin

.....

Director of Studies

MAGNETOSTRICTION HARMONICS IN (110) [001] SILICON IRON

by

C.E. WHITE

ABSTRACT

The contribution of the harmonics of magnetostriction to the overall noise spectrum of power transformers is discussed with reference to the domain theory of ferromagnetism, the development of electrical steels and transformer design, and current sound measurement practice.

An apparatus is described with which the precise measurements of magnetostriction harmonics can be obtained at any co-ordinate position within the boundaries of a grain of silicon-iron electrical steel. The magnetostriction is detected by a refined double transducer technique. The apparatus contains means for applying longitudinal stresses to a specimen of steel, for observing dynamic surface closure structures of domains and for controlling the flux waveshape.

Using this apparatus, values of the first three harmonics of magnetostriction have been measured for a single grain within a steel sample. The effects of variations in applied longitudinal stresses, flux density and flux waveshape have been observed and recorded for the strains measured in both the rolling direction and transverse to that direction.

The harmonic content is then shown to be dependent upon the stress level in combination with the extent of any flux waveshape distortion, and is particularly dependent upon the phase relationship between the flux harmonics and their fundamental. It is also shown how the third harmonic of flux has a determining influence on the second harmonic of magnetostriction, as well as the third, causing a reduction in magnitude under certain conditions.

A comparison between magnetostriction harmonics measured in the rolling direction and transverse to that direction is then made, and shows a 2:1 ratio for the same compressive stress level. This confirms a prediction by theory of such a relationship.

CONTENTS

CHAPTER ONE

INTRODUCTION AND OBJECTIVES

As society becomes increasingly aware of environmental pollution it is paradoxical that the major contributor to that pollution is the technology upon which modern society is founded. The technologists are therefore presented with the dilemma of continuing to investigate and improve the state of their art but at the same time consider the environmental aspects of their creations.

Noise is one of the major pollutants in the modern world, and anti-noise lobbies appear to revolt against a technology whose innovation has contributed to our society as it is today.

Simultaneously, society is becoming less tolerant of energy waste, but as yet the conservation of energy resources appears to be motivated by the technologist whereas the lay public does not appear to be making severe demands in that direction.

Noise, along with most other pollutants, does represent an energy loss in the overall energy-balance of the environment, and by satisfying the anti-noise lobbies in one direction the technologist is also contributing to the conservation of energy resources. This requires that the reduction of noise is made at the source, rather than just shielding its recipiants from it, since the latter needs additional expense.

It is necessary, therefore, to closely examine the processes by which noise is generated and to try and change such processes without detrimentally modifying the function of the device responsible for the noise generation. Thus, in the case of transformer noise, it is necessary to continue examining the process of magnetism within the material used and

to seek ways in which technology can adapt these processes to meet environmental requirements. Such research will also satisfy a need within the technology itself, that of continuing to further the scientific knowledge of one of the fundamental forces which modern physics now recognises - the electromagnetic force.

Power transformers play a vital role in the efficient distribution and utilisation of electricity energy, and it has become an economic necessity to position them close to centres of urban population. As will be shown, the noise created by a transformer is steady in nature, as opposed to the transient noises with which much noise-abatement is currently associated. The tendency, therefore, is for the overall background noise level in urban areas to be increased, and the treatment of the psycho-acoustical problems arising needs careful consideration.

It is known that the origin of most transformer noise lies in the cyclic strains (magnetostriction) set up in the core material during a.c. magnetisation of the core, and that this strain contains harmonics. As will be shown, the strain is dependant on certain physical properties of the core as well as the specific influences of external mechanical stresses and magnetic flux density. It is necessary to examine these dependancies in order to understand the mechanism by which the strains are produced. In addition, because of the characteristics of the human ear, it is the harmonic frequencies which are most offensive.

This research will therefore be concerned with investigating the phenomena of harmonic generation in magnetostriction and attempting to correlate this with specific structural properties of the core material. Two objectives are sought: (1) environmentally, to contribute to the design of quieter power transformers and (ii) scientifically, to further the understanding of basic magnetic processes.

CHAPTER TWO

BACKGROUND TO THE INVESTIGATION

2.1 Historical Development of Silicon-iron

Iron fulfils four of the most important requirements of a magnetic material for use in heavy-current engineering:-

(a) it has the highest saturation flux density of all ferromagnetics;

(b) it is readily available and the most abundant;

(c) it is not difficult to extract and work;

(d) it is, even today, relatively cheap.

These reasons were appreciated by the first manufacturers of transformers who used solid cores of unalloyed iron in their devices.

However, due to the low electrical resistance of iron (typically 0.1 μΩ - m) large eddy currents circulate normal to the direction of flux change resulting in excessive heating and intolerable losses.

It was soon realised that laminating the core would increase the specific resistance (being inversely proportional to the thickness) and reduce eddy current losses (which are proportional to the square of the thickness). Producing very thin laminations was, at that time, very expensive and at the thicknesses attempted to drastically reduce losses, poor stacking factors and reduced magnetic properties became apparent. Methods of increasing the specific resistance without detrimentally affecting the cost and magnetic properties were therefore sought.

In 1902, Barrett et.al. (1) published an enormous work concerning iron alloyed with other materials. In particular, alloys with silicon demonstrated a good increase in resistance to about 0.5 μΩ - m at 3.35% Si, but with only a small decrease in saturation flux density by about 0.15T (2). Additionally, with increasing silicon content, there is

an improvement in losses, permeability and coercivity; the losses appear to reach a minimum at about 6.5% Si. However, the brittleness of the material increases dramatically with silicon content and this sets a limit of about 3.5% Si; this effect can be counteracted by hot working of the material.

Efforts were then concentrated on producing alloyed Si-Fe laminations, and the major problem at that time was working with a virtually unrollable material. The resources of the vast German Steel industry solved most of these problems by 1903, and commercially produced "electrosheet" was readily available in England by 1906 containing about 3.4% Si. All sheets were produced by hot rolling methods.

Further advances occurred during the 1920's and 1930's when the effects of impurities were investigated, mainly in America. The harmful effects of carbon and oxygen were isolated, in that they hinder the formation of uniform crystal texture, and the detrimental effect on losses of such impurities as sulphur and manganese was established.

However, no real attempt had been made to utilize the anistropic properties of the crystal structure, all sheet being hot rolled which produces a virtually isotropic material from the point of view of magnetic properties. It was realised though, that if any anisotropic effects were present then the easiest direction of magnetisation usually lay along the rolling direction.

This led, in 1934, to the advent of cold rolling techniques designed to produce sheet steel with a marked anisotropy in the rolling direction, the so-called grain orientated sheet. The first successful attempts were patented by Goss in 1934, who, by a succession of cold rolling and annealing processes established the Goss, or cube-on-edge, texture. In terms of Miller indices this is expressed as (110)[001] texture and is shown diagrammatically in Fig. 2.1 (a), where the (110) planes of the crystal are parallel to the sheet surface and the [001] axis is parallel

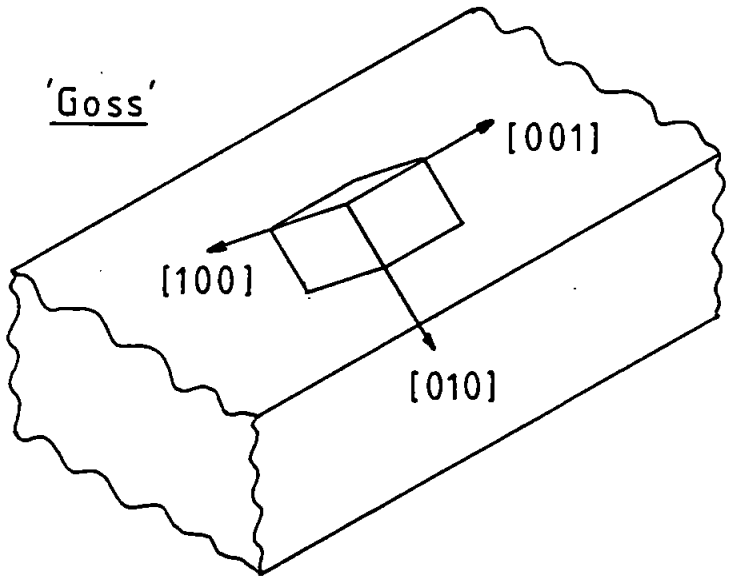

FIG. 2.1.(a). Texture (110)[001].

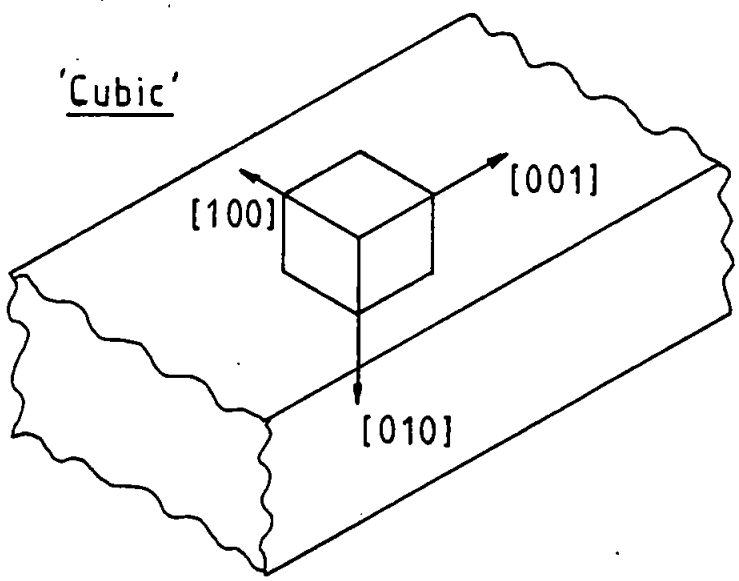

FIG. 2.1.(b). Texture (100)[001].

FIG. 2.1. Illustrating 'Goss' and 'Cubic' Textures in Grain-orientated Silicon-iron.

to the rolling direction.

As will be discussed in Chapter 3, the highly anisotropic nature of the ferromagnetic crystal gives the cube edges the easiest direction of magnetisation. Such a grain-orientated texture gives the bulk sheet material a highly preferred direction of magnetisation (3,4) and the magnetostriction as well as the losses will be reduced.

It is found that the presence of slight impurities is essential to achieve Goss texture and the growth of large grains. Manganese sulphide is used during this secondary re-crystallisation process which suppresses primary grain growth, and occurs during a high temperature batch anneal following the various cold rolling stages (5,6,7).

All modern electrical steels, or electrosheet, certainly for power transformers, are now produced in the Goss texture, and with modern techniques of fabrication large grain sizes with high orders of orientation (90-95%) can be achieved. Consequently the properties of modern steels have been greatly improved with notable reductions in losses and magnetostriction (8). All sheet is available in various sizes, usually graded in thickness of lamination and loss per kg, depending on the nature of the use required (9,10).

Other textures are, of course, possible, and attention has been given to the development of the so-called cubic texture, or (100)[001] texture shown in Fig. 2.1 (b), where the cube edges of the crystal lie both along the rolling direction and at right angles to it. Substantial reductions in losses have been reported with such material and it has an apparent advantage in transformer cores where the flux path needs to traverse 90^{o} at the corner joints. However, difficulties in manufacture have been experienced and there is a consequent cost penalty (11,12,13).

Advances have also been made concerning the application of various coatings to the sheet which, apart from giving the necessary inter-lamination insulation, also impart an effective tensile stress which may

off-set the effects of any compressive stresses applied during assembly of the laminations (14,15,16). As will be discussed in Chapter 3, this will have a beneficial effect on magnetostriction, as well as on any losses which may be stress sensitive.

2.2 Transformer Noise and the Effects of Design

The primary source of transformer noise has been recognised as originating from magnetostriction since the early 1940's (17,18,19) and the progress achieved since then now allows the designer to predict noise levels based on the transformer MVA rating (20).

These predictions are a consequence of statistical analyses of the core-emitted noise from a range of transformer sizes, and do not contain any element directly attributable to magnetostriction.

When actual noise levels are compared to those computed using magnetostriction as the origin of any core displacements, taking into account the transformer dimensions and allowing for attenuations due to oil and tank, it is found that the actual level is in the order of 10 dB(A) higher than was computed (21).

The differences are usually attributed to:-

(1) varying and often unknown stresses in the core (since, as will be described in Chapter Three, magnetostriction is highly stress sensitive);

(2) magnetic forces causing 'flapping' of individual laminations (particularly at joints where cross fluxing is occurring);

(3) mechanical resonances of the core-tank structures, especially at the higher harmonic frequencies of the noise (it will be described in Chapter Three how magnetostriction contains multiple harmonics of a single valued excitation frequency);

(4) inhomogeneous flux distribution and waveshape distortion.

Moses (22) states that the predominant causes of stress in the core are due to (a) clamping of the laminations, (b) the use of non-flat laminations and (c) the existence of temperature gradients and localised hot-spots, and that by far the worst stress effect is that due to wavy laminations.

Wilkins and Thompson (23) demonstrated how reductions in noise levels of the order of 10 dB could be achieved by carefully selecting flat laminations, thus reducing the stresses imparted by flattening of the undulations.

The effect of 'flapping' laminations, except in badly built cores, is generally considered to be far outweighed by the magnetostrictions (24), and this problem is very much more in the control of the designer. Of greater importance is the type of joint configuration, which greatly effects the natural frequencies of the core limbs and yokes.

Reinke (25) has shown how the joint design will influence the core response at the higher magnetostriction harmonics.

The results of core vibration due to resonances at the higher harmonic frequencies was studies by Thompson and Wilkins (26) who showed that these higher frequencies are radiated much more effectively by the core, and that the second harmonic was predominant in the overall noise level.

Thoeng (27) showed how resonances in the tank structure will greatly influence the transmitted noise, and in particular that the radiated noise power will be higher for the higher harmonics than for the fundamental frequency. This author also pointed out the necessity to prevent unequal flux distributions within the core.

Various methods are available to the designer in order to reduce the overall noise level, and a great deal of effort has been put into the reduction of core stresses. For example, the use of insulating coatings on laminations will be discussed further in Chapter Three, wherein it will be described how an effective tensile stress is imparted, tending to offset

the detrimental effects of any compressive stresses arising during core building.

Clamping stresses may be reduced by the elimination of core bolts and substituting resin-bonded, glass-fibre tape to bind the core stacks together. Moses (24,28) has shown an improvement in higher harmonic vibrations of the core by the use of flexible bonding of the laminations, although the overall noise reduction achieved was only 3 dB(A). Once again, this author emphasised how the noise output is controlled by the level of the higher harmonics.

Stresses due to wavy laminations can easily be controlled by careful heat-treatment (annealing) of the sheets (23). Since most laminations are cropped or sheared from sheet strip, this process is necessary anyway in order to reduce the stresses imparted by such mechanical treatment.

Limb-yoke T-joints in power transformers are now always of mitre construction, rather than simple overlap or butt joints, and this has the beneficial effect of ensuring more efficient flux transfer, as well as stiffening the joint and lowering its natural frequency (25). However, Moses and Thomas (29) have shown that, regardless of joint configuration, there can be large third harmonic fluxes circulating into the joints from the limbs and yokes, and rotational flux in the joint itself. Apart from increasing losses there could well be a detrimental increase in magnetostriction harmonics and hence noise.

It will also be necessary for the designer to dimension the core-tank assembly in a way to avoid resonances at the higher harmonic frequencies and, if necessary, to use some form of resilient mounting either between the core and its tank or between the tank and its mounting pad.

The final course left is to shield the transformer by enclosing it, an expensive procedure particularly for very large designs. This in itself adds further problems, since the influence of 'build-up' (30) due to reverberations inside the enclosure will reduce its effectiveness.

It is apparent from the preceeding discussion that it is the higher harmonics of magnetostriction which appear to have the greatest effect on transformer noise. Ruhlmann (31) studied the various influences described above and concluded that the predominant contributor to the harmonics of noise was the high harmonic content of a non-uniform flux distribution in the core, and that this would be greatly influenced by the presence of stresses.

2.3 Sound Measurement and Analysis

The effects of noise on the human ear, and particularly the harmonics in that noise, are most significant when taken in the context of the previous discussion of Section 2.2, from which it appears that the higher harmonics of transformer noise may be prevalent under some conditions.

This significance is due to the fact that the ear exhibits an apparent non-linear response.

Because it is true that there is no simple relationship between measured sound pressure and human perception of that sound (32) it is necessary to standardise such measurements to obtain meaningful, objective comparison. This has been done statistically from experiments over a large number of observations and, for example, normalised equal loudness level contours may be obtained for pure tones (33), which demonstrate how the subjective loudness of a tone varies with frequency.

From such curves it is deduced that the higher frequencies within a complex sound waveform, at least up to about 4 kHz, will have a greater effect on the overall loudness, as perceived by the listener, then may be apparent from a physical measurement of the pressure level of each frequency component (34).

These normalised relationships vary not only with frequency but also with the sound pressure level, tending to flatten as the S.P.L. increases.

It is noticeable from the published standards, however, that the greatest variations in response occur in the lower frequency ranges up to 400 Hz and for sound pressure levels up to 95 dB.

Thus for a noise containing 100 and 200 Hz components with equal S.P.L.'s of 50 dB, the second harmonic would appear approximately twice as loud as the fundamental to a 'normalised' listener.

In order to overcome the difficulties presented by these psycho-acoustical phenomena during interpretation of sound measurements, various kinds of instrumentation have been developed. In particular, to allow for the non-linear response of the ear, frequency weighting of the measured sound is employed; the 'A' weighting is now commonly accepted internationally as correlating extremely well with the subjective response of the ear.

The frequency response of the 'A' weighting shows an attenuation of - 3 dB(A) from 300 Hz to 200 Hz, and a further attenuation of - 9 dB(A) from 200 Hz to 100 Hz.

Since the measured sound spectra of power transformers fall within the frequency and pressure ranges mentioned above (35) it is clear that any higher harmonics of such noise will become much more significant in terms of annoyance to a listener than the fundamental (100 Hz) component.

2.4 Summary

It is apparent from the preceeding discussions that any reduction in the sound pressure levels of the higher harmonics (particularly the 200 Hz component) in transformer noise could result in a significant reduction of the overall sound level.

Several authors have pointed out the necessity for further investigations into the generation of such harmonics in the magnetostriction of the core (24,26), but there appears to be little published evidence of any direct measurements, and none attempting to correlate the harmonics with distortion of the flux waveform and under the influence of stress.

Before reporting on an Apparatus devised to fulfill such an objective, it will be necessary to discuss the magnetic processes which give rise to harmonics in magnetostriction. This will be dealt with in the next Chapter.

References to Chapter Two

1. W.F. Barrett, W. Brown, R.A. Hadfield, J.I.E.E., Vol. 31, 1902.

2. C. Heck, 'Magnetic Materials and Their Applications', Butterworths, London, 1974.

3. S. Chikazumi, 'Physics of Magnetism', Wiley, N.Y., 1964.

4. F. Brailsford, 'Physical Principles of Magnetism', Van Nostrand, London, 1966.

5. H.C. Fiedler, J.Appl.Phys., Vol. 29, No. 3, March, 1958.

6. J.R. Brown, Ibid.

7. A. Coombs, Steel Times, May, 1970.

8. S.M. Pegler, A.I.P. Conf. Proc., No. 24, May, 1974.

9. D. Hudson, Metal.Bull.Monthly, January, 1971.

10. G.R. Davies, Electrical Times, February, 1975.

11. J.E. Thompson, Electrical Times, December, 1963.

12. C.R. Boon, J.E. Thompson, Proc. I.E.E., Vol. 112, No. 11, November, 1965.

13. I.M. Stewart, I.E.E. Conf. Pub., No. 33, September, 1967.

14. P.J. Banks, E. Rawlinson, Proc. I.E.E., Vol. 114, No. 10, October, 1967.

15. K. Foster, J. Seidel, A.I.P. Conf. Proc., Vol. 5, September, 1971.

16. H. Shimanaka et.al., I.E.E.E. Trans. Mag., Vol.Mag. 15, No. 6, November, 1979.

17. B.G. Churcher, A.J. King, J.I.E.E., Vol. 87, No. 527, November, 1940.

18. J. Swaffield, J.I.E.E., Vol. 89, No. 17, May, 1942.

19. F. Brailsford, Ibid.

20. C.G. Gordon, I.E.E.E. Trans. PAS, Vol. PAS. 98, No. 3, June, 1979.

21. A. Coquard, I.E.E. Conf.Pub., No. 33, September, 1967.

22. A.J. Moses, J.Mat.Sci., Vol. 9, 1974.

23. J.T. Wilkins, J.E. Thompson, Electrical Times, February, 1962.

24. A.J. Moses, I.E.E.E. Trans.Mag., Vol.Mag. 10, No. 2., June, 1974.

25. H. Reinke, E. Reiplinger, C.I.G.R.E. Conf.Pub., No. 126, June, 1964.

26. J.E. Thompson, J.T. Wilkins, Electrical Times, November, 1963.

27. A.T. Thoeng, Holectechniek, Vol. 3, No. 2, 1973.

28. A.J. Moses, S.M. Pegler, J. Sound and Vib., Vol. 29, No. 1, 1973.

29. A.J. Moses, B. Thomas, I.E.E.E. Trans.Mag., Vol.Mag. 10, No. 2, June, 1974.

30. M. Milner, J. Dunsbee, Congres International D'Acoustique, Conf.Pub. No. F12, September, 1965.

31. R. Ruhlmann, Elektrotech. Z. (ETZ) A, Vol. 85, July, 1964.

32. J.R. Hassall, K. Zaveri, 'Acoustic Noise Measurements', Bruel & Kjaer Technical Publication, July, 1978.

33. I.S.O. Reccomendation R226, 'Normal Equal Loudness Curves For Pure Tones'.

34. L.L. Beranek, 'Noise and Vibration Control', McGraw-Hill, N.Y., 1971.

35. B. Berger et.al, Phil. Trans. A, Vol. 263, No. 1142, 1968.

CHAPTER THREE

MAGNETIC PROCESSES AND MAGNETOSTRICTION

Before investigating any relationships between magnetostriction and the crystalline structure of silicon-iron it is necessary to appreciate the fundamental process which gives rise to strains in the material during magnetisation and the way in which the physical structure of the material affects those processes. In the words of A.J. Leggett (1), "Ferromagnetism is one of the oldest and best known co-operative phenomena in nature. In a solid, the Pauli exclusion principle can give rise to an effective exchange interaction which may make it energetically advantageous for two neighbouring electrons to have their spins parallel. At sufficiently high temperatures this tendancy is off-set by the thermal disorder, but below the Curie temperature the system acquires a spontaneous magnetisation".

It is instructive to investigate in some detail the nature of the process summarised by the above statements as it will lead to an explanation of the phenomena of magnetostriction and its relationship to the material structure.

3.1 Ferromagnetism

Two possible sources of magnetism may be envisaged by considering the basic Bohr model of the free atom in which orbital motion of the charged electron around the nucleus and spin motion of the electron about its own axis constitute current paths with which there will be associated a magnetic moment. Both motions also possess angular momentum due to the mass and

velocity of the particle.

Improvements to the Bohr model quantise the orbital motions so that orbits exist at discrete levels which are integer multiples of Planck's constant, and are assigned a principle quantum number.

Spectroscopic analysis reveals that the spin angular momentum is also quantised, and as spin can exist in one of two directions this motion is assigned a quantum number, bing $\pm \frac{1}{2}$ of the orbital quantum number.

The ratio between the angular momentum and the magnetic moment for either type of motion is called the gyromagnetic ratio (ρ) and it can readily be shown (2) that for orbital motion

$$\rho_o = \frac{P_o}{M_o} = - \frac{m \omega r^2}{\frac{1}{2} \mu_o e \omega r^2} = - \frac{2m}{\mu_o e} \qquad \ldots\ldots\ldots\ldots 3.1$$

where the symbols are those accepted for the fundamental constants. Similarly, it can be shown that the gyromagnetic ratio for spin motion is given by

$$\rho_s = - \frac{m}{\mu_o e} \qquad \ldots\ldots\ldots\ldots 3.2$$

which is half that for orbital motion due to the 2:1 ratio between assigned quantum numbers. In general terms for either type of motion

$$\rho = \frac{-1}{g} \left(\frac{2m}{\mu_o e} \right) \qquad \ldots\ldots\ldots\ldots 3.3$$

where g is the Landé splitting factor which will have a value of 2 for spin motion, or unity for orbital motion. Since all the terms in the expression for ρ are universal constants, the factor $\left(\frac{g\ \mu_o\ e}{2m}\right)$ is called the gyromagnetic constant,

and suitably sophisticated experiments have been devised to enable this constant to be determined, (2,3).

When this is done for bulk ferromagnetic material it is found that the value obtained for g is approximately 2, being either slightly lower or higher depending on the experimental method employed, (2). The conclusion is, therefore, that the overall magnetic moment in ferromagnetic materials is due to spin motion of electrons, with a small contribution arising from the orbital motion.

Each electron spin can be assigned a vector of magnetic moment, $\bar{s}$, the sum of all the spins in the atom giving the overall atomic spin vector, $\bar{S} = \Sigma(\bar{s})$. Similarly for orbital motion, the overall atomic orbital vector is given by $\bar{L} = \Sigma(\bar{\ell})$. It can be demonstrated (2) that the two vectors are loosely coupled with a weak interraction called the Russell-Saunders coupling, such that $\bar{J} = \bar{L} + \bar{S}$.

In bulk ferromagnetic material the orbital moment vector, $\bar{L}$, is quenched since the overall magnetic moment is experimentally shown to be due to electron spin motion. However, the coupling referred to and the quenching of the orbital moment are necessary parts of the magnetisation process, as will be described later.

Unfortunately this explanation of the origins of ferromagnetism is not adequate for an explanation of the major characteristic of ferromagnetic materials - that they can be brought to saturation by the application of

very low field strengths (typically $< 10^3$A/m). Thus if a collection of free atomic magnetic moments is considered having a random arrangement of spin vectors, the field strength required to arrange these spin vectors in a parallel alignment (as required for magnetic saturation) can be shown to be in the order of 10^9 A/m, (2).

This anomaly is resolved by postulating that, below a critical temperature called the Curie temperature when the thermal energy of the electrons is sufficiently reduced, there will be a spontaneous interaction of energy between spin vectors such that they align themselves parallel to each other without the application of an external field. Thus a strong, internal field of the order of 10^9 A/m is spontaneously produced by the material when reduced below its Curie temperature; this is referred to as the Weiss molecular field.

Further, it is postulated that this field will exist in small areas within the bulk material, each of which will have a specific orientation to each other such that the flux of each area will be locally closed. Thus there will be no net magnetisation of the bulk material. Then only the application of a small, external field is required to bring into alignment the already saturated small areas, which are now referred to as domains. Most ferromagnetic phenomena can be explained in terms of domain behaviour, as will be discussed later in this chapter.

The problem now arises of explaining two phenomena: (a) the existence of the spin-spin interractions causing the spontaneous magnetisation and (b) the existence of specific ferromagnetic materials. To do this it is necessary to examine briefly the way in which the atomic structure of the known elements is derived.

This structure is produced by the building up of layers of electrons which can exist only in certain quantum levels and energy states. As the levels are gradually filled the total number of electrons allowed into each level is limited by the strictures of quantum mechanics. In particular, Pauli's Exclusion Principle applies which states that no two electrons having the same quantum number can exist in the same orbit. The implication of this is that two electrons having the same spin cannot be in the same orbit, but this will be contrary to the requirements of parallel spin alignment needed for ferromagnetism. As the principle quantum number for each orbit increases more electrons are allowed into the orbits, or shells, and in addition the shells sub-divide and go through the same processes. It is also possible for a shell with a higher quantum number to start filling up before the penultimate shell or sub-shell is complete. Thus many elements will exist having partially filled sub-shells which are capable of accepting additional electrons, provided they have the allowed quantum number.

In particular there is a group of elements called the Transition Metals which have partially filled, outermost (3d) sub-shells. This group includes the ferromagnetics of Fe, Co and Ni, which exist side-by-side in the Periodic Table of elements. One element lower than Fe, Mn, is not ferromagnetic although having only one electron less than Fe; the last element in the group, Cu, has a completed sub-shell and is not ferromagnetic either.

Closer examination of the comparative structures of these metals reveals two major factors: (a) the interatomic distances (lattice constants) are virtually similar and all have very compact crystal structures, and (b) the ratio of interatomic distances to sub-shell diameter is greater for Fe,

Co and Ni than for Mn. These properties are summarised in Table 3.1, (3,4).

Element	Mn	Fe	Co	Ni	
D. Atomic Separation	0.252	0.250	0.251	0.250	nm
d. Sub-shell Diameter	0.171	0.154	0.138	0.127	nm
Ratio of $^{D}/_{d}$	1.473	1.623	1.818	1.968	
Curie Temperature	____	770	1127	358	^{o}C
Saturation Level	____	2.15	1.76	0.61	T @ 20^{o}C
Crystal Structure		B.C.C.	C.P.H.	F.C.C.	

TABLE 3.1. Relative Properties of Transition Metals

Two further theories related to atomic structure also have to be considered before it is possible to have a situation whereby two or more electrons having the same spin can exist in the same atomic orbit. The first of these is Stoner's Band Theory, or the Collective Electron Model, (2,3), which follows from the concept of an atomic structure having its outermost sub-shells greatly removed from the nucleus and with adjacent atoms in the crystal structure being fairly close to each other. This allows the concept of energy bands which are not restricted to one particular atom but are spread through the bulk material, and in which electrons are envisaged as being free to wander throughout the crystal infrastructure. The second theory is the Brillouin Zone Theory which allows a particular sub-shell to

contain a large number of adjacent kinetic energy bands which are very close together and for which only a small quantity of energy is required to excite a given electron from one band to another (3). The Pauli Exclusion Principle still applies to each band, but it would now be possible for a free electron to exist in the same sub-shell as another electron having the same (parallel) spin, but at a slightly higher energy state.

Considering now the formation of a crystal structure from the basic constituent atoms; in the simplest case of a hydrogen molecule, a pair of positive nucleii share a pair of electrons in which strong forces of interraction, or coupling, exist between the electron spins. It is found that in this case the electrons have opposite, anti-parallel, spin vectors and the coupling forces are described as negative.

It is now postulated that the spontaneous molecular field in ferromagnetism is due to similar quantum forces of coupling between unpaired electron spins in adjacent atoms, but that the coupling is now positive so that parallel spin alignment occurs. This concept was introduced by Heisenberg's postulate of the Exchange Integral, used in quantum mechanics to relate the energy of the spin vectors of two neighbouring atoms, such that

$$W = \pm 2.J.\bar{S}i.\ \bar{S}j \qquad \ldots\ldots\ldots\ldots\ldots\ 3.4$$

where Si and Sj refer to the spin vectors of atoms i and j respectively. W is a minimum when the exchange integral, J, is negative and the spins are anti-parallel, and, most importantly, W is also at a minimum when J is positive and the spins are parallel. There is no classical analogy for this phenomena and it is explained purely on the basis of quantum analysis, but it is believed that exchange forces of this nature are as a result of electrostatic, Coulomb energy interaction between neighbouring electrons (2).

An extension of the exchange integral theory using a mathematical treatment due to Bethe (3) gives a theoretical possibility that positive coupling may arise when the distance between two adjacent nucleii, compared to the radius of the orbit in which uncompensated electron spins exist, exceeds a certain value. The estimates obtained for this value show it to be about 1.5, and, as has been shown in Table 3.1, this is indeed the case for Fe, Co and Ni, but not for Mn.

However, Pauli's Exclusion Principle will still not allow parallel spin alignment in the same energy band within a given quantum shell. Fortunately the Brillouin Zone Theory provides a large number of adjacent energy bands within the same sub-shell, so that if there is an unfilled energy level and if the positive exchange energy is acting in the system, then it is possible for negative or down-spin electrons to be excited up to a higher energy band and to reverse their spins, thus giving a net balance of unpaired, positive, parallel-aligned, spin electrons.

To summarise, the recipe required to produce the phenomena of ferromagnetism is as follows (4):

(1) There must be unfilled electron shells within the atom;

(2) There must be uncompensated electron spins in these shells;

(3) The lattice constant of the crystal structure must exceed 1.5 x the radius of the unfilled sub-shell.

When these conditions are fulfilled, then spontaneous parallel spin alignment will occur below the Curie Temperature, producing the Weiss Molecular Field, which is the origin of Ferromagnetism.

3.2 Magneto-Crystalline Anisotropy and Magnetic Domains

As previously mentioned the orbital motions of the electrons are quenched in bulk material, and this occurs during the formation of the

crystal structure of the material when orbit - orbit interractions or coupling determine the overall lattice structure. Thus the positions of the orbital magnetic moments are fixed in space relative to the crystal lattice, to the extent that there is no net magnetic moment arising from this source; this orbit-lattice coupling is so strong that the influence of an external field has no effect on it. However, in a ferromagnetic crystal there is the weak Russell-Saunders coupling between the spin and orbit magnetic moments, and therefore a weak coupling between the spin moment and the crystal lattice. So, in the absence of an external field, the spontaneously formed domains produced by the strong spin - spin interractions will tend to align with the crystal lattice. This gives the ferromagnetics their highly anisotropic nature; that is they show preferred or easy directions of magnetisation.

Now iron forms a body-centred cubic lattice structure, and it can be shown (3) that the energy associated with such magnetic anisotropy in a cubic crystal is given by:

$$W_A = K_o + K_1 (\ell^2 m^2 + m^2 n^2 + n^2 \ell^2) + K_2 (\ell m n)^2 \quad \ldots\ldots\ldots\ldots \quad 3.5$$

where ℓ, m, n are the direction cosines of the magnetisation vector arising from the domains (M_s), K_o is a constant independant of direction and so not required during dynamic investigations, and K_1, K_2 are the so-called anisotropy constants. Further, it can be shown (3) that for W_A to be a minumum, M_s must lie along a particular crystal axis, depending on the values of K_1 and K_2. For iron, it turns out that M_s will lie along the <100>, or cube-edge, directions for minimum anisotropy energy, and thus the preferred or easy directions for magnetisation in iron will be coincident with the cube-edges of the crystal structure. This, indeed, has been experimentally verified (3). Thus in demagnetised crystals it would be

expected to find the domains distributed among the six equivalent directions of cube-edges such that the resultant magnetisation in any direction was zero.

Considering now the formation of domains in a lamination of iron in which the crystal structure is assumed to have perfect orientation to the lamination, i.e., all the {100} planes lie along the plane of the sheet and all the [001] directions are parallel to the largest side. If the length of the sheet is greater than its width, and both are considerably greater than its thickness, then any domains will be expected to lie in the plane of the sheet parallel to its length. This will be so since the smallest demagnetising factor for such a shape can be shown to exist for magnetisation parallel to the longest axis, as compared to axes normal to, and transverse to, that direction, (2,3). Hence the magnetostatic energy, which is related to the demagnetisation factor by the relationship $E_m = \frac{1}{2} N M_s^2$ (4), will be a minimum in that direction.

If one continuous domain was to be formed throughout the sheet then E_m will still be extremely great, due to the creation of free poles at each end of the sheet (Fig. 3.1, (a)). This energy will be reduced if the domain sub-divides into two anti-parallel domains (Fig. 3.1, (b)), and will be eliminated if closure, or transverse, domains appear, creating flux closure paths (Fig. 3.1, (c)). However, the presence of the transverse domains requires the M_s vector to rotate through 90^o, and, as will be discussed in Section 3.3, this imposes a strain on the crystal lattice. Thus a component of magnetoelastic energy (E_x) is introduced. E_x will be reduced if the volume of the transverse domains is decreased which can be achieved if the domain further sub-divides (Fig. 3.1 (d)). However, as this occurs, more boundaries (called 180^o boundaries) are created between the domains; these boundaries, or Bloch Walls, have finite thickness in which takes place a gradual rotation through 180^o of the M_s vectors. It can be shown (3) that

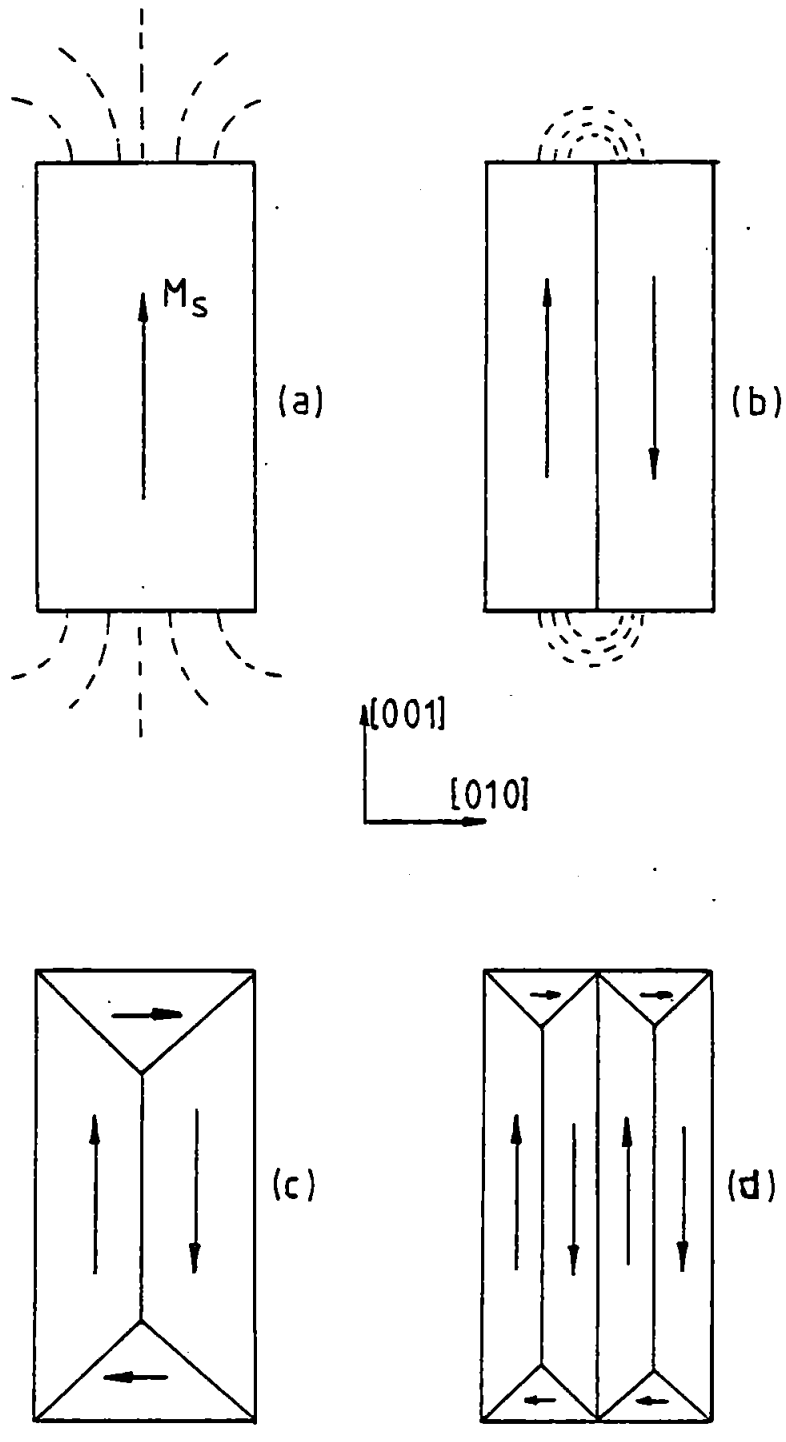

FIG. 3.1. Showing the formation of Basic Domain Structures

these walls have an associated energy made up of an exchange energy due to interaction between adjacent, non-parallel spin vectors, and an anisotropic energy due to the width of the wall. Hence, as the domain sub-divides, there will be an increase in wall energy :-

$$E_w = E_x + E_A$$

The likeliest, stable domain arrangement will occur when the total energy of the system becomes a minimum (5,6). Thus if the magnetostatic energy is eliminated by the presence of the closure domains, the main, 180° domains will sub-divide until the sum of the boundary wall energy and the magnetoelastic energy is a minimum.

Following the development of techniques for domain observation (see Chapter 4), domain structures, formed as described above, have been observed, and as mentioned in Section 3.1., the study of domain behaviour is now completely used to explain all ferromagnetic processes. Thus for the simple domain structure depicted by Fig. 3.1 (d), when an external field is applied along the major axis of the material, those domains already magnetised to saturation in that direction will grow by means of domain wall motion (2) at the expense of the oppositely magnetised, anti-parallel domains. Eventually, for increasing applied field strength, the material will be completely magnetised in this direction at the saturation level, M_s, of the domains.

If the crystal orientations within the material are now such that the {110} planes are parallel to the plane of the sheet, but still with the [001] directions parallel to the longest side, then sub-division of the domain structure into anti-parallel 180° walls will still occur in order to reduce the magnetostatic energy. However, closure domains of the type shown in Fig. 3.1 (d) will not now be expected, since these directions are

coincident with the <110> direction, or non-easy direction, associated with much higher anisotropy energy. In this case, the closure deomains at the ends of the specimen will lie along the [100] or [010] directions inclined at 45^{o} to the sheet plane.

This type of material having a (110)[001] crystallographic orientation is now commonly in use as an electrical sheet steel, and in all subsequent discussions this will be the material referred to. Unfortunately, such perfect orientation in polycrystalline material is not realisable in practice, although electrical steels containing iron alloyed with silicon have now been developed in which 90 - 95% orientation with the preferred direction has been achieved.

Since the properties of silicon-iron, such as magnetic anisotropy and saturation magnetisation, are sufficiently like those of iron (4), then it may be expected that the same domain patterns will occur in both materials.

Thus in Polycrystalline material it might be expected to find individual grains (each composed of many, similarly orientated crystals) having varying angles of the crystal axes with respect to the axes of the bulk material. Thus the [001] axis may be tilted out of the plane of the sheet, or rotated about the normal to the plane of the sheet, or the (110) plane may be rotated about the [001] axis. These correspond to angles of pitch (ϕ), yaw (θ) and roll (α) as depicted in Fig. 3.2. Obviously grains having combinations of various values of ϕ, θ and α may be expected to occur.

In an investigation of over 200 grains having a wide variation of misorientation angles, Paxton and Nilan (7) found that, at least in the demagnetised state, the domain configurations appeared to be independant of θ, and that, at least for small values of α, the angle α had little effect on domain patterns. The most important conclusion of this work was that the type of domain pattern expected to be observed at the material surface

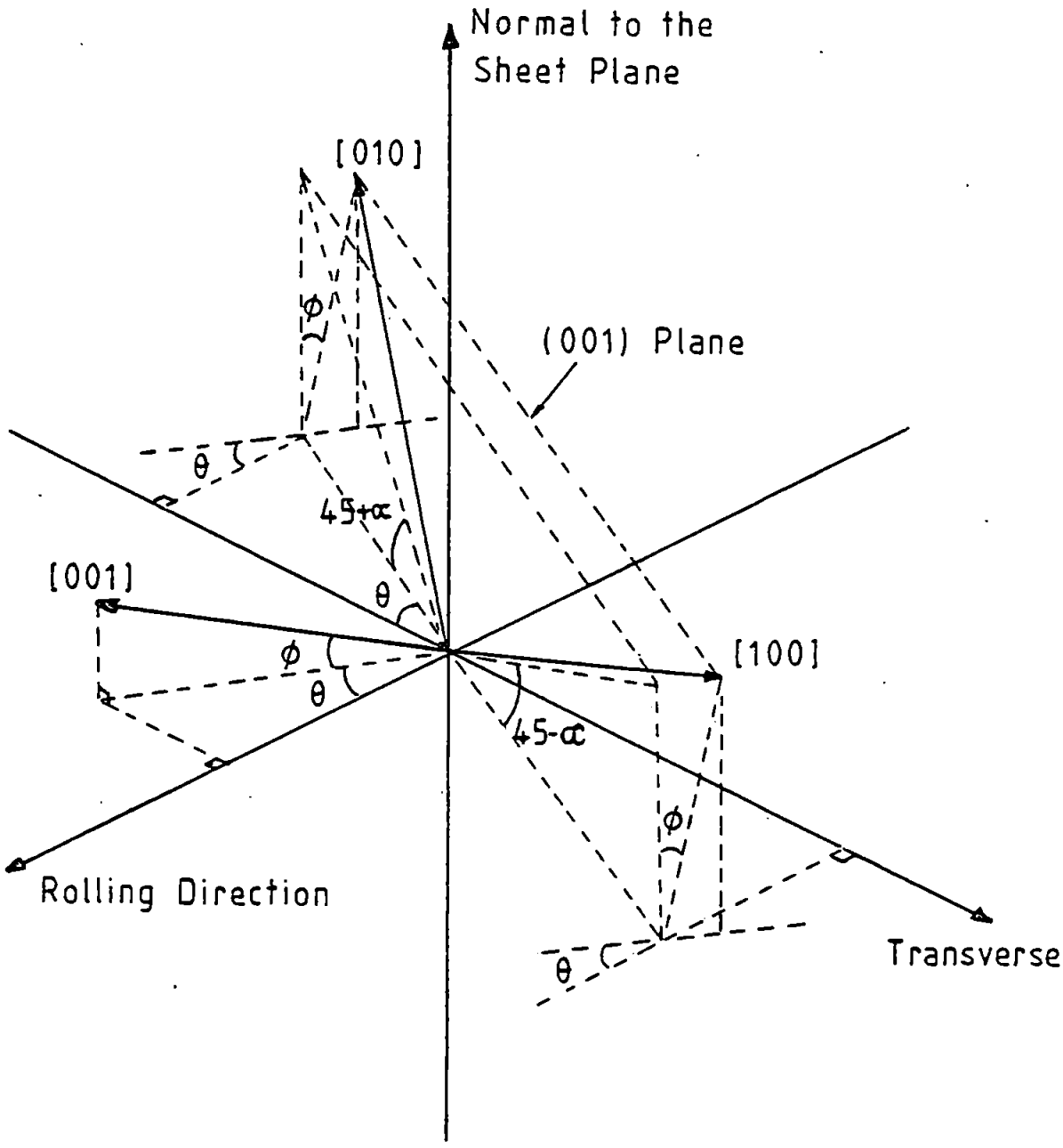

FIG. 3.2. The Mis-orientation Angles.

(the so-called surface closure structure) will be determined solely by the angle ϕ. Further, Paxton and Nilan classified five types of domain structure, designating them Wall, Spike, Lozenge, Lace and Maze patterns, the names arising from the physical manifestations of the observed patterns. More significantly they were identified as corresponding to angles of ϕ in the ranges $0 - 2^{o}$, $2 - 4^{o}$, $4 - 7^{o}$, $7 - 13^{o}$ and greater than 13^{o} respectively.

More recent work by Daniels (8) has complemented the work of Paxton and Nilan and enabled more precise correlation of ϕ with domain patterns, allowing ϕ to be measured to within 1^{o} from the surface closure structure, and extending the ranges of ϕ to include $8 - 9^{o}$ and greater than 9^{o}.

Various models have been proposed by way of explanation for the different types of domain patterns, and most are based on the fact that it is necessary for flux closure domains to occur in order to reduce the magnetostatic energy which would otherwise arise due to free poles being produced when the main, 180^{o} domains reach the surface of the material (5, 7). Such studies have shown that this structure is not merely a surface effect but that the domains apparent at both surfaces of a lamination are interconnected through the thickness of the material by transverse domains lying along the easy directions perpendicular to the $[\bar{0}0\bar{1}]$ direction. Hence possible domain structures, as proposed to exist through the sheet thickness, are shown in Figs. 3.3, (a) and 3.3, (b) for the cases when $2^{o} < \phi < 4^{o}$ (5, 7). Such structure is referred to as "supplementary structure", as distinct from "main" structure which refers to the large, flux carrying slab domains.

The volume and behaviour of the supplementary structure is now known to be responsible for the levels of power loss and magnetoelastic energy in electrical sheet steels, (5, 9) and, as will be shown in Section 3.3.2,

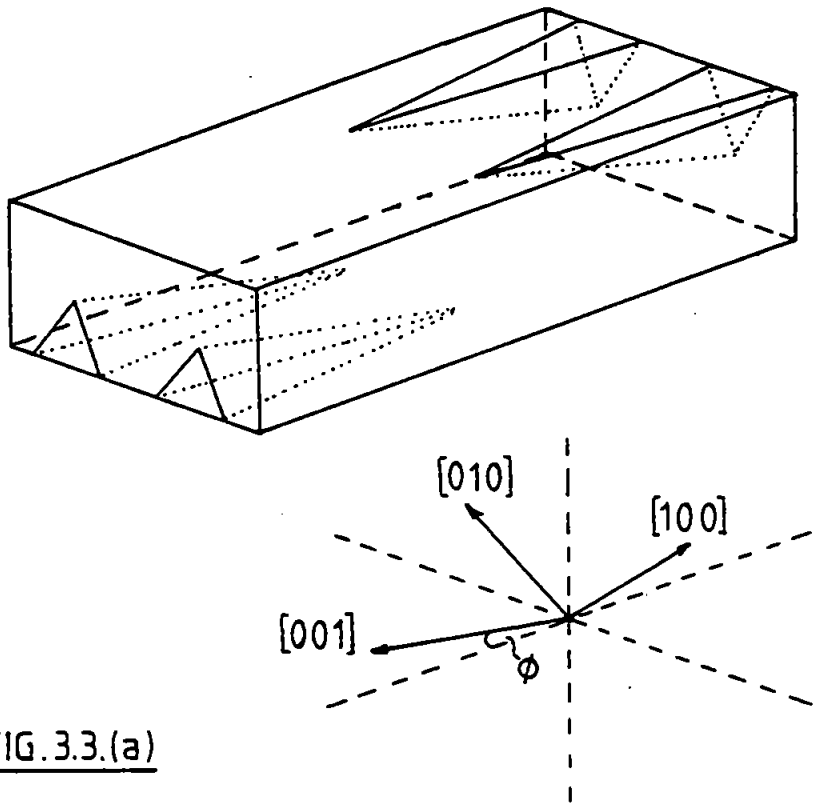

FIG. 3.3.(a)

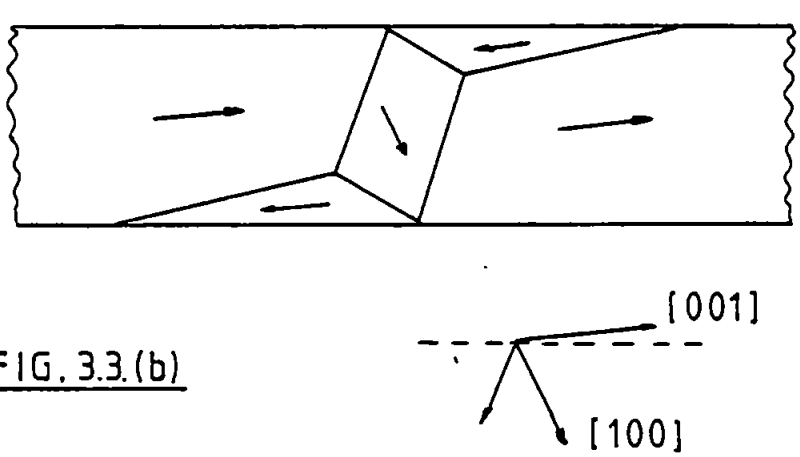

FIG. 3.3.(b)

FIG. 3.3. Illustrating the formation of "Supplementary" Domain Structure in a Mis-orientated Grain.

the supplementary structure is dramatically affected by the application of external stresses to the material.

The formation of flux closure obeys a fundamental principle originally stated by Néel, but summarised in the light of modern investigations by Shilling and Houze (5). This states that for materials with large cubic anisotropy (thus for 3% Si-Fe, $K_1 = 3.5 \times 10^4$ J/m^3, $K_2 = 0$) domains will arrange themselves along the six easy directions, <001>, such that the net induction is parallel to the applied field; that is, parallel to the sheet plane since applied fields are usually orientated so. This may be explained by again considering the relative demagnetising factors, N, such that for long, thin sheets the value of N along the length of the sheet is very small. Thus if the crystal axis is rotated out of the sheet plane ($\phi > 0$), then magnetisation spin vectors will not rotate down into the sheet, but domains will form along the $\pm[0\bar{1}0]$ and $\pm[\bar{1}00]$ directions such that the volume weighted vector sum of domain magnetisation is parallel to the (110) surface plane.

A further feature of polycrystalline material is that the main, 180° slab domains tend to be continuous along the sheet, passing through grain boundaries. The essential difference between adjacent grains is then apparent due to differences in supplementary structure (due to variations in ϕ) and differences between the $[00\bar{1}]$ direction and the axis of the sheet (variation in θ). Thus it is apparent that variations in induction will occur from grain to grain.

Shilling and Houze (5) have shown, at least at the knee of the magnetisation curve, that the value of the net induction, B_N, parallel to the applied field in a misorientated grain (θ, $\phi > 0$) is given by

$$\frac{B_N}{M_S} = \frac{1}{\cos\theta.\cos\phi + \frac{\sqrt{2}}{2}\left[\cos\theta.\sin\phi + \sin\theta + \left|\cos\theta.\sin\phi - \sin\theta\right|\right]} \qquad \ldots\ldots\ldots\ldots\ldots\ldots 3.6$$

where M_s is the domain saturation magnetisation. Above the knee of the curve rotation of domains out of the easy directions will be required, necessitating larger increases in applied field energy, thus producing the knee.

Radley (10) used the above relationship between the permeability and misorientation angle as a way of predicting the grain orientation, since changes in either θ or ϕ will produce the same change in B and will be governed by the larger of the two angles, the smaller having little effect (5). However, this would not enable the determination of which angle of misorientation was present, and this can only be done by observation of the domain surface closure structure. Techniques for achieving this will be dealt with in Chapter 4.

3.3 Magnetostriction Phenomena and Derived Theory

3.3.1 The Origin of Magnetostriction

Due to the marked anisotropy of ferromagnetic material, any domains tend to lie along preferred directions, such as the cube edges of silicon-iron crystals. If an external field is applied at some angle to these preferred directions then the spin vectors will experience a torque tending to align them with the easy direction of magnetisation nearest to the direction of the applied field. In addition, this torque will be exerted on the orbit moment axes through the spin-orbit coupling discussed in Section 3.1. Since the orbit moment vectors are strongly coupled to the crystal axes, and since rotation of the spin vectors involves rotation of the unfilled 3 d sub-shells (in which the aligned spin-vectors exist) which are not spherically symmetrical, then a change in the lattice dimensions of the crystal has to occur in order to re-establish a condition of minimum energy. This sets up a strain in the material which is referred to as the Joule effect, or linear or longitudinal magnetostriction, or simply

magnetostriction. As, in this case, it occurs with variations in the applied field, it may be referred to as dynamic magnetostriction.

A similar effect occurs at the instant of spontaneous domain formation when the material is cooled below its Curie temperature, and when the otherwise cubic lattice inside each domain is spontaneously deformed in the direction of domain saturation magnetisation, M_s. This may be referred to as the static magnetostriction or static magnetostrictive strain.

Two important considerations arise from this explanation:

(a) no dynamic strain will be observed unless there is a re-arrangement of domains within the material,

(b) that any externally applied stresses will obviously strain the material and influence the process of magnetostriction.

The usual definition of magnetostriction accepted by users and suppliers of electrical sheet is the net strain measured parallel to the applied field when the material is magnetised from its demagnetised state to some given level of induction (5).

By consideration of the lattice strain and elastic constants it may be shown (2,5) that an equilibrium lattice strain exists when the total magnetoelastic energy (the sum of the elastic strain energy and the lattice magnetoelastic energy) is minimised. From this may be derived an expression for the equilibrium magnetostriction in terms of two experimentally measured, equilibrium lattice strains λ_{100} and λ_{111} where λ_{100} the strain in the $[\bar{1}00]$ direction when the magnetisation is in that direction, and λ_{111} is the strain in the $[\bar{1}\bar{1}1]$ direction when the magnetisation is in that direction. Thus

$$\lambda = \frac{\delta \ell}{\ell} = \frac{3}{2} \lambda_{100} \left[(\ell_1^2 m_1^2 + \ell_2^2 m_2^2 + \ell_3^2 m_3^2) - \frac{1}{3} \right]$$

$$+ 3 \lambda_{111} (\ell_1 \ell_2 m_1 m_2 + \ell_1 \ell_3 m_1 m_3 + \ell_2 \ell_3 m_2 m_3)$$

..... 3.7

where λ is the strain in a domain measured in a direction whose direction cosines are ℓ_1, ℓ_2, ℓ_3 with respect to the cube edges as reference directions, and having a saturation magnetisation, M_s, in a direction whose direction cosines are m_1, m_2, m_3 with respect to the cube edges.

Hence the strain in any direction of a material may be obtained when the material contains cubic crystals aligned in some way to the material, those crystals being contained by saturated domains at some other orientation. Thus for the simple case when M_s lies along cube edges and the $[\bar{0}0\bar{1}]$ axis is parallel to the direction of strain measurement, then $\ell_1 = m_1 = 1$, $\ell_2 = \ell_3 = m_2 = m_3 = \cos 90^\circ = 0$. Hence

$$\lambda = \frac{3}{2} \lambda_{100} \left(1 - \frac{1}{3}\right) = \lambda_{100} \qquad \ldots\ldots\ldots\ldots\ldots\ldots\ldots\ldots 3.8$$

If the strain is now measured in the same direction but for domains lying along the $[\bar{0}1\bar{0}]$ or $[\bar{1}0\bar{0}]$ axis at right angles to the $[\bar{0}0\bar{1}]$ axis, then $m_2 = 1$, $m_1 = m_3 = 0$, $\ell_1 = 1$, $\ell_2 = \ell_3 = 0$ or $m_3 = 1$, $m_1 = m_2 = 0$, $\ell_1 = 1$, $\ell_2 = \ell_3 = 0$. For either case

$$\lambda = \frac{3}{2} \lambda_{100} \left(0 - \frac{1}{3}\right) = -\tfrac{1}{2} \lambda_{100} \qquad \ldots\ldots\ldots\ldots\ldots\ldots\ldots\ldots 3.9$$

So if domains change orientation by rotating through 90° from the $[\bar{0}0\bar{1}]$ axis to the $[\bar{1}0\bar{0}]$ or $[\bar{0}1\bar{0}]$ directions, then the net strain in the $[\bar{0}0\bar{1}]$ direction will be given by the difference between equation 3.8 and 3.9, such that

$$\lambda = -\tfrac{1}{2} \lambda_{100} - \lambda_{100} = -\frac{3}{2} \lambda_{100} \qquad \ldots\ldots\ldots\ldots\ldots\ldots\ldots\ldots 3.10$$

If the reverse procedure occurs i.e., rotation from the $[0\bar{1}0]$ or $[\bar{1}00]$ direction into the $[00\bar{1}]$ or measuring direction then the net strain will be given by

$$\lambda = \lambda_{100} - (-\tfrac{1}{2}\lambda_{100}) = +\frac{3}{2}\lambda_{100} \qquad \ldots\ldots\ldots\ldots\ldots\ldots 3.11$$

Thus the strain can be positive or negative (that is, an elongation or a contraction) depending on the relative direction of domain movement.

3.3.2 The Effects of Stress

If the magnetostriction described above is produced in a crystal structure whilst that crystal is being subjected to an externally applied stress, then strain energy in the form of magnetoelastic energy will be stored by the domains responsible for the strain. It might be expected, therefore, that the domain structure would alter in order to reduce the total free energy of the system.

It can be shown (3) that the increase in magnetoelastic energy in a crystal of cubic structure under stress is given by

$$E_\lambda = -\lambda\sigma \qquad \ldots\ldots\ldots\ldots\ldots\ldots 3.12$$

where λ is given by equation 3.7, and σ is the stress assumed to be applied in the same direction as which λ is measured, i.e., direction cosines ℓ_1, ℓ_2, ℓ_3. The stress, σ, is positive for tension and negative for compression. Thus if σ is tensile, E_λ will be negative or reduced, but if σ is compressive E_λ will be positive or increased. Thus it may be expected that little, if any, domain changes will occur under the application of tensile stress but that domain structure will modify under compression of the material.

The effects of stress on domain structure have been observed by many workers. Dijkstra and Martius (11) investigated the effect of tensile stress applied in the $[1\bar{1}0]$ direction at 90° transverse to the $[00\bar{1}]$ direction, and noted that the predominant, 180° domain structure of Fig. 3.4, (a) broke down at fairly low levels of stress until the so-named Stress Induced Pattern I was produced (Fig. 3.4, (b)). On further increase of the stress this pattern became more distinct and narrower in spacing until eventually this in turn changed into the Stress Induced Pattern II as shown in Fig. 3.4, (c). The stresses did not exceed the elastic limit of the material which was grain-orientated S_i-F_e.

Neurath (12) noted the decrease in magnetostriction measured in 3% S_i-F_e for tensile stress applied along the $[00\bar{1}]$ direction, and an increase for compressive stress applied in that direction, and interpreted this as due to changes in domain structure.

Gniewek (13) observed domain surface closure structures in 3½% S_i-F_e for tensile stresses applied transverse to the $[00\bar{1}]$ direction, i.e., along $[1\bar{1}0]$, and also along the $[00\bar{1}]$ direction. In the former case similar effects to those reported by Dijkstra and Martius were noted and in the latter case it was observed that a reduction in what is now called supplementary structure occurred as well as a refinement in the 180° wall patterns.

Corner and Mason (14) noted that tension applied in the $[1\bar{1}0]$ direction had the same effect as compression applied in the $[00\bar{1}]$ direction, the effect being similar to that reported by Dijkstra and Martius, and that tension applied in the $[00\bar{1}]$ direction had little effect, in well orientated grains ($\phi = 0$) but caused a reduction in supplementary structure for grains tilted into the plane of the material ($\phi > 0$). Further, Corner and Mason suggested models to account for the Stress Induced Patterns I and II of Dijkstra and Martius and also predicted theoretically that a compressive stress along $[00\bar{1}]$ would have the same effect as a tension of twice the magnitude along $[1\bar{1}0]$.

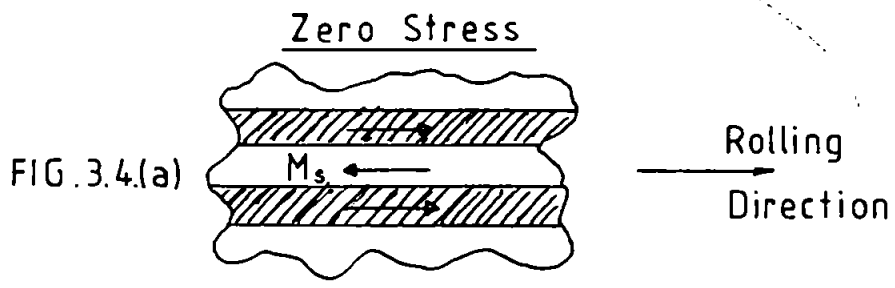

FIG. 3.4.(a)

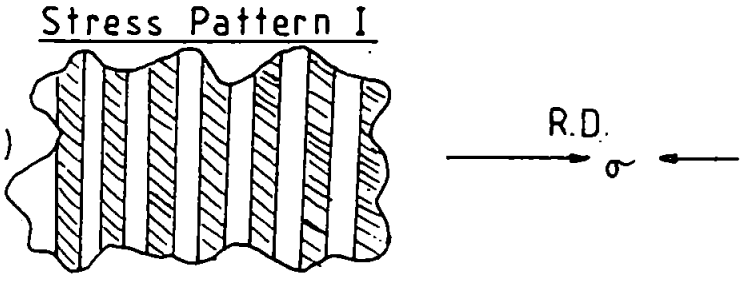

FIG. 3.4.(b)

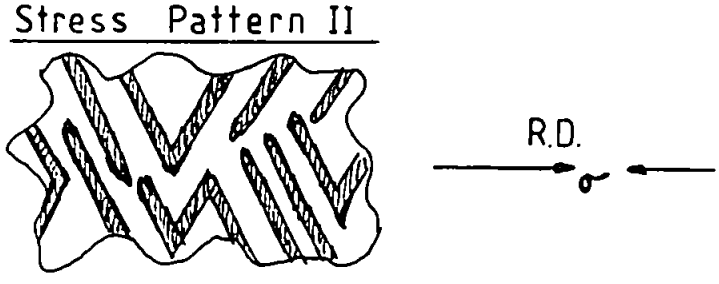

FIG. 3.4.(c)

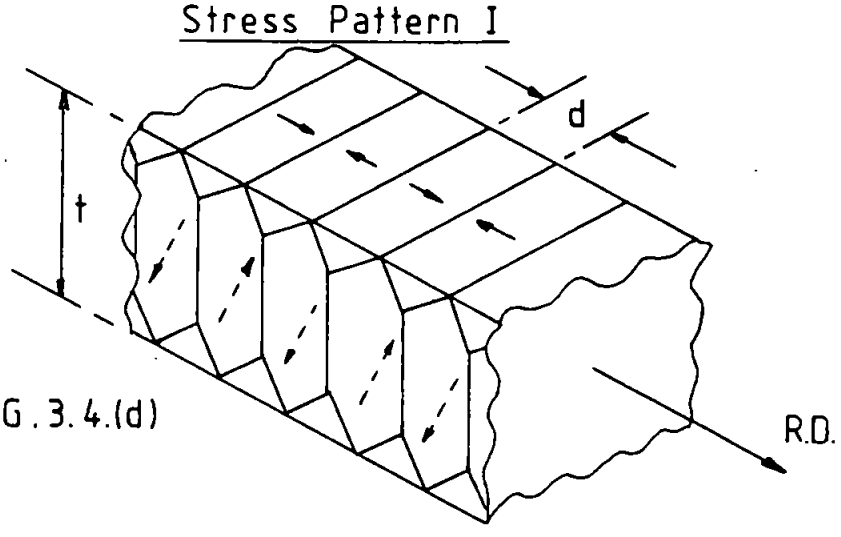

FIG. 3.4.(d)

FIG. 3.4. Illustrating the effects of Compressive Stress on Domain Structure.

The structure predicted by Corner and Mason to account for Stress Pattern I is reproduced in Fig. 3.4, (d) where the unstressed state is assumed to be the 180° bar structure of a well aligned grain (Fig. 3.4, (a)). It will be seen that the bulk of domains are in the transverse directions, $[\bar{1}00]$ and $[0\bar{1}0]$, the magnetostatic energy being reduced by flux closure domains in the $[00\bar{1}]$ direction.

It can be shown (15) that the $[\bar{1}00]$ and $[0\bar{1}0]$ directions are energetically favourable for a compression applied to the $[00\bar{1}]$ direction or a tension applied along $[1\bar{1}0]$. Hence for increasing compression along $[00\bar{1}]$ the transverse directions become more favourable for domain orientation and the volume of such supplementary structure increases at the expense of domains in the $[00\bar{1}]$ direction.

Further, by consideration of equation 3.7 and 3.12 for the case when M_s is the same direction as a compressive stress ($-\sigma$) applied parallel to the $[00\bar{1}]$ axis then

$$E_\lambda = + \lambda_{100}\, \sigma \qquad \ldots\ldots\ldots\ldots\ldots\ldots\ldots\ldots \quad 3.13$$

since $\ell_1 = m_1 = 1, \quad \ell_2 = m_2 = \ell_3 = m_3 = 0$

Alternatively, when a tensile stress ($+\sigma$) is applied transverse to the $[00\bar{1}]$ direction along $[1\bar{1}0]$ then

$$E_\lambda = + \tfrac{1}{2} \lambda_{100}\, \sigma \qquad \ldots\ldots\ldots\ldots\ldots\ldots\ldots\ldots \quad 3.14$$

since $\ell_1 = 0, \quad \ell_2 = \ell_3 = \cos 45^\circ, \; m_1 = 1, \; m_2 = m_3 = 0$

This is exactly the prediction of Corner and Mason since comparison of equation 3.13 and 3.14 shows compression along $[00\bar{1}]$ has the same effect on E_λ as has a tension of twice the magnitude along $[1\bar{1}0]$. Such a result has been experimentally confirmed (16).

If the stress applied along $[00\bar{1}]$ is now tensile, then equation 3.13 becomes

$$E_\lambda = -\lambda_{100}\,\sigma \qquad \ldots\ldots\ldots\ldots\ldots\ldots\ldots\ldots \quad 3.15$$

showing that the total free energy is reduced for the main, 180° domains. However, if any supplementary structure is present it will experience an increase in magnetoelastic energy given by

$$E_\lambda = \tfrac{1}{2}\,\lambda_{100}\,\sigma \qquad \ldots\ldots\ldots\ldots\ldots\ldots\ldots\ldots \quad 3.16$$

since $\ell_1 = 1$, $\ell_2 = \ell_3 = 0$, $m_2 = 1$, $m_1 = m_3 = 0$ for a domain magnetised along $[0\bar{1}0]$ with the tensile stress along $[00\bar{1}]$. Thus to minimise the total free energy, the transverse structure will re-orientate into the (110) plane; but as this will increase the magnetostatic energy of the main, 180° domains they will then further sub-divide to reduce this energy as discussed previously in Section 3.2. This has been experimentally confirmed by V.M. Bichard et. al. (17).

The effects of compressive stress applied normally to the plane of a sheet of Si-Fe have also been investigated (18, 19, 20). Again, by consideration of equation 3.7 and 3.12, an expression for the increase in magnetoelastic energy for such a stress is given by

$$E_\lambda = +\tfrac{1}{2}\,\lambda_{100}\,\sigma \qquad \ldots\ldots\ldots\ldots\ldots\ldots\ldots\ldots \quad 3.17$$

since $\ell_1 = 0$, $\ell_2 = \ell_3 = \cos 45^\circ$, $m_1 = 1$, $m_2 = m_3 = 0$. This is equivalent to the change due to the transverse stress of equal magnitude. However, in practical transformer cores the normal stresses will be several orders of magnitude less than any planar stresses (also a high demagnetising field perpendicular to the sheet) and the domain changes expected would consequently only be minor. Experimental evidence (18, 19) shows that the stress sensitivity of magnetostriction and losses in well orientated

material for normally applied stresses is significantly less than that for any planar stresses of similar magnitude.

Thus it may be concluded from the above discussion that the effect of stresses on domains is to cause a re-arrangement of the supplementary structure consisting mainly of transverse domains; tensile stresses applied parallel to the rolling direction remove supplementary structure and re-align the main, 180° domains whilst compressive stresses in the rolling direction increase the volume of supplementary structure.

3.3.3 Negative Magnetostriction

The experimentally measured magnetostriction constants λ_{100} and λ_{111} have values in the order of $+ 24.10^{-6}$ and $- 4.10^{-6}$ respectively for Goss-orientated, 3% Si-Fe (5). By substituting these values into equations 3.7 to 3.16 above it will be anticipated that the net strain measured in the $[\bar{0}0\bar{1}]$ direction will be positive (elongation) for domain rotations from $[\bar{0}1\bar{0}]$ or $[\bar{1}0\bar{0}]$ directions into the $[\bar{0}0\bar{1}]$ axis, regardless of the level of stresses applied along the rolling direction (assumed nearest to $[\bar{0}0\bar{1}]$). Equally the strain would be negative (contraction) for domain rotation in the reverse direction.

Since, at any stress level, net magnetisation of the material involves growth of 180° domains by wall movement (which does not produce magneto-striction) and rotation of the supplementary structure into the $[\bar{0}0\bar{1}]$ direction, then it would be expected that all measured magnetostriction would be positive. This is contradictory to experimentally determined values (16, 21) wherein negative levels of strain have been reported, particularly at, or near, zero stress and at relatively high inductions near to the knee of the magnetisation curve.

Langham (22) produced a magnetostriction model based on 90° wall domain motion at low inductions (< 1.5 T) and rotation of 180° wall domains at high inductions (> 1.5 T). This accounted for small, positive values of λ at zero stress, but did not include negative levels. Anyway, current domain theory discounts 180° wall rotations in the plane of the sheet except at very high field strengths above the knee of the magnetisation curve (5).

Brownsey and Maples (23) accounted for negative values of λ by considering the rotation of 180° wall domains away from the [001] crystal axis which was dipped into the plane of the sheet. This account was subsequently modified by Holt and Robey (24) to include rotation in the plane of the sheet. As this requires moving the domains away from their easy directions, the field strengths required would be greater than those normally experienced with modern materials in practice (5).

Simmons and Thompson (21) observed negative λ at low stresses for the cases when the [001] axis was in the plane of the sheet ($\phi = 0$) and with no evidence of any supplementary structure in the form of surface closure domains which would, in any case, have produced a positive strain under magnetisation.

Banks and Rawlinson (16) also observed negative λ, but for samples of orientated Si-Fe subjected to various degrees of coating material. This was interpreted as indicating that the samples were under an effective tensile stress due to the coatings since uncoated samples gave small, positive values of λ at zero stress, and negative λ for increased tensile stress.

All these phenomena can now be explained in terms of the behaviour of supplementary structure of domains. Simmons and Thompson produced a model based on the assumption that, during the process of magnetisation under

stress free conditions, transverse domains were created in the [010] and [100] directions by rotation of spin vectors away from the [001] axis. This would minimise the magnetostatic energy due to the angle of rotation, θ, between the 180° main domain and the applied field by enabling the net induction in the grain to remain parallel with the applied field in the plane of the sheet, parallel to the rolling direction. This is consistent with the principle stated in Section 3.2 concerning the formation of flux closure structure.

These authors then derived an expression relating the strain measured in the rolling direction to the misorientation angle θ (between the [001] axis and the rolling direction) by consideration of the volume weighted algebraic sum of the domain magnetisations in each easy direction before and after magnetisation to some induction B. The expression derived is

$$\lambda = \frac{3}{\sqrt{2}} \cdot \lambda_{100} \cdot \frac{B}{M_s} \cdot \sin\theta \left(\tfrac{1}{2}\sin^2\theta - \cos^2\theta\right) \quad \ldots\ldots\ldots\ldots\ldots\ldots 3.18$$

where M_s is the domain saturation magnetisation.

In the case of the phenomena observed by Banks and Rawlinson, it has previously been shown that tensile stresses remove supplementary structure, since the [001] direction has become energetically favourable. If this is the case, then on applying an external field, it will be necessary for the supplementary structure to reform, for the same reasons as given by Simmons and Thompson, so that the net induction may remain parallel to the applied field. Thus the conclusion reached by Banks and Rawlinson is correct, in that the coating applied to the material is applying an effective tensile stress large enough to remove supplementary structure which then reforms during magnetisation. This requires transfer of spin vectors through 90° from [001] to ± [010] or ± [100] direction, which, as has been shown

earlier, results in negative strains in the crystal structure.

Shilling (5) shows that an expression for λ can be derived for this case which is identical to equation 3.18 above but with θ replaced by the angle of tilt, ϕ.

An analysis may be undertaken to include all three misorientation angles (θ, ϕ, α) on an assumption that in the demagnetised state no supplementary structure exists, either due to ϕ being zero, or because a tensile stress of sufficient magnitude has been applied to remove any supplementary structure due to $\phi > 0$.

The analysis is as follows:-

Consider a grain having angles of misorientation θ (yaw), ϕ (pitch) and α (roll) as shown in Fig. 3.5. Then the direction cosines of the cube edges corresponding to the easy directions of magnetisation [001], [010] and [100] will be:

$$\ell_1 = \cos\theta . \cos\phi$$

$$\ell_2 = \sin\theta . \cos(45 + \alpha) + \cos\theta . \sin\phi . \sin(45 + \alpha)$$

$$\ell_3 = |\sin\theta . \cos(45 - \alpha) - \cos\theta . \sin\phi . \sin(45 - \alpha)| \quad \ldots\ldots\ldots \quad 3.19$$

with respect to the sheet rolling direction;

and

$$n_1 = \sin\phi$$

$$n2 = \cos\phi . \sin(45 + \alpha)$$

$$n_3 = \cos\phi . \sin(45 - \alpha) \quad \ldots\ldots\ldots\ldots\ldots\ldots\ldots \quad 3.20$$

with respect to the normal to the sheet plane;

and $t_1 = \sin\theta \cdot \cos\phi$

$$t_2 = \left|\cos\theta \cdot \cos(45 + \alpha) - \sin\theta \cdot \sin\phi \cdot \sin(45 + \alpha)\right| \quad \ldots\ldots\ldots \quad 3.21$$

$t_3 = \cos\theta \cdot \cos(45 - \alpha) + \sin\theta \cdot \sin\phi \cdot \sin(45 - \alpha)$

with respect to the transverse direction, at right angles to the rolling direction.

Assuming that domains will only form along the six edges of the cubic structure corresponding to the <001> or easy direction, then let the volume fractions of such domains within the grain be:

ν_1 parallel to $[001]$, $\bar{\nu}_1$ parallel to $[00\bar{1}]$
ν_2 parallel to $[010]$, $\bar{\nu}_2$ parallel to $[0\bar{1}0]$
ν_3 parallel to $[100]$, $\bar{\nu}_3$ parallel to $[\bar{1}00]$ 3.22

when the grain is in a demagnetised state such that the net induction is zero;

and ν^1_1 parallel to $[001]$, $\bar{\nu}^1_1$ parallel to $[00\bar{1}]$
ν^1_2 parallel to $[010]$, $\bar{\nu}^1_2$ parallel to $[0\bar{1}0]$
ν^1_3 parallel to $[100]$, $\bar{\nu}^1_3$ parallel to $[\bar{1}00]$ 3.23

when the grain is magnetised to some net induction, Bg, measured in the plane of the sheet parallel to the applied field, which is taken as being parallel to the rolling direction. The $[001]$ direction is assumed to be nearest to the sheet rolling direction.

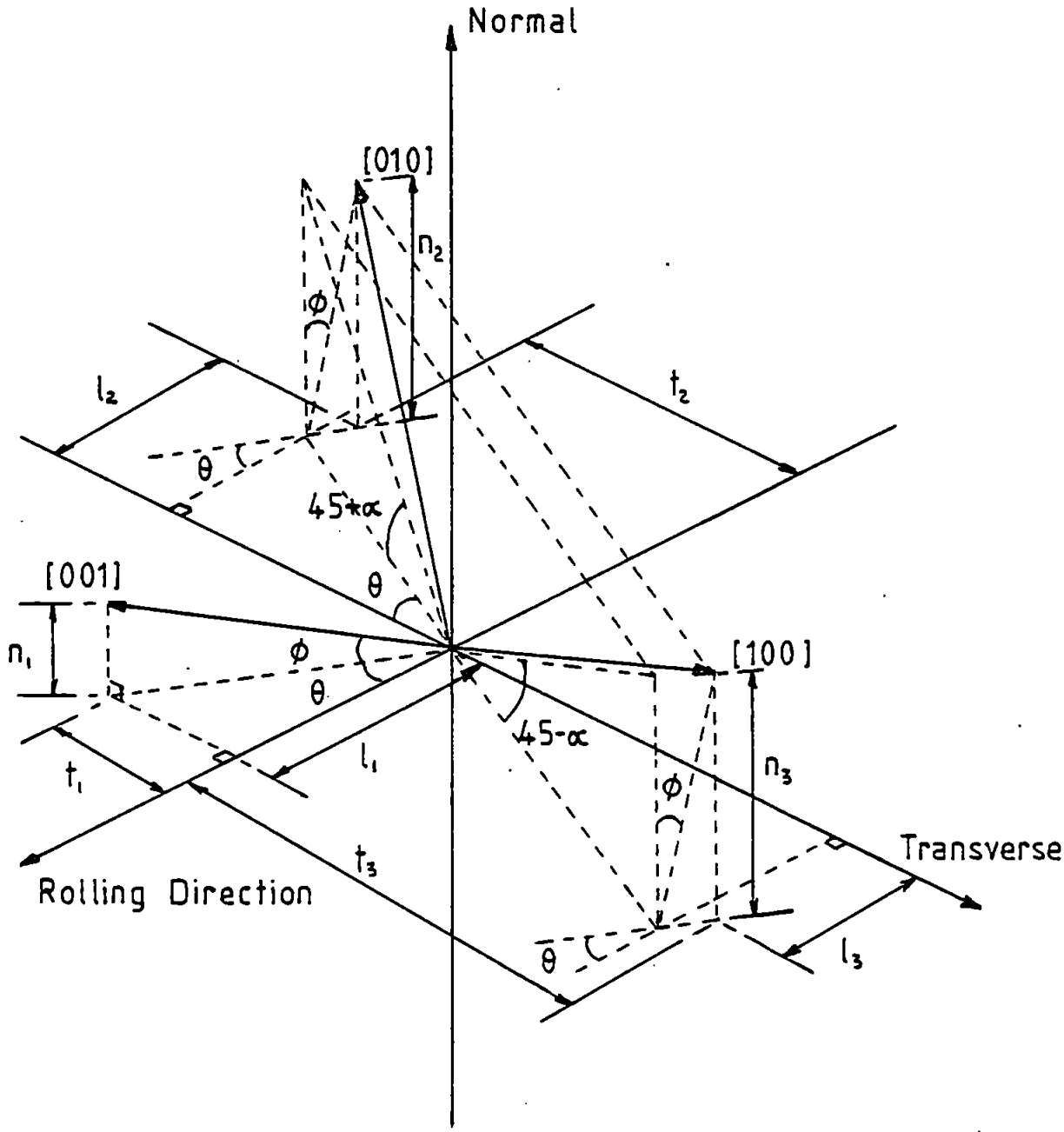

FIG. 3.5. Direction Cosines for a Mis-orientated Grain.

In addition, since 'ν' represents a volume expressed as a fraction of the total volume of the grain, then

$$\sum_{i=1,2,3} (\nu_i + \bar{\nu}_i) = 1 \quad \text{and} \quad \sum_{i=1,2,3} (\nu^1{}_i + \bar{\nu}^1{}_i) = 1$$

..... 3.24

Domains existing in the $[\bar{0}0\bar{1}]$ or $[00\bar{1}]$ directions will be referred to as 'parallel' or 'anti-parallel' main domains, all others being referred to as 'transverse' domains or supplementary structure.

If the only restraint governing domain behaviour during magnetisation is based on the principle that, for a material with large cubic anisotropy K_1, domains will arrange themselves among the six <001> easy directions of magnetisation in such a way that the net induction will always be parallel to the applied field, then there will be no net induction normal to the sheet plane or transverse to the rolling direction. This fundamental principle is quoted by Shilling and Houze (5) from the works of Néel, and Becker and Doring.

Thus for the rolling direction:

$$Bg = (\nu^1{}_1 - \bar{\nu}^1{}_1) M_s \ell_1 - (\nu^1{}_2 - \bar{\nu}^1{}_2) M_s \ell_2 + (\nu^1{}_3 - \bar{\nu}^1{}_3) M_s \ell_3$$

..... 3.25

And, for the normal to the sheet plane:

$$0 = (\nu^1{}_1 - \bar{\nu}^1{}_1) M_s n_1 + (\nu^1{}_2 - \bar{\nu}^1{}_2) M_s n_2 + (\nu^1{}_3 - \bar{\nu}^1{}_3) M_s n_3$$

..... 3.26

And, for the transverse direction:

$$0 = (\nu^1{}_1 - \bar{\nu}^1{}_1) M_s t_1 + (\nu^1{}_2 - \bar{\nu}^1{}_2) M_s t_2 - (\nu^1{}_3 - \bar{\nu}^1{}_3) M_s t_3$$

..... 3.27

M_s is the domain saturation magnetisation. The negative signs arise in order to be consistant with the misorientation angles shown in Fig. 3.5.

Expressing equation 3.25, 3.26 and 3.27 in matrix notation, and applying Kramers rule to obtain solutions for the net volume fractions parallel to the $[\bar{0}0\bar{1}]$, $[\bar{0}1\bar{0}]$ and $[\bar{1}0\bar{0}]$ direction, then

$$\begin{bmatrix} \nu^1_1 - \bar{\nu}^1_1 \\ \nu^1_2 - \bar{\nu}^1_2 \\ \nu^1_3 - \bar{\nu}^1_3 \end{bmatrix} = \frac{Bg}{M_s} \begin{bmatrix} \ell_1 & -\ell_2 & \ell_3 \\ n_1 & n_2 & n_3 \\ t_1 & t_2 & -t_3 \end{bmatrix}^{-1} \begin{bmatrix} 1 \\ 0 \\ 0 \end{bmatrix}$$

whereby
$$(\nu^1_1 - \bar{\nu}^1_1) = \frac{Bg}{M_s} \left(\frac{-n_2 t_3 - n_3 t_2}{D} \right)$$

$$(\nu^1_2 - \bar{\nu}^1_2) = -\frac{Bg}{M_s} \left(\frac{-n_1 t_3 - n_3 t_1}{D} \right)$$

$$(\nu^1_3 - \bar{\nu}^1_3) = \frac{Bg}{M_s} \left(\frac{n_1 t_2 - n_2 t_1}{D} \right)$$

where $D = \ell_1 (- n_2t_3 - n_3t_2) + \ell_2 (- n_1t_3 - n_3t_1) + \ell_3 (n_1t_2 - n_2t_1)$

Substituting for the relevant values of the direction cosines then

$$- n_2t_3 - n_3t_2 = -\ell_1, \qquad - n_1t_3 - n_3t_1 = -\ell_2$$

$$n_1t_2 - n_2t_1 = -\ell_3 \qquad D = - \ell^2_1 - \ell^2_2 - \ell^2_3 = -1$$

Therefore $$(\nu^1_1 - \bar{\nu}^1_1) = \left(\frac{Bg}{M_s}\right) \ell_1$$

$$-(\nu^1_2 - \bar{\nu}^1_2) = \left(\frac{Bg}{M_s}\right) \ell_2$$

$$(\nu^1_3 - \bar{\nu}^1_3) = \left(\frac{Bg}{M_s}\right) \ell_3 \qquad \ldots\ldots\ldots\ldots\ldots\ldots \quad 3.28$$

The negative sign arising for $(\nu^1_2 - \bar{\nu}^1_2)$ suggests that $\bar{\nu}^1_2$ is greater than ν^1_2 such that the net volume fraction involved should be orientated parallel to the $[\bar{0}1\bar{0}]$ direction. By inspection of Fig. 3.5 this is seen to be correct in order that the fundamental principle governing domain configuration shall hold.

Equations 3.28 are valid for grains exhibiting yaw only ($\phi = \alpha = 0$) with θ taken in the direction shown in Fig. 3.5 provided that $\nu^1_1 > \bar{\nu}^1_1$, $\bar{\nu}^1_2 > \nu^1_2$ and $\nu^1_3 > \bar{\nu}^1_3$. Similarly they will be valid for grains exhibiting pitch only ($\theta = \alpha = 0$) with ϕ taken in the direction shown in Fig. 3.5, provided that in this case $\bar{\nu}^1_3 > \nu^1_3$. For angles of θ, ϕ in any other quadrant, the direction cosines of equations 1, 2 and 3 will be modified accordingly and equations 3.28 will still be obtained in the form shown.

If a constraint is now applied to the domain structure such that only those directions nearest to the applied field can be occupied, then $\bar{\nu}^1_1 = \nu^1_2 = \bar{\nu}^1_3 = 0$. This state is proposed to exist at the knee of the magnetisation curve (25). Hence, from equation 3.28 and 3.24

$$\nu^1_1 + \bar{\nu}^1_2 + \nu^1_3 = \frac{B_n}{M_s} \cdot (\ell_1 + \ell_2 + \ell_3)$$

and

$$\nu^1_1 + \bar{\nu}^1_2 + \nu^1_3 = 1$$

where Bn is the net induction at the knee of the B-H curve. Therefore,

$$\frac{Bn}{M_s} = \frac{1}{\ell_1 + \ell_2 + \ell_3} \qquad \ldots\ldots\ldots\ldots\ldots\ldots\ldots\ldots 3.29$$

This relationship has also been shown to hold (2) at the remanence point when Bg will become the retentivity Br, and the resulting relationship is known as Kaya's Law.

In addition for this state

$$\left.\nu_i^1\right|_{i=1,2,3} = \frac{\ell_i}{\ell_1 + \ell_2 + \ell_3}, \qquad \sum_{i=1,2,3}\left(\nu_i^1\right) = 1 \qquad \ldots\ldots\ldots\ldots\ldots\ldots\ldots\ldots 3.30$$

For any intermediate induction, Bg, between the demagnetised state and the knee of the B-H curve then equations 3.28 apply and the net induction in the grain will depend on the degree of misorientation of the grain and the relative volumes of main domains and supplementary structure.

Shilling and Houze (5) have shown that Bn will depend on the larger of the two angles θ or ϕ so that a measurement of Bn will only indicate the general degree of misorientation. Observation of the domain surface closure structure will reveal which of the two angles is dominant.

Equations 3.28 may also be used to determine the change in magnetostriction in a misorientated grain when the induction varies, provided that it is possible to describe the domain configuration at each level of induction. Then, the net strain measured along the rolling direction in the grain can be obtained from the algebraic sum of the strains due to domains existing along each of the six easy directions, weighted according to the volumes involved.

The strains due to domains along each of the easy axes may be obtained from the fundamental relationship (2, 5):-

$$\lambda_s = \frac{3}{2} \lambda_{100} \cdot \sum_{i=1,2,3} (\ell_i^2 m_i^2 - \frac{1}{3}) + 3 \lambda_{111} \cdot \sum_{i \neq j} \ell_i \ell_j m_i n_j$$

..... 3.31

For domains along $[00\bar{1}]$ and $[00\bar{1}]$, $m_1 = 1$, $m_2 = m_3 = 0$, and so

$$\lambda_{s_1} = \frac{3}{2} \lambda_{100} (\ell_1^2 - \frac{1}{3})$$

Similarly, for domains parallel to $[0\bar{1}0]$ and $[0\bar{1}0]$, or $[\bar{1}00]$ and $[\bar{1}00]$,

$$\lambda_{s_2} = \frac{3}{2} \lambda_{100} (\ell_2^2 - \frac{1}{3}), \text{ or } \lambda_{s3} = \frac{3}{2} \lambda_{100} (\ell^2_3 - \frac{1}{3})$$

Thus for the volume fractions stated in equation 3.22 and 3.23, the net change is strain between the demagnetised state and some induction Bg will be given by

$$\lambda_{net} = \frac{3}{2} \lambda_{100} \cdot \sum_{i=1,2,3} \left[(\nu_i^1 + \bar{\nu}_i^1) - (\nu_i + \bar{\nu}_i) \right] (\ell_i^2 - \frac{1}{3})$$

..... 3.32

and where Bg will be defined by equation 3.28 such that

$$Bg = \left(\frac{M_s}{\ell_1 + \ell_2 + \ell_3} \right) \cdot \sum_{i=1,2,3} (\nu_i^1 - \bar{\nu}_i^1)$$

..... 3.33

But from equation 3.24

$$(\nu_1 + \bar{\nu}_1) = 1 - (\nu_2 + \bar{\nu}_2 + \nu_3 + \bar{\nu}_3)$$

and

$$(\nu_1^1 + \bar{\nu}_1^1) = 1 - (\nu_2^1 + \bar{\nu}_2^1 + \nu_3^1 + \bar{\nu}_3^1)$$

Therefore, equation 3.32 simplifies to

$$\lambda_{net} = \frac{3}{2} \lambda_{100} \cdot \sum_{i=2,3} \left[(\nu_i^1 + \bar{\nu}_i^1) - (\nu_i + \bar{\nu}_i) \right] (\ell_i^2 - \ell_1^2) \quad \ldots\ldots\ldots\ldots\ldots\ldots\ldots\ldots 3.34$$

It is now necessary to determine the volume fractions (ν). This may easily be done for certain simple cases exhibiting well defined domain structure. Thus in the demagnetised state it may be assumed that ν_2, $\bar{\nu}_2$, ν_3 and $\bar{\nu}_3$ are all zero, corresponding to a grain under stress-free conditions having an angle of yaw (θ) only, when equal volumes of parallel and anti-parallel main domain would exist; or a grain to which sufficient tensile stress has been applied such that all supplementary structure has been removed.

After magnetisation to some induction Bg the supplementary structure will reform in both cases in order to keep the net induction in the grain parallel to the applied field (along the rolling direction). Then, equations 3.28 apply such that:

$$\bar{\nu}_2^1 = \frac{Bg}{M_s} \cdot \ell_2 \quad \text{and} \quad \nu_3^1 = \frac{Bg}{M_s} \cdot \ell_3$$

for which it is assumed that $\nu_2^1 = \bar{\nu}_3^1 = 0$ and that domain formation corresponding to $\bar{\nu}_2^1$ and ν_3^1 is sufficient to satisfy the fundamental principle of domain configuration.

Substituting the above conditions into equation 3.34, the net strain will be given by

$$\lambda_{net} = \frac{3}{2} \lambda_{100} \cdot \frac{Bg}{M_s} \left| \ell_2 (\ell_2^2 - \ell_1^2) + \ell_3 (\ell_3^2 - \ell_1^2) \right| \quad \ldots\ldots\ldots \quad 3.35$$

For the case when $\phi = \alpha = 0$, that is, a grain exhibiting yaw only, then

$$\ell_1 = \cos\theta, \quad \ell_2 = \ell_3 = \frac{\sqrt{2}}{2} \sin\theta$$

Thus

$$\lambda_{net} = \frac{3}{2} \lambda_{100} \frac{Bg}{M_s} \left| \sqrt{2} \sin\theta \left(\tfrac{1}{2} \sin^2\theta - \cos^2\theta\right) \right|$$

or

$$\lambda_{net} = \frac{9}{4} \lambda_{100} \frac{Bg}{M_s} \sqrt{2} \sin\theta \left(\tfrac{1}{3} - \cos^2\theta\right) \quad \ldots\ldots\ldots\ldots\ldots \quad 3.36$$

Hence for $\cos^2\theta > \frac{1}{3}$, corresponding to $\theta < \sim 55^\circ$, λ_{net} will be negative.

A similar expression may be obtained in terms of dip angle ϕ for a grain in which $\theta = \alpha = 0$. Both these expressions are identical to those derived by Simmons and Thompson (21), and Shilling and Houze (5), who considered the specific cases only in isolation from the general conditions.

Hence in the unstressed condition λ will be positive, negative or even zero depending on the relative values of the misorientation angles. For small values of θ or ϕ, which will be usual for well orientated $S_i - F_e$, λ will be negative due to reformation of supplementary structure during magnetisation in order to keep the net induction parallel to the applied field, and thus minimise the magnetostatic energy.

The expressions derived above have been shown to be in good agreement with experimentally measured values (5, 20), and recent work by Allia et.al. (26) has produced a theoretical model to account quantitatively for negative strains as a function of both induction and applied tensile stress, which confirm the general observations of the proceeding discussion.

3.34 Magnetostriction Harmonics

Under the application of an external field which produces a cyclically varying magnetisation of the material, domain vectors will re-orientate into the easy directions nearest to the applied field, firstly in one direction and then in the reverse direction, corresponding to alternate half cycles of magnetisation.

The material will be strained similarly for both half cycles and it would be expected to observe a dynamic magnetostriction of fundamental frequency equal to twice that of the excitation.

Even if the induction is sinusoidal of a single frequency the dynamic strain will not necessarily be so since this will be determined by the λ - B relationship.

It has been verified (27) that the localised flux waveform within the bulk of the material does, however, contain harmonics and other workers have shown that this factor is predominant in the increase of losses due to large circulating harmonic fluxes, (28, 29, 30). This is particularly so in completed transformers and when the effects of stress are considered.

Holt (31) has reported a wide range of stress sensitivities for magnetostriction harmonics but was not able to conclude with any satisfactory explanations.

Ruhlmann (32) has derived simple relationships to demonstrate the increase in harmonic content of transformer noise due to localised flux waveform distortion, and has demonstrated the variation of harmonic amplitudes with changes in induction. In particular, evidence for maxima and minima in the harmonics was produced where, for example, the second harmonic of magnetostriction decreased with increasing induction.

This latter phenomena has also been observed in the sound spectra of power transformers when the excitation was varied (33).

An analysis now follows which attempts to relate the level of magnetostriction harmonics to the level of harmonics in the induction within a grain of the material.

Magnetostriction Harmonic Analysis

In the previous discussion on negative magnetostriction (Section 3.3.3), a direct, linear relationship was deduced between λ and B. This was for the specific case of a misorientated grain, with no supplementary domain structure in the demagnetised state (equation 3.36).

If, as will be usual, the above specific conditions are not met, then some volume of supplementary structure will exist in the demagnetised state due to grain misorientation ($\phi > 0$) or to the presence of external stress, or both.

This condition needs to be analysed to obtain the λ-B relationship, and certain simplyfying assumptions may be made by considering the cases when $\phi = \alpha = 0$, or $\theta = \alpha = 0$, corresponding to grains having yaw only or pitch only.

For either case

$$\ell_1 = \cos \beta, \ \ell_2 = \ell_3 = \frac{1}{\sqrt{2}} \sin \beta$$

where β represents either θ or ϕ respectively. Equation 3.34 then becomes

$$\lambda_{net} = \frac{3}{2} \cdot \lambda_{100} \left(\tfrac{1}{2} \sin^2 \beta - \cos^2 \beta\right) \sum_{i=2,3} \left[(\nu_i^1 + \bar{\nu}_i^1) - (\nu_i + \bar{\nu}_i) \right]$$

or

$$\lambda_{net} = \frac{9}{4} \lambda_{100} \left(\frac{1}{3} - \cos^2 \beta\right) \sum_{i=2,3} \left[(\nu_i^1 + \bar{\nu}_i^1) - (\nu_i + \bar{\nu}_i) \right] \quad \ldots\ldots\ldots\ldots\ldots\ldots\ldots\ldots 3.37$$

Equation 3.33 for Bg simplifies to

$$Bg = \left(\frac{M_s}{\cos \beta + \sqrt{2} \sin \beta} \right) \cdot \sum_{i=1,2,3} (\nu_i^1 - \bar{\nu}_i^1) \quad \ldots\ldots\ldots\ldots\ldots\ldots 3.38$$

The resulting λ - B relationship for the misorientated grain can now be obtained from equation 3.37 and 3.38 provided that the various values of ν can be enumerated.

From equation 3.24

$$\nu_2 + \bar{\nu}_2 + \nu_3 + \bar{\nu}_3 = 1 - (\nu_1 + \bar{\nu}_1)$$

and

$$\nu_2^1 + \bar{\nu}_2^1 + \nu_3^1 + \bar{\nu}_3^1 = 1 - (\nu_1^1 + \bar{\nu}_1^1)$$

Therefore, equation 3.37 further simplifies to

$$\lambda_{net} = \frac{9}{4} \cdot \lambda_{100} \left(\frac{1}{3} - \cos^2 \beta\right) \left[(\nu_1 + \bar{\nu}_1) - (\nu_1^1 + \bar{\nu}_1^1)\right] \quad \ldots\ldots\ldots\ldots\ldots\ldots\ldots\ldots \quad 3.39$$

Simmons and Thompson (21) have shown, for a grain exhibiting yaw only and having a domain structure corresponding to a well defined Stress Pattern I (as postulated by Corner and Mason (14) due to an external compressive stress along the rolling direction) that a value for $(\nu_1 + \bar{\nu}_1)$ - the total volume fraction of domain along $[\bar{0}01]$ and $[00\bar{1}]$ - is given by

$$\nu_1 + \bar{\nu}_1 = \frac{d\sqrt{2}}{4t} \quad \ldots\ldots\ldots\ldots\ldots\ldots\ldots\ldots\ldots\ldots\ldots\ldots \quad 3.40$$

where d is the average spacing between the $[\bar{0}01]$ direction surface closure domains, and t is the sheet thickness. This structure has been shown in Fig. 3.4 (d).

A value for $(\nu_1^1 + \bar{\nu}_1^1)$ was also found by these authors on the assumptions that (1) the volume fractions ν_3^1 and $\bar{\nu}_3^1$ are equal in the magnetised state and that $\nu_2^1 = \bar{\nu}_2^1 = 0$, so that there will be no net component of flux normal to the sheet plane; (2) that all anti-parallel main domains $(\bar{\nu}_1^1)$ have been eliminated.

Thus from equation 3.25

$$Bg = \nu_1^1 M_s \ell_1 \qquad \text{or} \qquad \nu_1^1 = \frac{Bg}{M_s \cos \beta}$$

$$\ldots\ldots\ldots\ldots\ldots\ldots\ldots\ldots\ldots\ldots\ldots\ldots \quad 3.41$$

Substituting the above conditions into equation 3.39 gives, for the net change in strain during magnetisation to Bg of a grain exhibiting Stress Pattern I in the demagnetised state:

$$\lambda_{net} = \frac{9}{4} \lambda_{100} \left(\frac{1}{3} - \cos^2 \beta\right) \left[\frac{d\sqrt{2}}{t} - \frac{Bg}{M_s \cos \beta} \right] \quad \ldots\ldots\ldots\ldots\ldots\ldots\ldots\ldots 3.42$$

This is identical to the equation derived by Simmons and Thompson from the particular instance of a grain exhibiting an angle of yaw (θ) only.

From equation 3.36 and 3.42, if the time-variation of the induction is known then the time variation of λ can be deduced, since both equations show a direct relationship between λ and B. By expressing the magnitude of any harmonics as a percentage of the fundamental, a comparison of these harmonics may be made for changes in the induction without the need to know the constants in the equations for a given grain.

A generalised solution would be arduous if B is taken to contain a series of 'n' harmonics. However, an indication of the effects produced may be assessed by assuming that B consists of a fundamental and a 3rd harmonic only.

This is not unreasonable since, assuming that the excitation voltage is sinusoidal of a single frequency (ω), B cannot contain even harmonics since the B-H relationship is an odd function (34). Furthermore, the 3rd harmonic is experimentally known to be predominant (29, 30).

Not only must the magnitude (p) of the harmonic be considered but also its phasor relationship (γ) to the fundamental. Since the two phasors are rotating at different angular velocities, it is necessary to define γ, and this has been done with reference to Fig. 3.6 (a) such that γ represents the angle between the zero crossings of the phasors when they are both going positive.

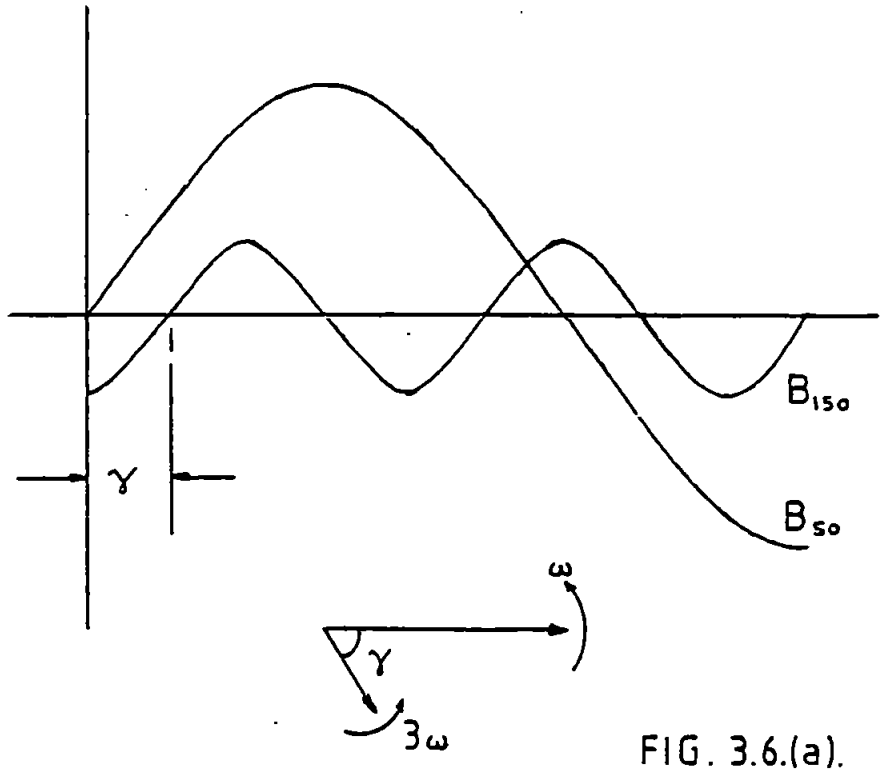

FIG. 3.6.(a).

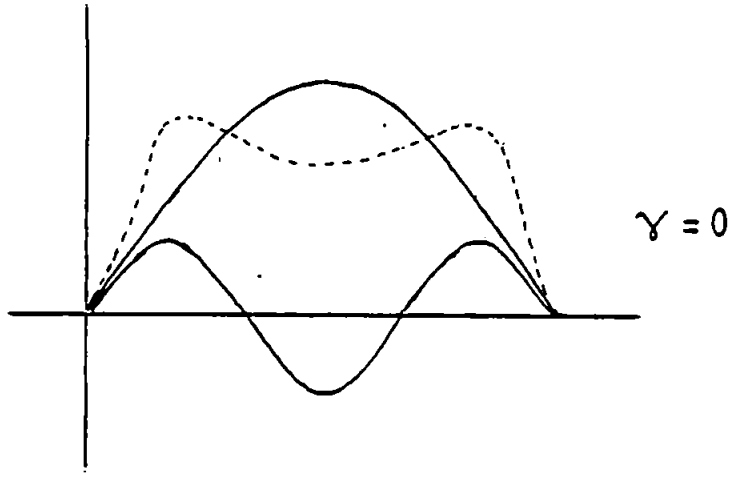

FIG. 3.6.(b).

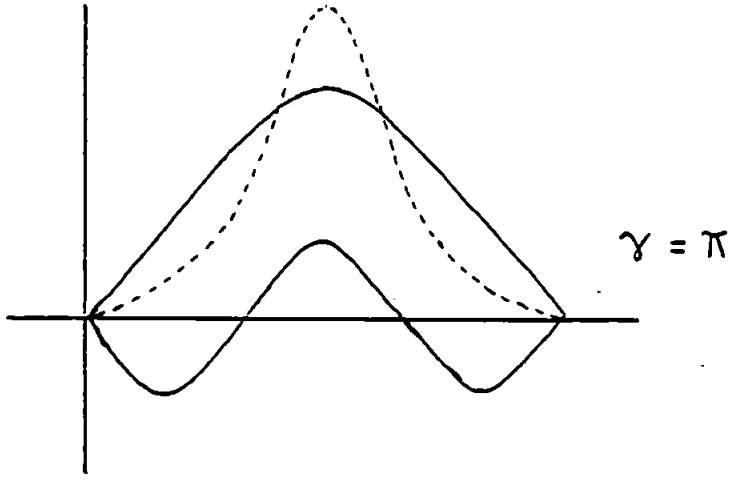

FIG. 3.6. Defining the Phasor Relationships of the Induction 1st & 3rd Harmonics.

The magnitude of γ will be related to the period of the third harmonic, as shown in Fig. 3.6 (b).

In addition, the effects of hysteresis must be taken into account whereby the magnetostriction appears to lag the induction, as shown in the typical "butterfly" loop of Fig. 3.7 (a) taken during the course of this investigation. The extent to which any hysteresis is present may be approximated by the angle α, representing the lag, as shown in Fig. 3.7 (b).

Therefore the induction may be expressed as a function of time, with respect to the magnetostriction, by the equation

$$B(t) = \hat{B} \left[\sin(\omega t + \alpha) + p \sin (3\omega t + \alpha \pm \gamma)\right] \quad \ldots\ldots\ldots\ldots 3.43$$

Now equation 3.36 or 3.42 may be written in the form

$$\lambda(t) = k_1 + k_2 \left|B(t)\right| \quad \ldots\ldots\ldots\ldots\ldots\ldots 3.44$$

where k_1, k_2 represent the constants contained in those equations. The magnitude of B is considered since the strain will be unidirectional for each half cycle of magnetisation.

Hence, from equation 3.43 and 3.44

$$\lambda(t) = k_1 + k_2 \hat{B} \left|\sin(\omega t + \alpha) + p \sin (3\omega t + \alpha \pm \gamma)\right| \quad \ldots\ldots 3.45$$

Equation 3.45 may be written in terms of the Fourier series:

$$\lambda(t) = \frac{a_o}{2} + \sum_{n=1}^{\infty} (a_n \cos 2n\omega t + b_n \sin 2n\omega t) \quad \ldots\ldots\ldots 3.46$$

where the coefficients are obtained (34) from the standard Fourier expressions:

$$\left.\begin{aligned} an &= \frac{2\omega}{\pi} \int_0^{\pi/\omega} \lambda(t).\cos 2n\omega t.dt. \\ bn &= \frac{2\omega}{\pi} \int_0^{\pi/\omega} \lambda(t).\sin 2n\omega t.dt. \end{aligned}\right\} \quad \ldots\ldots\ldots\ldots\ldots 3.47$$

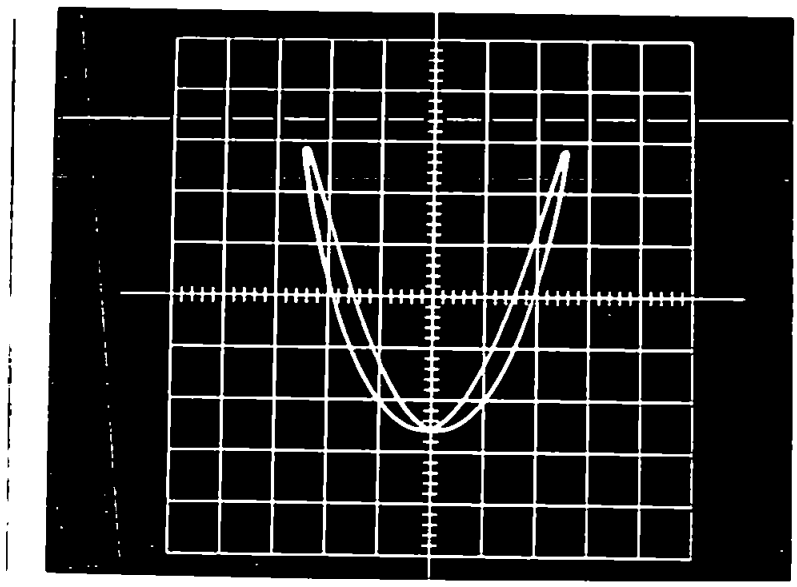

FIG. 3.7.(a). Typical Magnetostriction "Butterfly" Loop.

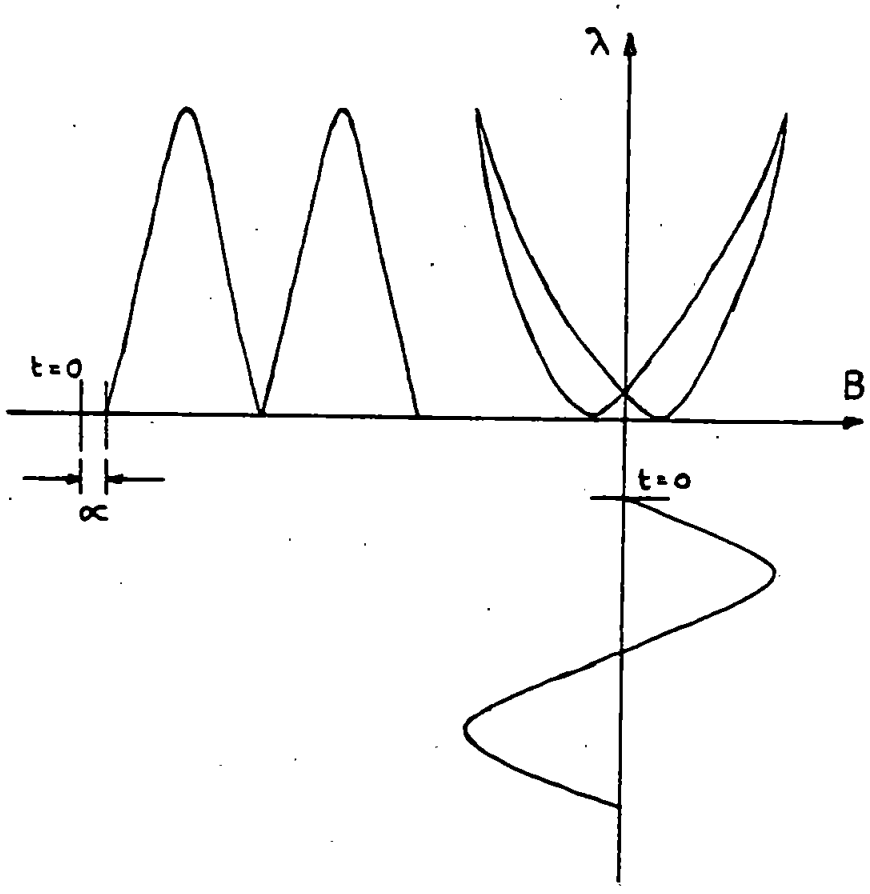

FIG. 3.7.(b). Demonstrating the Angle of Lag Representing Magnetostriction Hysteresis.

By expanding equation 3.45, substituting into equations 3.47 and solving,

$$a_n = \frac{4k_2 \hat{B}}{\pi} \cdot \left[\frac{\cos \alpha}{1-4n^2} + \frac{3p \cos (\alpha \pm \gamma)}{9-4n^2} \right]$$

$$b_n = \frac{4k_2 \hat{B}}{\pi} \cdot \left[\frac{2n \sin \alpha}{4n^2 - 1} + \frac{2np \sin (\alpha \pm \gamma)}{4n^2 - 9} \right]$$

Taking values for n of 1, 2 and 3, corresponding to the first three harmonics of magnetostriction λ_1, λ_2 and λ_3, then

$$\lambda_1 \propto \left[\frac{3p}{5} \cos (\alpha \pm \gamma) - \frac{1}{3} \cos \alpha \right] \cos 2\omega t + \left[\frac{2}{3} \sin \alpha - \frac{2p}{5} \sin (\alpha \pm \gamma) \right] \sin 2\omega t$$

$$\lambda_2 \propto - \left[\frac{3p}{7} \cos (\alpha \pm \gamma) + \frac{1}{15} \cos \alpha \right] \cos 4\omega t + \left[\frac{4}{15} \sin \alpha + \frac{4p}{7} \sin (\alpha \pm \gamma) \right] \sin 4\omega t$$

$$\lambda_3 \propto - \left[\frac{3p}{27} \cos (\alpha \pm \gamma) + \frac{1}{35} \cos \alpha \right] \cos 6\omega t + \left[\frac{6}{35} \sin \alpha + \frac{6p}{27} \sin (\alpha \pm \gamma) \right] \sin 6\omega t$$

By allowing α, γ and p to take selected values, and by expressing the second and third harmonics as a percentage of the fundamental so that the constants may be ignored, then the relative dependance of the harmonics upon α, γ and p may be examined.

The levels of p chosen are typical of the experimentally measured values in the T-joints of power transformers (30). The values of α were selected by drawing "butterfly" loops corresponding in shape to those experimentally observed, and measuring the angle of lag (see Fig. 3.7 (b)). Values of γ were taken arbitrarily in the range 0 to $\pm\pi$.

Solution of the equations was made on a Z80 micro-computer, and the programme used is shown in Fig. 3.8. A set of solutions for the case when p = 10% is shown in Fig. 3.9 in which J represents α over the range 0^{o}, 5^{o}, 10^{o} and 15^{o}, and R represents γ over the range $-\pi$ to $+\pi$.

The results are shown in the graphs of Figs. 3.10 and 3.11, for the cases when $\alpha = 0^{o}$ and 10^{o}, for the 2nd and 3rd percentage magnetostriction harmonics.

The following observations may be made from these results:-

(1) there is a dramatic increase in both the 2nd and 3rd harmonics of magnetostriction for increases in 3rd harmonic of induction;

(2) there may be large variations in both higher harmonics of magnetostriction for changes in the phase relationships between the 1st and 3rd harmonics of induction.

3.4 Summary

The proceeding theoretical discussion indicates the dependance of magnetostriction harmonics upon stress and induction levels within the material, and also on the distortion of the flux waveshape, particularly with regard to the phasor relationships of the flux harmonics.

In order to test these relationships it is necessary to build an Apparatus with which the individual magnetostriction harmonics within a grain may be measured, whilst varying the levels of stress and induction, and also measuring the amount of flux waveshape distortion present.

Such an Apparatus will now be described in the following Chapter, and the results obtained with it will be described in Chapter 5.

```
10 REM THEORETICAL % MAGNETOSTRICTION HARMONICS
20 P=0
30 J=0
40 R=-3.142
50 FOR N=1TO3
60 A(N)=(COS(J)/(1-4*N↑2))+(3*P*COS(J+R)/(9-4*N↑2))
70 B(N)=(2*N*SIN(J)/(4*N↑2-1))+(2*N*P*SIN(J+R)/(4*N↑2-9))
80 NEXTN
90 K1=(A(1)↑2+B(1)↑2)↑0.5
100 K2=(A(2)↑2+B(2)↑2)↑0.5
110 K3=(A(3)↑2+B(3)↑2)↑0.5
120 PR(2)=INT((K2/K1)*100*100)/100
130 PR(3)=INT((K3/K1)*100*100)/100
140 PRINT "R="R, "J="J, "P="P, "PER2="PR(2), "PER3="PR(3)
150 R=INT((R+3.142/6)*1000)/1000
160 IFR<3.5 THENGOTO50
170 LPRINT:LPRINT
180 J=INT((J+(5/180)*3.142)*100000)/100000
190 IFJ<0.34THENGOTO40
200 LPRINT:LPRINT
210 P=INT((P+0.1)*10)/10
220 IFP<0.35THENGOTO30
230 FOR P=0.1TO0.3STEP0.1
240 NEXTP
250 END

>READY
```

FIG.3.8. Computer Programme for the solution of % Magnetostriction Harmonics.

R=-3.142	J= 0	P= .1	PER2= 6.05	PER3= 4.43
R=-2.619	J= 0	P= .1	PER2= 10.64	PER3= 5.68
R=-2.096	J= 0	P= .1	PER2= 18.34	PER3= 8.21
R=-1.573	J= 0	P= .1	PER2= 26.12	PER3= 10.77
R=-1.05	J= 0	P= .1	PER2= 33.06	PER3= 12.82
R=-.527	J= 0	P= .1	PER2= 38.13	PER3= 14.09
R=-4E-03	J= 0	P= .1	PER2= 40.06	PER3= 14.51
R= .519	J= 0	P= .1	PER2= 38.19	PER3= 14.1
R= 1.042	J= 0	P= .1	PER2= 33.15	PER3= 12.84
R= 1.565	J= 0	P= .1	PER2= 26.23	PER3= 10.8
R= 2.088	J= 0	P= .1	PER2= 18.46	PER3= 8.25
R= 2.611	J= 0	P= .1	PER2= 10.74	PER3= 5.72
R= 3.134	J= 0	P= .1	PER2= 6.05	PER3= 4.43
R=-3.142	J= .0872	P= .1	PER2= 7.54	PER3= 5.47
R=-2.619	J= .0872	P= .1	PER2= 8.38	PER3= 4.99
R=-2.096	J= .0872	P= .1	PER2= 15.15	PER3= 6.57
R=-1.573	J= .0872	P= .1	PER2= 22.77	PER3= 8.87
R=-1.05	J= .0872	P= .1	PER2= 30.16	PER3= 11.23
R=-.527	J= .0872	P= .1	PER2= 36.55	PER3= 13.51
R=-4E-03	J= .0872	P= .1	PER2= 40.56	PER3= 15.46
R= .519	J= .0872	P= .1	PER2= 40.68	PER3= 16.36
R= 1.042	J= .0872	P= .1	PER2= 36.8	PER3= 15.71
R= 1.565	J= .0872	P= .1	PER2= 30.2	PER3= 13.69
R= 2.088	J= .0872	P= .1	PER2= 22.3	PER3= 10.87
R= 2.611	J= .0872	P= .1	PER2= 14.2	PER3= 7.88
R= 3.134	J= .0872	P= .1	PER2= 7.6	PER3= 5.49
R=-3.142	J= .1744	P= .1	PER2= 10.65	PER3= 7.65
R=-2.619	J= .1744	P= .1	PER2= 8.53	PER3= 6.24
R=-2.096	J= .1744	P= .1	PER2= 13.5	PER3= 6.79
R=-1.573	J= .1744	P= .1	PER2= 20.82	PER3= 8.77
R=-1.05	J= .1744	P= .1	PER2= 28.68	PER3= 11.53
R=-.527	J= .1744	P= .1	PER2= 36.23	PER3= 14.75
R=-4E-03	J= .1744	P= .1	PER2= 41.86	PER3= 17.73
R= .519	J= .1744	P= .1	PER2= 43.47	PER3= 19.32
R= 1.042	J= .1744	P= .1	PER2= 40.43	PER3= 18.86
R= 1.565	J= .1744	P= .1	PER2= 34.04	PER3= 16.7
R= 2.088	J= .1744	P= .1	PER2= 26.06	PER3= 13.65
R= 2.611	J= .1744	P= .1	PER2= 17.83	PER3= 10.42
R= 3.134	J= .1744	P= .1	PER2= 10.72	PER3= 7.68
R=-3.142	J= .2616	P= .1	PER2= 13.96	PER3= 9.99
R=-2.619	J= .2616	P= .1	PER2= 10.69	PER3= 8.35
R=-2.096	J= .2616	P= .1	PER2= 13.81	PER3= 8.45
R=-1.573	J= .2616	P= .1	PER2= 20.58	PER3= 10.22
R=-1.05	J= .2616	P= .1	PER2= 28.69	PER3= 13.22
R=-.527	J= .2616	P= .1	PER2= 36.96	PER3= 16.91
R=-4E-03	J= .2616	P= .1	PER2= 43.51	PER3= 20.33
R= .519	J= .2616	P= .1	PER2= 45.99	PER3= 22.16
R= 1.042	J= .2616	P= .1	PER2= 43.5	PER3= 21.7
R= 1.565	J= .2616	P= .1	PER2= 37.3	PER3= 19.39
R= 2.088	J= .2616	P= .1	PER2= 29.33	PER3= 16.17
R= 2.611	J= .2616	P= .1	PER2= 21.13	PER3= 12.83
R= 3.134	J= .2616	P= .1	PER2= 14.04	PER3= 10.02

FIG. 3.9. Typical Results of the Computer Programme.

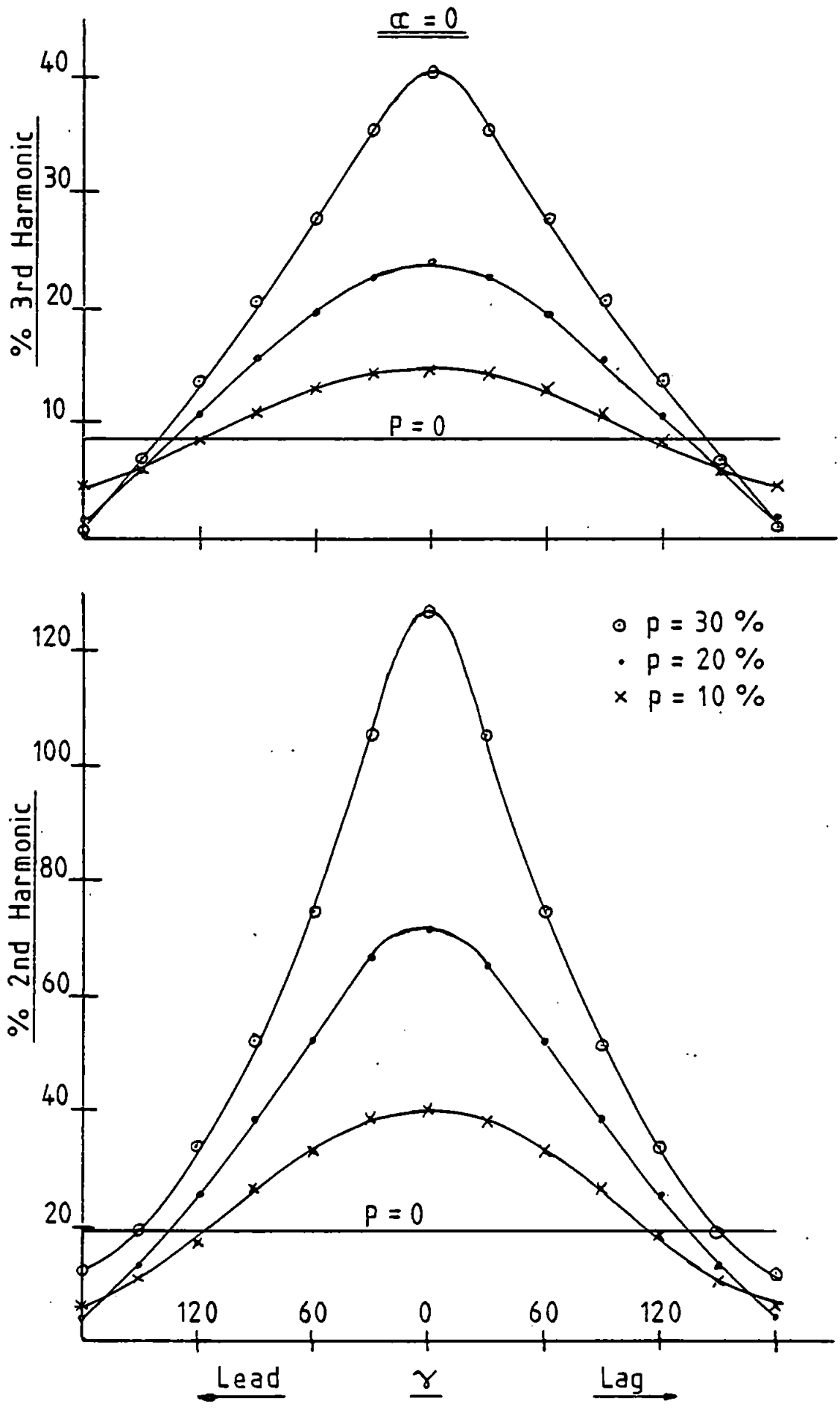

FIG. 3.10. Theoretical Variation in % Magnetostriction Harmonics due to Distorted Induction.

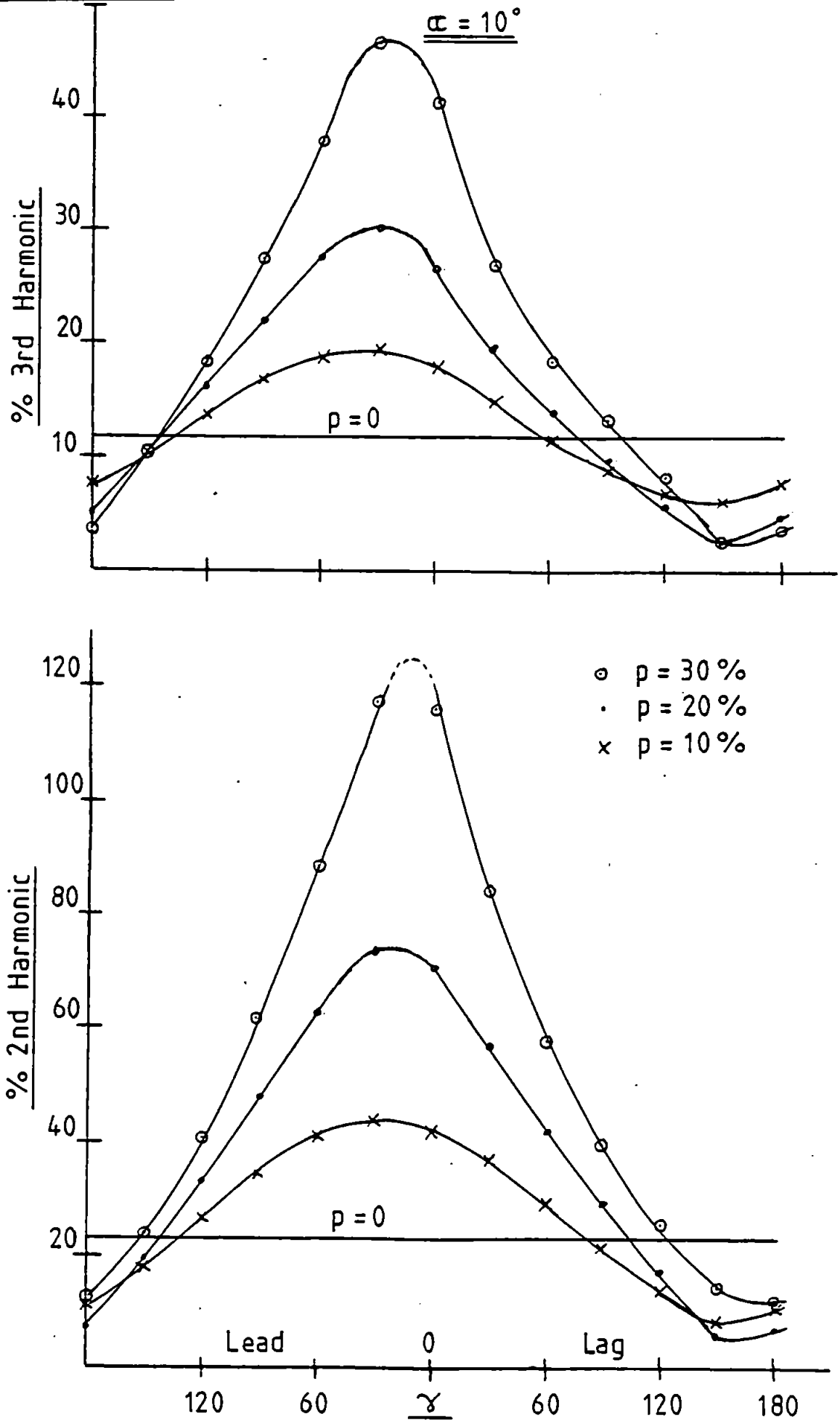

FIG. 3.11. Theoretical Variation in % Magnetostriction Harmonics due to Distorted Induction.

REFERENCES TO CHAPTER THREE

1. A.J. Leggett, Phys. Bull., Vol. 29, p.252, June 1978.

2. S.Chikazumi, 'Physics of Magnetism', Wiley, N.Y., 1964.

3. F. Brailsford, 'Physical Principles of Magnetism', Van Nostrand, London, 1966.

4. C. Heck, 'Magnetic Materials and their Applications', Butterworths, London, 1974.

5. J.W. Shilling, G.L. Houze, I.E.E.E. Trans.Magn. Vol Mag. 10, No. 2, June, 1974.

6. R. Carey, E.D. Isaac, 'Magnetic Domains and Techniques for their Observation', E.U.P., London, 1966.

7. W.S. Paxton, T.G. Nilan, J. Appl. Phys., Vol. 26,No.8, August, 1955.

8. M.R. Daniels, I.E.E. Conf.Pub., No.33, September 1967.

9. J.W. Shilling et al., I.E.E.E., Trans.Magn., Vol. Mag.14, No.3, May, 1978.

10. G.S. Radley, 'Magnetorestriction and Dynamic Elasticity in Magnetic Sheet Steel', Ph.D. Thesis, Liverpool Polytechnic, 1977.

11. L.J. Dijkstra, U.M. Martius, Rev. Mod. Phys, Vol. 25, No.1, January, 1953.

12. P.W. Neurath, Elec. Eng., November, 1954.

13. J.J. Gneiwek, J. Appl. Phys., Vol. 34, No.12, December, 1963.

14. W.D. Corner, J.J. Mason, Brit. J. Appl. Phys., Vol.15, 1964.

15. A.J. Moses, J. Matl., Sci., Vol. 9, 1974.

16. P.J. Banks, E. Rawlinson, Proc. I.E.E., Vol.114, No.10, October, 1967.

17. V.M. Bichard, A. Coombs, M.R. Daniels, I.E.E.E. Trans. Magn. Vol. Mag. 14, No.5, September, 1978.

18. C. Holt, J.A. Robey, I.E.E.E., Trans. Magn. Vol. Mag. 5, No. 3, September, 1969.

19. P.C. Joslin, A.J. Moses, J.E. Thompson, Proc. I.E.E., Vol.119, 1972.

20. P.J. Banks, I.E.E.E., Trans. Magn., Vol. Mag. 13, No.3, May, 1977.

21. G.H. Simmons, J.E. Thompson, Proc. I.E.E., Vol.118, No.9, September, 1971.

22. E.J. Langham, Brit. J. Appl. Phys., Vol. 14, 1963.

23. C.M. Brownsey, G.C. Maples, Proc. I.E.E., Vol.113, No.11, November, 1966.

24. C. Holt, J.A. Robey, Proc. I.E.E., Vol. 114, No.9, September, 1967.

25. K.H. Stewart, 'Ferromagnetic Domains', C.U.P., Cambridge, 1954.

26. P. Allia et al., I.E.E.E., Trans. Magn. Vol. Mag. 14, No. 5, September, 1978.

27. F. Brailsford, V.R. Mazza, Proc. I.E.E., Vol. 109, No.44, April, 1962.

28. A.J. Moses, B. Thomas, I.E.E.E. Trans. Magn., Vol. Mag. 9, No. 4, December, 1973.

29. M.A. Jones, A.J. Moses, I.E.E.E. Trans. Magn., Vol. Mag. 10, No. 2, June, 1974.

30. A. Basak, A.J. Moses, I.E.E.E. Trans. Magn., Vol. Mag. 14, No.5, September, 1978.

31. C. Holt, I.E.E. Conf. Pub., No.33, September, 1967,

32. R. Rhulmann, Electrotech. Z. (E.T.Z.)A, Vol. 85, July, 1964.

33. B. Berger, G. Blaylock, J.G. Charles, A.B. Dobie, Phil. Trans. A, Vol. 263, No. 1142, 1968.

34. F.F. Kuo, 'Network Analysis and Synthesis', Wiley, N.Y., 1964.

CHAPTER FOUR

THE EXPERIMENTAL DEVELOPMENT

4.1 Domain Observation

4.1.1. Introduction

One of the first experiments demonstrating the electro-magnetic nature of light was performed by Faraday, who noted that plane polarised light had its plane of polarisation rotated when transmitted through material magnetised along the direction of polarisation - the Faraday Effect.

A similar effect was observed by Kerr in 1876 for plane polarised light reflected from the polished surface of an electro-magnet pole piece. The reflected light is elliptically polarised, with the major axis of the ellipse rotated slightly with respect to the incident beam. This is the polar Kerr Effect; the longitudinal Kerr Effect was discovered four years later for the case when the magnetisation lay along the surface of a magnetised mirror.

Not until theoretical knowledge of domain behaviour and likely structures had been developed, and with the availability of better prepared materials, did the first direct observation of domains occur. Bitter (1) and Van Hamos and Thiessen (2) independantly suggested in 1931 that if a fine powder of magnetic material is sprinkled on the surface of a magnetised specimen then stray fields on the surface, particularly at domain boundaries and other discontinuities, will aggregate the particles, enabling those discontinuities to be observed.

First attempts by Bitter and Van Hamos used a fine powder (the Powder Technique) but it was soon found advantageous to use magnetic particles in true colloidal suspension. This technique was first satisfactorily employed by McKeehan and Elmore (3) in 1934 and has been refined over the years to enable high contrast patterns to be obtained, particularly when a polarising field is

applied normal to the surface (4). The colloid particles are attracted to domains having a normal component of magnetisation in the same sense as the applied field and represent an image of the domain surface. When domain magnetisation is wholly in the plane of the specimen only the domain walls will be made visible. Various recipes for colloids are given by Carey and Isaac (5).

The Colloid Technique has proved to be successful on a wide range of materials and surfaces, but is limited to static or quasi-static conditions of domain motion, and so will not be suitable for this investigation under dynamic conditions.

Alternative techniques for domain observation utilise the various adaptions of electron beam technology, or the use of field probes.

Transmission microscopy requires a material transparent to the electron beam - not the case in this investigation. Reflection microscopy requires extreme care in image interpretation and the apparatus is excessively complex and expensive - beyond the scope of this investigation. A third technique involves passing a high intensity electron beam at grazing incidence to the specimen surface; this Shadow Technique also requires careful image interpretation and elaborate equipment.

The Hall Effect field probe was extensively developed by Kostysheyn et. al. (6) in 1959 for domain mapping and the technique has recently been refined to produce domain boundary maps (7). However, due to its limited resolution, and the consequences of large stray fields in magnetised specimens producing spurious Hall voltages, its use on bulk specimens in any condition other than the demagnetised state reduces its use to plotting a static condition. The Permalloy Probe, first described by Kaczer (8) in 1955, is as limited as the Hall Probe, and both require sophisticated manipulating techniques.

The electro-magnetic, optical effects of Faraday and Kerr thus appear to be the only suitable alternatives for this investigation. The rotation experienced by the plane of polarisation of light is dependant on the direction of magnetisation, amongst other variables (9). In the case of two adjacent domains with anti-parallel magnetisation, rotations will occur in opposite directions, and if the reflected or transmitted beam is viewed through an analysing polariser the two domains will appear as adjacent light and dark patterns.

The Faraday Effect is obviously limited to naturally transparent materials or those which can be made thin enough to become transparent. It was first used by Fowler and Fryer (10) in 1956 on nickel-iron films, but is of no consideration for this investigation using bulk materials.

The Kerr Effect appears ideally suited for surface observation of underlying domain structures. The Polar Effect, first discovered, where the magnetisation is normal to the reflecting surface, has been used for the study of crystals by Williams, Foster and Wood (11), but its uses in ferromagnetic studies are limited mainly because polar magnetisation rarely occurs. The Transverse Effect, where the magnetisation is in the plane of the reflecting surface but also in the plane normal to the plane of incidence has rarely been used in domain studies. Although the contrast that can be obtained is very high, it is necessary to perfect a very precise and accurately phase adjusted light system (5).

The longitudinal Kerr Effect, when the magnetisation lies in the plane of incidence as well as the plane of the reflecting surface, was first used by Fowler and Fryer (12) in 1952 on silicon-iron crystals, and has since been extensively developed for domain observations in bulk ferromagnetic material. Due to the limitations of the other techniques discussed, and the relative ease with which the longitudinal Kerr Effect can be set up and operated for dynamic domain observations, this technique was chosen for use in this investigation.

4.1.2 Apparatus

The Optical System

The Longitudinal Kerr Effect system used in this investigation is shown diagrammatically in Fig. 4.1, and a photograph of the complete system is shown in Fig. 4.2.

The source (S) is a 'Strobex' Model 70 high intensity stroboscopic light powered from a 'Strobex' Model 99 power supply and triggering circuit. (The electronic circuits derived to supply the triggering circuit are discussed in the next section). This source is mounted at the centre of curvature of a concave mirror (M) producing an inverted, real image at the source. The intensified source is placed well within the focal plane of the first of two achromatic doublets (C_1) which produce a divergent beam of light from a magnified, virtual image. The second achromatic doublet (C_2) is then positioned at the focal point of C_1 producing a beam of near parallel light. This beam illuminates an adjustable iris (I) placed next to C_2 and the intensely illuminated hole of the iris becomes the source for the rest of the optical system. The iris is set at a diameter of 6 mm. The achromatic doublets are chosen to give minimum spherical aberration and good chromatic correction, as well as having low f-numbers and large apertures for maximum light transmittance (13).

Lens' L_1 and L_2 then focus the light spot onto the specimen surface. L_2 is chosen to have a large focal length so that the incident beam remains nearly parallel; thus when passed through the first polariser (P_1) a reasonably plane, polarised light beam is achieved. However, since the length of the incident beam was restricted to about 300 mm, and as it is necessary to focus the light spot at the specimen surface, the first focussing lens (L_1) is introduced. This lens is positioned so that the source lies within its focal plane, and a virtual, magnified image is produced effectively increasing the source distance for L_2.

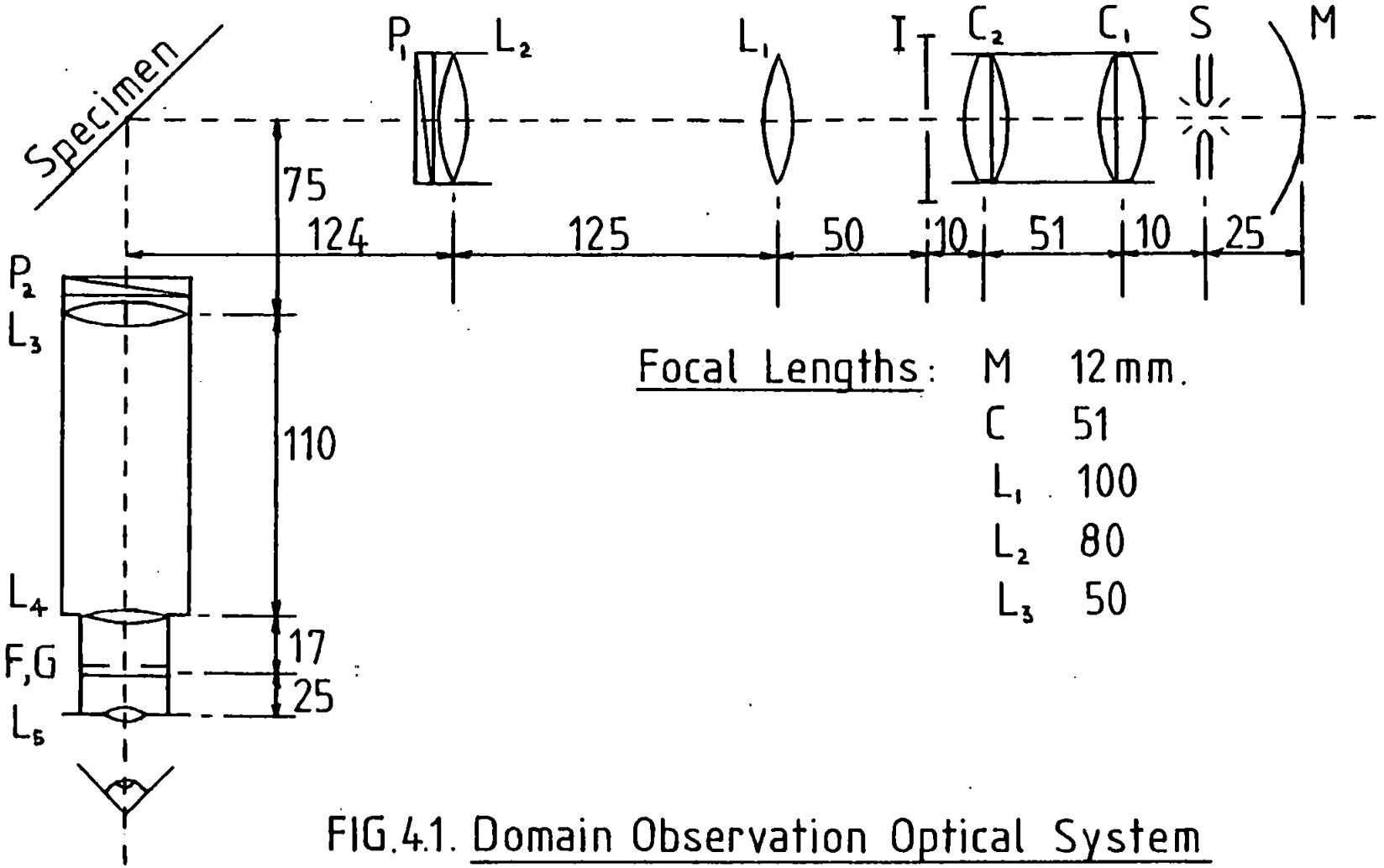

FIG.4.1. Domain Observation Optical System

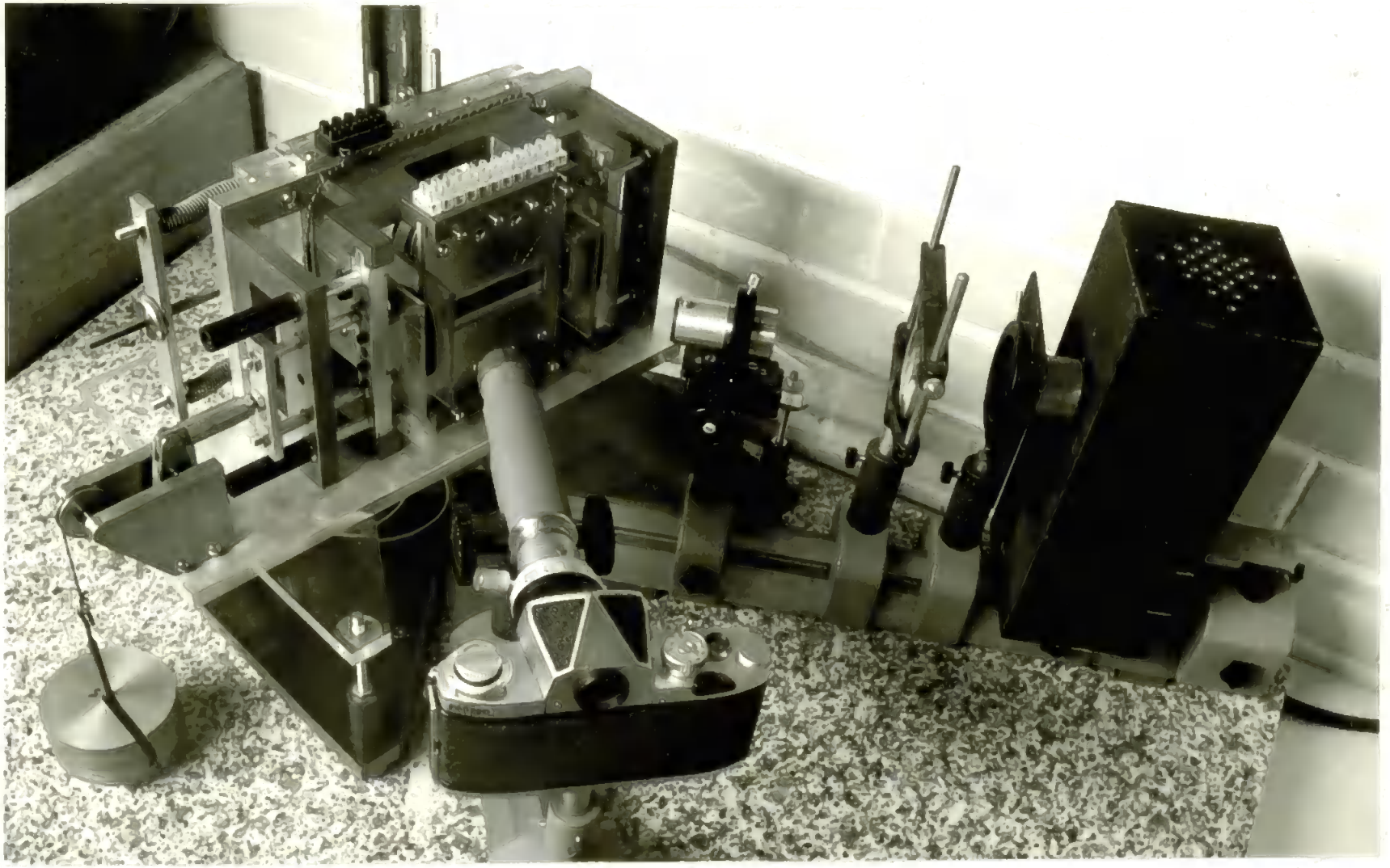

FIG. 4.2. The Domain Observation Optical System.

The lens L_2 can then focus the spot onto the specimen at the required position by judicious manipulation of the positions of L_1 and L_2. In addition the image formed by L_2 will be diminished, and the overall magnification will depend on the position of L_1 and L_2. For the dimensions shown in Fig. 4.1 the overall magnification of the light source is -1.1X, giving a light spot of about 7 mm. major axis at the specimen.

The reflected light beam is then passed through the second polariser (P_2) and a low power microscope. The objective lens (L_3) has a long focal length to achieve a large depth of field and reduce focussing problems at the edges of the light spot. This lens would form a magnified real image further along the light path, but the beam is interrupted by the microscope ocular. The ocular used is a standard Huygens eye-piece of magnification 7X, and the field lens (L_4) focuses the image at the field stop (F).

As F is at the focal point of the eye-lens (L_5) a parallel beam of light is produced which is refocussed by the observers' eye. In addition, a micrometer graticule is placed at the field-stop, and by focussing the microscope onto a metric scale placed at the specimen position the magnification can be adjusted so that the apparent size of the object at the eye-piece can be measured. For the positions shown in Fig. 4.1 the overall magnification is -14X.

Rotational adjustment of the polarisers was achieved by mounting them in tubes which were sliding fits into an outer sleeve. The polarising elements chosen were of the colloid film type having an orientated molecular structure, enabling very high extinction ratios to be achieved, with a crossed transmittance of 0.00015%, representing an extinction ratio of -100 dB.

With this system satisfactory domain observations were achieved for a range of angles of incidence, but mainly for practical convenience in the space available the final angle was set at 44°.

For permanent reproduction of domain structures a camera having a microscope ocular attachment was used, fitted to the steel carriers for alignment of the optical system. The camera is shown in position in Fig. 4.2.

Specimen Preparation:

Because of surface stresses induced by mechanical finishing, which obscure the true nature of domain structures in ferromagnetic specimens, and also because the Kerr Longitudinal Effect must be enhanced by non-reflecting coating techniques, specimen preparation is critical. Mechanically finished (lapped) specimens must be strain-relief annealed and the Kerr Effect enhanced using a zinc-sulphide layer to obtain multiple reflections, as described by Kranz and Dreschel (14).

It was decided to work with half-Epstein samples of material, these being the size conventionally adopted for such investigations as covered by this work as well as being convenient to obtain and handle. The first step is to remove the insulating surface coating put on during the manufacturing process by pickling the samples in a 50% solution of hydrochloric acid for about thirty minutes. The specimens were then neutralised by dilute sodium hydroxide solution and washed throughly. Polishing of the surface to produce the high level of reflectivity required was commenced with 300 grit size 'wet and dry' hand polishing under running water, with the specimen mounted on a mangetic block. Only the central 25 mm. were polished. As the surface improved, the grit size was decreased through 400 to 600 grit until an 'eye-flat' mirror was produced.

The final polish was achieved using a mechanical rotary polisher with 2 μm. diamond paste. This was only carried out for about one minute as it has been found that excessive polishing can give rise to an 'orange-peel' effect when subsequently viewing the specimen under high intensity illumination required by the Kerr Effect (9).

In order to enhance the degree of rotation of the reflected polarised light beam, a quarter-wavelength layer of zinc-sulphide is then vacuum electro-deposited on the surface. Judgement of this process is very critical and the author was pleased to use the experience of other workers to obtain this surface blooming (see Aknowledgements).

Since all the above processes will stress the specimen, which will be detrimental to the domain structure, it is then necessary to stress-relieve anneal the material. This was achieved by mounting several prepared specimens in a clamp made from non-magnetic stainless steel, whereby the weight of a 6 mm. thick plate provided adequate pressure to flatten the specimens. This assembly was then placed in a vacuum furnace and the temperature raised to 800°c in about one hour, held at that temperature for one hour, and then allowed to cool slowly over about twenty-four hours.

Stroboscope Triggering

Since the specimen is under dynamic excitation, direct observation of domain surface closure structures will only be possible if the light source is stroboscopically triggered from either the specimen excitation or some waveform locked to it. An advantage is obtained if the triggering point can be derived from any point on the waveform, enabling domain patterns to be observed at any value of excitation and to be slowly 'swept' through a range of magnetisation levels.

Various methods of achieving this have been achieved by other workers (4, 9, 27), all based on the method of varying the time constant of passive R-C networks which control the operating characteristic of a valve or operatical amplifier. This indeed was the basic method employed for this investigation, but a novel means of determining the initial triggering point was selected in order to achieve 'sweeping' of the excitation waveform over a full 360°, and even through the zero crossings of that waveform.

The complete circuit diagram for the trigger circuit is shown in Fig. 4.4 with a schematic diagram illustrating the various stages of operation shown in Fig. 4.5.

The input stage of the circuit is a SN 710 Voltage Comparator, the output of which changes state from a high to a low logic level when the driving signal

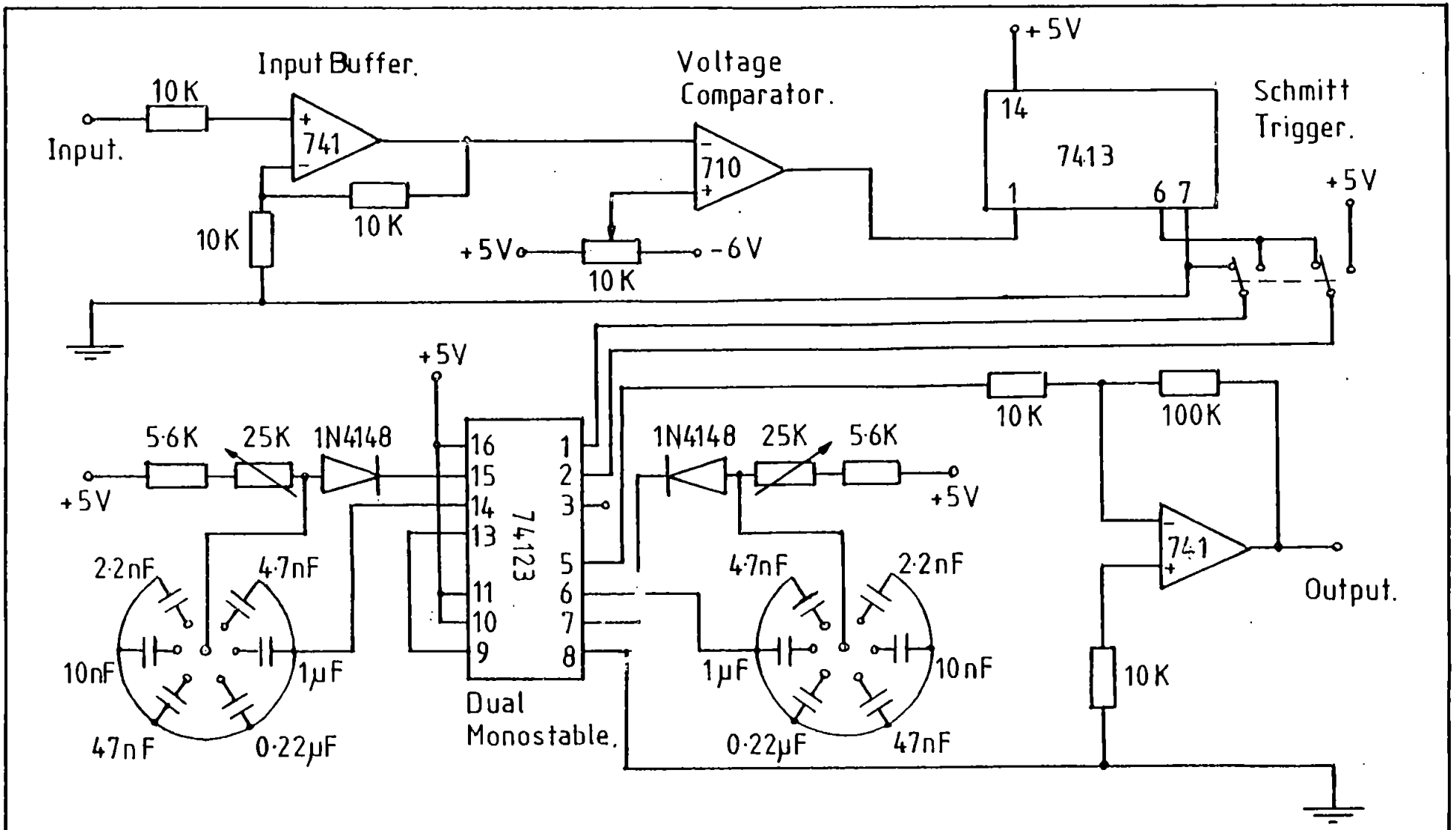

FIG. 4.4. Stroboscope Trigger Circuit.

exceeds a reference voltage, and vice-versa. By making the reference level ground potential, the pulse generator can be made virtually independant of driving signal level down to about 100 mV. Alternatively, by varying the reference level either side of ground potential the edges of the output pulse from the imput stage can be moved about the zero-crossings of the driving signal waveform. This may be of advantage when the driving signal is derived from the specimen magnetisation, when the reversals of domain behaviour around the zeros of flux density will be of interest. It also avoids the necessity to switch the driving signal in order to achieve a full 360° sweep of the input period.

The first stage output pulse exhibits undesirable qualities such as hysteresis, noise and overshoot of the pulse edges. The pulse is cleaned-up by passing through a 7413 Schmitt Trigger, before going to the next stage which is one half of a 74123 Dual Monostable Vibrator.

This monostable can be triggered by either the leading or trailing edges of the Schmitt trigger output, by switching at its input terminals. This increases the overall versatility of the pulse generator, although complete coverage of the driving signal waveform can be achieved without it. The length of the output pulse derived from the first half of the monostable is controlled by external, timing capacitors and resistors, the values of which are adjusted so that the negative-going edge of the pulse may be swept across virtually the complete driving signal period to within a few degrees of the zero crossings. Adjustment of the reference level at the input stage completes the sweep, passing up to and through the zero-crossings.

The pulse thus formed is then passed to the second half of the dual monostable which is triggered by the negative going edge which can, as described above, be positioned at any point with reference to the driving signal period. The length of the output of the second half is again controlled by external, passive, timing resistors and capacitors which are selected to produce a pulse

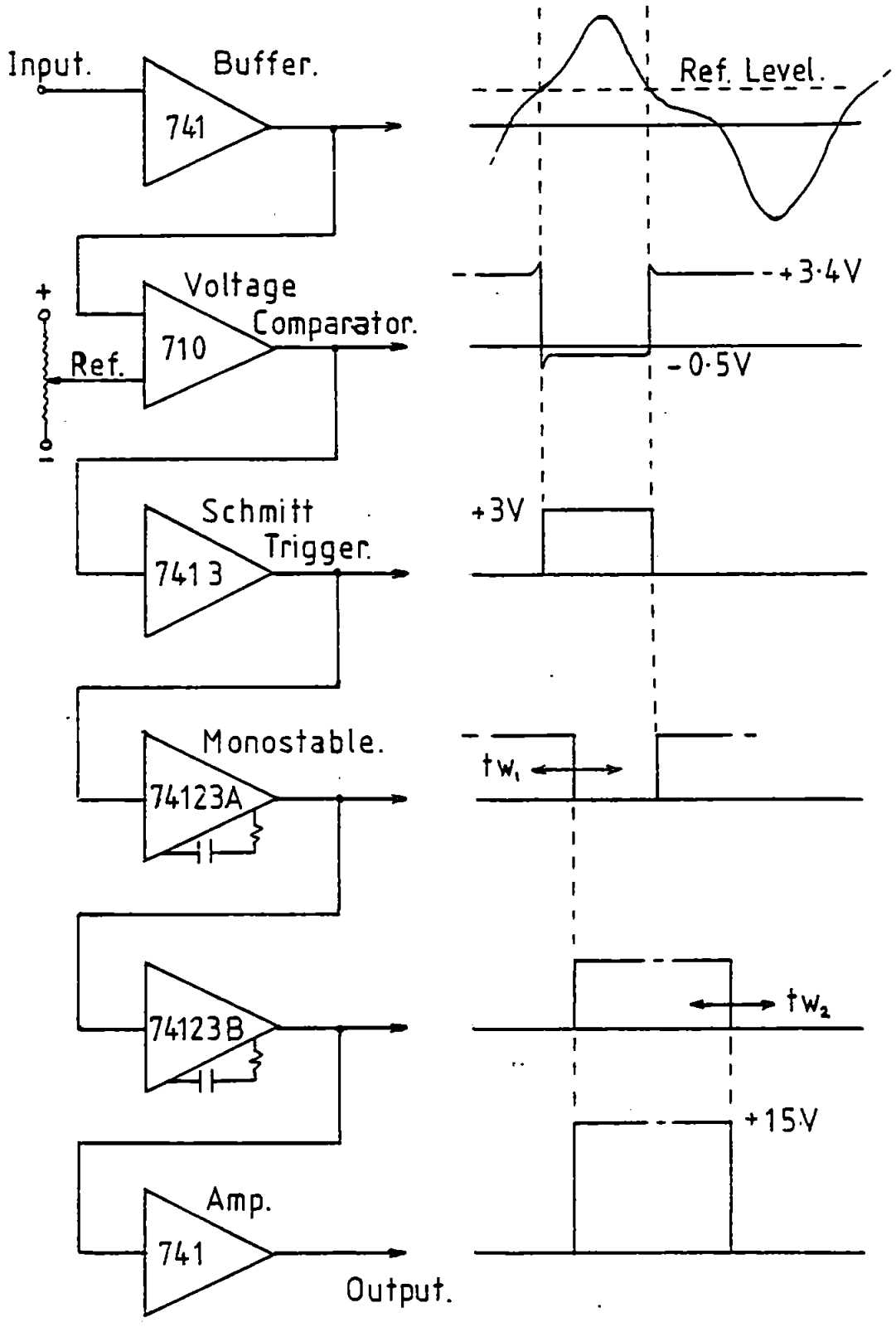

FIG. 4.5. Stroboscope Trigger Circuit.
Schematic Diagram.

width much smaller than the period of the input driving signal. This output pulse may be swept smoothly across the period of the driving signal by adjustment to the input stage reference level and/or the adjustable resistor in the first half of the dual monostable. Sweeping is continuous through the zero crossings of the input waveform, in either direction.

Finally, a fixed gain 741 operational amplifier is used to increase the pulse from its positive logic level to about 13V as required by the Strobex Trigger Circuit.

The pulse generator will accept virtually any waveshape driving signal, provided that the signal level does not exceed the reference level more than once per half cycle in either direction. The frequency response is limited at the top end by the influence of stray capacitance, and will work down to a 'one-shot' type of operation provided that the reference level is exceeded once.

A disadvantage becomes apparent if, when examining domain structures at a particular point on the magnetisation curve, the effect of frequency variation is required. As the pulse widths are determined by passive devices their positions will not be fixed to the driving signal waveform if the frequency is changed. However, by making the pulse width of the first half of the dual monostable very small compared to the driving signal period, the leading edge of the output pulse from the generator is virtually at the same point on the waveform as the initial triggering point of the first stage voltage comparator. This point is fixed to the driving signal and will stay at the same point on the waveform as the frequency is varied. As previously described, this reference point may be adjusted, but as the input level must exceed the reference level in either direction, complete coverage of the waveform cannot now be obtained. However, by switching the input to the first half of the dual monostable as described both sides of the waveform may be swept to within about 100 mV of the peaks, on a waveform of approximately 5 V peak to peak amplitude.

A further disadvantage is apparent if, when examining domain structure at a particular point on the magnetisation curve, the amplitude of the driving

signal is required to be varied. If the pulse is being derived by adjustment of the reference level, then the triggering point will effectively move as the input amplitude varies. This is easily overcome by putting the reference level to ground potential, and setting the pulse position by adjustment to the timing controls of the first half monostable.

It will be appreciated, therefore, that this device is versatile enough to cover most requirements for domain observation under varying conditions of both frequency and amplitude, as well as satisfying the basic requirement for smooth, continuous pulse positioning with respect to an input signal. In practice the input signal was derived from a master oscillator which also supplied the specimen excitation and waveshape control circuits (to be described in later sections), but any waveform locked to the specimen excitation would be satisfactory.

4.2 Magnetostriction Measurement

4.2.1 Introduction

Various methods are available for the measurement of bulk strain in a material, that is, the total displacement over the whole length. Capacitive transducers relying on a change in plate separation have been used (15, 16, 17) and inductance transducers as well (18). Direct observations using optical systems with high magnification (light levers) have been developed (19, 20) and the principles of interferometry have also been applied (21). The disadvantage of the transducer method is that it cannot be applied to measurements within the bulk of the material, and a disadvantage of optical methods is the level of sophistication required by the apparatus.

Strain gauges have been successfully developed for magnetostriction measurement (22, 23, 24) with the advantages of being relatively cheap, and having relatively simple associated electronics. They are also easily adapted to measuring axial components of strain - rosette gauges for example. The major disadvantage of strain gauges for the purposes of this investigation is that they are permanent fixtures and, even with the miniature devices now available,

will be resolving a strain component over a finite area, not at a point or between two points on the surface.

For those reasons it was decided to adopt the method first used by Neurath (25) and developed by Brownsey and Maples (26), who used ceramic pick-ups of the type employed in record players. This method has been highly developed, notably by Simmons (27), who adapted it by the use of two transducers set up to measure the differential displacement occuring between the two stylii points set a small distance apart on the specimen surface.

A commercially manufactured instrument consisting of a piezo-electric crystal having two needles fixed 23 mm. apart is available and has been employed for magnetostriction measurements (28), but it was felt that the permanent fixing of the needles, as well as the relative inaccuracy of the instrument, were a disadvantage to this investigation. As will be shown, the separation of the measuring points greatly affects the accuracy of measurement.

Fig. 4.6 shows the essential constructional features of a stereo ceramic cartidge commonly available for record players. For an ideal transducer having identical piezo-electric crystals in both channels with perfect alignment, the output signals from each channel due to vertical motion of the stylus will be equal in magnitude and phase, since the bending moment for each crystal will be vertical in both magnitude and sense. With horizontal motion of the stylus, the outputs in the two channels will be equal in magnitude but opposite in polarity i.e., anti-phase. For transverse motion the stylus is constrained by its fixing arrangement but if such motion is allowed to occur then the two outputs will be equal in magnitude and, as for vertical motion, in phase. This arrangement assumes that terminals 1 and 3, as depicted in Fig. 4.6, are used as the 'common' terminals.

Hence, if the difference between the two output signals is taken by connection to a differential amplifier of suitable input impedence, then any response due to vertical or transverse motion will be cancelled, leaving a signal entirely due to horizontal motion of the stylus.

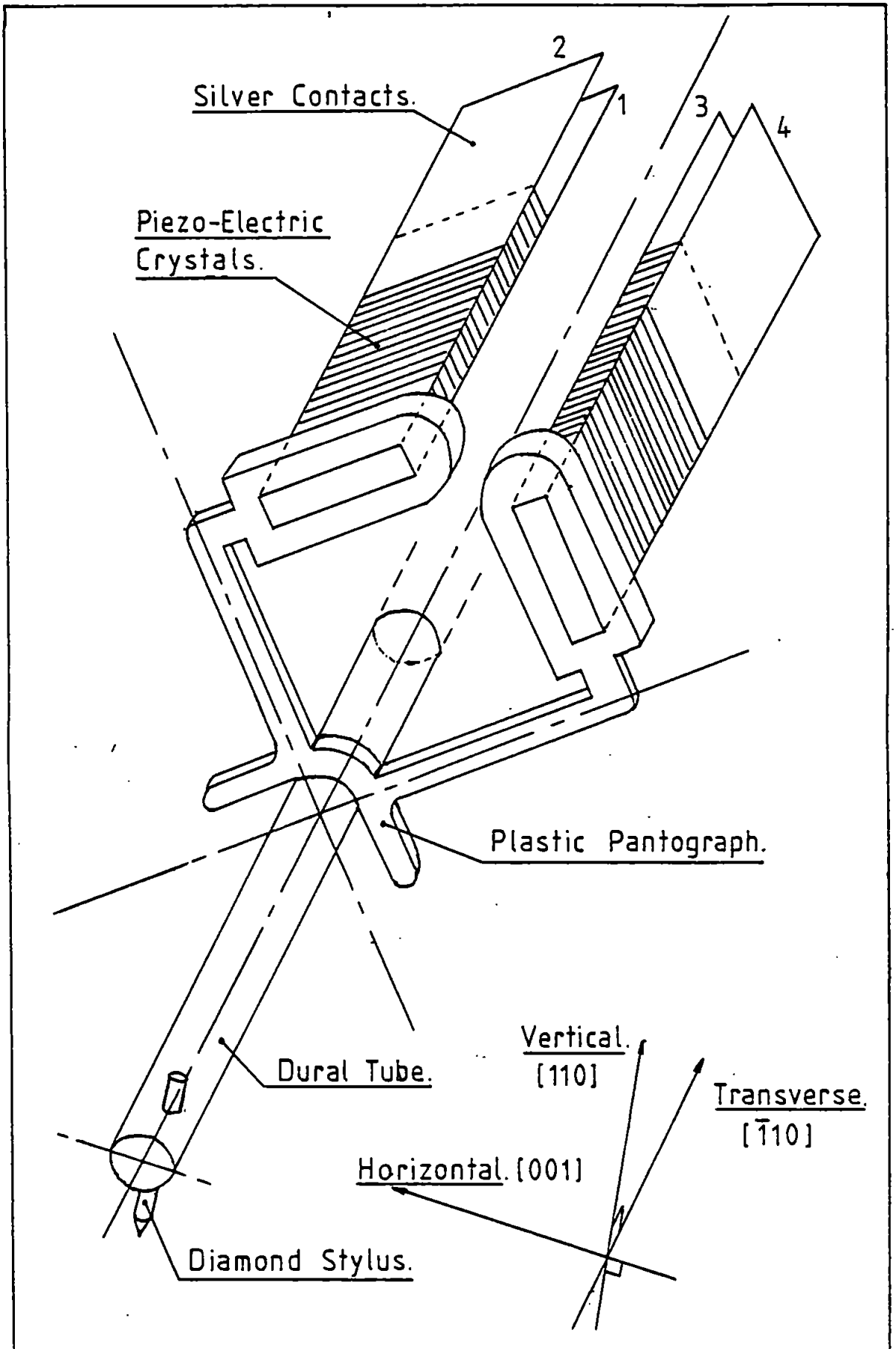

FIG. 4.6. TRANSDUCER ASSEMBLY.

If two such transducers are now positioned so that each is experiencing a complex motion containing components along each of the three axes, and the outputs from the two differential amplifiers connected to each transducer are connected to a further difference amplifier, then the final output will be proportional to the difference in motion along the horizontal axis. No component due to vertical or transverse motion will appear.

This arrangement is ideal for the measurement of magnetostrictive strains occurring in silicon-iron, when it is required to measure the differential motion between two points within the boundaries of a grain, and at the same time eliminating any vertical (i.e., normal to the sheet plane) vibration due to magnetisation under compressive stress and any vibration transverse to the direction of interest.

Of course, in practice, it is necessary to depart from the ideal, and consideration has to be given to the fact that the transducer will not behave as previously described. Thus the two crystals will not be identical or symmetrically positioned so that the output sensitivities will be dependant on vibration magnitudes and frequency. Even with transducers carefully built by hand it was found that sensitivities varied significantly, not only between channels but between transducers. Thus it would be necessary, in the case of a double-transducer arrangement, to have to deal with twelve different sensitivities.

To simplify the problem, the response of one axial motion would have to be ignored. The transverse direction was selected for this since, not only is the stylus physically restrained in this direction, but later experimental evidence showed that the transducer output due to transverse motion was less than 5% of that due to vertical or horizontal motion. Further, it was found that the sensitivities to this axial motion were much more equal between channels then for the other two axial displacements.

It remained, therefore, to provide a system requiring only the nulling of vertical components and catering for the difference in sensitivities between channels and transducers. In addition, it was necessary to improve the technique to allow for measurements at the harmonic frequencies in the magnetostriction.

This approach has extended and improved on the double-transducer technique developed by Simmons (27).

In order to assess the degree of refinement required, an error analysis was undertaken as follows.

4.2.2. Error Analysis

The error in the output from the differential pre-amplifier fed from the two transducers will be due to

(1) any phase shifts introduced by the transducers, the pre-amplifier, or both

and (2) any differences in gain between the two channels of the pre-amplifier or differences between the transducer sensitivities.

Consider the two signals to be measured, A_1 and A_2, where $A_1 > A_2$ and $A_1 - A_2$ ($= \Delta A$) is the required result. Assume that A_1 and A_2 are in phase, as shown in Fig. 4.7, (a).

Let the overall gains of the two channels (which will include the transducer sensitivities) be K_1 and K_2, where $K_1 > K_2$, and let the total phase shifts introduced by each channel be θ_1 and θ_2.

The resulting output from the system will then be as shown in Figs. 4.7, (b) or (c) where R_n is the output when the channel with the higher gain is sensing the larger of the two signals, and R_r is the output when the channel with the higher gain is sensing the lower of the signals.

R_n and R_r will be defined by

$$R_n \cos \phi_n = K_1 A_1 \cos \theta_1 - K_2 A_2 \cos \theta_2 \quad \ldots\ldots\ldots\ldots\ldots 4.1$$

$$R_n \sin \phi_n = K_1 A_1 \sin \theta_1 + K_2 A_2 \sin \theta_2 \quad \ldots\ldots\ldots\ldots\ldots 4.2$$

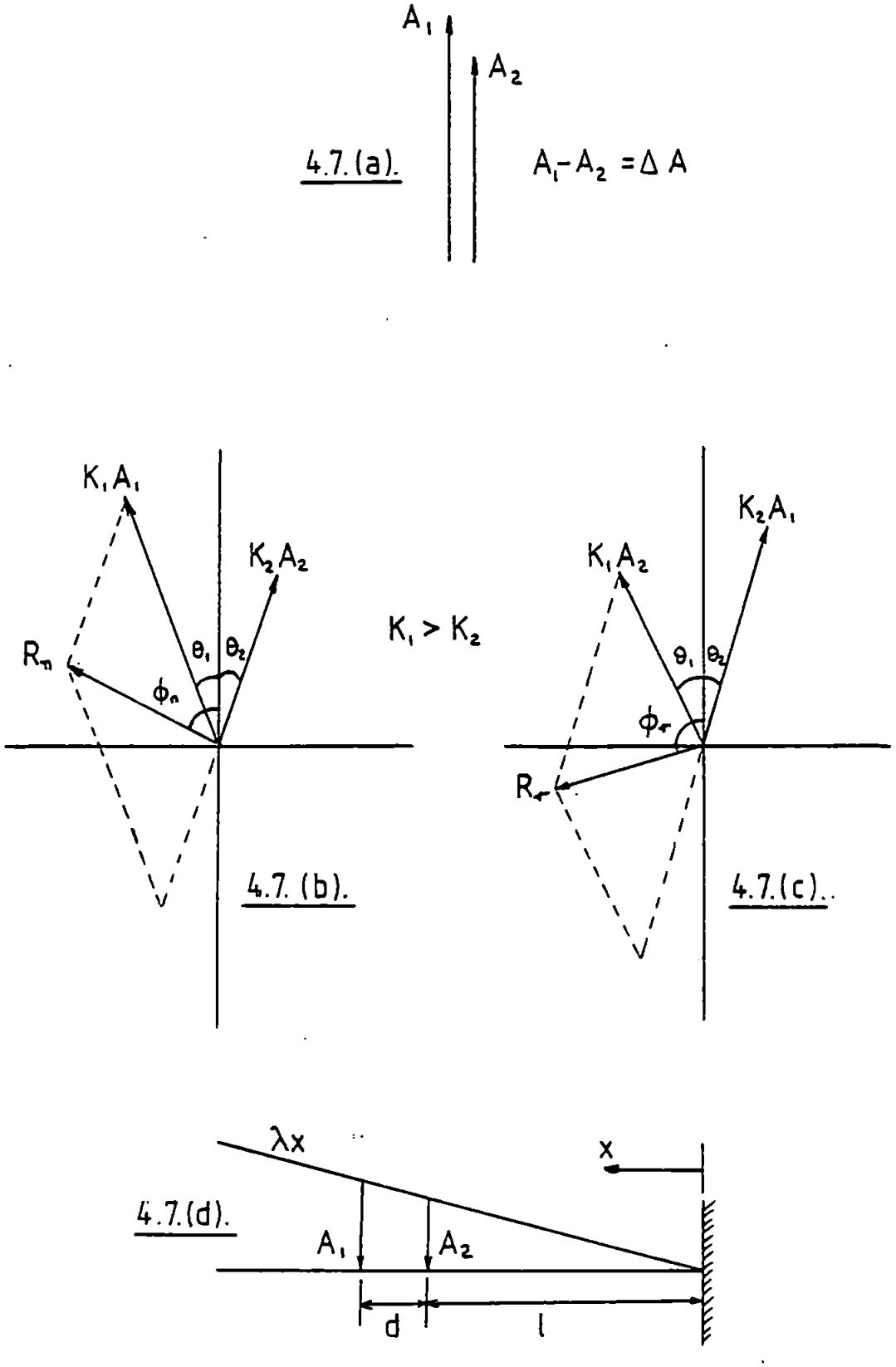

FIG. 4.7. Relationships for the Error Analysis.

$$R_r \cos \phi_r = K_1 A_2 \cos \theta_1 - K_2 A_1 \cos \theta_2 \quad \ldots\ldots\ldots\ldots\ldots 4.3$$

$$R_r \sin \phi_r = K_1 A_2 \sin \theta_1 + K_2 A_1 \sin \theta_2 \quad \ldots\ldots\ldots\ldots\ldots 4.4$$

Squaring and adding equation 4.1 and 4.2, and equations 4.3 and 4.4 gives

$$R_n^2 = (K_1 A_1)^2 + (K_2 A_2)^2 - 2K_1 K_2 A_1 A_2 \cos (\theta_1 + \theta_2)$$

or $$R_n^2 = (K_1A_1 - K_2A_2)^2 + 2K_1 K_2 A_1 A_2 [1 - \cos (\theta_1 + \theta_2)] \quad \ldots\ldots\ldots 4.5$$

and $$R_r^2 = (K_1 A_2)^2 + (K_2 A_1)^2 - 2K_1 K_2 A_1 A_2 \cos (\theta_1 + \theta_2)$$

or $$R_r^2 = (K_2 A_1 - K_1 A_2)^2 + 2K_1 K_2 A_1 A_2 [1 - \cos (\theta_1 + \theta_2)] \quad \ldots\ldots 4.6$$

In addition, the phase angles of the outputs with respect to the input signals will be given by

$$\tan \phi_n = \frac{K_1 A_1 \sin \theta_1 + K_2 A_2 \sin \theta_2}{K_1 A_1 \cos \theta_1 - K_2 A_2 \cos \theta_2} \quad \ldots\ldots\ldots\ldots\ldots 4.7$$

$$\tan \phi_r = \frac{K_1 A_2 \sin \theta_1 + K_2 A_1 \sin \theta_2}{K_1 A_2 \cos \theta_1 - K_2 A_1 \cos \theta_2} \quad \ldots\ldots\ldots\ldots\ldots 4.8$$

A complete analysis of equations 4.5 to 4.8 is extremely arduous, but certain simplyfying assumptions may be made in order to determine the worst possible error, so that the significant factors contributing to that error may be identified.

Thus if there is no phase error ($\theta_1 = \theta_2 = 0$) the error in magnitude may be eliminated by taking the sum of R_n and R_r, since, for this case,

$$R_n = K_1 A_1 - K_2 A_2 \qquad \text{and} \qquad R_r = K_2 A_1 - K_1 A_2$$

Hence

$$R_n + R_r = K_1 (A_1 - A_2) + K_2 (A_1 - A_2)$$

or $$\frac{R_n + R_r}{K_1 + K_2} = A_1 - A_2 = \Delta A,$$ the required result.

There is no similar, easy solution when the phase error is introduced.

Expressions for the total percentage error in the output signal may be obtained from equation 4.5 and 4.6 as follows.

Referring all quantities to their lowest values, let

$$\frac{y}{100} = \frac{A_1 - A_2}{A_2} = \frac{\Delta A}{A_2} \quad \text{so that} \quad A_1 = \left(1 + \frac{y}{100}\right) A_2 \qquad \ldots\ldots\ldots\ 4.9$$

where y represents the percentage difference is the signals to be measured, and let

$$\frac{X}{100} = \frac{K_1 - K_2}{K_2} \quad \text{so that} \quad K_1 = \left(1 + \frac{X}{100}\right) K_2 \qquad \ldots\ldots\ldots\ldots\ 4.10$$

where X represents the percentage difference in channel gains, and let

$$\frac{E}{100} = \frac{R/K_2 - \Delta A}{\Delta A} \quad \text{so that} \quad \frac{R}{K_2\ \Delta A} = 1 + \frac{E}{100} \qquad \ldots\ldots\ldots\ 4.11$$

where E represents the percentage error in the resulting output signal (R).

In addition, if the magnetostriction (λ) of the specimen is assumed to increase linearly with distance from the fixed end of the specimen, as shown in Fig. 4.7, (d), then

$$A_1 = \lambda\ (d + \ell), \quad A_2 = \lambda\ \ell, \quad \Delta A = \lambda\ d$$

Thus

$$\frac{\Delta A}{A_2} = \frac{y}{100} = \frac{d}{\ell} = r \quad \text{so that} \quad A_1 = (1 + r)\ A_2 \qquad \ldots\ldots\ldots\ 4.12$$

where r represents the ratio between the transducer separation (d) and the distance of the nearest transducer to the fixed end of the specimen (ℓ).

From equations 4.5, 4.9, 4.10, 4.11 and 4.12 the percentage error (E_n) in the output signal when the channel with the higher gain in sensing the larger of the two input signals will be given by

$$\frac{R_n^2}{K_2^2 A_2^2} = \left[(1 + \frac{X}{100})(1 + r) - 1\right]^2 + 2\,(1 + \frac{X}{100})(1 + r)\left[1 - \cos\,(\theta_1 + \theta_2)\right]$$

$$= (1 + \frac{E_n}{100})^2\, r^2$$

If it is also assumed that $\theta_1 = \theta_2 = \theta$ then

$$(1 + \frac{E_n}{100})^2\, r^2 = \left[(1 + \frac{X}{100})(1 + r) - 1\right]^2 + 2\,(1 + \frac{X}{100})(1 + r)(1 - \cos\,2\,\theta)$$

..... 4.13

Similarly, from equations 4.6, 4.9, 4.10, 4.11 and 4.12 the percentage error (E_r) in the output, when the channel with the highest gain is sensing the lower of the two input signals, will be given by

$$\frac{R_r^2}{K_2^2 A_2^2} = \left[(1 + \frac{X}{100}) - (1 + r)\right]^2 + 2\,(1 + \frac{X}{100})(1 + r)\left[1 - \cos\,(\theta_1 + \theta_2)\right]$$

$$= (1 + \frac{E_r}{100})^2\, r^2$$

Again assuming that $\theta_1 = \theta_2 = \theta$ then

$$(1 + \frac{E_r}{100})^2\, r^2 = \left[(1 + \frac{X}{100}) - (1 + r)\right]^2 + 2\,(1 + \frac{X}{100})(1 + r)(1 - \cos\,2\,\theta)$$

..... 4.14

Expressions for ϕ_n and ϕ_r, the total phase errors in the outputs for the two conditions of channel connections, may also be obtained in a similar fashion. Assuming that $\theta_1 = \theta_2 = \theta$ then, from equations 4.7, 4.9, 4.10, 4.12,

$$\tan \phi_n = \tan \theta \left[\frac{(1 + \frac{X}{100})(1 + r) + 1}{(1 + \frac{X}{100})(1 + r) - 1} \right] \quad \ldots\ldots\ldots\ldots\ldots\ldots 4.15$$

and $$\tan \phi_r = \tan \theta \left[\frac{(1 + \frac{X}{100}) + (1 + r)}{(1 + \frac{X}{100}) - (1 + r)} \right]$$ from equations 4.8, 4.9, 4.10 and 4.12.

Note that for $\frac{X}{100} = r$, ϕ_r will be 90^o. For $\frac{X}{100} < r$, which, as will be shown later, is usual, then $\phi_r < 90^o$ and so the expression for ϕ_r becomes,

$$\tan (180 - \phi_r) = \tan \theta \quad \frac{2 + \frac{X}{100} + r}{r - \frac{X}{100}} \quad \ldots\ldots\ldots\ldots\ldots\ldots 4.16$$

Examination of equations 4.13 and 4.14 shows that, for $X > 0$, E_n will be larger than E_r, so that the worst magnitude error will occur for the condition when the channel with the highest gain is sensing the larger of the two input signals. Similarly by examination of equation 4.15 and 4.16, when $X > 0$, the largest phase error will occur for the opposite condition of channel connections, since $\phi_r > \phi_n$, and will be 90^o or greater, approaching 180^o as θ tends to zero.

By taking values of r in the range 0.05 to 0.3 (which represents transducer separations of 0.5 mm. to 3.0 mm. for every centimetre along the specimen from the fixed end), values of X in the range 0.1 to 1% and values of θ of 0.5 and 1^o, then the variation of E and ϕ may be plotted as functions of r for the different combinations of X and θ. These results are shown in Figs. 4.8 and 4.9, for the two conditions of "normal" (n) and "reversed" (r) transducer positions.

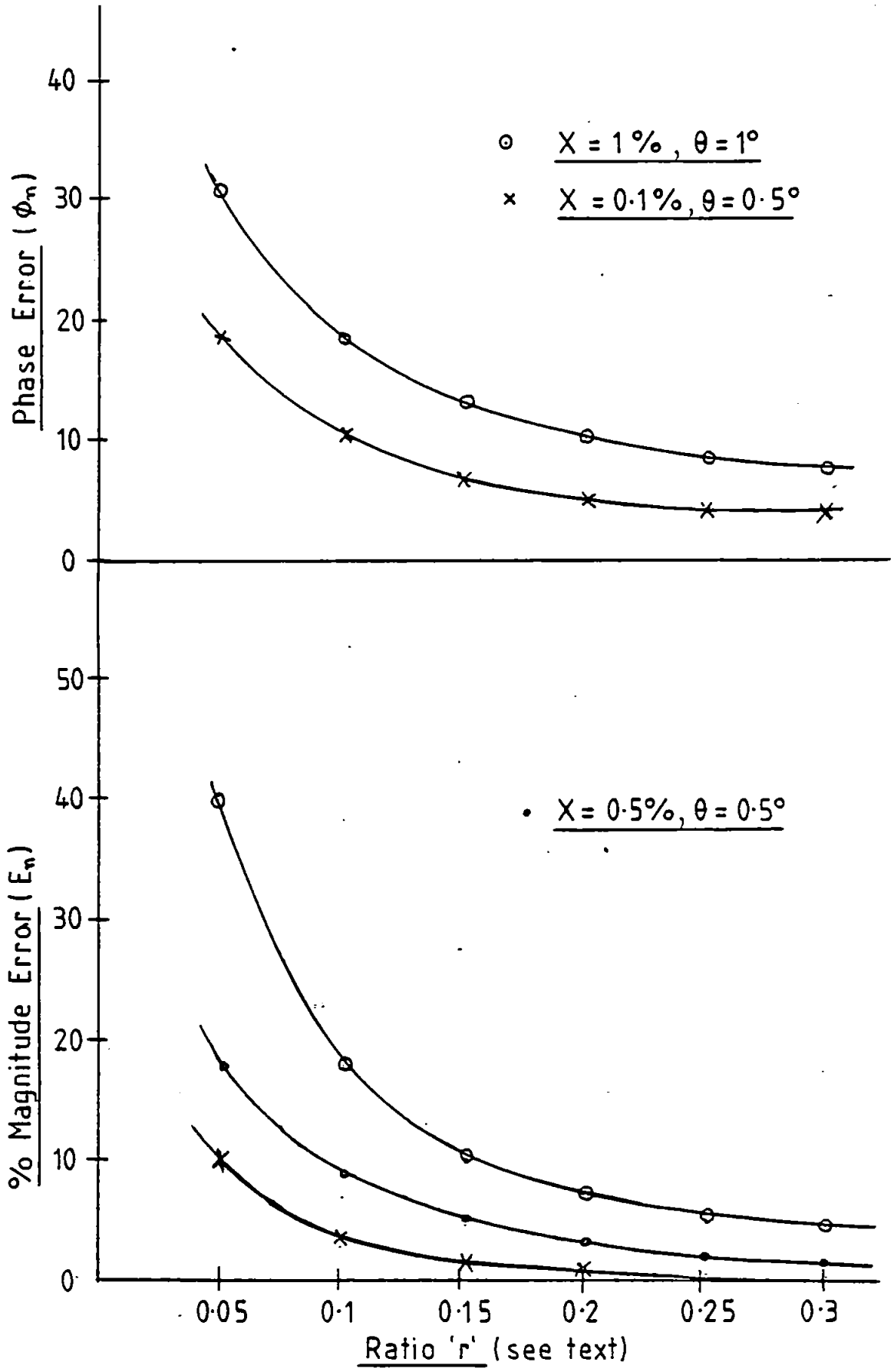

FIG. 4.8. Magnitude & Phase Errors for "Normal" Transducer Position.

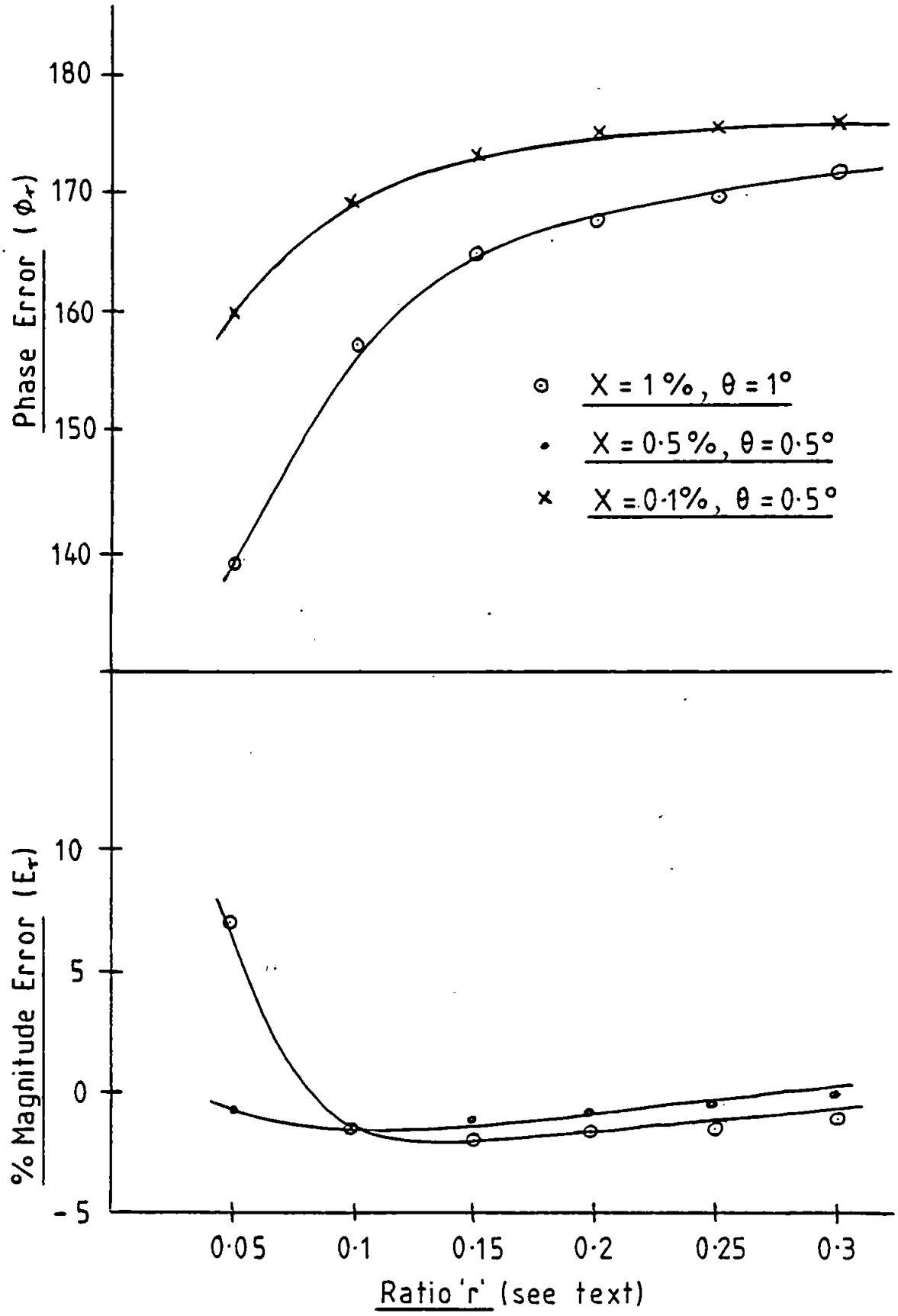

FIG. 4.9. Magnitude & Phase Errors for "Reversed" Transducer Position.

Close examination of these results enables the following observations to be made concerning the accuracy of the method used to measure ΔA.

(1) For an output error better then +5% it is necessary to restrict the difference in channel gains to 0.5% and any phase shifts to 0.5^{o}, and to restrict the transducer separation to a minimum of 1.5 mm. for every 10 mm. from the fixed end of the specimen. This will cater for the worst conditions.

(2) Even if this condition is met, there could still be a phase error of about 10^{o}.

(3) On reversing the transducer position, with the above conditions still in effect, the output error will fall to about -2.25% and the phase error increase to about 170^{o}.

(4) Any improvements in phase error beyond that given in (2) will mean reducing the level of X and/or θ, and increasing the separation of the transducers. Thus for a phase error less than 5^{o}, it will be necessary to restrict $\bar{R}$ to 0.1%, θ to 0.5^{o} and the transducer separation to about 2.2 mm. for every 10 mm. from the fixed end of the specimen.

4.2.3 Apparatus for Magnetostriction Detection

The apparatus constructed to accomplish reasonable accuracy of measurements as outlined above is based on two stereo cartridges similar to those shown in Fig. 4.6.

Transducer Mounting

Several requirements need to be satisfied for satisfactory positioning of the transducers at the specimen. They are:

(1) Vertical motion, normal to the sheet, for setting the stylus contact force;

(2) Rotation about the normal to the sheet for examining axial strain variations;

(3) Tilt motion to cater for non-perfect alignment of the stylii and allow both to make simultaneous contact;

(4) Variable separation between the two stylii;

(5) X-Y motion about the sheet surface for positioning within grain boundaries.

To accommodate all these variables a single transducer head was designed and built, and is shown in Fig. 4.10 with a sectionalised view shown in Fig. 4.11. It is best described by explaining how the various motions are achieved.

Vertical motion, normal to the sheet, is performed by screwing the main ring in or out, which bears on the top plates held together by a brass sleeve. The transducer plate is connected to the top plates by three tie rods which are free to be screwed in or out.

To achieve rotation about the normal, the top plates are manually rotated within the main ring. Having set the required position, the top plates are then locked in position by means of the nylon gears shown in Fig. 4.10. Lowering of the transducers onto the specimen can then commence, without disturbing their axial position relative to the sheet.

Tilt motion is performed by screwing in or out of the through bolts which terminate at the base plate. As there are three such bolts, movement of one will tilt the transducers about the axis of the other two. To facilitate this a knob was attached to the through bolts, one of which is shown clearly in Fig. 4.10.

The assembly is accurately machined from perspex and brass with a central hole running through all the component parts to enable viewing of the transducer stylii, and passage for their leads. Spring pressure is used to maintain firm contact between the different rotating parts.

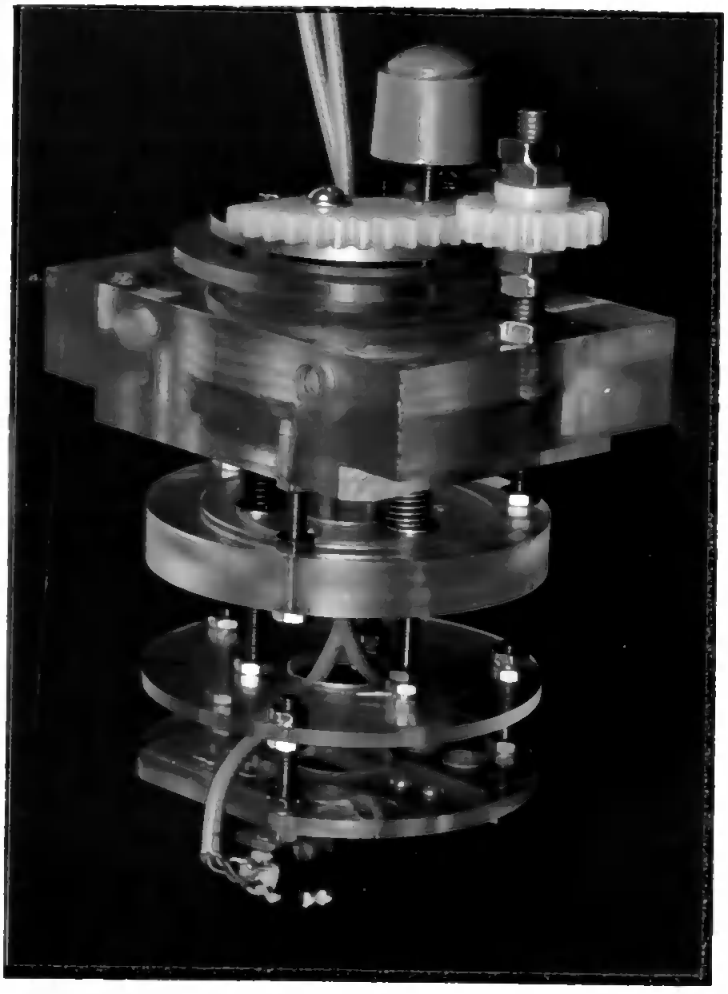

FIG. 4.10. The Transducer Mounting and Positioning Head.

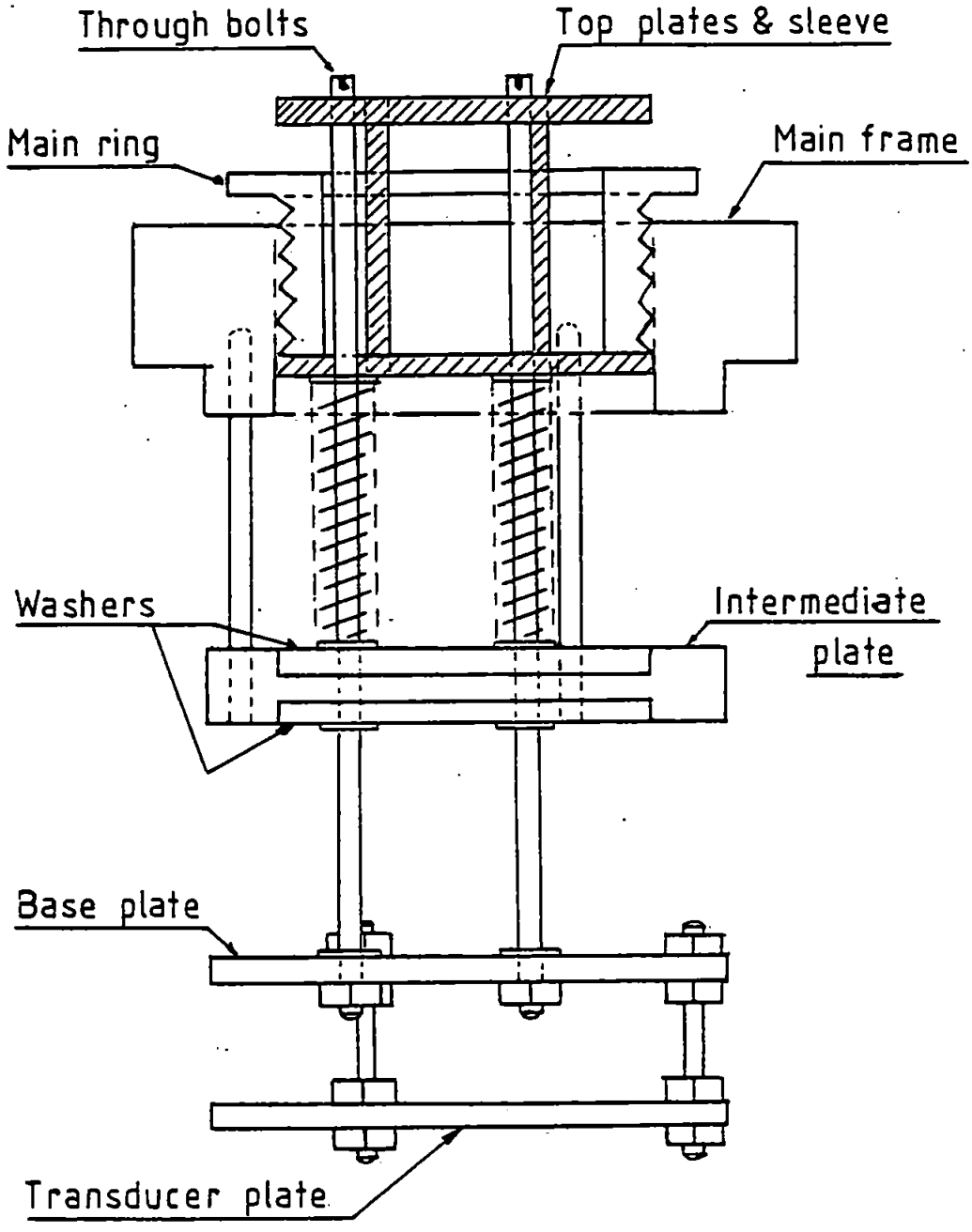

FIG . 4.11. THE TRANSDUCER MOUNTING AND POSITIONING HEAD.

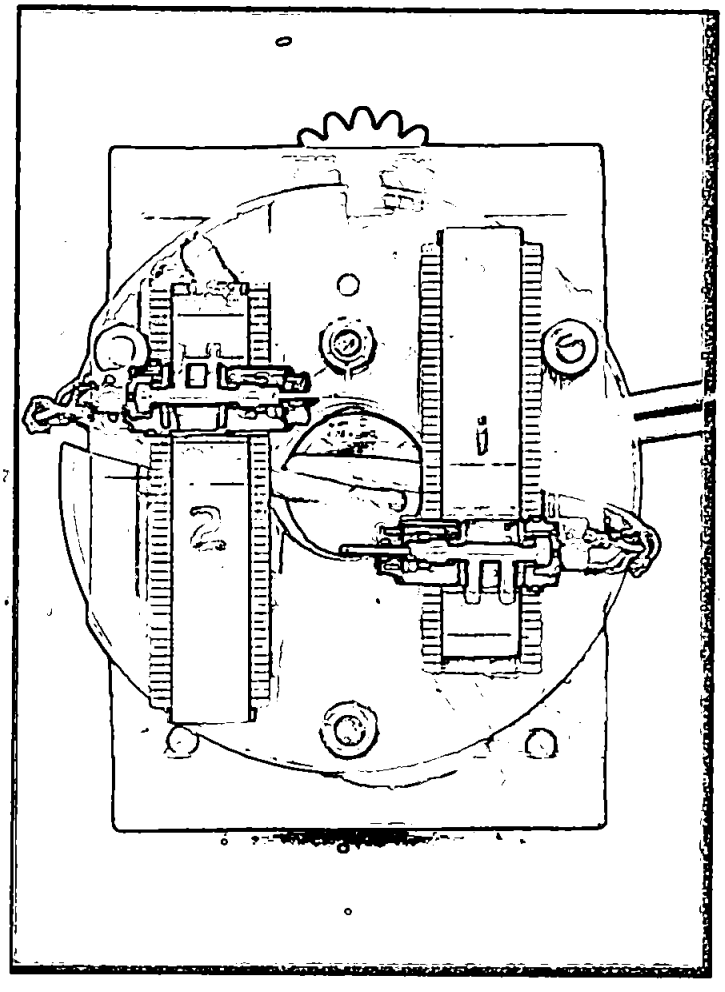

FIG. 4 12. The Double Transducer Mounting Arrangement.

A close-up view of the two transducers mounted on the head is shown in Fig. 4.12, where the arrangement for providing variable separation between the two stylii can clearly be seen. Each transducer is fixed to a brass slide running in brass guides, firm contact between the two being made by phosphor bronze spring strips under the slide. The brass mounts were machined from door catches, and as can be seen, marks were accurately machined at 1 mm. intervals to enable setting of the stylii separation. The mounts are screwed to the transducer plate in such a position that the motions of the two stylii are parallel and along the centre axis between the mounts.

Fig. 4.13 shows the transducer head fitted to the specimen stage, (to be described in section 4.3), with the specimen omitted.

A rear view of the complete specimen stage with the transducer head fitted is shown in Fig. 4.14. This demonstrates the arrangement providing X-Y motion of the transducers, across the specimen surface.

The transducer head is a sliding fit into a rectangular perspex frame which runs in aluminium guides screwed to the top and bottom edges of the specimen stage base plate. The frame is attached to four aluminium rods which slide in perspex guides also rigidly screwed to the base plate. One pair of rods carries a cross arm which can be moved longitudinally by screwing a knurled thumb nut against spring pressure. This provides motion along the rolling direction of the specimen.

Transverse motion is provided by a similar arrangement ulitising screw motion against spring pressure except that in this case the main frame of the transducer head (see Fig. 4.11) is guided by four lengths of brass studding running through the rectangular perspex frame.

Having set the required transducer position by reference to the scales fitted to the apparatus (clearly seen in Fig. 4.14), the transducer head is then locked to the specimen stage by screwing up two nuts running on the brass studding in the main frame. Lowering of the transducers onto the specimen can then commence as previously described.

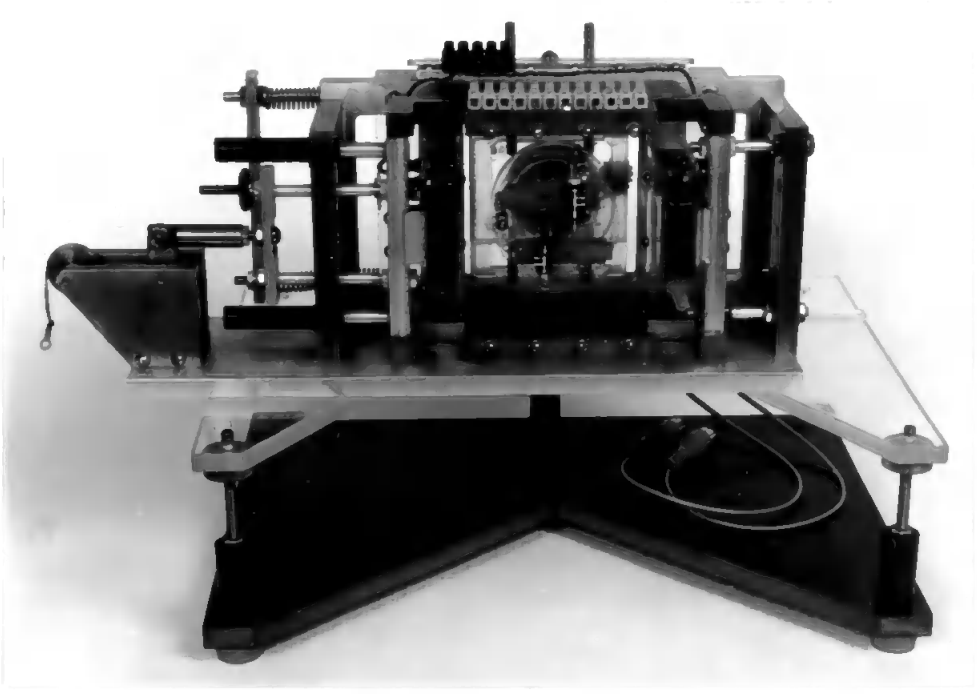

FIG. 4.13. The Transducer Head fitted to the Specimen Mounting Stage.

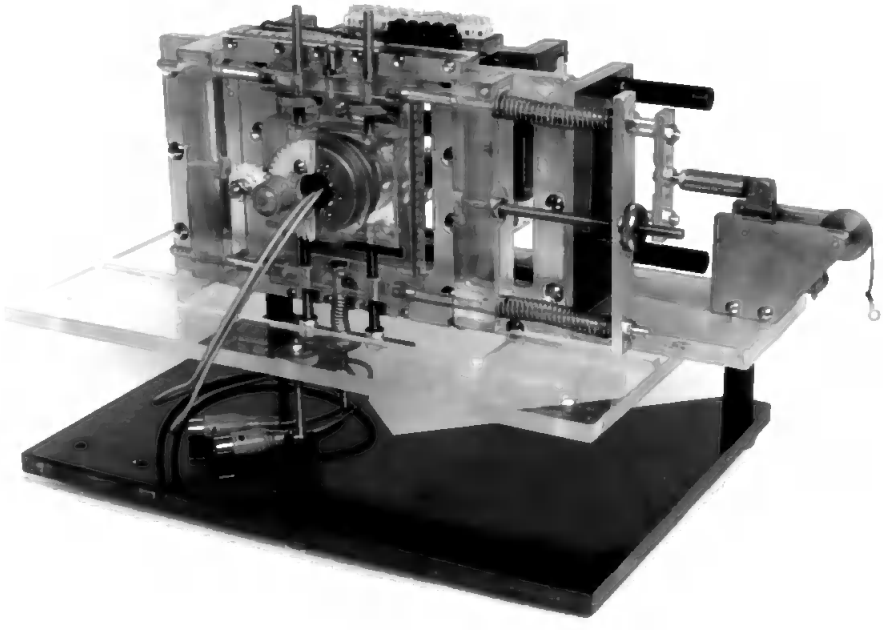

FIG. 4.14. Showing the Arrangements for the X-Y Motion of the Transducers.

Signal Conditioning Circuits

It has previously been indicated that it will be necessary to cater for differences in channel sensitivities between various transducers employed, and for variation in frequency response of the transducers. Therefore, it was decided at this stage to treat each set of harmonic measurements as a seperate entity; that is, to position the transducers and measure variations in fundamental strains; then to remove, recalibrate at the second harmonic frequency and reposition the transducers at the same place on the specimen and measure variations in the second harmonic; and so on for the third harmonic.

The basic electronic circuits for conditioning the magnetostriction signals were therefore designed around these premises.

The first circuit made is shown in Fig. 4.15. A full description of the circuits will be given as they are crucial to the precise functioning of the apparatus.

Since the transducers are capacitive devices of about 800 pF per channel, it is necessary to provide very high input impedance amplifiers. This is easily overcome using MOSFET devices, but as there will be no path for d.c. bias current to flow at the inputs, bias resistors will be required; initially 10 MΩ resistors were employed as shown. Charged-coupled amplifiers were tried but serious d.c. drift problems were encountered which gave rise to phase distortions when a.c. coupling was introduced at a later stage.

In addition it is necessary to provide high C.M.R. at the inputs to eliminate any 50 Hz pick-up by the floating transducer terminations. To achieve this each channel was fed to a pair of cross-coupled variable-gain differential-input, F.E.T. operational amplifiers. This circuit eliminates the dependance of C.M.R.R. on resistor matching (29) and the overall C.M.R.R. is equal to that of any following amplifier multiplied by the differential gain of the proceeding stage (29). Working at a typical gain of 100, the overall C.M.R.R. is 130 dB.

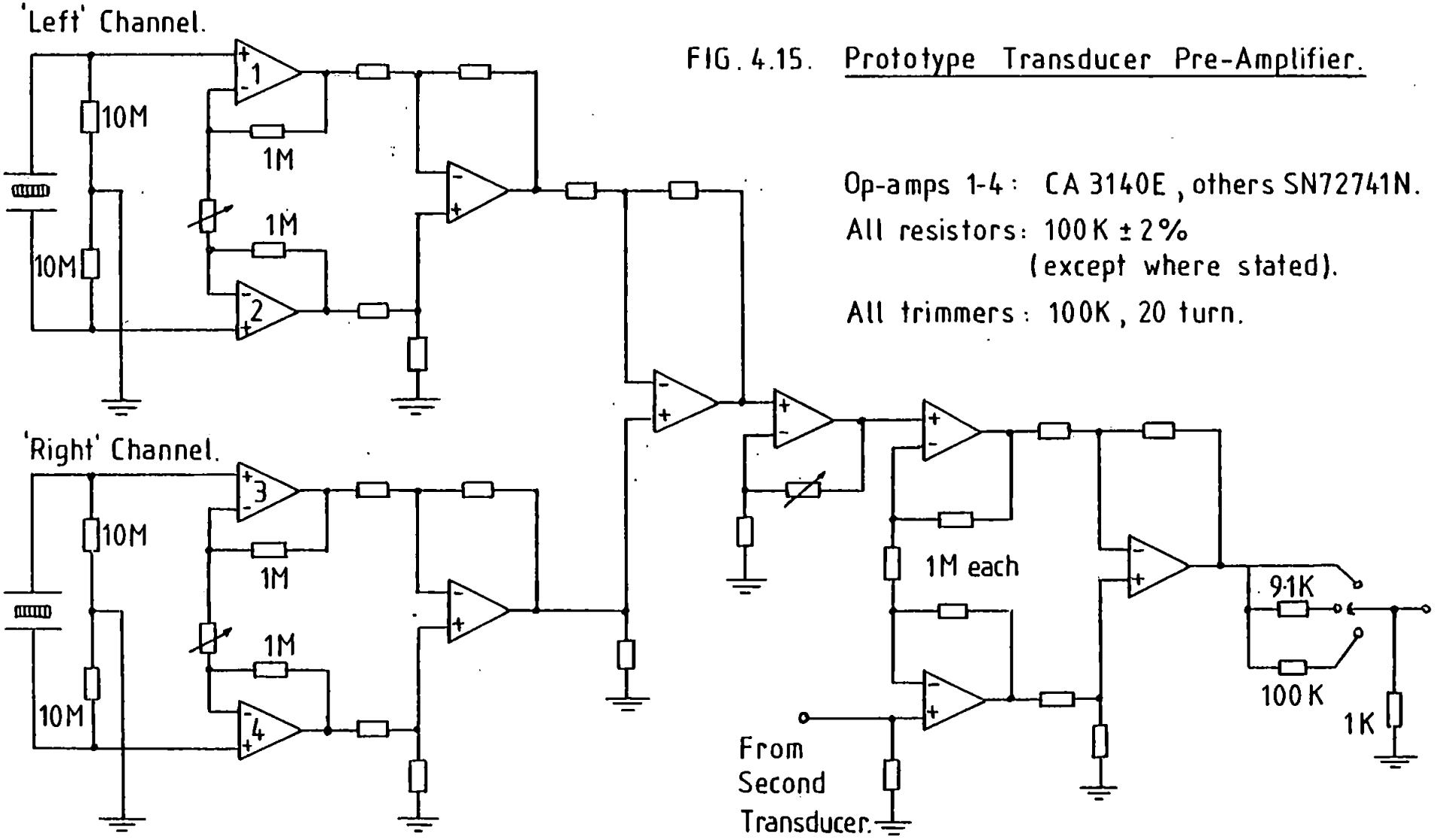

FIG. 4.15. Prototype Transducer Pre-Amplifier.

Op-amps 1-4: CA 3140E, others SN72741N.
All resistors: 100K ± 2%
(except where stated).
All trimmers: 100K, 20 turn.

Each differential pair is followed by a single, differentially connected amplifier, giving a single-ended output per channel. That is, four outputs each containing signal components proportional to both horizontal and vertical motion of the stylii.

To clarify the references to 'horizontal' and 'vertical' motion, 'horizontal' refers to that motion which it is desired to measure, whereas 'vertical' refers to movement of the specimen normal to its plane. This is illustrated in Fig. 4.16. In this illustration it will also be seen that the two transducers are placed on the specimen from opposite sides, as will have already been noticed from 4.12. This is necessary to allow the two stylii to be positioned virtually next to each other if required, without interference from the transducer bodies. Thus it will be necessary to connect one transducer to the circuit in the opposite manner to the other i.e., right and left channels reversed. This will become clear when an analysis of the calibration process for the transducers is given later.

Each pair of channels is then connected to a single stage differentially connected amplifier to obtain the difference in channel signals. This difference signal then passes to a variable gain amplifier, and both the difference signals from each transducer are connected to the final stage, which is a pair of cross-coupled, fixed-gain, differential input op. amps. Hence the single ended output will be proportional to the difference between the two transducer signals.

As will be discussed later, adjustment of the gains of the various stages is used to eliminate unwanted vertical mode signals and to compensate for the variation in sensitivities between transducer channels.

Since a large range of signals was anticipated, a simple resistive divider was provided at the output with carefully selected values to give 20 dB and 40 dB attenuations.

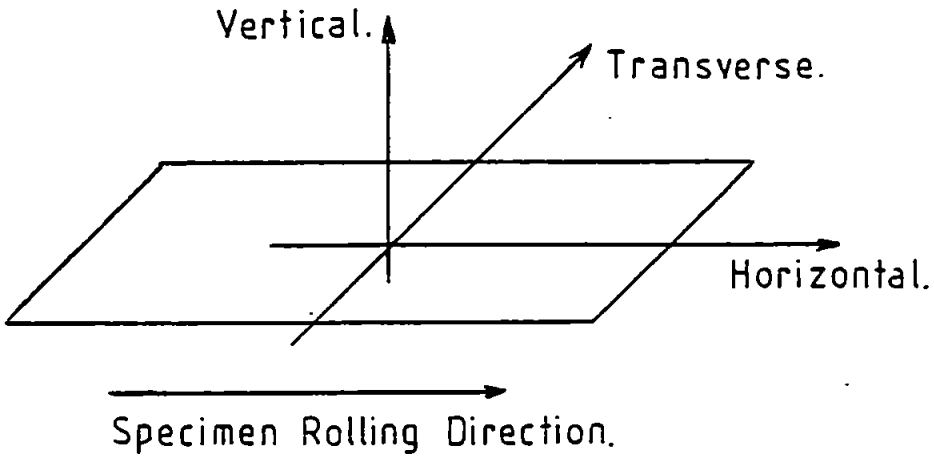

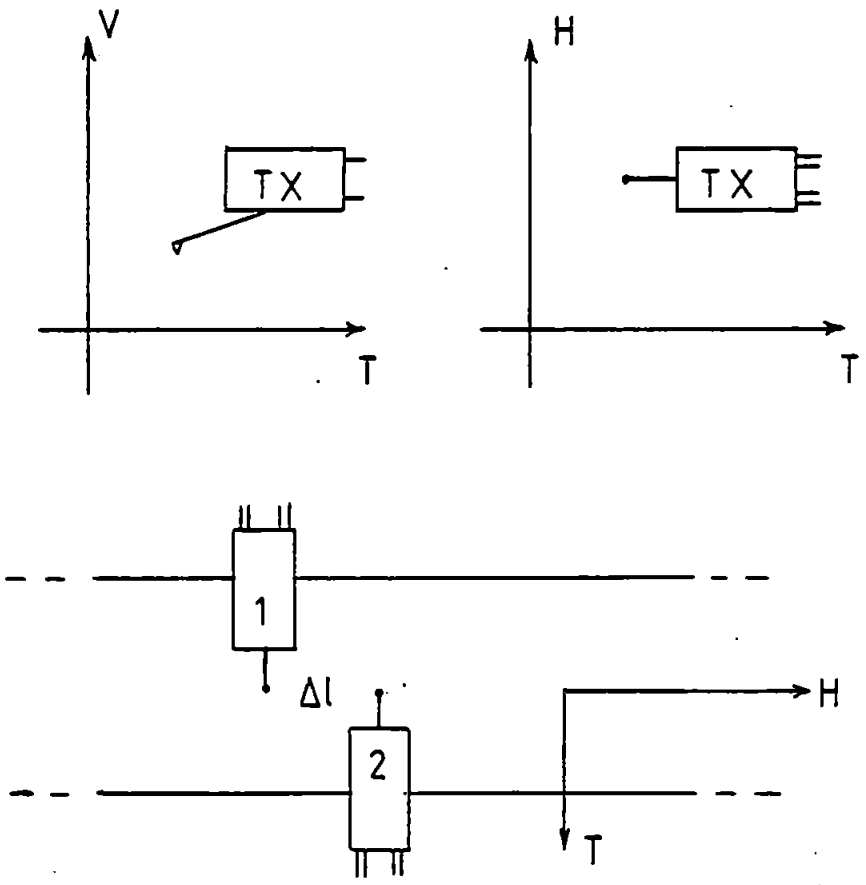

FIG. 4.16. Reference Directions for the Transducer Signals.

The Filters

For reasons already established it is now necessary to filter the transducer signal for analysis of the harmonic content. A B. & K. Type 2120 Frequency Analyser was available, but this was planned for other use in the frequency analysis of the flux waveforms. It was therefore considered desirable to design and build a separate analyser specifically for the purpose of this investigation.

The band-pass filter was designed around the second-order transfer function obtainable by connecting integrating amplifiers in series, as shown in Fig. 4.17.

It can readily be shown (29) that the transfer function of this circuit is given by

$$H(s) = \frac{\omega_{o_1}\ \omega_{o_2}\ S}{\omega_{o_2}\ S^2 + \frac{3R_B}{R_A + R_B}\ \omega_{o_1}\ \omega_{o_2}\ S + \omega_{o_1}\ \omega_{o_2}^2} \qquad \ldots\ldots\ldots\ldots\ldots\ldots\ 4.17$$

where $\omega_{o_1} = \frac{1}{R_1\ C_1}$, $\omega_{o_2} = \frac{1}{R_2\ C_2}$ $\ldots\ldots\ldots\ldots\ldots\ldots\ 4.18$

with reference to Fig. 4.17.

This is of the same form as a general second order band-pass function (30) and will have a magnitude and frequency response given by

$$H(j\omega) = \frac{Q}{\sqrt{Q^2\left(\frac{\omega}{\omega_{o_1}} - \frac{\omega_{o_2}}{\omega}\right)^2 + 1}} \qquad \ldots\ldots\ldots\ldots\ 4.19$$

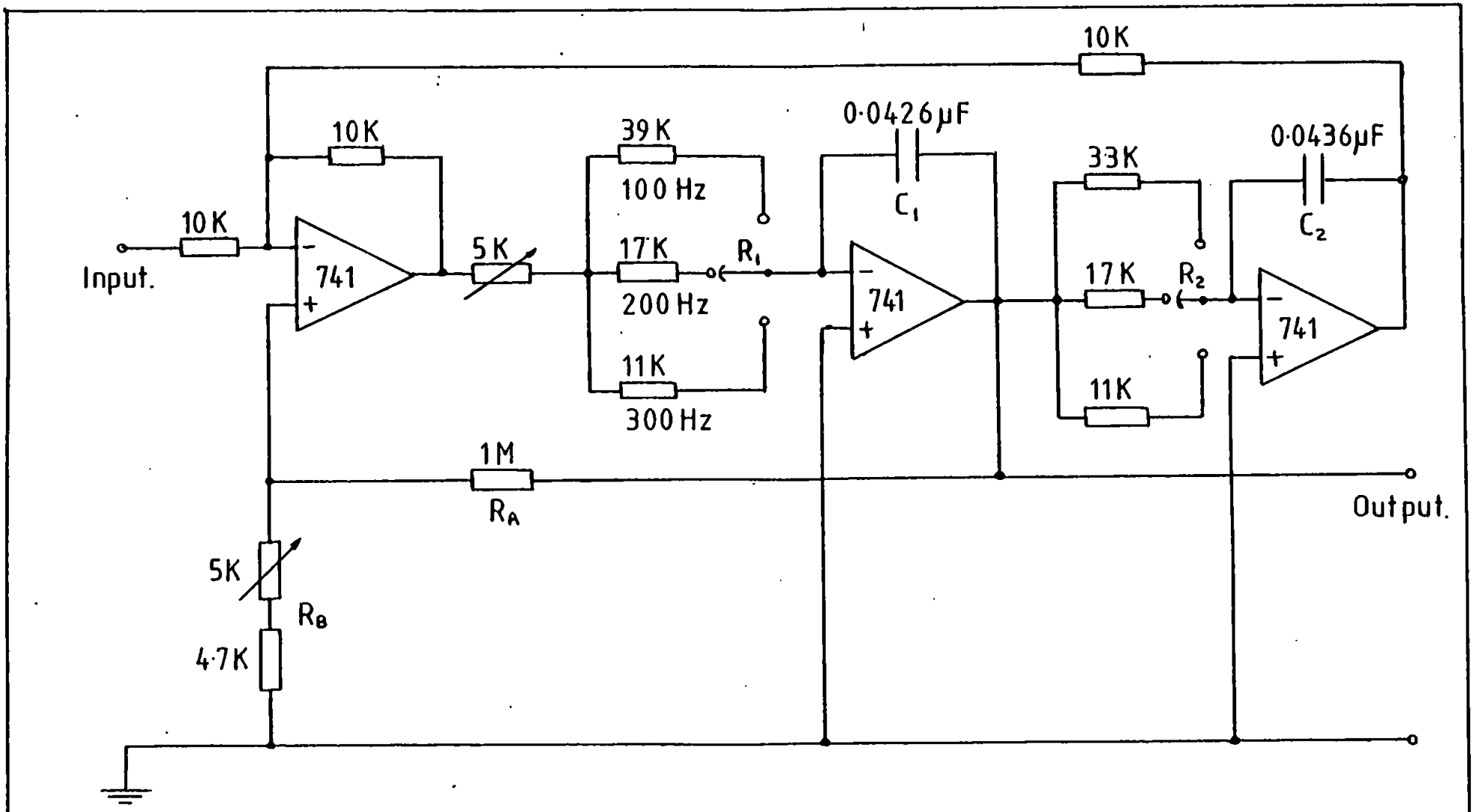

FIG. 4.17. The Band-Pass Filter.

$$\theta = \tan^{-1} Q \left(\frac{\omega}{\omega_{o_1}} - \frac{\omega_{o_2}}{\omega} \right) \qquad \ldots\ldots\ldots\ldots\ldots\ldots\ldots 4.20$$

where

$$Q = \frac{R_A + R_B}{3 R_B} \qquad \ldots\ldots\ldots\ldots\ldots\ldots\ldots 4.21$$

Thus when $\omega^2 = \omega_{o1} \cdot \omega_{o2}$ i.e., at resonance,

$$H(j\omega) = Q \text{ and } \theta = 0$$

Therefore, at resonance, the gain of the filter will be independant of frequency and there will be no phase shift through the filter. These are considered to be highly desirable qualities for this investigation.

By making ω_{o_2} have fixed values higher than the required centre frequency. and by making ω_{o_1} variable over a small frequency range below the required centre frequency, then ω_o may be varied over a small range. This was considered necessary to cater for small variations in 'main' frequency. For example, at ω_o of 200 Hz, the frequency range was 191 to 217 Hz.

Unlike other types of active filters using operational amplifiers, this circuit stability is not restricted by the level of Q (29). Hence Q could be made large and variable by the adjustment of R_B. At a Q value of 50, the filter response will be -38 dB at $\frac{1}{2}\ \omega_o$ and 2 ω_o, and the measured response is shown in Fig. 4.18.

4.2.4 Improvements to the Transducer Pre-amplifier

Initial magnetostriction measurements attempted with the pre-amplifier revealed significant phase shifts between transducers, creating disturbed 'butterfly loops' and large errors in measured strains. As has been described in the Error Analysis, very small phase shifts will contribute to large magnitude errors.

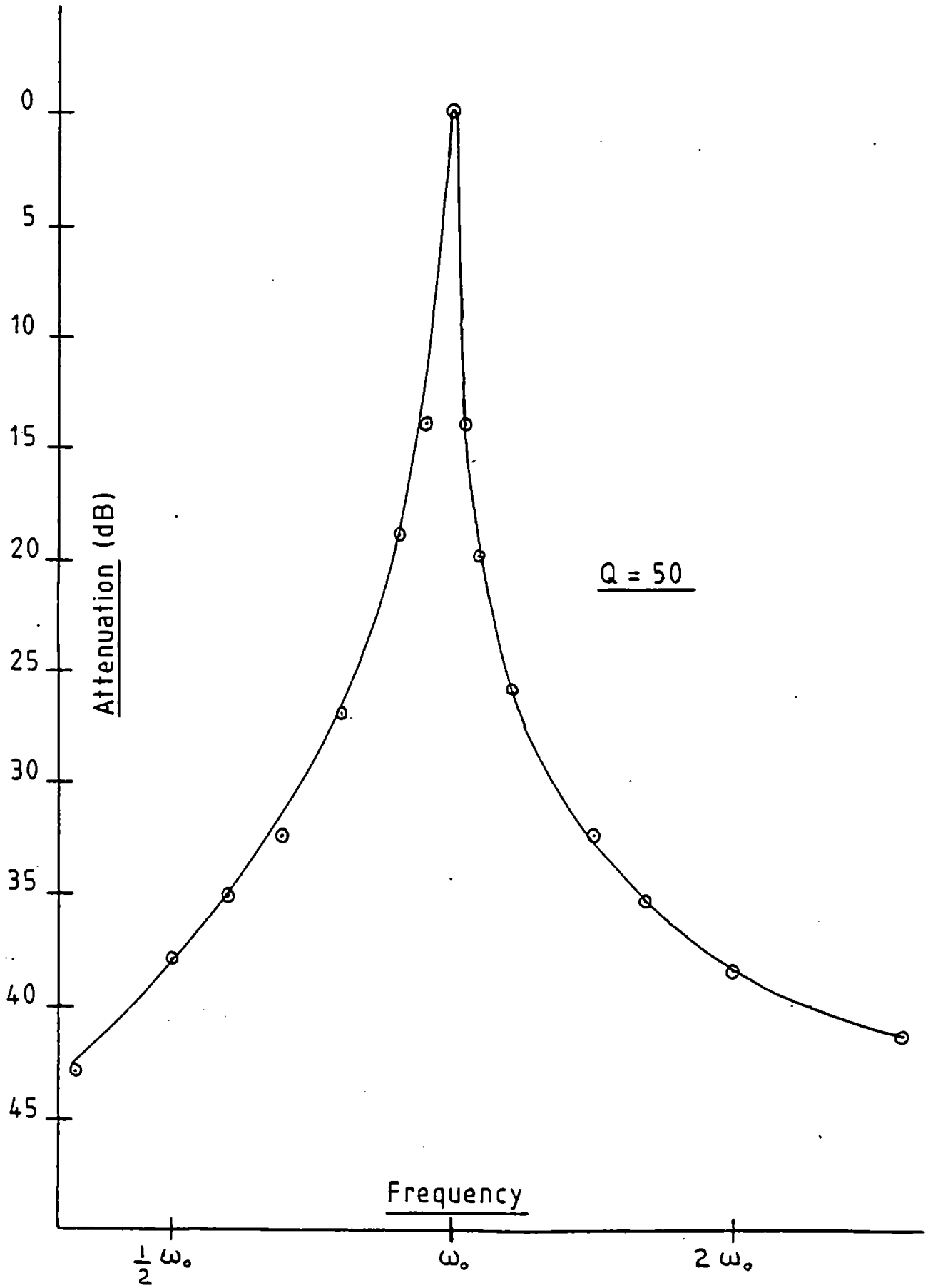

FIG. 4.18. Band-Pass Filter Response.

By driving the two transducers from equal sinewave sources at magnitudes equivalent to those of a typical magnetostriction signal, and by observing Lissajou figures of the two outputs, it was verified that small phase shifts, of the order of 2 - 8°, were indeed occurring between the transducers. The driving source used is described in a later section dealing with Calibration of the transducers.

Measurements of the capacitances of the transducers showed variations of up to ± 10% between channels and between transducers. This was the source of the phase errors since this capacitance is in parallel with the 10 MΩ. input resistances of the pre-amplifiers.

The circuit diagram of the pre-amplifier input stage for a single channel is reproduced in Fig. 4.19, (a), with an equivalent circuit shown in Fig. 4.19, (b).

The gain, K, of the cross-coupled input stage is given by (29)

$$K = 1 + \left(2 \frac{R_A}{R_B}\right) \qquad \ldots\ldots\ldots\ldots\ldots\ldots\ldots\ldots 4.22$$

and the magnitude and phase response of the input stage may be deduced as (30)

$$H(j\omega) = \frac{K}{\left[1 + \frac{1}{4\omega^2 C^2 R_p^{\,2}}\right]^{\frac{1}{2}}} \qquad \ldots\ldots\ldots\ldots\ldots\ldots\ldots\ldots 4.23$$

$$\phi(j\omega) = \tan^{-1}\left[\frac{1}{2\omega C R_p}\right] \qquad \ldots\ldots\ldots\ldots\ldots\ldots\ldots\ldots 4.24$$

For the values of the components selected, and with transducer channel capacitances lying between 720 and 880 pF, the phase shift at 100 Hz will lie between 5.2 and 6.3°.

In addition, the maximum gain of the input stages is ∞, creating too large an incremental gain when the 100 KΩ. trimmer is varied to adjust for differences between channel sensitivities.

To improve this circuit in the light of the Error Analysis previously conducted, the following modifications were made.

The gain of the input stage was reduced by simply adding a fixed resistor of 10 KΩ. in series with the 100 KΩ. trimmer. The maximum gain is thus limited to K = 201.

The phase shift may be reduced by increasing the value of R_p (see Fig. 4.19). However, this will reduce the bias current to the input stages, causing an increase in d.c. drift and jitter. Experiment put a limit of 33 MΩ. on R_p, for which phase shifts of the order of 2° will still occur at 100 Hz. Further decreases may be achieved by the inclusion of parallel capacitance, as shown schematically in the equivalent circuit of Fig. 4.19, (c). For this circuit the magnitude and phase responses will be (30):

$$H(j\omega) = \frac{2KC/2C + C_p}{\left[1+\frac{1}{\omega^2 R_p{}^2(2C + C_p)^2}\right]^{\frac{1}{2}}} \qquad \ldots\ldots\ldots\ldots\ldots\ldots\ldots\ldots 4.25$$

$$\phi(j\omega) = \tan^{-1}\left[\frac{1}{\omega R_p(2C + C_p)}\right] \qquad \ldots\ldots\ldots\ldots\ldots\ldots\ldots\ldots 4.26$$

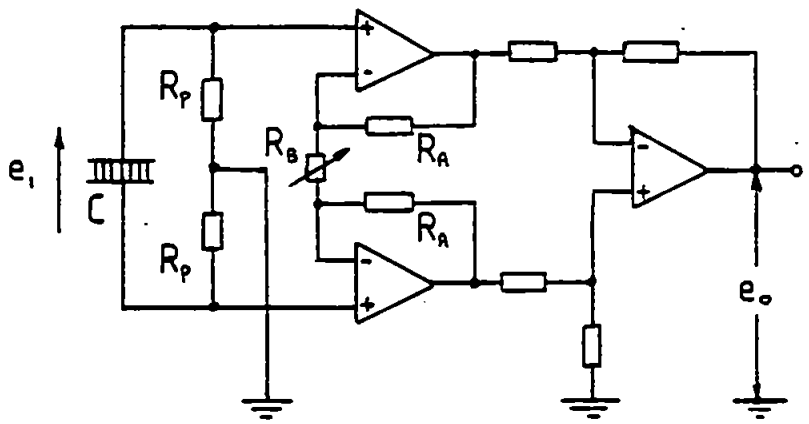

FIG. 4.19 (a). Input Stage Circuit Diagram.

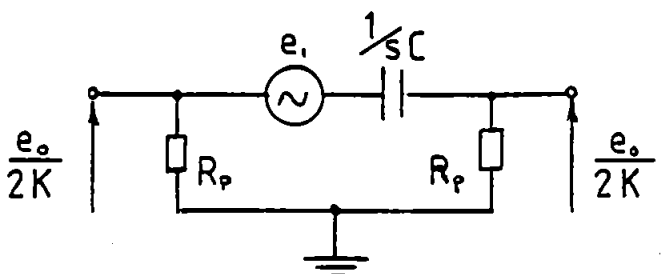

FIG. 4.19 (b). Equivalent Circuit of (a).

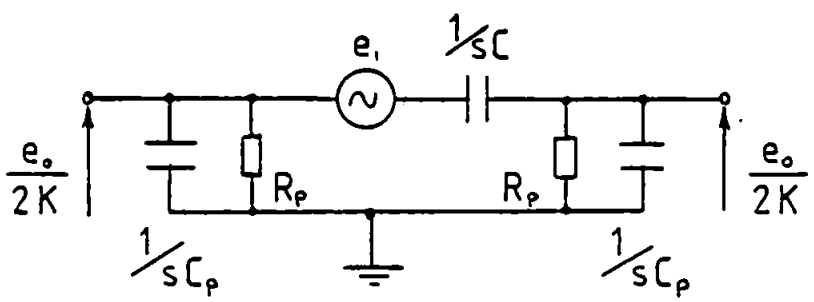

FIG. 4.19 (c). Equivalent Circuit of Modified Input Stage.

FIG. 4.19. Transducer Pre-amplifier Input Stage.

However, C_p cannot be made too large as this will attenuate the input by a factor of $2C/(2C + C_p)$, and, since it has been necessary to reduce the gain of the input stage, the overall design will be a compromise between the levels of C_p, R_p and K.

After experimentation, C_p was made 0.01 μF, for which the phase shift will be 0.25° at 100 Hz with a transducer channel capacitance of 800 pF. The overall channel gain will then be 0.138 K, having a maximum value of 28. Experiments showed this to be acceptable.

The final design of the input stages incorporated into the overall pre-amplifier circuit is shown in Fig. 4.20.

Lissajou figure analysis of each individual transducer now showed that there was no detectable phase shift between channels, but that a phase shift was apparent between the two transducers, being of the order of 2°. The Error Analysis showed that this was unacceptable, and in order to compensate for it a phase shifting network was incorporated into the pre-amplifier.

A circuit diagram of the phase shifter is shown in Fig. 4.20, connected between the two halves of the pre-amplifier dealing with each transducer, and before the final, cross-coupled, differential output stage, (points A and B in Fig. 4.20). It was decided to switch the phase-shifter between three, equal capacitors so that for the frequencies of interest (100, 200 and 300 Hz) the characteristic time of the circuit could be kept constant without re-adjustment of the trimmer resistor. The magnitude and phase response of this circuit is given by (30):

$$H(j\omega) = \frac{1}{\sqrt{(1 + \omega^2 C^2 R^2)}} ; \phi(j\omega) = \tan^{-1} \omega RC \quad \ldots\ldots\ldots\ldots 4.27$$

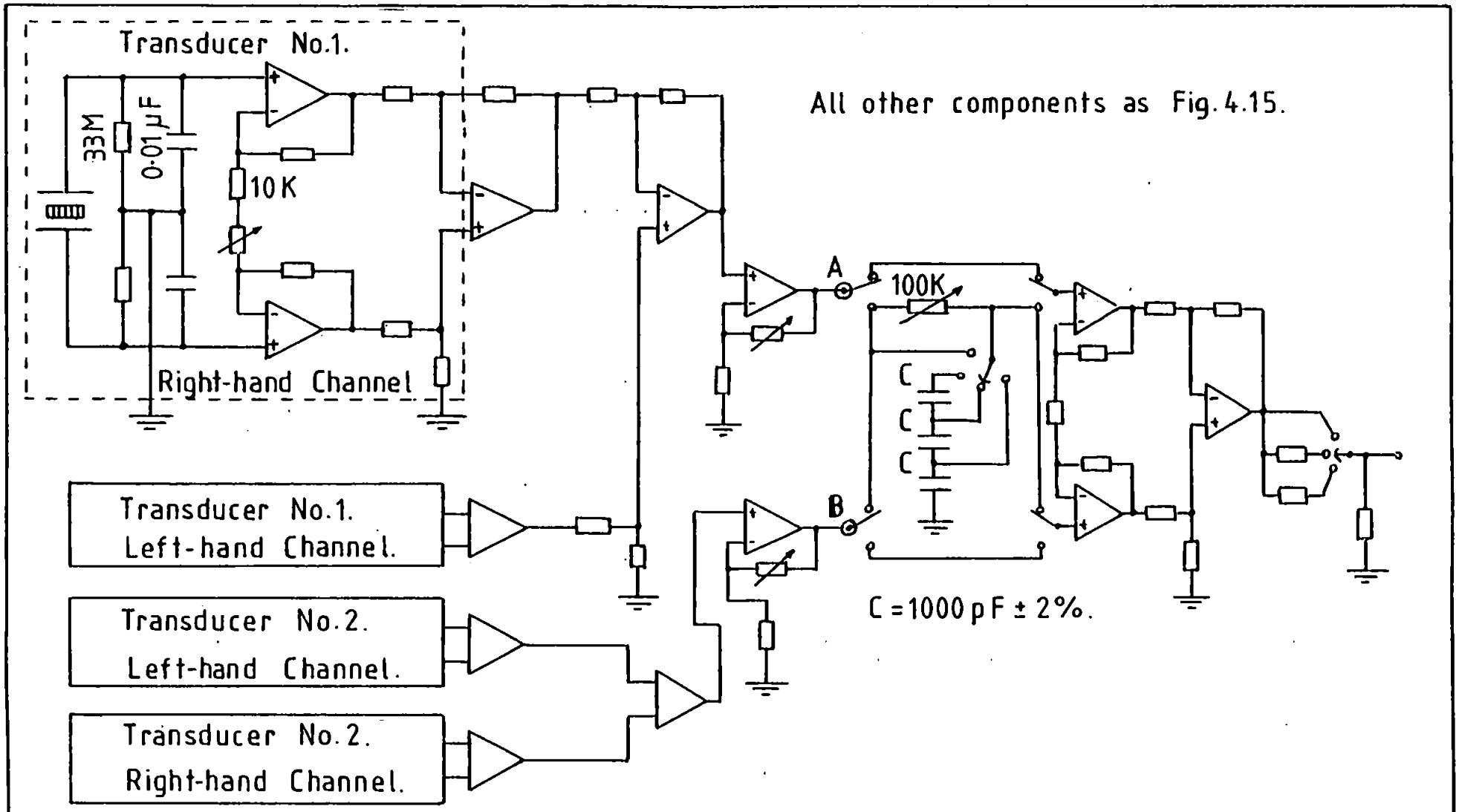

FIG. 4.20. The Modified Transducer Pre-Amplifier.

The values of R, C, were chosen so that there was negligible attenuation, and so that the maximum phase shift was about 3^{o}. Thus, for a 20 turn trimmer resistor, small adjustmants in the order of 0.1^{o}, as required by the Error Analysis, could be made.

Lissajou figure analysis of the complete system, driving the transducers simultaneously from a sine-wave source over a range of frequencies and magnitudes, showed that there was now negligible phase shifts between the input and output.

4.2.5. Magnetostriction Calibration

As the magnetostriction system relies on the nulling of 'vertical' components of vibration, it is essential to provide a uni-axial source of known displacement with which to set up and calibrate the system.

For this purpose, a vibrating block constrained to move along only one axis was built, and this is shown in Figs. 4.21 and 4.22.

Basically it consists of a steel cube, of side 25 mm., with machined flat surfaces, supported by leaf springs made from strips of silicon-iron. The springs allow longitudinal motion of the block, but not transverse or vertical motions. The block is excited by a small vibrator, driven directly from a signal generator. The vibration amplitude is detected by a B and K type 4331 accelerometer connected to the Frequency Analyser already mentioned.

Vibration amplitudes are obtained by measurement of the acceleration level at a known sinusoidal frequency, and then computing the displacement from well known S.H.M. relationships.

The transducer head can be inserted into the calibration apparatus in either vertical or horizontal modes, thus detecting the equivalent of horizontal or vertical motions as represented by the specimen. Both these positions are shown, along with the accelerometer and associated pre-amplifier.

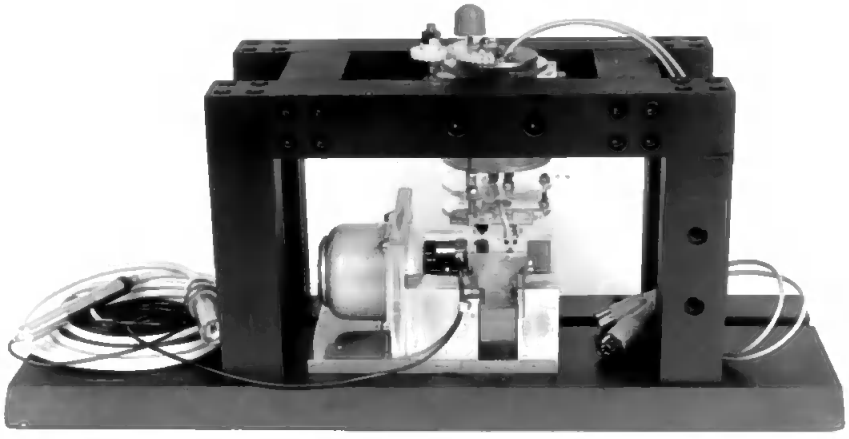

FIG .4.21. The Vibrating Block showing Horizontal Calibration.

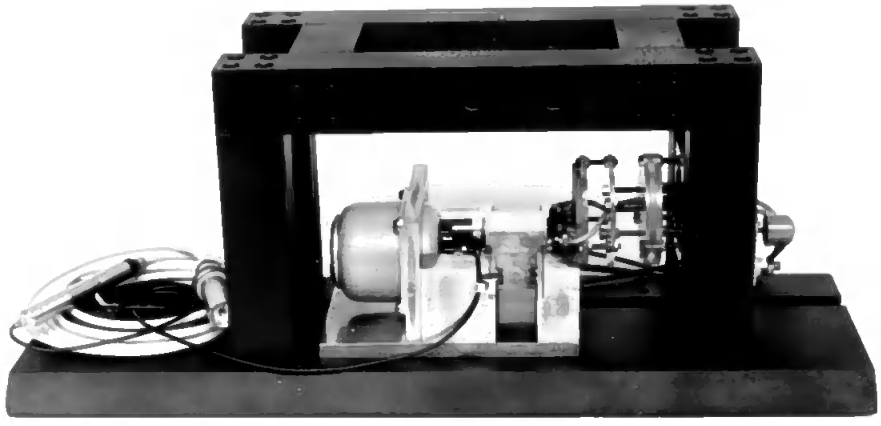

FIG .4.22. The Vibrating Block showing Vertical Calibration.

A substantial steel structure was built to carry the vibrating block and transducer head to avoid any resonance effects whereby the mounting frame would be energised with some phase shift with respect to the block.

A description of the calibration process now follows, which includes an analysis of the behaviour of the transducer amplifier circuits. A schematic diagram of the circuit is shown in Fig. 4.23.

Considering two transducers, TX1 and TX2, connected to the pre-amplifier in the fashion previously discussed such that the "right" and "left" channels are reversed for one transducer.

Let the sensitivities to "horizontal" deflections be A and B for the "left" and "right" channels respectively of one transducer, and D and C the corresponding sensitivities for the second transducer. Let the appropriate sensitivities to "vertical" deflection be P, Q, S and R respectively.

Assume that both transducers are now driven from a source equivalent to a horizontal motion H, or from a source equivalent to a vertical motion V, where H and V can represent peak, peak to peak, r.m.s. or instantaneous values of the dynamic vibration. The response of the system will now be considered for each type of motion.

The signal levels to each differential input amplifier will be as shown in Fig. 4.23 where the "vertical" responses of the transducers will have the same sign for all four channels (as indicated by + or -) and for which terminal 1 was arbitrarily taken as being negative with respect to terminal 2. The responses to "horizontal" signals was also arbitrarily selected with terminal 1 positive with respect to terminal 2 for transducer TX1. This immediately determines the polarity of the other terminals since, as discussed in section 4.2.1, "left" and "right" channels will produce opposite polarity outputs due to "horizontal" motions, and since the two transducers have been connected in the reverse fashion. It is important to realise that the following

description will still apply even if the arbitrarily chosen polarities are reversed for either, or both, "horizontal" or "vertical" motions.

Further examination of the schematic diagram of Fig. 4.23 will show that the resultant signal produced by each transducer at points X and Y in the circuit is given by:

$$+ \ 2H \ (Ak_1 + Bk_2) \quad \text{for TX1} \quad \text{at point X,}$$

and

$$+ \ 2H \ (Ck_3 + Dk_4) \quad \text{for TX2} \quad \text{at point Y}$$

due to a "horizontal" driving source and:

$$+ \ 2V \ (Qk_2 - Pk_1) \quad \text{for TX1} \quad \text{at point X,}$$

and

$$+ \ 2V \ (Sk_4 - Rk_3) \quad \text{for TX2} \quad \text{at point Y}$$

due to a "vertical" driving source. The variable gains of each differential input amplifier are represented by k_1, k_2, k_3 and k_4 respectively.

Thus assuming that there are no phase shifts (introduced due to the transducers) between the relevant signals, the "vertical" components of the resultant signals can be set to zero by judicious adjustment of the variable gains. In practice it was found possible to achieve this by adjustment of one gain control per transducer, leaving the other control set at minimum to avoid over-driving the input stages.

Having set the "vertical" responses to zero, the response to "horizontal" motions can be considered. Each transducer signal is now passed to a stage of variable gain shown by amplifiers k_5 and k_6 in Fig. 4.23 and the two signals are then combined in the differential output stage k_7. It will be seen that the total output signal due to "horizontal" motions is given by

$$2H \ [k_6 \ (Ck_3 + Dk_4) - k_5 \ (Ak_1 + Bk_2)] \ k_7$$

where k_7 is the gain of the output stage.

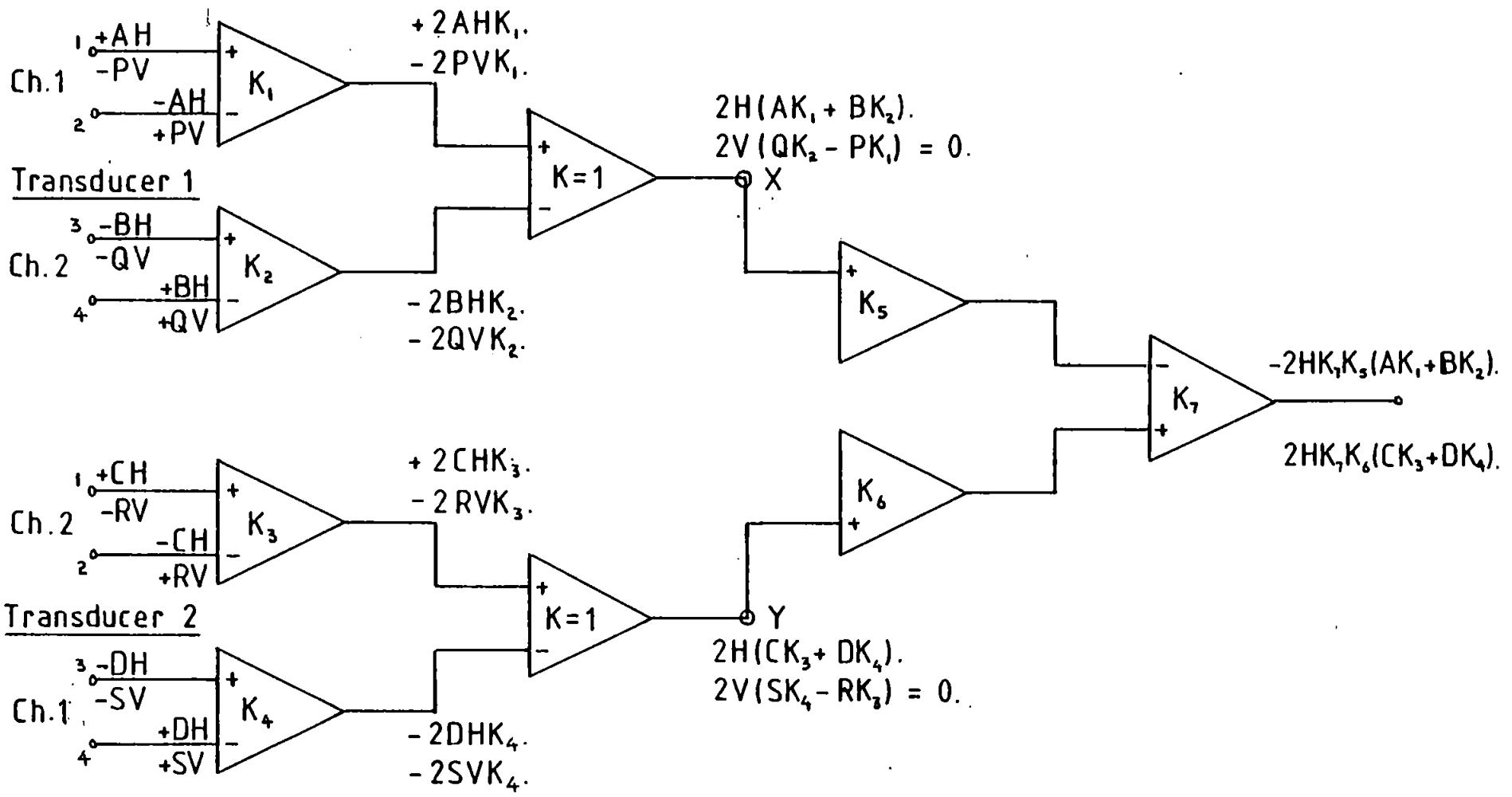

FIG. 4.23. Schematic Diagram of Transducer Pre-amplifier.

Due to the adjustments made to k_1, k_2, k_3 and k_4 during cancellation of the "vertical" signals, and due to the differences in channel sensitivities A, B, C and D inherent in the transducer design, the quantities $(Ck_3 + Dk_4)$ and $(AK_1 + Bk_2)$ will in all probability be different. Adjustment of the gain k_5 and k_6 can then be made so that the above expression will become zero, again assuming no phase shifts between the relevant signals. As before, it was found possible to achieve this by adjustment of one gain control only, the other being set at its minimum value, having established by experiment which channel was producing the lower output and re-connecting the inputs accordingly.

Thus by subjecting both transducers to equal "horizontal" or "vertical" motions in the calibration process, the final output of the pre-amplifier will be zero for either type of motion.

Now let the "horizontal" motion experienced by one transducer (e.g., TX1 in Fig. 4.23) change to $H \pm \Delta H$ and the "vertical" motion change to $V \pm \Delta V$ between the two tranducers. The resultant signals produced at points X and Y by each transducer will then be

$$2(Ak_1 + Bk_2).(H \pm \Delta H) \quad \text{or} \quad 2(Qk_2 - Pk_1).(V \pm \Delta)$$

and

$$2(Ck_3 + Dk_4).\ H \qquad \text{or} \quad 2(Sk_4 - Rk_3).\ V$$

But by previous calibrations the quantities $(Qk_2 - Pk_1)$ and $(Sk_4 - Rk_3)$ have been made zero, so that the outputs due to "vertical" motions will still be zero.

The total output signal due to the "horizontal" motions will now be given by:

$$2[k_6(Ck_3 + Dk_4)H \ - \ k_5(Ak_1 + Bk_2)(H \pm \Delta H)]k_7$$

But by previous calibrations the quantities $k_6(Ck_3 + Dk_4)$ and $k_5(Ak_1 + Bk_2)$ have been made equal in magnitude, so that the resultant, total output signal will be:

$$\pm \; 2k_5(Ak_1 + Bk_2).\Delta H.k_7$$

or

$$\pm \; 2k_6(Ck_3 + Dk_4)\Delta H.k_7$$

That is, the output is proportional to ΔH and contains no signal proportional to V or ΔV. Hence the device is now responsive only to the differential, horizontal motion between the two transducers.

The calibration process, to be performed prior to any new set of magnetostriction measurements and for each discrete frequency of interest, is therefore as follows.

The transducer head is set up to sense 'vertical' motion, as in Fig. 4.22 and the pre-amplifier gain controls adjusted to give a null output. The driving source magnitude is then manually swept and the controls readjusted as required for best nulling. It was found possible to achieve 'vertical' mode cancellations to within 1% of maximum signal levels, up to 1 mm. peak-peak displacements at 100 Hz.

The transducer head is then set up to sense 'horizontal' motions, as in Fig. 4.21. At the same frequency as before, the vibrating block is set to vibrate at the maximum amplitude anticipated. For example, with a transducer position equivalent to 5 cm. from the clamped end of the specimen and a strain of 30 με, the equivalent longitudinal motion would be 1.5 μm (peak-peak). At 100 Hz this corresponds to an r.m.s. acceleration signal of 0.02135g, as detected by the accelerometer attached to the vibrating block. For an accelerometer sensitivity of 35.3 mV/g, a signal level of 753.7 μV (r.m.s.) is available.

The pre-amplifier gain controls (amplifiers k_5 and k_6 in Fig. 4.23) and the phase shifter trimmer resistor are now successively adjusted to give a null

output. Manual sweeping of the driving source checks the linearity of the system, and the calibration process is repeated as often as necessary to achieve the best null over the range of amplitudes. At the null point, the percentage error in magnitudes and any phase shift is measured, using an X-Y oscilloscope, and, from the Error Analysis, the minimum transducer separation can be calculated for a 5% error at the measuring position chosen on the specimen.

One transducer is then disconnected, so that the output will be that due to the known amplitude of vibration at the block. This level can be used to set a deflection sensitivity on an X-Y plotter (to be described in section 4.5). The driving signal can then be swept, and linearity/calibration curves obtained, typical examples of which are shown in Fig. 4.24.

4.3 The Stressing Apparatus

4.3.1 Introduction

This apparatus is required to hold a half-Epstein sample and to apply longitudinal stresses without buckling the material but yet not restricting free motion of it. An important consideration is that no ferromagnetic material may be used in its construction.

As consideration also needs to be given to obtaining access to both flat surfaces of the specimen, in order that simultaneous strain measurements and domain observations can be made from opposite sides, it was decided to mount the specimen on edge, with its long side horizontal.

4.3.2 The Apparatus

Various views of the mounting stage are shown in Figs. 4.25 and 4.26. The specimen is mounted between two aluminium stretchers, each consisting of two parts; the smaller part into which the specimen fits has a 0.4 mm. wide slot milled precisely along its centre line, into which the specimen is finally glued. This part is detachable from the longer, vertical part, which is in turn clamped rigidly to the aluminium, L-shaped base plate at one end of the specimen, the

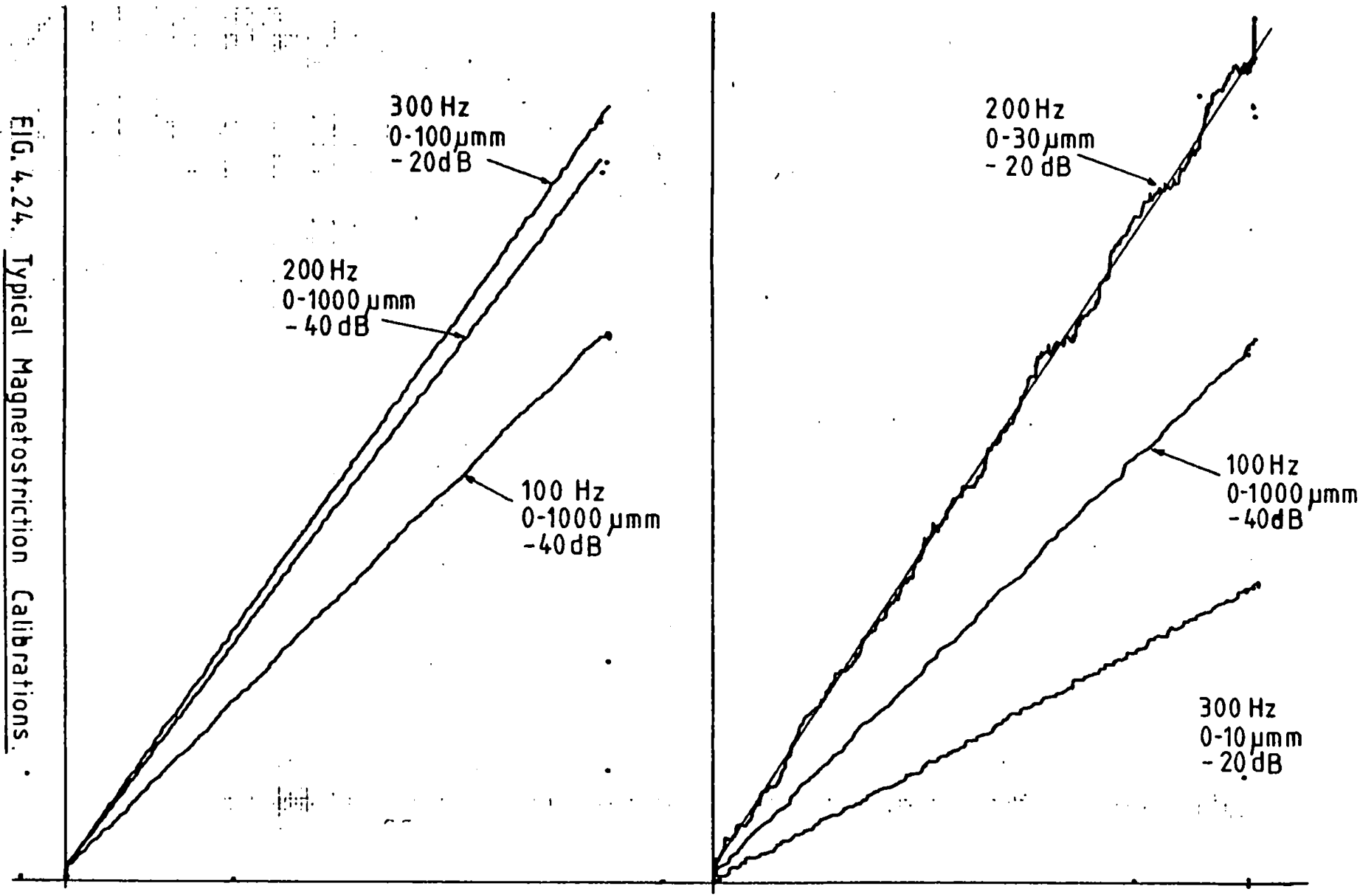

FIG. 4.24. Typical Magnetostriction Calibrations.

other stretcher being constrained to move along the longitudinal axis of the specimen by means of aluminium guides running in polished tufnol tubes. It is at this end that the stressing will be applied. The basic assembly is carefully machined and assembled so that the specimen lies precisely along a horizontal axis within a tolerance of 0.125 mm.

To restrain buckling of the specimen when under compressive stress, anti-buckling rails are provided along its length allowing ± 0.080 mm. lateral movement. These rails are made from 18/8 austenitic stainless steel which is non-magnetic and allows a high quality of machining accuracy. A complete sheet covers one side of the specimen with a central rectangle removed to allow access by the domain observation equipment. Slots are provided for positioning of search soils around the whole specimen. The back face of this sheet has an 0.5 mm. groove milled along its length and of the width of the specimen, into which the specimen lies. On the other side of the specimen two sheets of stainless steel extend only to cover 0.80 mm. of each edge, these sheets being clamped to the front sheet. Thus the specimen is lying in a slot of width 0.5 mm. The assembled anti-buckling rails are clamped into top and bottom brass runners which are securely screwed to the base plates.

During assembly the rails are shimmed in the runners so that the centre line of the 0.5 mm. slot is consistent with the slots in the aluminium stretchers. This is achieved by sliding a dummy specimen through the rails until it mates without interference into the stretcher slots.

Fig. 4.27 shows a rear view of the specimen stage revealing the back face of the anti-buckling rails.

The original design for applying longitudinal stresses to the specimen was by means of two compression springs acting in opposition. This arrangement is shown in Fig. 4.25. An extension arm is connected to the moveable stretcher and spring forces are applied to the extension arm by screwing down on knurled thumb nuts which run along studding fitted securely to the base frame of the

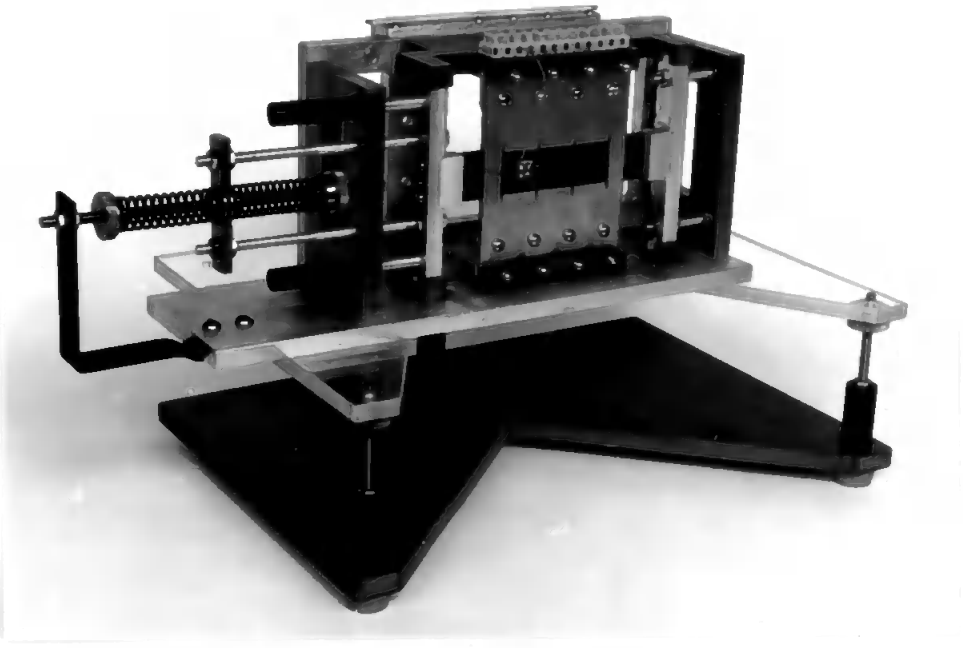

FIG. 4.25. The Specimen Mounting Stage showing 'Spring-loaded' Stressing.

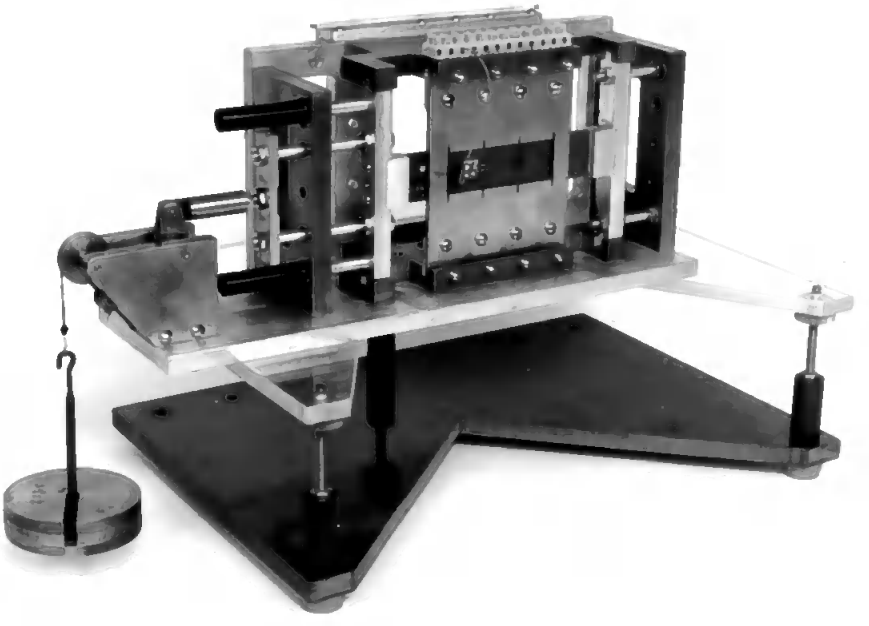

FIG. 4.26. The Specimen Mounting Stage showing 'Dead-weight' Stressing.

assembly and along the centre line of the specimen. Depending on which spring is the more compressed will determine whether compressive or tensile loads are applied. The springs used had stiffnesses of about 25 kg/m. enabling movements of up to 25 mm. for loads up to 7 MN/m^2 at the specimen.

Subsequent attempts at calibration of this system revealed considerable hysteresis in the strain-load relationships. This was due to the springs 'winding-up' when rotating the thumb nuts. In an attempt to alleviate this, roller bearings were fitted at each end of the spring - a single bearing can be seen in place in Fig. 4.25 - to allow free rotation. However, a significant level of hysteresis was still obtained, and since calibration of compression springs is notoriously difficult, this method of loading was abandoned.

The method finally adopted is shown in Fig. 4.26. Again, an extension arm on the moveable stretcher is used to pick up the loading forces, but this time the load is applied by dead-weights whose effect is transmitted via a pulley and lever arm. A section of this system is shown in Fig. 4.28. The pulley, lever arm and extension arm of the lever are all mounted on small roller bearings in order to reduce friction to a minimum. The lever arm is designed to give a 2:1 ratio to the loading forces so that excessive weights would not be required. Depending on which side of the pulley the weights are suspended will determine whether compressive or tensile loads are applied to the specimen. Each dead-weight was machined individually so that after calibration of the stressing system the overall applied stress could be determined with reference to the weight used.

Subsequent strain measurements revealed no hysteresis with the dead-weight system adopted.

4.3.3 Calibration of the Stressing Apparatus

Due to the elastic properties of silicon-iron varying with the state of stress because of the magnetostriction, no single figure of Young's modulus

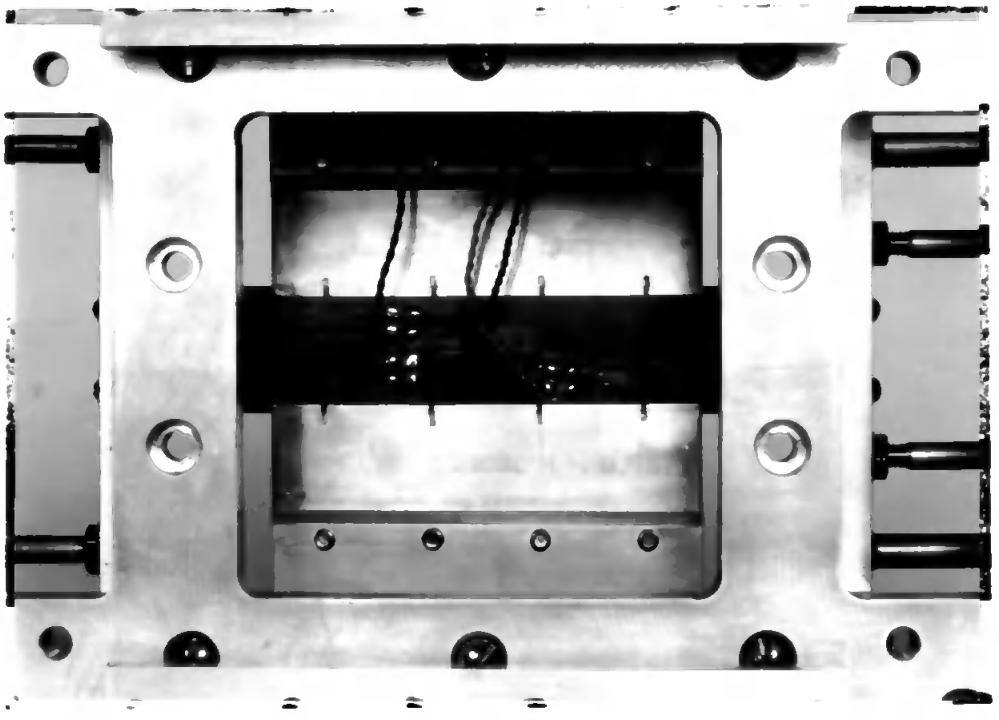

FIG. 4.27. A Rear View of the Specimen Stage showing the Anti-buckling Rails & a Strain-gauged Copper Specimen.

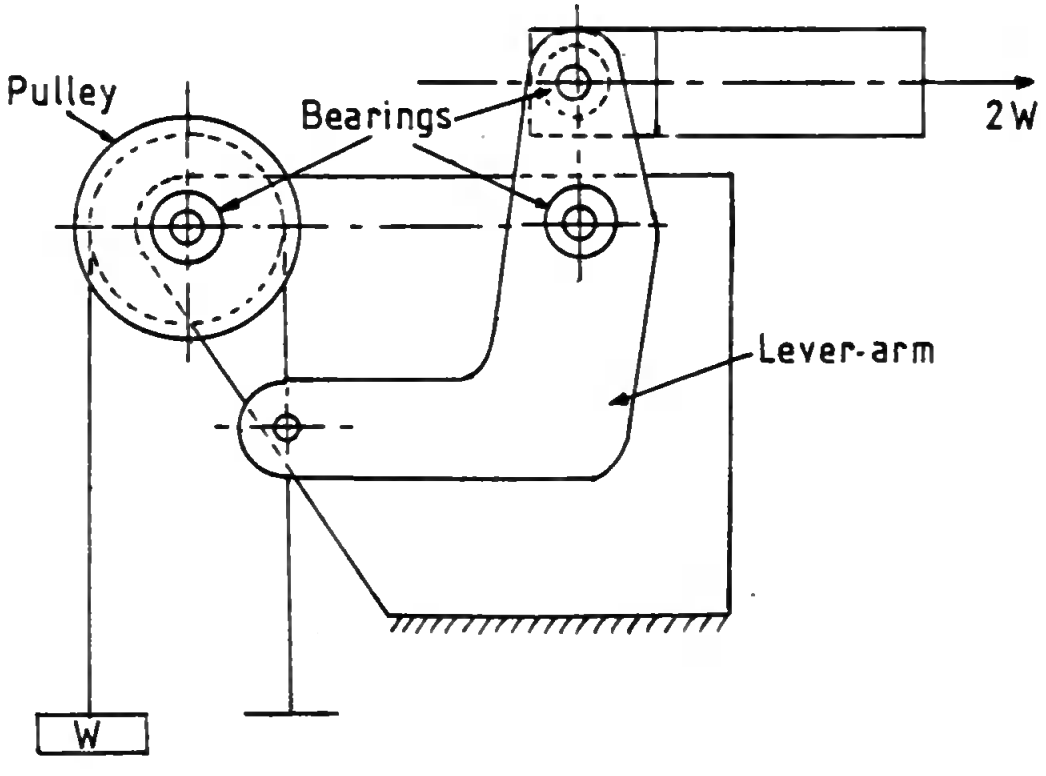

FIG. 4.28. The 'Dead-weight' Stressing Apparatus.

can be used to describe the stress/strain behaviour of such material, since the stress/strain curves will be non-linear at low stresses. This phenomenon, known as the ΔE effect, has been well described by other workers (4, 31). It is, therefore, necessary to use a non-magnetic, homogeneous material to replace the silicon-iron specimen during calibration.

To achieve this, cold rolled copper to BS 1432:1970 , was used, cropped to the same shape as the specimens (i.e., half-Epstein lengths) and assembled into the mounting stage in an identical fashion as the specimens. Strain gauges were attached to the copper strips, with three gauges spaced symmetrically on one side, and a single gauge on the reverse side, as previously shown in Fig. 4.27. The gauges used were temperature compensated for stainless steel, which has a temperature coefficient very similar to copper, and the cement used was a cyanoacrylate-based adhesive.

Young's Modulus for the material was determined as follows. Further half-Esptein strips were cut from the same sheets as the original strips used for strain gauging. Three strips of each thickness were then cropped into dumbell shapes suitable for mounting into a Tensile Testing machine. All the strips were then strain relief annealed at 450° for 1 hour using the same technique as used for sample preparation of the silicon-iron specimens (see section 4.1.2).

The cross sectional area of each strip was determined by averaging micrometer readings along the test length, and the test length was measured by a vernier-caliper. Each prepared strip was then mounted in turn into the tensile testing machine and stress/strain curves produced up to a stress of 20 MN/m^2.

At this stage it was discovered that the copper had a non-linear stress/strain relationship, as will be seen by reference to Fig. 4.29. Further investigation led to the discovery that this phenomen has been the subject of research (32) and that the determination of E for copper at low stress levels does present problems.

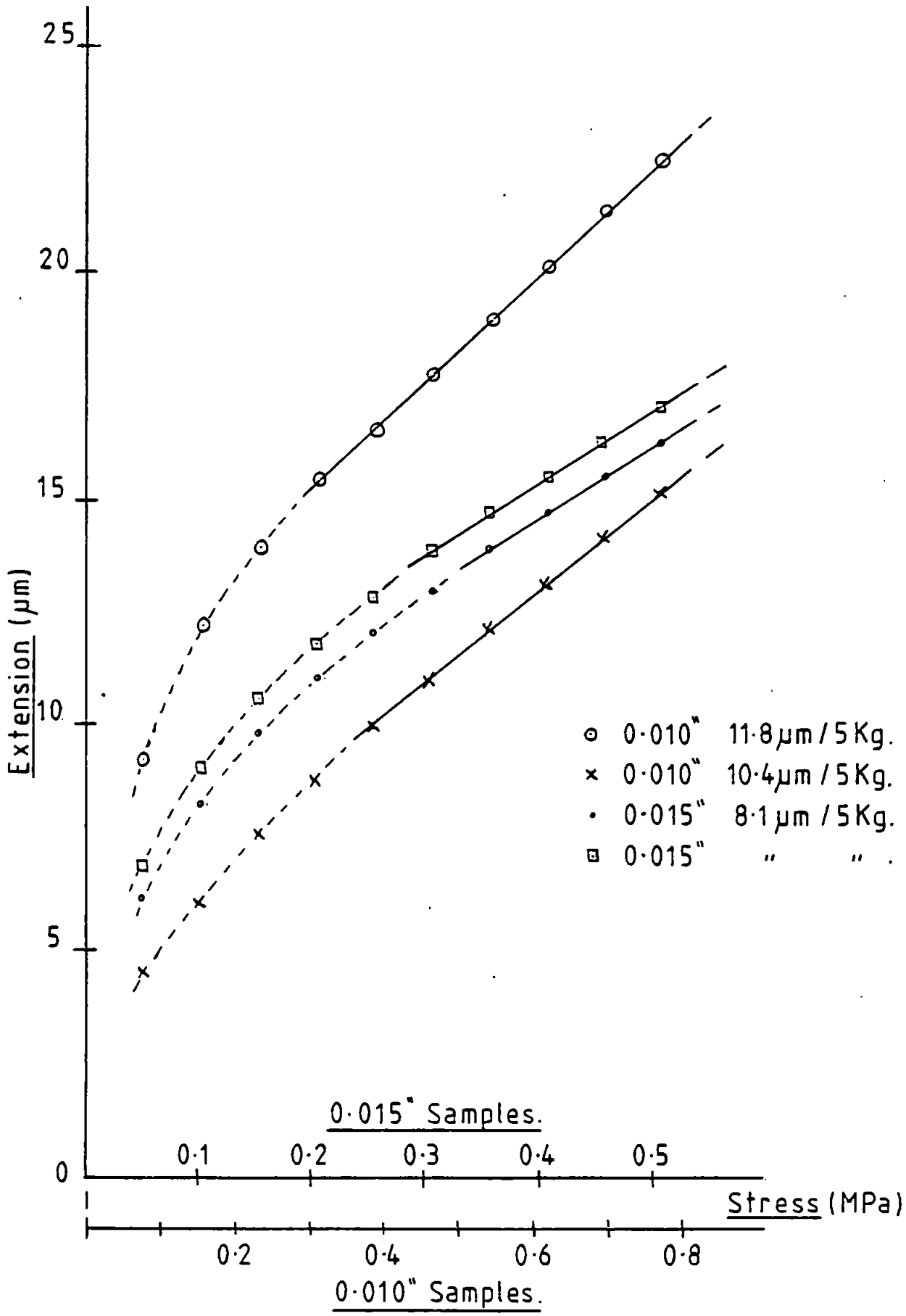

FIG. 4.29. Stress-Extension Curves for Copper at Low Stress Levels.

However, by averaging out the readings of the linear portions of the curves obtained, a value of E was determined which was not dissimilar from manufacturer's figures for the type of copper being used. It was, therefore, decided to use this figure during the calibration of the stressing equipment.

With a suitably strain gauged strip mounted into the specimen stage, the strain as detected from each gauge in turn was measured by connecting the relevant gauge into a four arm bridge, the other three arms being three gauges on a spare strip placed close to the mounted strip. Thus full temperature compensation was employed. The bridge output was monitored on a strain meter and strain levels recorded for increasing and decreasing compressive and tensile stress, applied by dead weights hung onto the lever arm.

Using the value of Young's Modulus previously determined, the levels of stress were computed and compared to values obtained from the mass of the weights divided by the cross sectional area of the strip.

By this means it was found that the stresses in the specimen could be determined from the known mass of the weights, to a tolerance of ± 10%, as shown in Fig. 4.30. It is considered that this error is acceptable, since the actual stresses occurring in built-up transformer cores are not exactly known.

4.4 Specimen Excitation

4.4.1 Excitation and Flux Measurement

The basic assembly is again shown in Fig. 4.31 but with the anti-buckling rails omitted and the magnetising coils fitted. Each coil consists of 750 turns of 27 SWG wire wound on a rectangular Perspex former, the internal dimensions of the coil being 22 x 40 mm. The two coils are connected in parallel to the source of excitation which is described below. The specimen shown in Fig. 4.31 has search coils mounted at 10 mm. intervals about the centre line to enable the symmetry of flux distribution along the length of

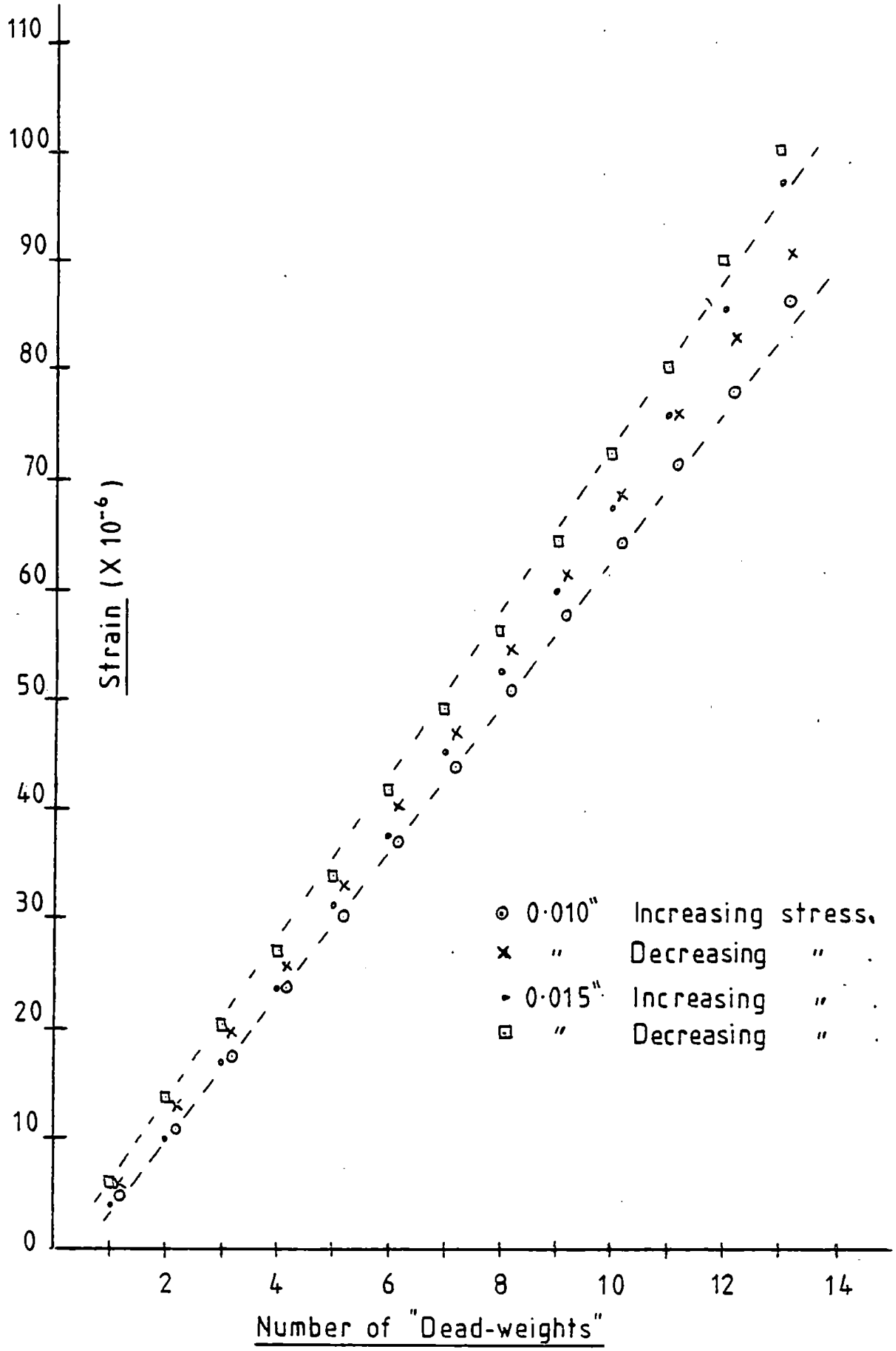

FIG. 4.30. Stress Calibration of Specimen Stage.

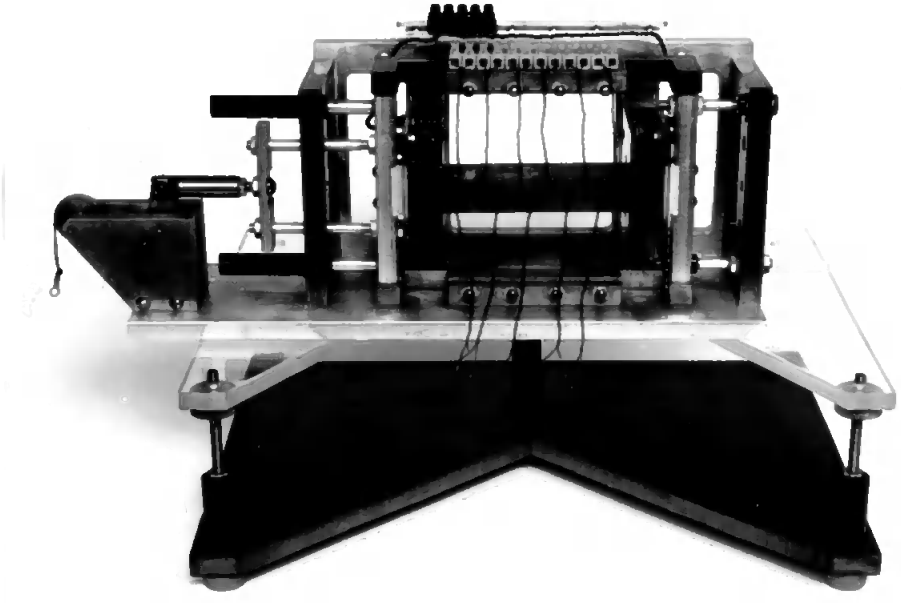

FIG. 4.31. The Specimen Stage showing the Magnetising Coils and a Multi-Search-coil Specimen.

the specimens to be determined. The magnetising coils are mounted in slots in the vertical base plates so that optimum positioning could be achieved for good flux uniformity. By this means it was determined that the flux density was consistent within 2% up to 40 mm. each side of the specimen centre and 3% up to 50 mm. each side. This was achieved at levels up to 1.9T flux density.

The source of excitation was an 'Advance' Type J1B A.F. signal generator driving a 'Texan' 25W Audio Stereo Amplifier, only one channel being driven. The circuit diagram is shown in Fig. 4.32 which also includes the flux measuring circuits and flux waveshape control circuits to be described later. A 1Ω resistor is included in series with the magnetising coils enabling a signal proportional to magnetising current to be obtained. This is used to derive a signal proportional to magnetising force for subsequent oscilloscope display of the magnetising characteristics of specimens.

In order to obtain a signal proportional to flux density, single turn search coils were employed, either wound around the entire specimen or through 0.25 mm. holes drilled at grain boundaries during the specimen preparation stage. Since the e.m.f. induced in the coil is a function of the rate of change of flux linkage, it is necessary to integrate the search coil output, and by including the cross section of the specimen, the flux density may be obtained.

As an approach to producing an integrator, a high input impedance, F.E.T., operational amplifier with capacitive feedback was used. However, at the very high levels of gain required to produce a satisfactory signal level from the very small search coil output it was found that such an arrangement was unstable, due to the d.c. drift inherent in such devices, and due to this d.c. charging up the capacitor to supply rail voltages. A passive RC integrator was therefore used, made from a 1 MΩ resistor and 1 μF capacitor. This circuit is d.c. coupled into a stage of high gain followed by a buffer amplifier. Accurate comparison of input and output signals showed the device to be integrating

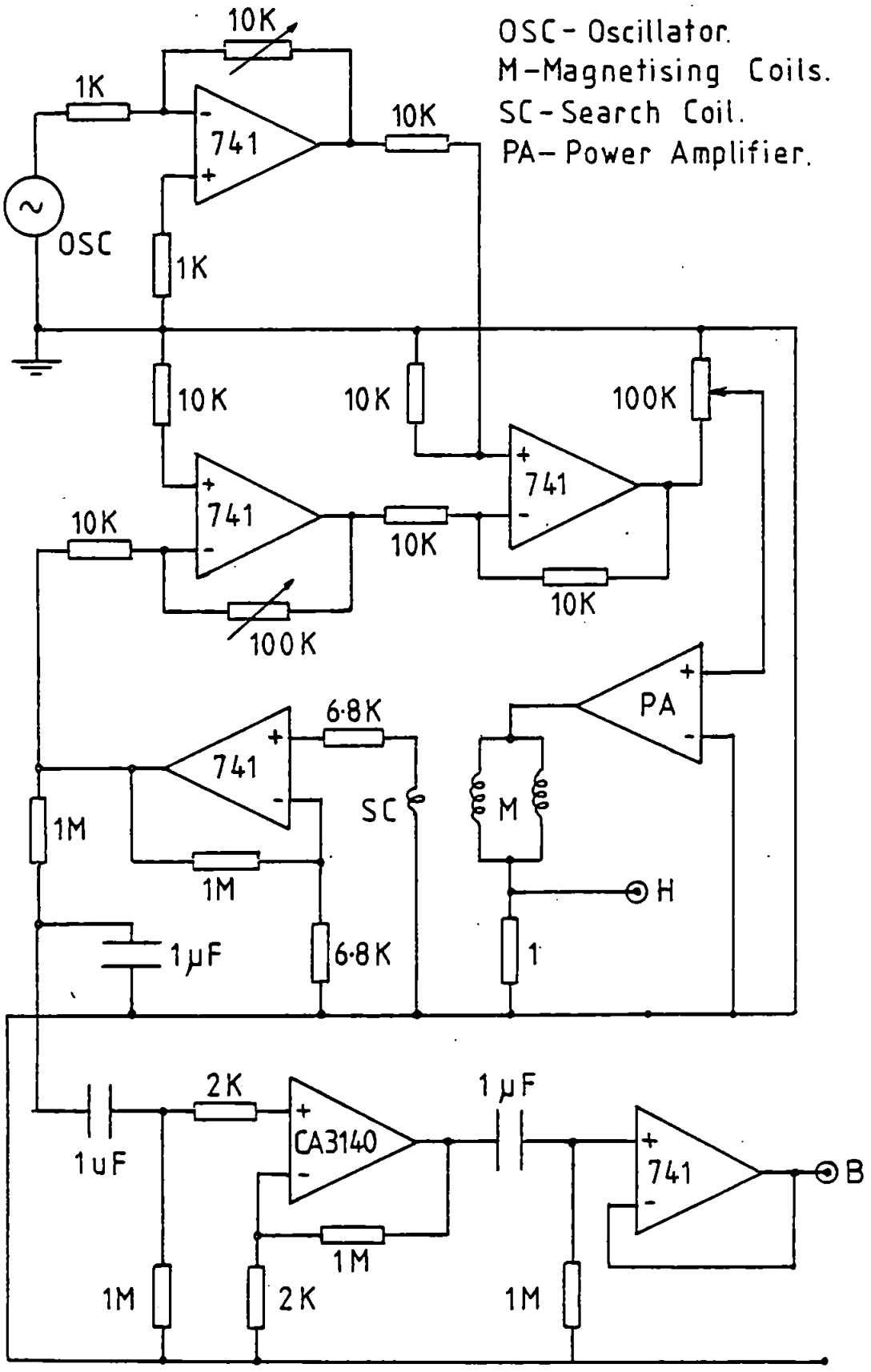

FIG. 4.32. Specimen Excitation, Flux Waveshape Control and Integrator Circuits.

satisfactorily between 50 Hz and 1 kHz, adequateley covering the intended range of 50 to 300 Hz.

4.4.2 Flux Waveshape Control

During the process of single sheet testing it has always been noticeable that the flux waveform distorts considerably, particularly under conditions of compressive stress. It is therefore necessary to exert some measure of control on this distortion, and particularly since the influence of the flux harmonics on magnetostriction harmonics is a crucial part of this investigation, it is necessary to deal with this aspect in some detail.

The method of employing negative feedback in the specimen excitation developed by McFarlane and Harris (33) was adopted. The theoretical analysis of this procedure is well known and has been extensively documented by other workers (4, 27). However, an original circuit was developed for this investigation and this will now be described, but without recourse to the original theoretical analysis.

The circuit has already been shown in Fig. 4.32 along with the specimen excitation and flux detection circuits. A schematic diagram of the waveshape control circuit alone is shown in Fig. 4.33.

An oscillator is used as the source of fundamental excitation frequency and is set at a fixed output level since it is also used as the source for triggering the circuits of the domain observation equipment (see section 4.1). It thus becomes the master oscillator for the complete apparatus. The oscillator output is, therefore, controlled by a stage of variable gain (k_2 in Fig. 4.33), and then fed to the non-inverting input of a differentially connected, operational amplifier. The ouput of this stage feeds the power amplifier connected to the magnetising windings. By variation of the gain controls of both the oscillator output amplifier and the P.A., excitation of the specimen may be obtained without regard for waveshape control.

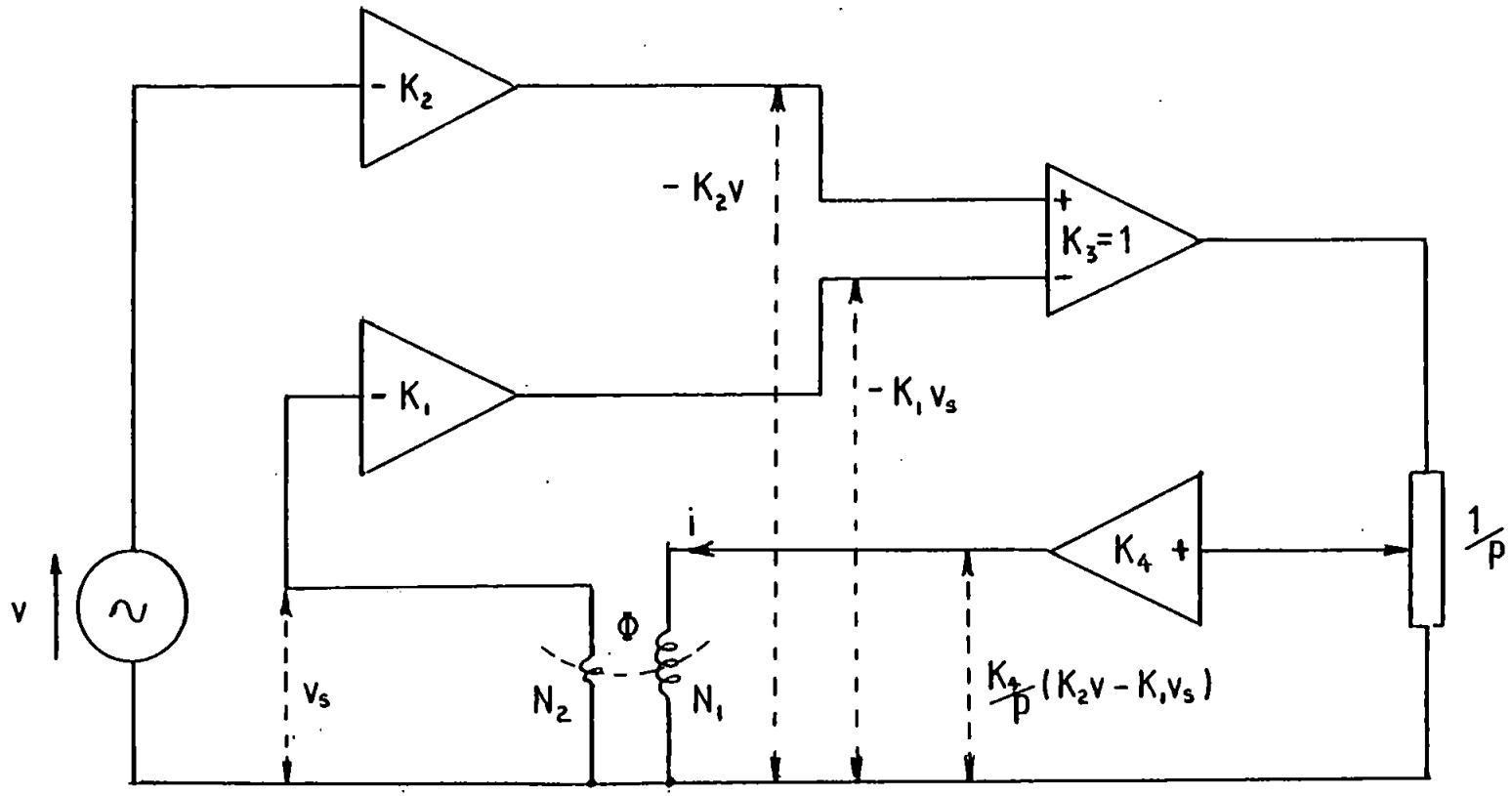

FIG. 4.33. Flux Waveshape Control — Schematic Circuit.

Feedback is then provided in the manner prescribed by McFarlane and Harris, from the same search coil which is used to derive the measure of flux density within the specimen. The search coil output is fed to a single stage of high, variable gain (k_1 in Fig. 4.33) the output from which feeds the integrator previously described, but also feeds the inverting input of the differential amplifier (k_3 in Fig. 4.33). Provided the gain stage has some finite level the power amplifier will then see the difference signal between the oscillator sine-wave output and the distorted search coil e.m.f.

Judicious selection of the various gain controls will enable various reductions in the harmonic content of the flux waveshape, as consistent with the original theory. In practice, with maximum levels of feedback consistent with stable operation, the harmonic content was typically reduced from 18% to less than 1% at a flux density of 1.96T. Careful control enabled determined levels of distortion to be set if required, but as no control was available over any individual harmonic frequency, this approach was not pursued. Further, it was intended to measure strain levels under the two conditions of no feedback and full feedback, and to analyse the levels of individual harmonic components in each case.

4.4.3 Flux Distortion Measurement

In order to investigate any variation of magnetostriction harmonics with flux harmonics, it is necessary to measure the level of distortion occurring. This was achieved by feeding the signal from the integrator to a B. & K. Type 2120 Frequency Analyser. This device incorporates a d.c. output proportional to the peak level of the filtered signal, and could thus be used directly on one channel of an X-Y plotter to be described in Section 4.5. By simultaneously feeding the total signal from the integrator to the other channel of the X-Y plotter via a separate peak voltage detector (see Section 4.5), and by automatically increasing the specimen magnetisation by means of a motor driven potentiometer in the excitation circuit, automatic plots of the various

harmonics in the specimen induction, as a function of the total peak induction, could be achieved without recourse to laborious point-by-point plotting. Calibration of the X-Y plotter was made by setting a fixed level of induction and calculating the percentage harmonic from the frequency analyser recordings.

Typical automatically recorded graphs of the third and fifth harmonics are shown in Fig. 4.34 in which can also be seen the reductions due to the flux waveshape control circuits previously described.

Flux Measurement Calibration

The signal proportional to B, which is finally a d.c. level available at the X-Y plotter, will be modified by all the gains throughout the circuits involved. To evaluate the sum of these gains, a sinusoidal signal of known amplitude and frequency is fed into the circuit at the point where the search coil would normally be connected.

Input and output waveforms at any point in the circuits can then be compared for both magnitude and phase. It was found that no phase errors were being introduced at any point, and the total gain was adjusted to give adequate signal levels at all the measuring points. This gain was noted.

The cross sectional area of the specimen surrounded by the search coil was measured by micrometer readings of the specimen thickness averaged from at least three readings across the coil width, and from the coil width measured either by micrometer when the whole specimen was encompassed, or by vernier calipers in the search coil holes.

Thus from knowledge of the system gain, the cross section of the coil and the characteristic time of the integrator, the level of B can be deduced.

The signal level for B is then displayed on the X-Y plotter enabling that device to be calibrated in T per cm. of deflection. By sweeping the induction from zero to saturation, the linearity of the system could be checked, as shown in Fig. 4.35 which also indicates the effects achieved by the waveshape control circuits.

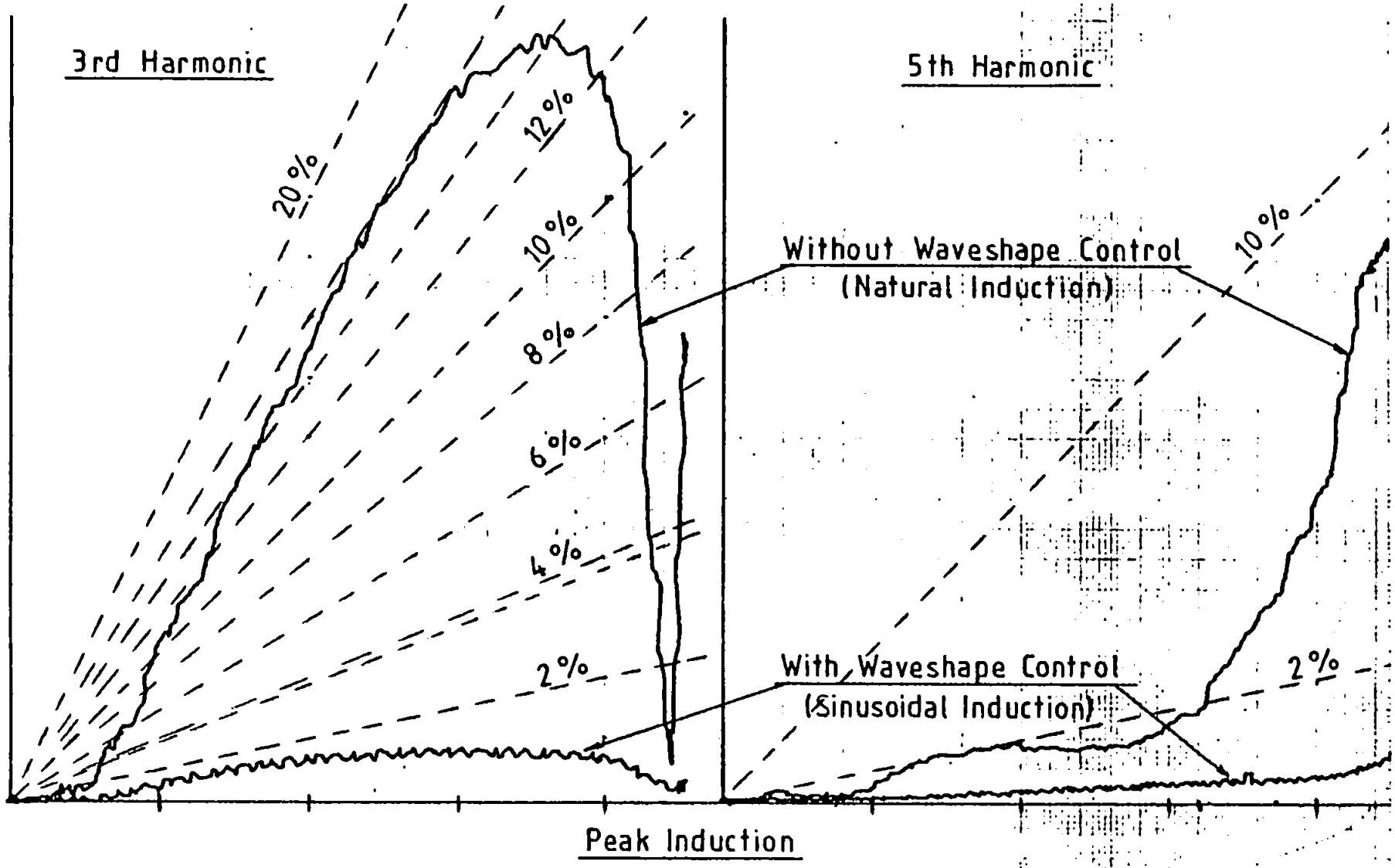

FIG. 4.34. Typical Variation in Induction 3rd & 5th Harmonics with Peak Induction.

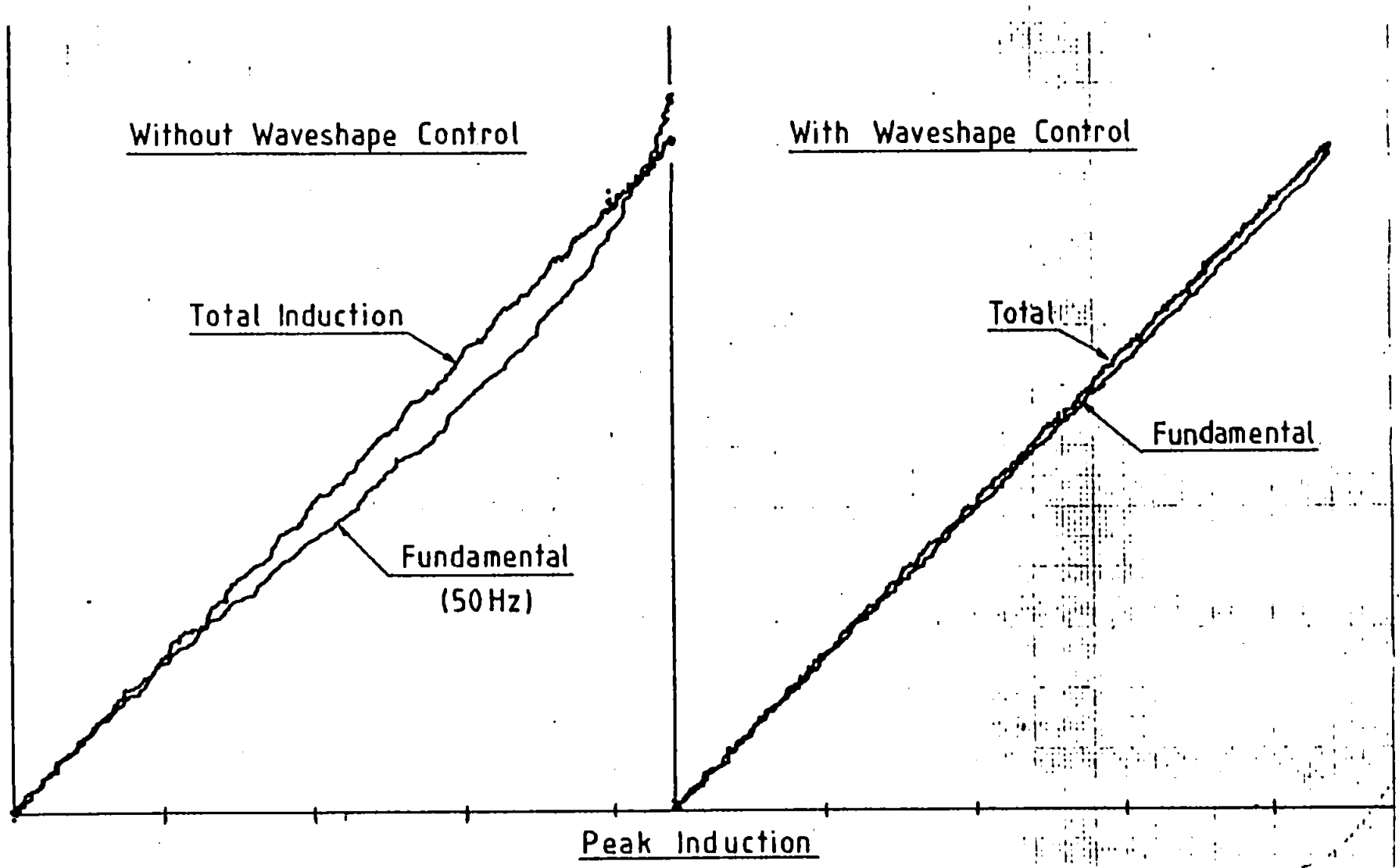

FIG. 4.35. Typical Variation of Total and Fundamental Peak Induction

4.5 The Complete Apparatus

All the previously described parts of apparatus are now combined into a complete system along with the devices to be used for measurement of the variables. A schematic diagram of the complete system is shown in Fig. 4.36.

Since frequency analysis of both the magnetostriction and flux density is planned, then any measuring devices will be dealing with sinusoids only, not complex waveforms. In addition it is usual to describe these variables in terms of their peak values.

It was therefore decided to convert both signals into d.c. levels equivalent to their peak values for subsequent easy recording on a flat-bed pen plotter. For this purpose a pair of precision, peak-voltage detectors were designed and built, and the circuit is shown in Fig. 4.37.

The circuit consists of two stages: a precision full-wave rectifier formed by operational amplifiers OP1 and OP2, and a peak voltage detector formed by OP3 and D3.

Diodes alone are not precise rectifiers since at low input signals the forward voltage will be below the knee of the diode characteristic and virtually open circuit to input signals. The circuit of Fig. 4.37 overcomes this, since when the forward voltage is below the knee of the diodes employed (about 600 mV), both D_1 and D_2 are open circuit and consequently zero negative feedback is applied to OP1. This op-amp is therefore operating in its open loop mode with a gain of about 100 dB; consequently an input voltage of only about 6 μV. is required to raise the diode forward voltage above the knee. Once the forward voltage is exceeded the diodes act as virtual short circuits and the gain will be determined by R_2 and R_3 as usual. This gain was made unity.

For positive half cycles at the inputs the output of OP1 will be negative, D_2 conducts via resistor R_2, but diode D_1 is reverse biased and does not conduct. Thus negative half cycles will appear at position A, whilst position B will be at zero potential.

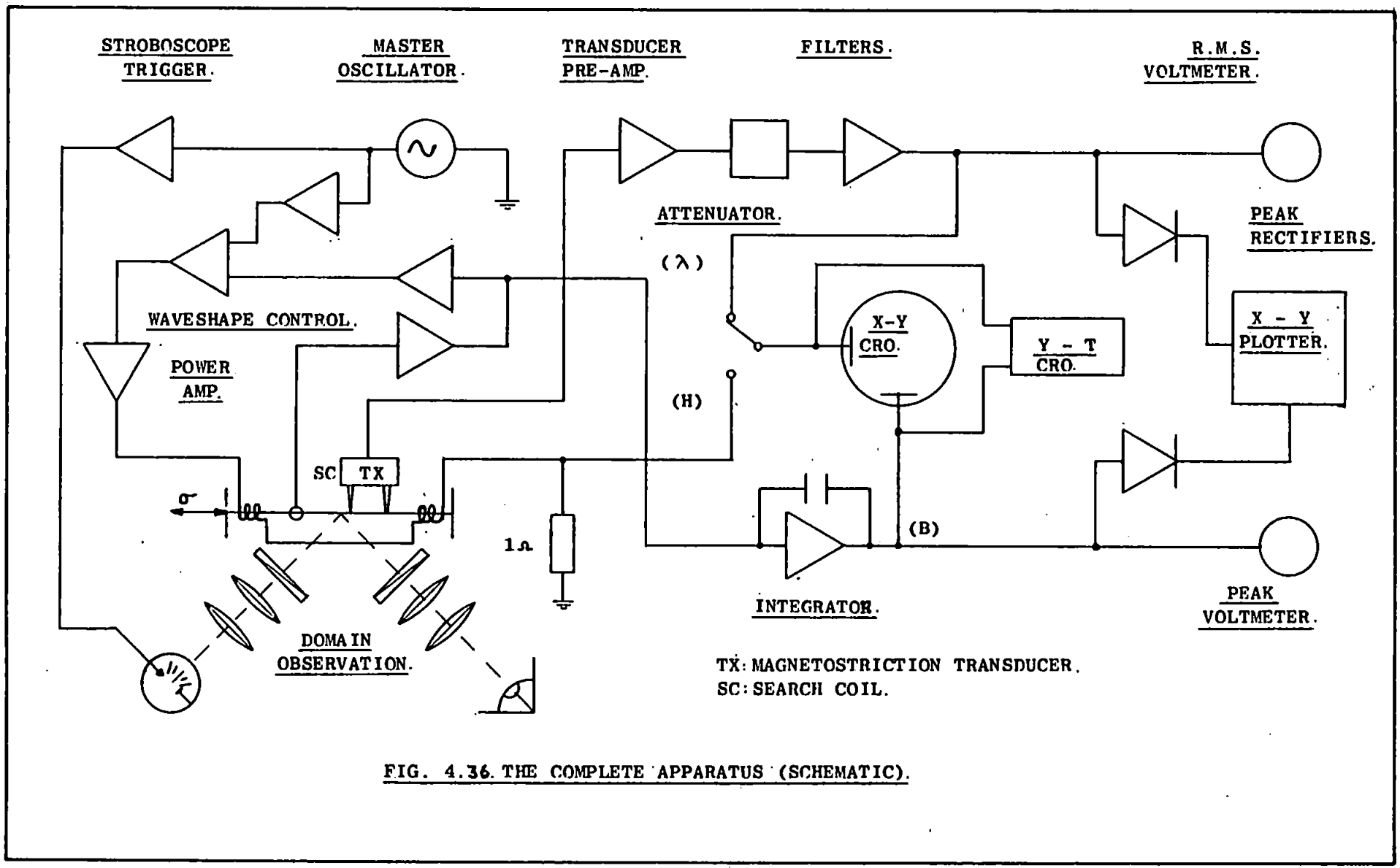

FIG. 4.36. THE COMPLETE APPARATUS (SCHEMATIC).

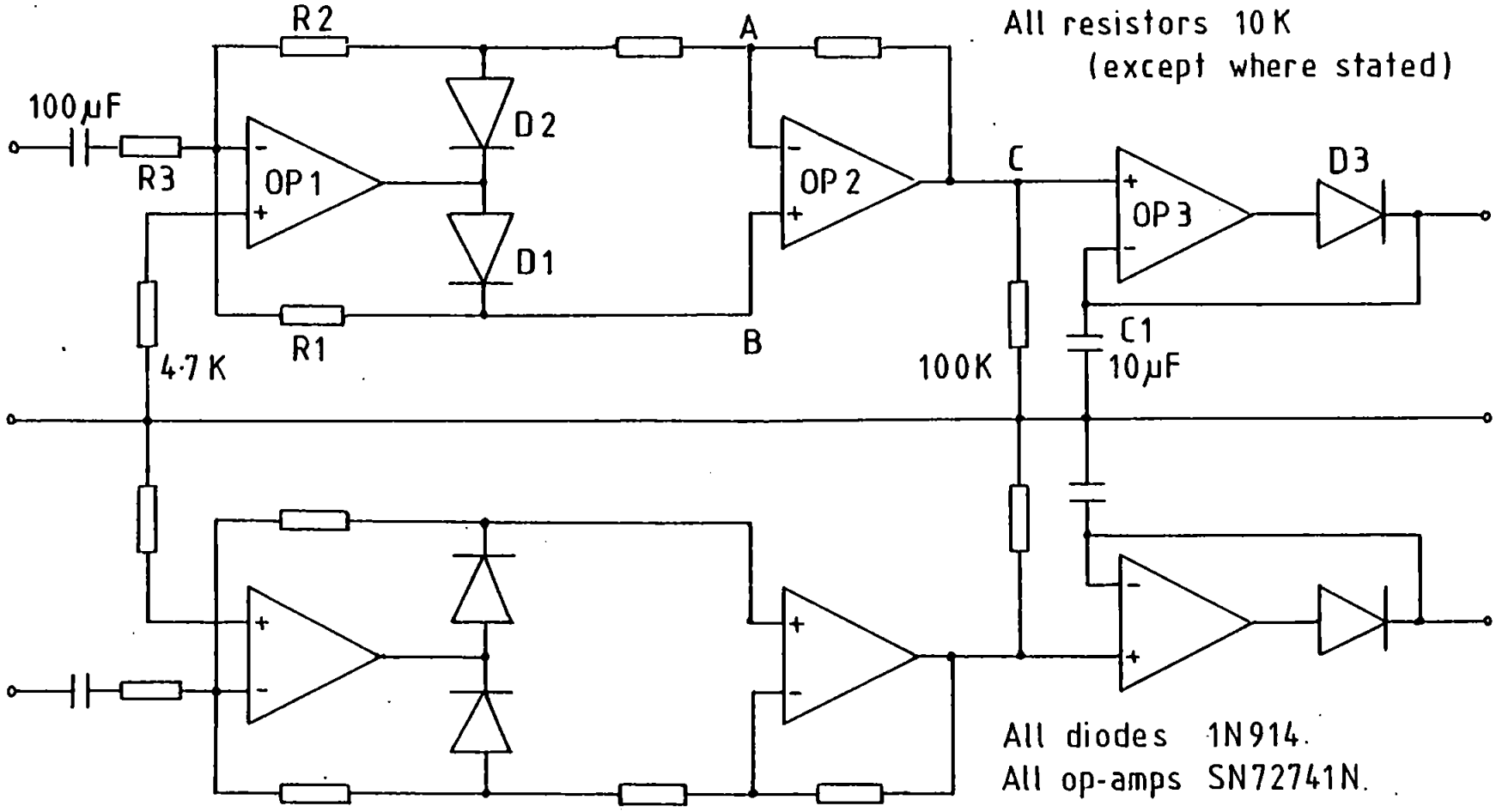

FIG. 4.37. PRECISION PEAK VOLTAGE DETECTORS.

For negative half cycles, the output of OP1 will be positive, diode D_1 conducts via R_1 and D_2 is reverse biased. Therefore, positive half cycles will appear at B whereas A goes to zero.

Position A is connected to the inverting input of the differential amplifier OP2 so that the negative half cycles will appear as positive half cycles at the output C. Similarly position B is connected to the non-inverting input and the positive half cycles will appear at the output. That is, the output will be positive, full wave rectification of the input.

This output is connected to the non-inverting input of OP3 so that capacitor C_1 can charge rapidly through the small forward resistance of diode D_3 to the peak value of the input. The discharge path for C_1 is only through the input resistance of the inverting input of OP3; since this is in the order of 1 MΩ, the discharge time constant is very large (about 10 secs). Hence the output will be the peak value of the input waveforms.

The outputs from the magnetostriction filters and flux integrator are also fed to X-Y and Y-T oscilloscopes to enable magnetostriction butterfly loops and waveshapes to be displayed. The signal proportional to magnetising force (H) is available for display of magnetisation characteristics.

Analogue voltmeters are also included in the circuits of λ and B to facilitate calibration and provide visual monitoring during measurements.

To avoid the difficulties associated with 'earth loops' when several items of 'mains' powered equipment are connected together, the critical electronic circuits (flux waveshape control and magnetostriction signal conditioning) are powered by two heavy-duty batteries, supplying $\pm$ 12V for the operational amplifiers.

A further innovation introduced was to drive the potentiometer controlling the level of specimen induction from a small, geared electric motor, allowing B to rise from the demagnetised state to saturation in about 1 minute. Thus

X-Y plots of magnetostriction variation with induction could be obtained automatically without recourse to manual plotting.

A photograph of the complete apparatus is shown in Fig. 4.38, in which it will be seen that the specimen stage is mounted on a slab of granite. This in turn is de-coupled from the bench by pieces of foam rubber, in order to provide some degree of vibration isolation from the movement of the building due to an adjacent carpark and machine-shop.

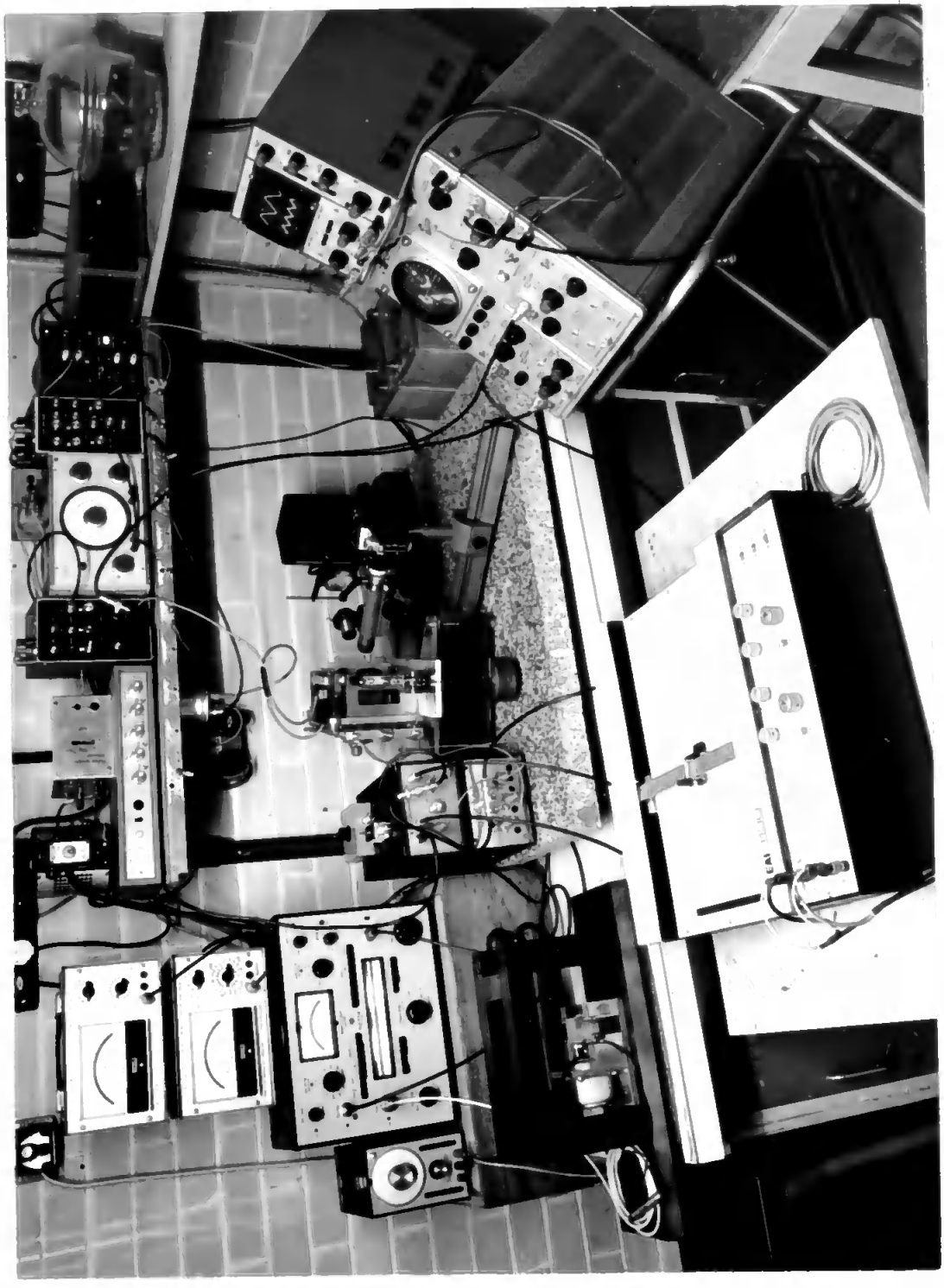

FIG. 4.38. THE COMPLETE APPARATUS.

REFERENCES TO CHAPTER FOUR

1. F. Bitter, Phys. Rev., No. 38, p. 1903, 1931.

2. L. von Hamos and P.A. Thiessen, Zeit. fur Phys., No. 49, p. 619, 1931.

3. L.W. McKeehan and W.C. Elmore, Phys. Rèv., No. 46, p. 226, 1934.

4. D.J. Mapps, Ph.D. Thesis, U.W.I.S.T., September 1969.

5. R. Carey and E.D. Isaac, "Magnetic Domains and Techniques for their Observation", E.U.P., London, 1966.

6. B. Kostyshyn, "A Hall Probe and Scanning Apparatus for determining Magnetic Fields with High Resolution and Sensitivity", I.B.M. (New York, undated).

7. K. Mohri and T. Fujimoto, Memoirs of the Kyushu Inst. of Tech. Engineering No. 7, March 1977.

8. J. Kaczer, Czech. J. Phys., Vol. 5, p. 239, 1955.

9. W. Swindell, Ph.D. Thesis, Sheffield University, 1964.

10. C.A. Fowler and E.M. Fryer, Phys. Rev., Vol. 104, p. 552, 1956.

11. H.J. Williams, F.C. Foster and E.A. Wood, Phys. Rev., Vol. 82, p. 119, 1951.

12. C.A. Fowler and E.M. Fryer, Phys. Rev. Vol. 86, p. 426, 1952.

13. H.E. White, "Fundamentals of Optics".

14. J. Kranz and W. Dreschel, Z. Physik, No. 150, p. 632, 1958.

15. J.D. Whitaker, Elec. Times, Vol. 137, p. 675, April 1960.

16. J.T. Wilkins and J.E. Thompson, Elec. Times, p. 233-235, February 1962.

17. R. Risch, Brown Boveri Review, November/December 1962.

18. V.A. Nezhizhim and E.A. Prokopchenko, Soviet Phsy. J. No. 5, p. 110-115, May 1977.

19. V.A. Zaykova and Ya. S. Shur, Fiz. Met. and Metalloved, Vol. 14, No. 5, p. 785-787, 1962.

20. Ibid, Vol. 21, No. 5, p. 664-673, 1966.

FSGABB

21. H. Bittel, W. Gross-Nobis and W. Schonfelder, Physica 80 B, p. 83-94, 1975.

22. P.J. Banks and E. Rawlinson, Proc. I.E.E., Vol. 114, No. 10, October 1967.

23. R.D. Greenough, C. Underhill and P. Underhill, Physica 81 B, p. 24-34, 1976.

24. A.J. Moses and P.S. Phillips, I.E.E.E. Trans. Magn., Vol. Mag - 14, No. 5, September 1978.

25. P.W. Neurath, Elect. Eng., Vol. 73, p. 991-994, November 1954.

26. C.M. Brownsey and G.C. Maples, Proc. I.E.E., Vol. 113, No. 11, 1966.

27. G.H. Simmons, Ph.D. Thesis, U.W.I.S.T., 1970.

28. A.J. Moses, I.E.E.E. Trans. Magn., Vol. Mag - 10, No. 2, June 1974.

29. C.B. Clayton, "Linear Integrated Circuit Applications", MacMillan, London 1975.

30. F.F. Kuo, "Network Analysis and Synthesis", Wiley, N.Y., 1964.

31. P.J. Banks, I.E.E.E. Trans. Mag., Vol. Mag - 8, No. 2, June 1972.

32. D.C. Plane, Ph.D. Thesis, University of London, 1975.

33. J. MacFarlane and M.J. Harris, Proc. I.E.E. Paper No. 2554M, February 1958.

FSGABB

CHAPTER FIVE

EXPERIMENTAL RESULTS AND DISCUSSION

5.1 The Measuring Procedure.

It has been established in Chapter Four (Section 4.2.2) that the errors in the magnetostriction measurement will depend on the effective cancelling of any phase shifts between the two transducers, and on the equality of the gains between channels. It has also been described (Chapter Four, Section 4.2.5) how the calibration procedure for magnetostriction measurement involves the effective nulling of any "vertical" (i.e. normal to the sheet) components of vibration.

Initial measurements had, as described in Section 4.2.4, revealed severely distorted butterfly loops and erroneous levels of magnetostriction, particularly at 100 Hz. The former effect was found to be due to phase shifts, but the latter was found to be due to the unwanted "vertical" vibrations. A first attempt to reduce these was made by reducing the clearance between the specimen and the anti-buckling rails into which it is mounted. After experimenting with lubricated, thin rubber sheet and strips of paper, a technique difficult to apply to the sharp edges of the specimens, it was found that effective damping could be achieved using 0.08 mm stainless steel shims between the specimen and the rails. However, a component of "vertical" motion was still in evidence which could be damped by light finger pressure at the specimen surface.

Since the "vertical" vibrations are an unknown quantity, and since it was found impossible to completely null these motions, it will be necessary to measure this component of vibration under all the anticipated measuring conditions. Then, knowing the level of attenuation produced by the nulling process, the percentage of signal

component due to that source can be calculated and compared to the level of the desired "horizontal" signal.

Measurement of the "vertical" vibrations is achieved by the same calibration process as for magnetostriction, except that in this case the transducer outputs due to "horizontal" motion will need to be nulled. The following procedure was therefore adopted as a routine operation prior to any new set of measurements.

The transucer head is set up in the Calibration Vibrating Block (see Fig 4.21 Page 115) so as to sense "horizontal" motion with the system set up for 100 Hz measurements. The amplitude of vibration is set to the maximum anticipated; this will be determined by the distance of the furthest transducer from the clamped end of the specimen at the desired measurement position. Thus for investigation in a grain 40 mm from the clamp with a maximum strain of say, 30 με, the block is set to vibrate at 1.2 μm (peak-peak). Then as described in Section 4.2.5, the gains of the transducer pre-amplifier are adjusted to give a null output. By removing the input from one transducer the output due to the other transducer may be measured, and the null signal expressed as a percentage of the "horizontal" sensitivity. In all cases, including measurements at 200 and 300 Hz, this error was found to be less than 1%, being typically 0.8% at 100 Hz.

The transducer head is then mounted on the Vibrating Block so as to sense "vertical" motion. By successive adjustments to the pre-amplifier, output-stage gains, and to the phase shifter, the output can be nulled as described in Section 4.2.5. In this mode it was found possible to null to 0.4% at 100 Hz with undetectable phase error between outputs of each transducer. Whilst in this mode, the sensitivity to "vertical" signals is obtained by removing one transducer input and noting the output level. Since the level of "vertical" motion is unknown, the system was calibrated up to the maximum possible, this being a

vibration of 0.25 mm (peak-peak).

The transducer head is next mounted into the Apparatus at the position in which magnetostriction measurements will eventually be taken. Observations are made over the complete range of stress levels and induction levels of the transducer reponse at 100 Hz due to vertical motion of the specimen under 50 Hz excitation, both with and without feedback in the excitation.

The whole of the above procedure is then repeated, but with the system calibrated to sense vertical motion at 200 Hz, and then at 300 Hz.

Fig 5.1 shows a typical result for the "vertical" signal obtained at 300 Hz. Note that this graph does not show the true vertical motion of the specimen but shows the difference between the motions experienced by the two transducer needles.

The measurement procedure then continues for the desired "horizontal" motion, either longitudinal or transverse magnetostriction. The calibration process is then as set out in Chapter Four, which is exactly as outlined above except that the "vertical" and "horizontal" modes are interchanged. As reported above, it was found possible to null the output due to "vertical" motions to better than 1% at all frequencies, and also found possible to null the output due to equal "horizontal" inputs to better than 0.5%, at phase shifts less than 0.5^{o} between transducers.

Examination of subsequent magnetostriction measurements showed that, over the range of stress and induction used, the maximum error due to inclusion of 1% of any vertical motion as measured above was never greater than 2%.

In order to reduce the error due to phase

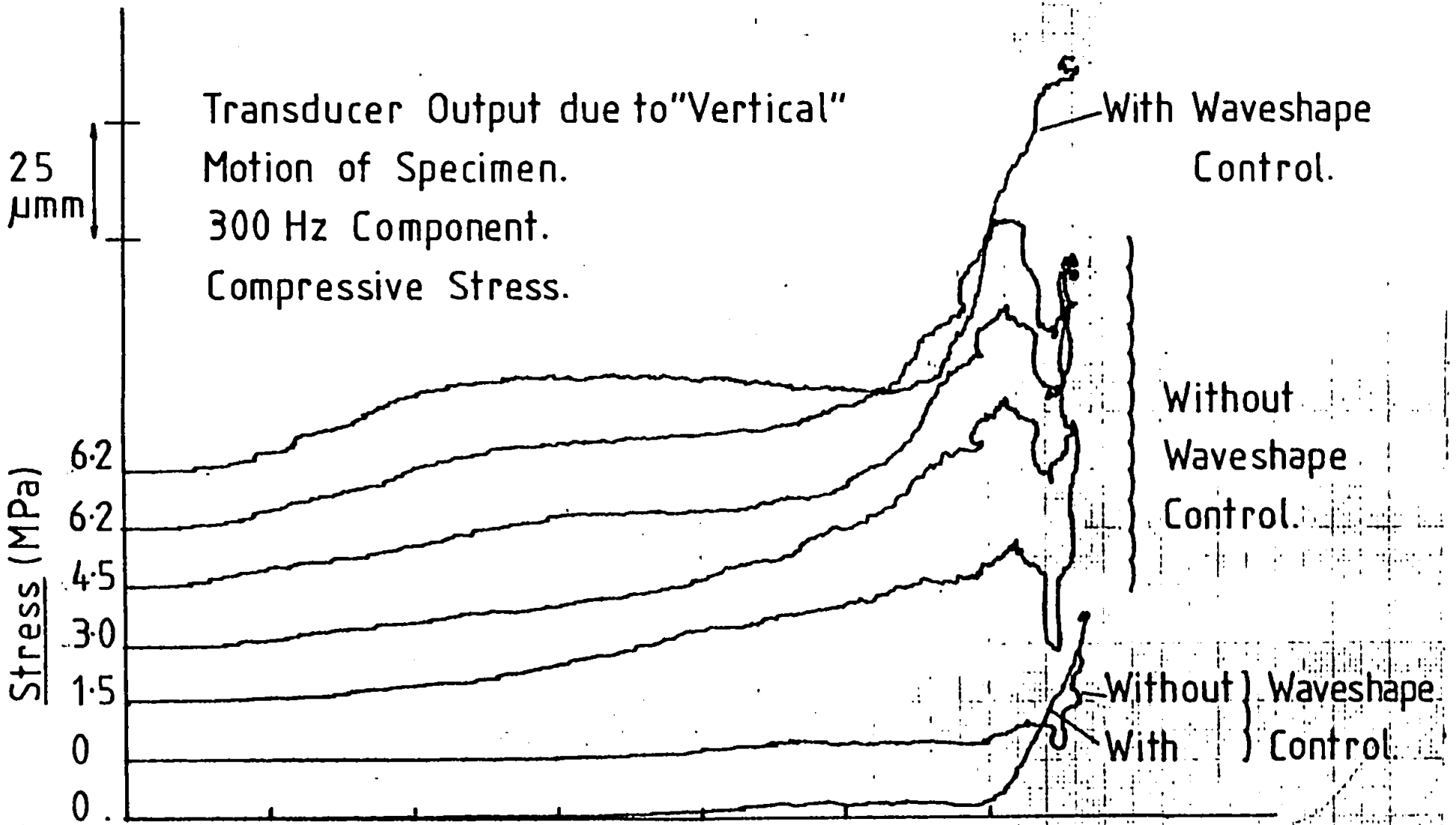

FIG.5.1."Normal" Component of Specimen Vibration

shifts, it was decided to restrict the transducer separation to 2 mm for every 10 mm from the clamped end of the specimen. Reference to the Error Analysis of Chapter Four shows that, for 0.5% error in nulling and 0.5° phase shift, the worst output error will be 3.5%, and the phase error less than 5°. This was considered acceptable since all the calibration results were better than the limits mentioned above.

The noise level of the system was also assessed as a possible source of error. With the output attenuator (as shown in Fig. 4.15 of Chapter Four) set at zero attenuation, the gain of the X - Y plotter used to record all results was increased at each centre frequency of interest and the peak - peak fluctuations recorded. Then, by setting a deflection corresponding to a known displacement level from the transducers mounted on the Vibrating Block, the noise amplitude could be determined. This was found to have a worst peak - peak amplitude equivalent to 0.4 μmm, corresponding to a strain of 0.05 με for a transudcer separation of 8 mm. This was considered acceptable.

Attention to detail in the measuring procedure was completed by ensuring that the specimen was demagnetised prior to any measurement. Thus, after application of a new level of stress by addition to the weights hung on the lever arm described in Chapter Four, the induction (as sensed by the search coil around the grain under examination) was increased to saturation (observed on a B/H loop). The excitation, at 50 Hz, was then reduced to zero at a uniform rate.

5.2 Grain Selection and Position.

Several half - Epstein samples of large-grained Silicon-Iron had been prepared for examination. Each of these was examined in turn by the domain observation equipment. Most of the specimens exhibited either poor surface preparation causing domain patterns of poor contrast

(inadequate for high quality photography of the patterns) or insufficient stress relief annealing causing Complex Stress Pattern II types of domain structure (1) even in the unstressed state.

Eventually a grain was found near to the centre of a specimen having a typical structure in well aligned material; it exhibited a Spike domain structure, classified by Paxton & Nilan (2) as having an angle of dip in the range of 2^{o} - 4^{o}, and its [001] axis was yawed away from the longitudinal axis of the specimen by 5^{o}. This angle was estimated by rotation of the graticule in the eye piece of the domain observation equipment away from the horizontal.

The grain size was approximately 20 mm longitudinally by 14 mm transversely, being roughly trapezoidal in shape. Its centre was 42 mm from the clamped end of the specimen. It had previously been located as one of many possible grains by the use of a device marketed as a Magnetic Tape Viewer. This consists of a colloidal suspension of magnetic particles contained in a clear plastic container. Placing this onto a specimen and tapping the device causes the particles to align with domain walls, much in the way of the Colloid Technique outlined in Chapter Four, Section 4.1. All of the possible grains so obtained showed a reasonably well defined bar pattern of domains, and they were all prepared for search coils prior to surface preparation.

The position of this grain determined the minimum separation of the transducer needles as decided by the Error Analysis of Chapter Four, and the calibration process outlined above. This has been established as 2 mm for every 10 mm from the clamped end of the specimen; so for the grain chosen, the needle separation was set at 8mm.

5.3 Magnetostriction Measurement Parallel to the Rolling Direction.

With increasing compressive stress in the range

0 - 6.2 MPa (0-900 P.S.I) applied in the plane of the sheet, parallel to the rolling direction, longitudinal magnetostriction was measured in the grain described above, with the transducer needles spaced symmetrically about the centre of the grain. Measurements were made at each discrete frequency of 100, 200 and 300 Hz for each increment of stress over an induction range between the demagnetised state and saturation as detected by the search coil around the grain. This was done for the two conditions of sinusoidal induction (feedback applied to the excitation as described in Chapter Four Section 4.4.2) and natural induction (no feedback). Examples of the effects of feedback are demonstrated in the photographs of Figs 5.2 and 5.3, which show the magnetising current and overall grain induction near to saturation both with and without feedback.

5.3.1 Sinusoidal (Controlled) Flux Waveshape.

The graphs of Figs 5.4., 5.5 and 5.6 (a), (b), (c) show the results obtained for longitudinal harmonic magnetostriction with the overall grain induction controlled to be sinusoidal. The photograph of Fig. 5.7 shows a typical overall magnetostriction waveform along with the corresponding level of induction, and the photograph of Fig. 5.8 shows a typical "butterfly" loop obtained for the fundamental magnetostriction harmonic.

From the graphs, curves of magnetostriction as a function of the compressive stress may be obtained at discrete levels of induction. These are shown in Figs. 5.9 and 5.10 for each of the first three harmonics, at induction levels of 0.9, 1.2, 1.5 and 1.8T.

The shape of the curves obtained at 100 Hz are similar to those reported by other workers(3, 4, 5). The large increase occuring in the range 0-2 MPa (0 - 300 P.S.I) relates to the changeover between the predominant bar domain structure of the demagnetised state and the Stress Induced PatternI of Corner and Mason (6) as described in Chapter Three, Section 3.3.2.

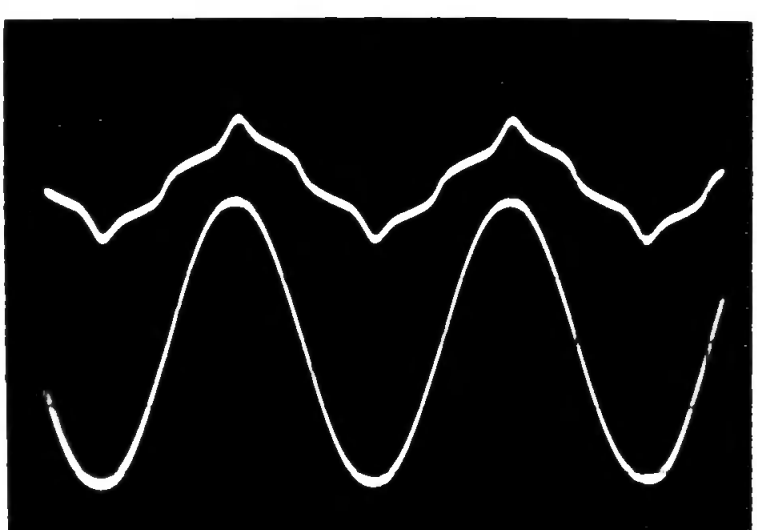

FIG.5.2. Typical Magnetising Current and Induction Waveforms with Feedback Control.

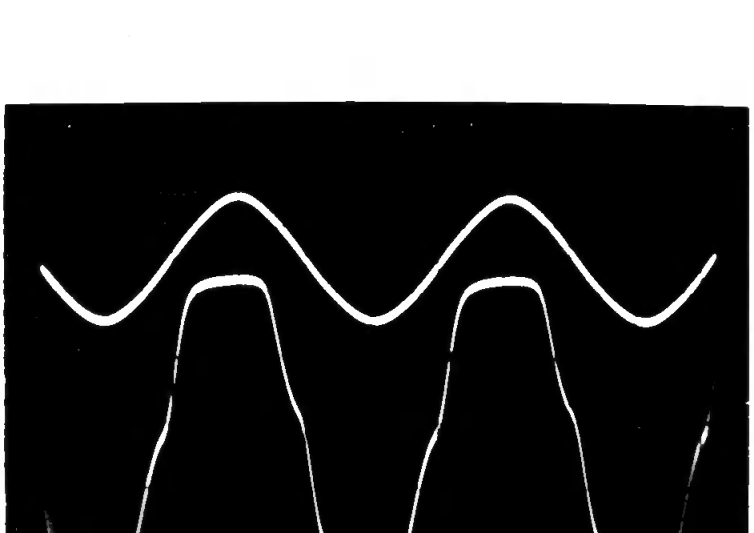

FIG.5.3. Typical Magnetising Current and Induction Waveforms without Feedback Control.

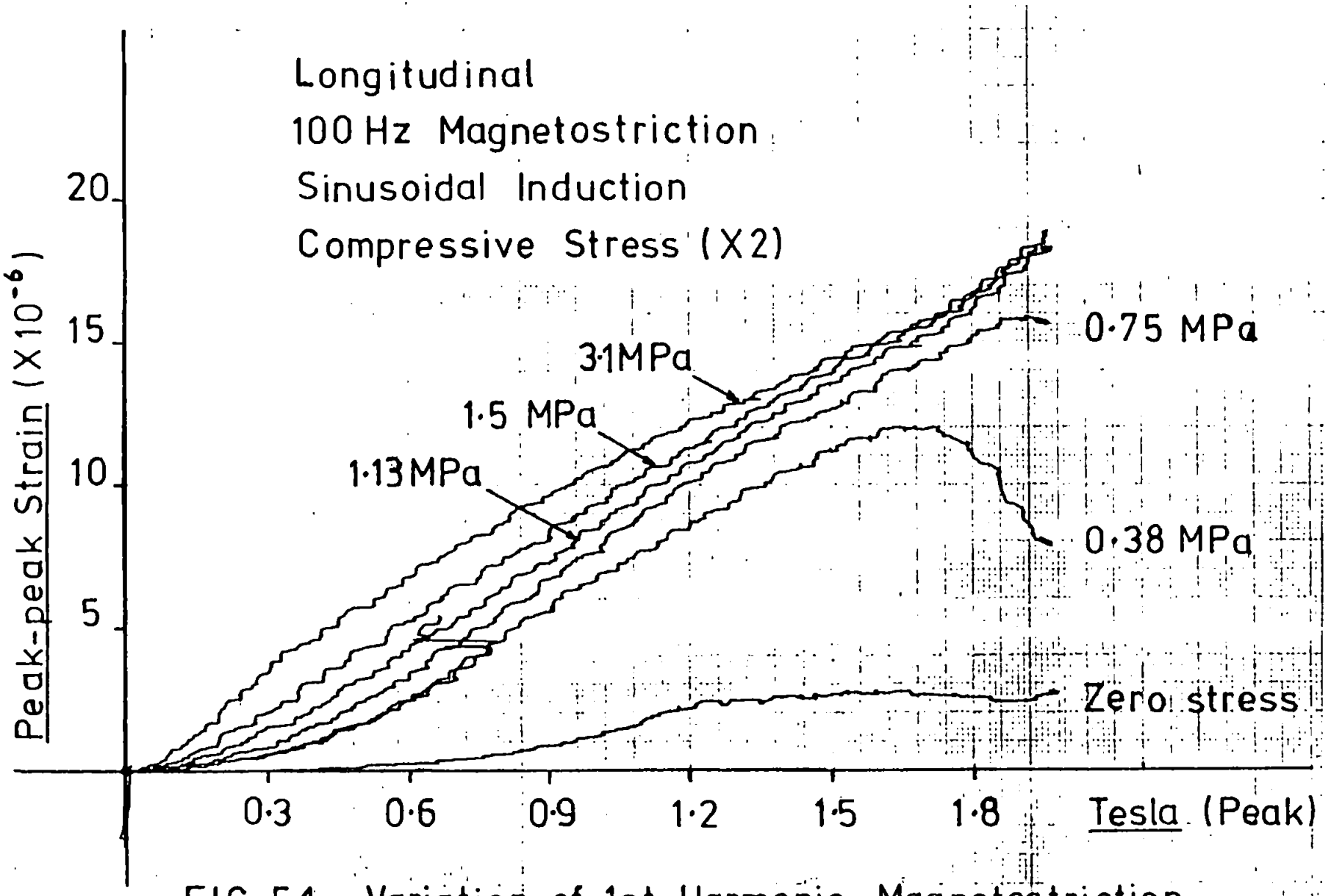

FIG: 5.4. Variation of 1st Harmonic Magnetostriction

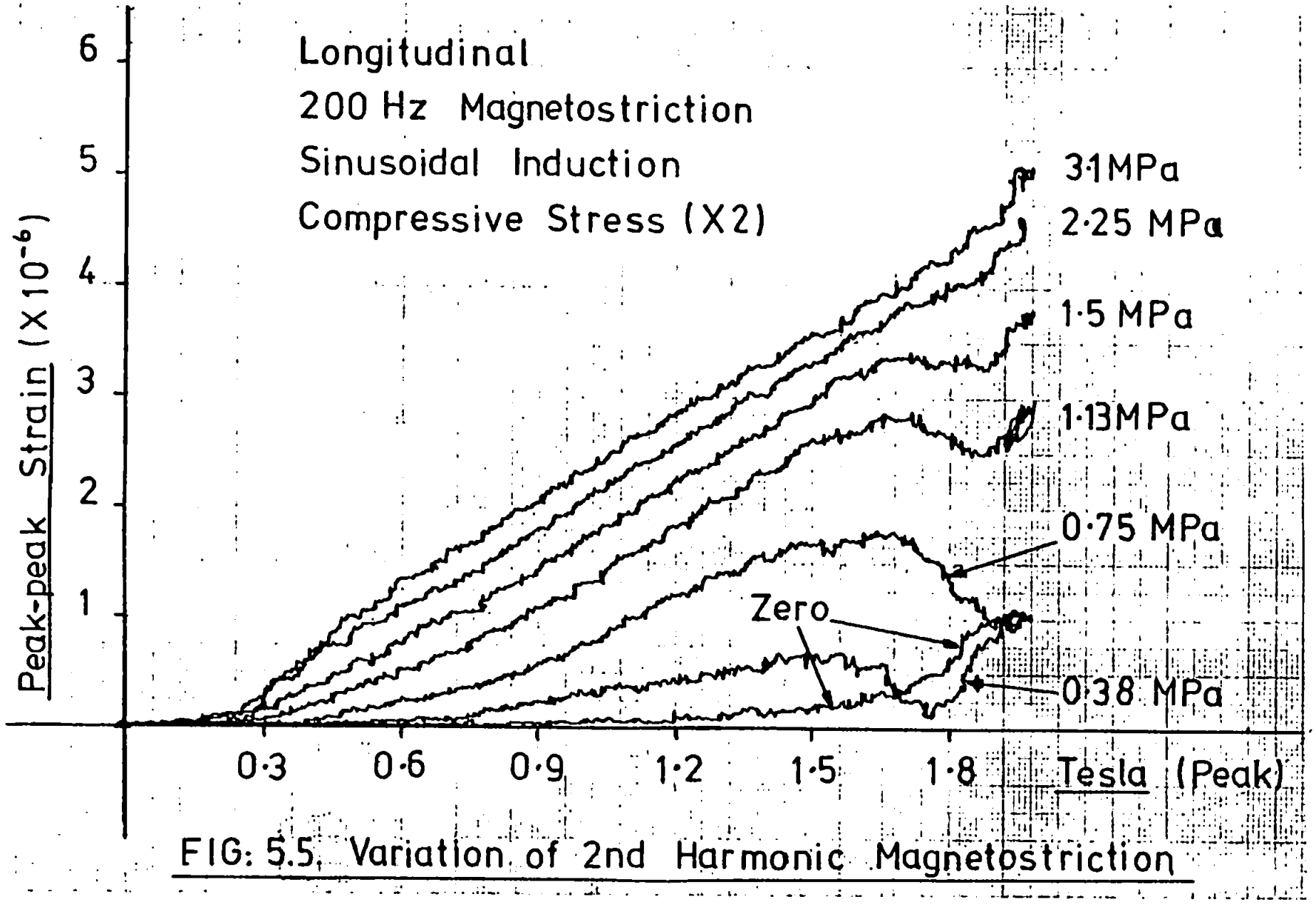

FIG: 5.5. Variation of 2nd Harmonic Magnetostriction

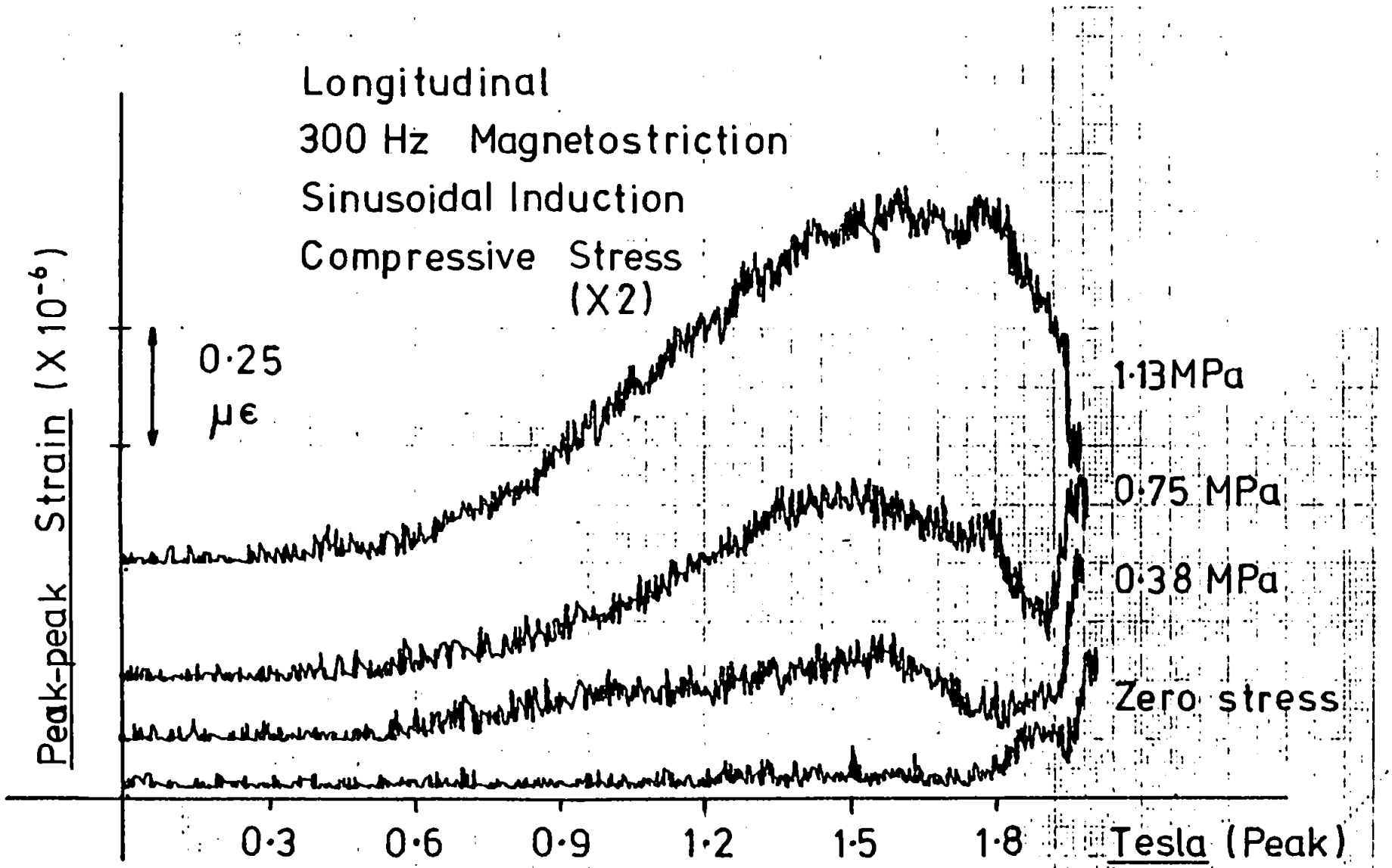

FIG: 5.6.a. Variation of 3rd Harmonic Magnetostriction

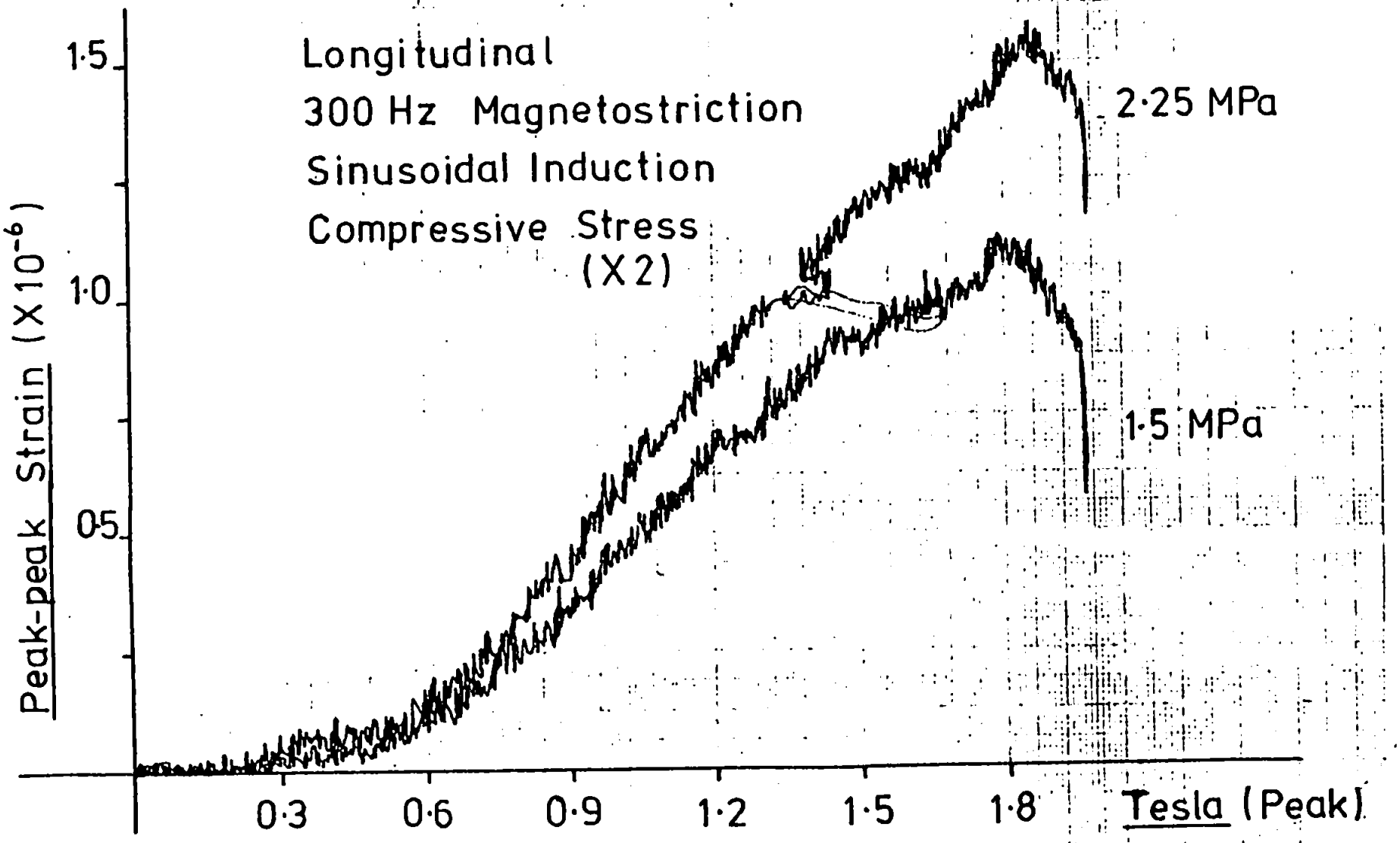

FIG:5.6.b. Variation of 3rd Harmonic Magnetostriction

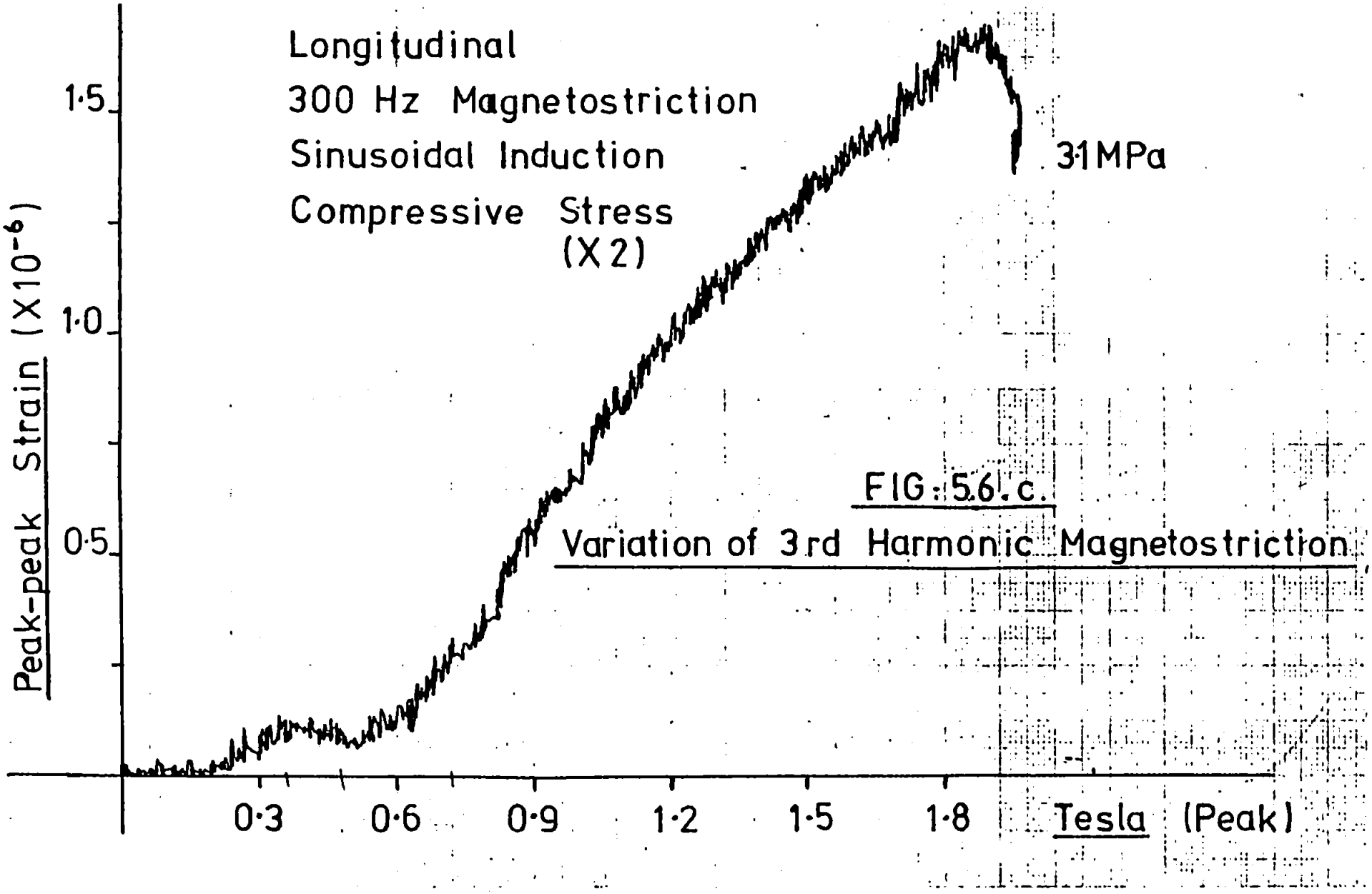

FIG: 5.6.c.

Variation of 3rd Harmonic Magnetostriction

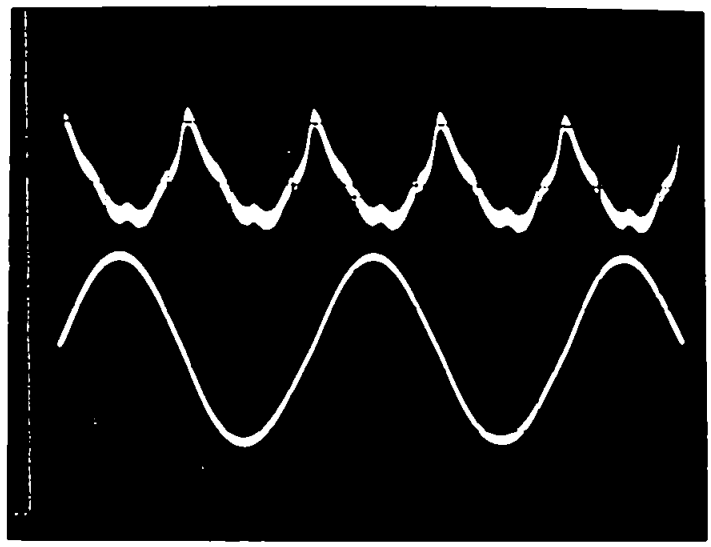

FIG 5.7. Typical Magnetostriction and Induction Waveforms with Feedback Control.

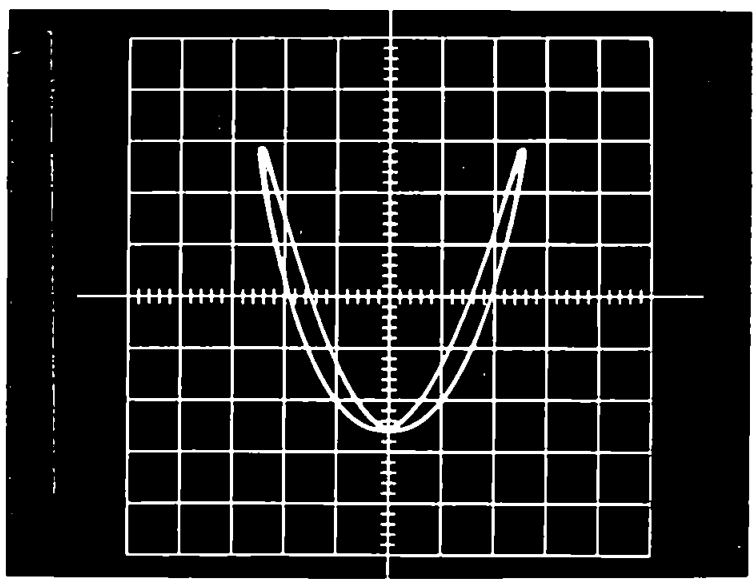

FIG. 5.8. Typical 100 Hz Magnetostriction 'Butterfly' loop with Feedback Control of Induction.

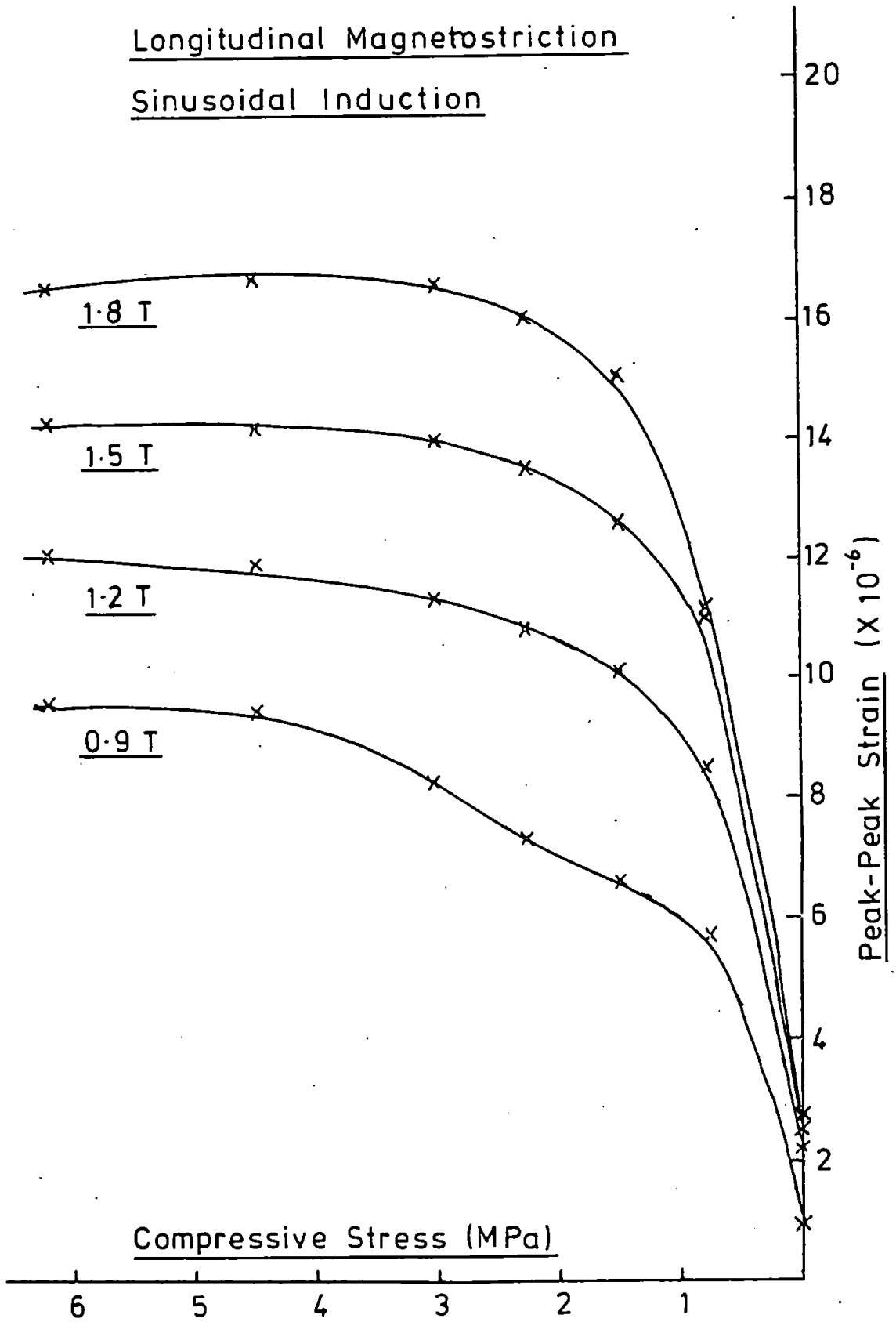

FIG. 5.9. First Harmonic (100 Hz) Stress Sensitivity.

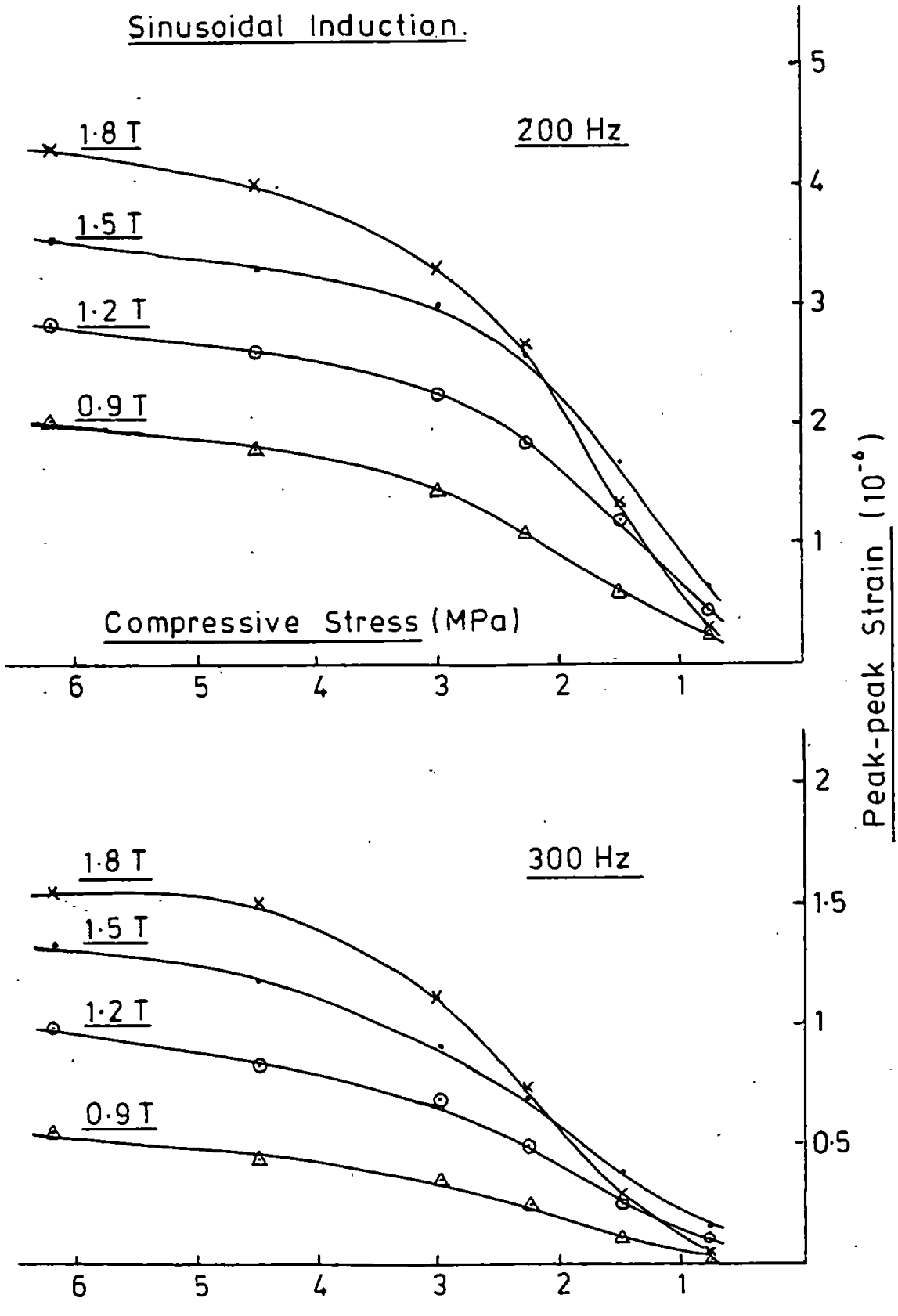

FIG. 5.10. Second (200 Hz) & Third (300 Hz) Harmonic Stress Sensitivities.

The curves obtained for the 2nd and 3rd magnetostriction harmonics are new, not having previously been reported. They show a similar behaviour to the fundamental (100 Hz) relationship with stress, although the large increase during the onset of Stress Pattern I is not as marked as for the fundamental strain.

5.3.2 Natural (Uncontrolled) Flux Waveshape.

The measurements of section 5.3.1. are repeated but without feedback in the excitation circuits, allowing the induction to distort in order to accommodate the B/H loop when a sinusiodal excitation voltage is applied.

The results obtained are shown in Figs 5.11, 5.12, and 5.13 (a), (b). Photographs of a typical overall magnetostriction waveform and a fundamental "butterfly" loop are shown in Figs 5.14 and 5.15.

The corresponding derived curves of magnetostriction harmonics versus compressive stress are shown in Figs 5.16 and 5.17.

As for the previous case with Controlled Induction, the fundamental curves are similar to those already reported, but again the 2nd and 3rd harmonics show a flatter response particularly at lower inductions. These latter curves are new, not having been reported before.

5.3.3 Comparison of Results for Longitudinal Magnetostriction

A comparison of the curves of Figs 5.4 and 5.11 for the fundamental magnetostriction at 100 Hz show similar features in both shape and magnitude. However there are significant differences between the behaviour of the 2nd and 3rd harmonics for the conditions of Controlled and Uncontrolled induction. These differences are highlighted by a direct comparison measured on the same graph: Fig 5.18 shows the 2nd harmonic at a stress of 4·5 MPa and Fig 5.19 shows the 3rd harmonic at the same stress level. These

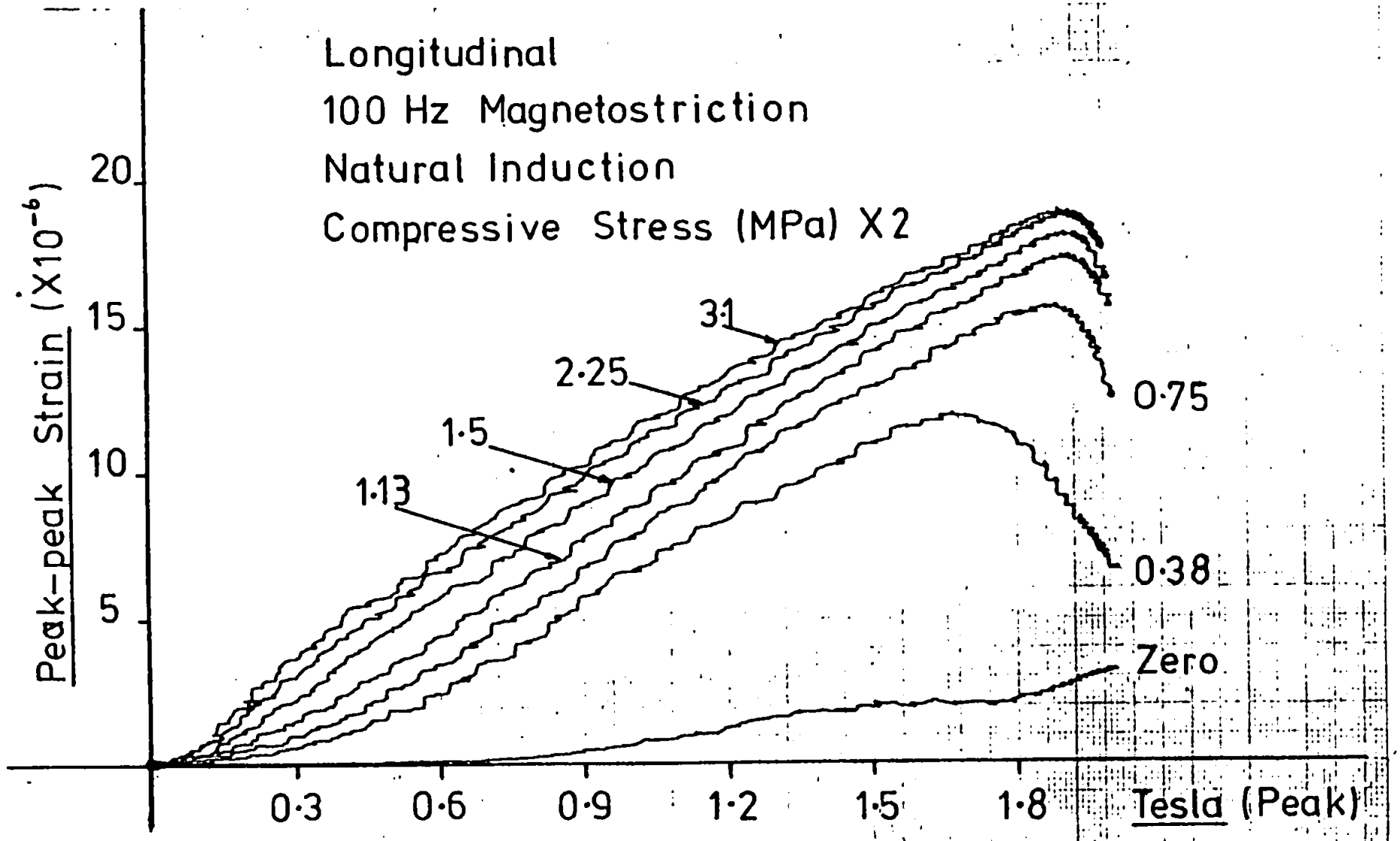

FIG:5.11. Variation of 1st Harmonic Magnetostriction

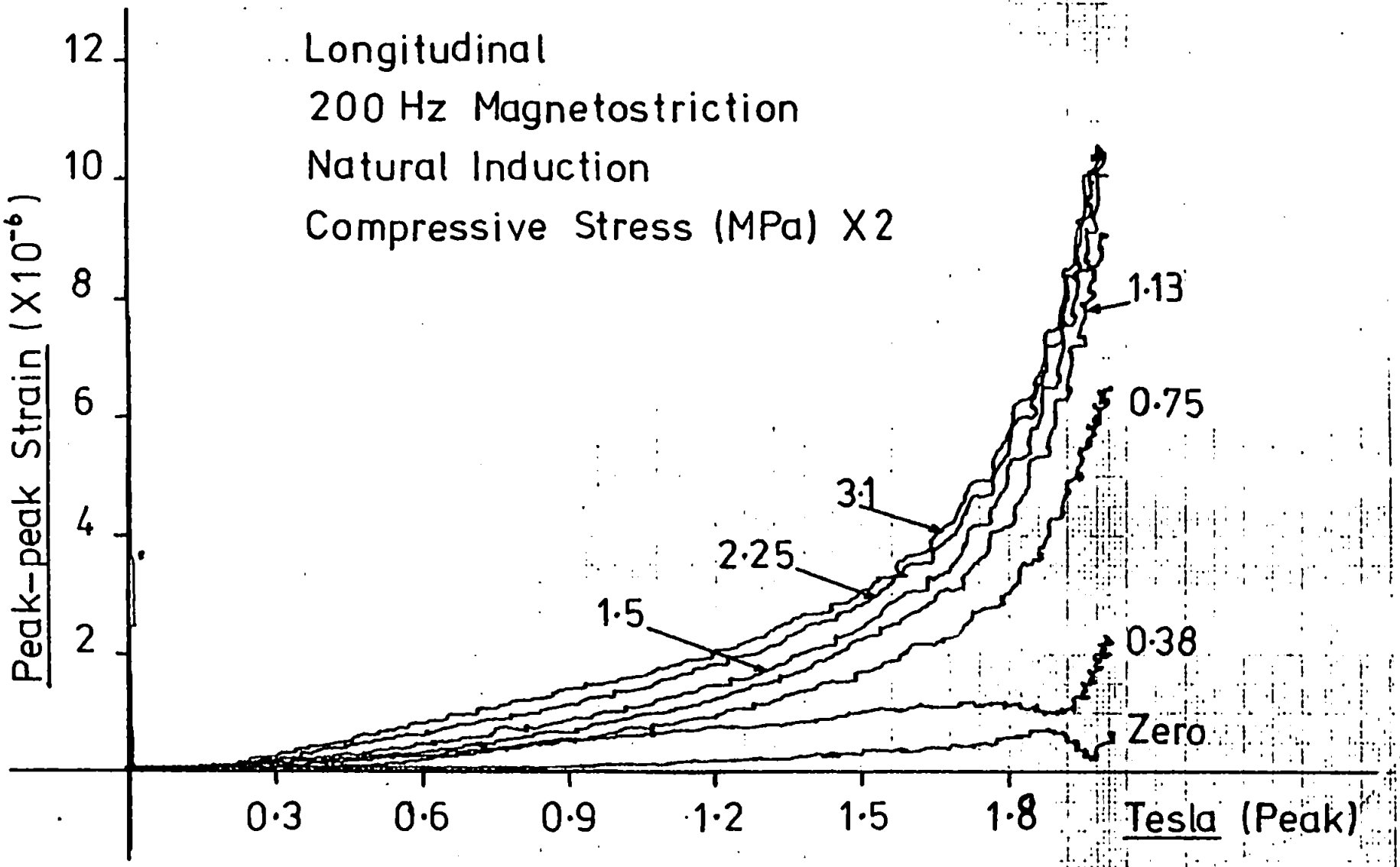

FIG: 5.12. Variation of 2nd Harmonic Magnetostriction

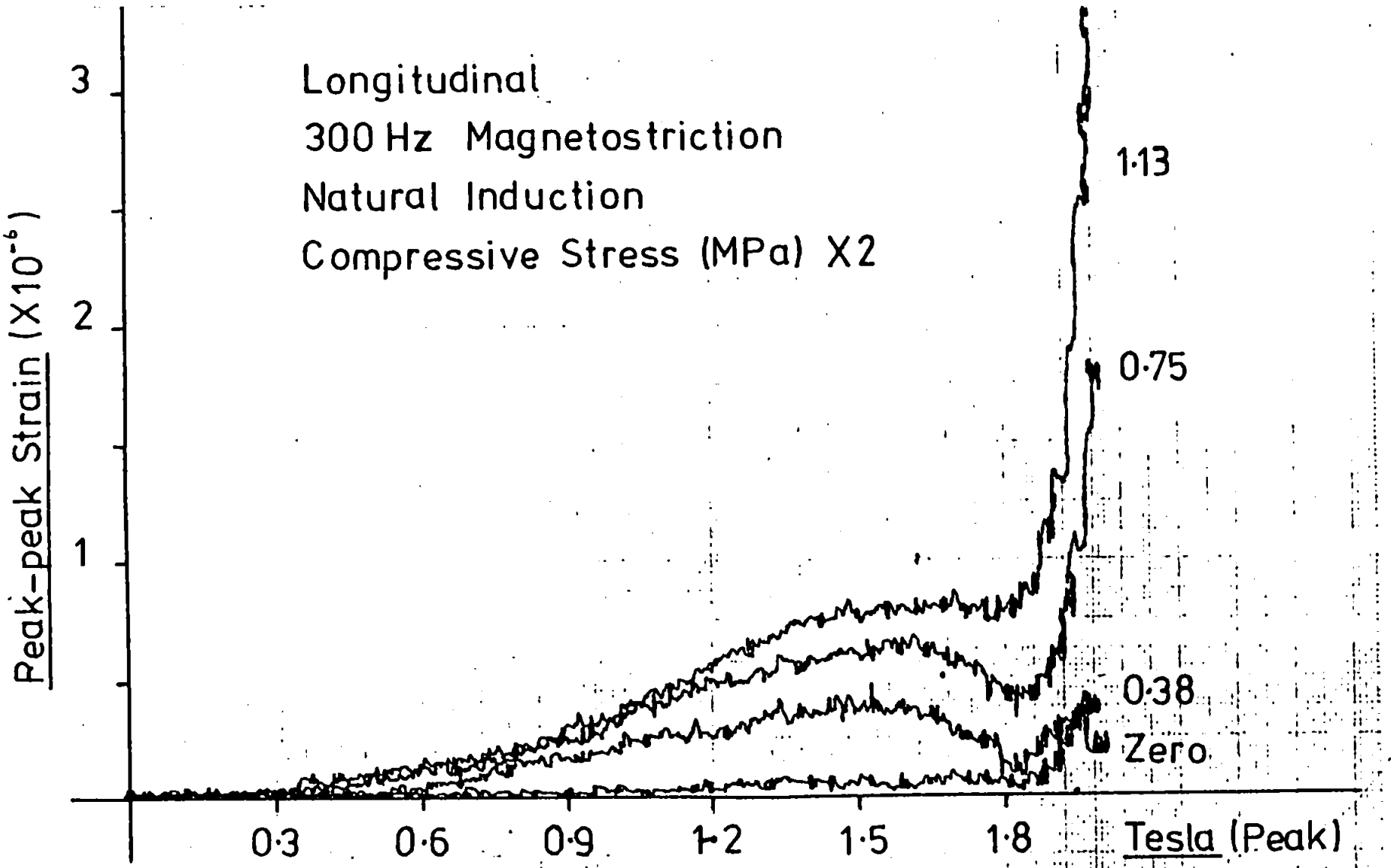

FIG:513.a. Variation of 3rd Harmonic Magnetostriction

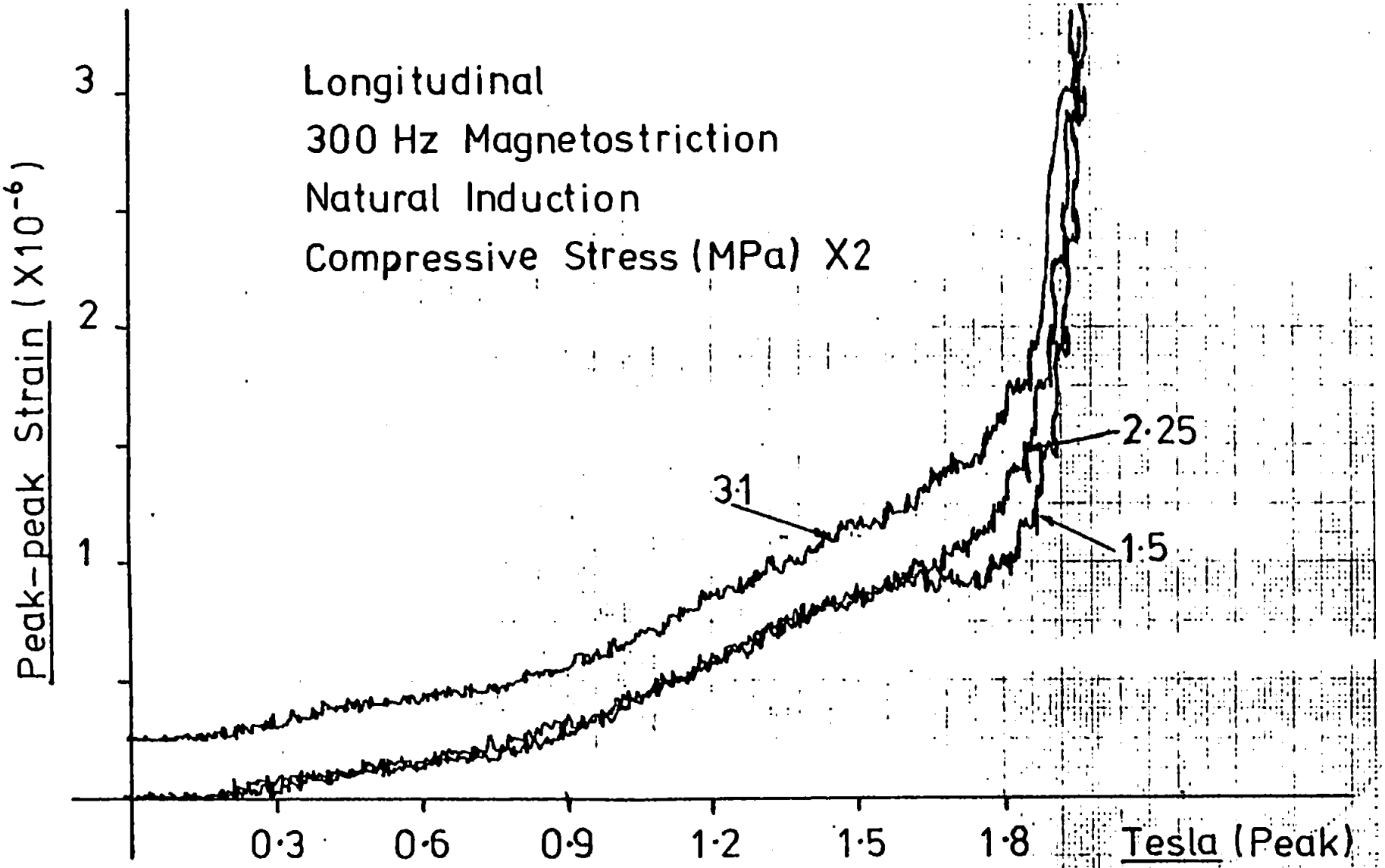

FIG: 5.13.b. Variation of 3rd Harmonic Magnetostriction

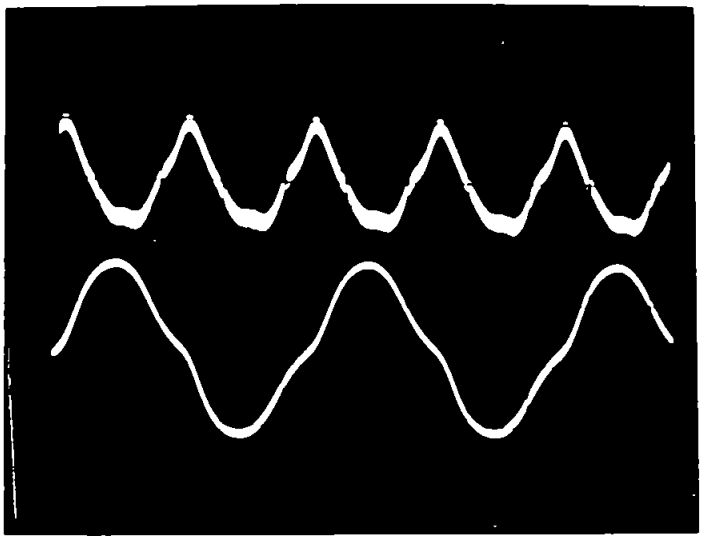

FIG. 5.14. Typical Magnetostriction and Induction Waveforms without Feedback Control.

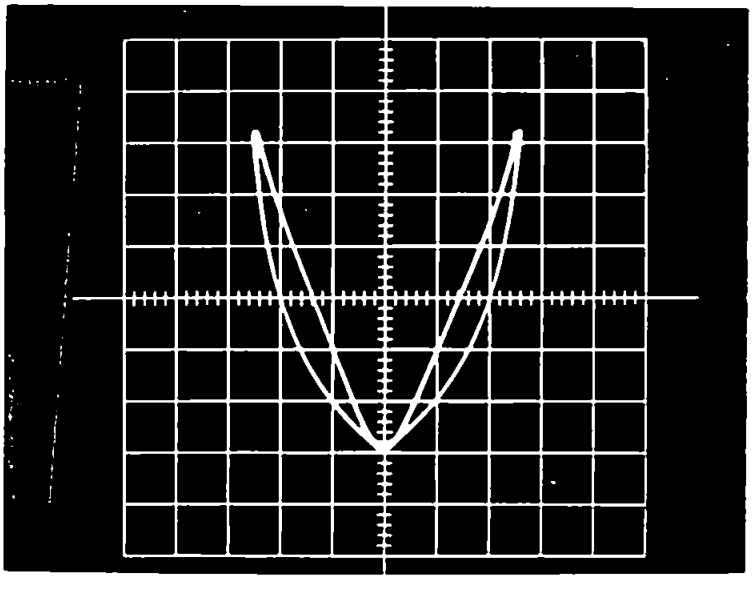

FIG. 5.15. Typical 100 Hz Magnetostriction 'Butterfly' loop without Feedback Control of Induction.

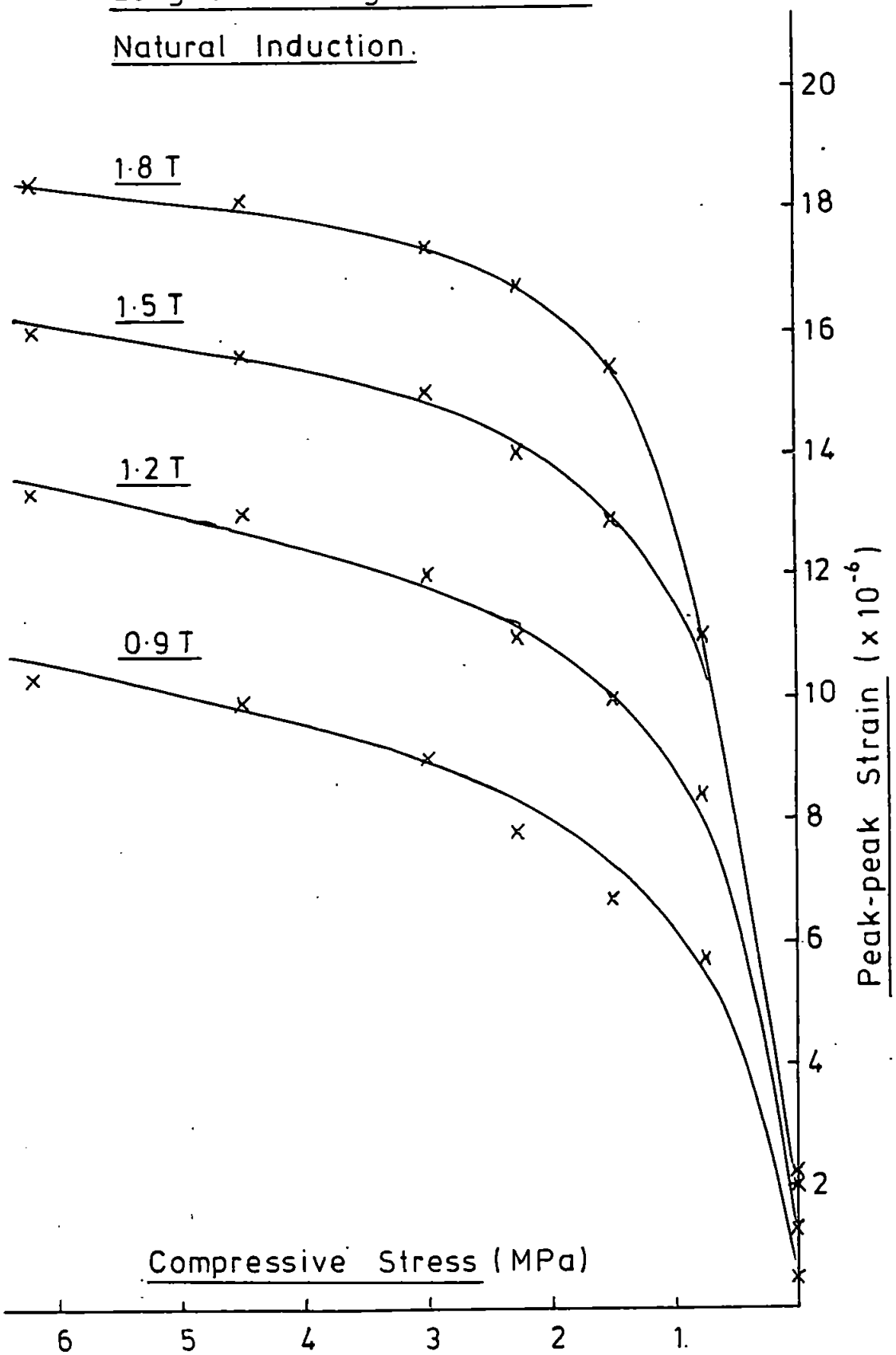

FIG. 5.16. First Harmonic (100 Hz) Stress Sensitivity.

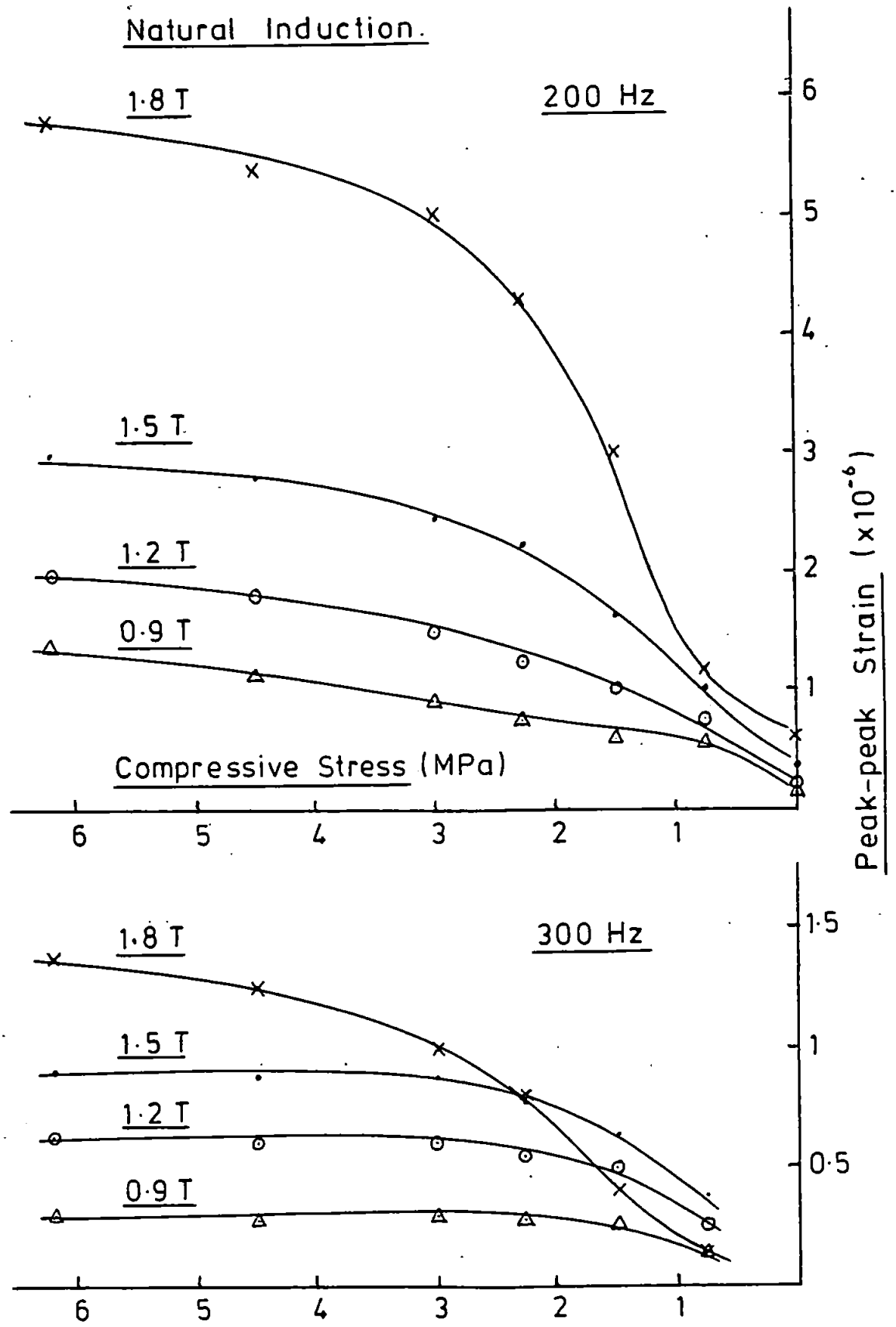

FIG. 5.17. Second (200 Hz) & Third (300 Hz) Harmonic Stress Sensitivities.

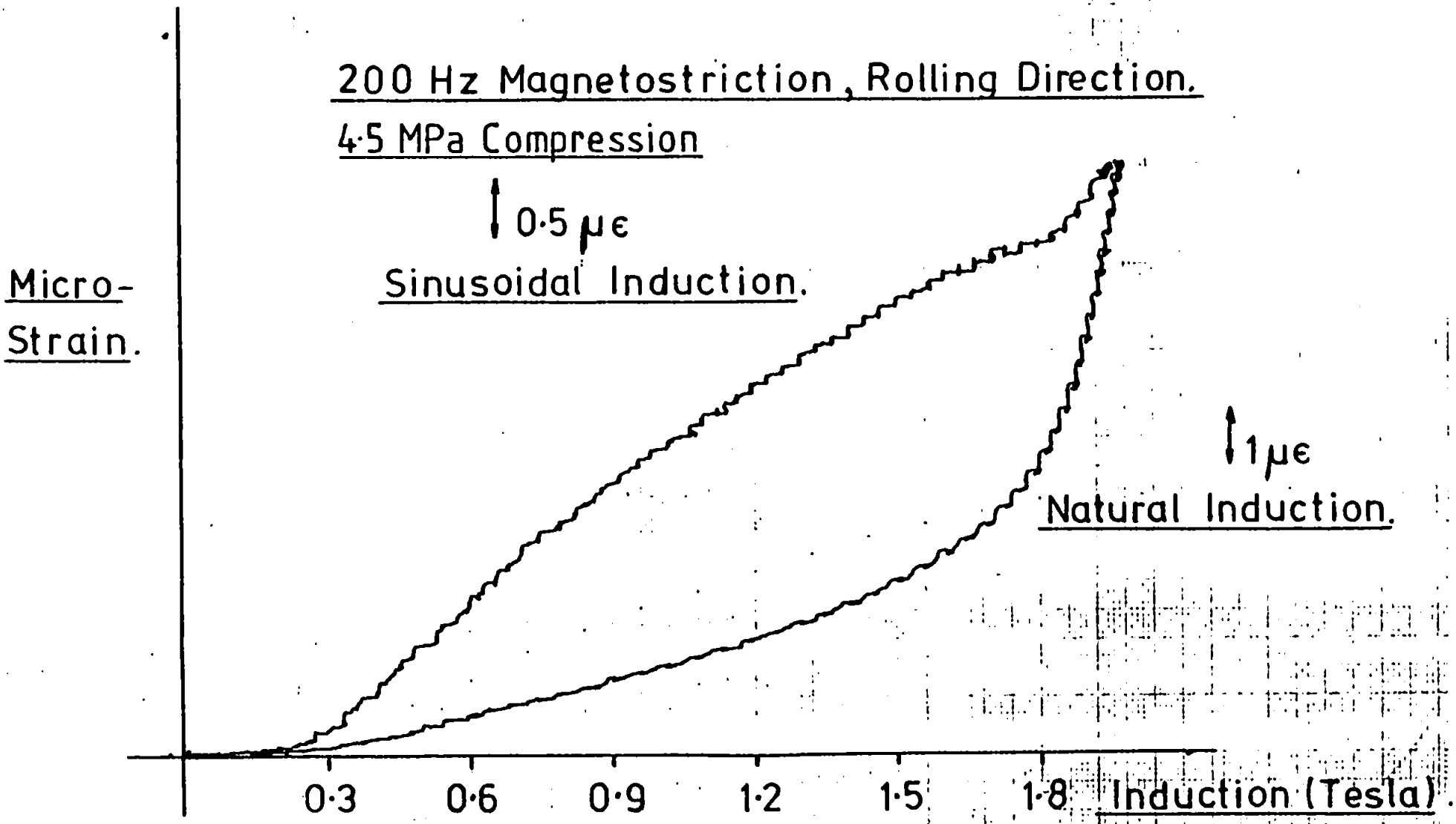

FIG. 5.18. 2nd Harmonic with & without Controlled Induction.

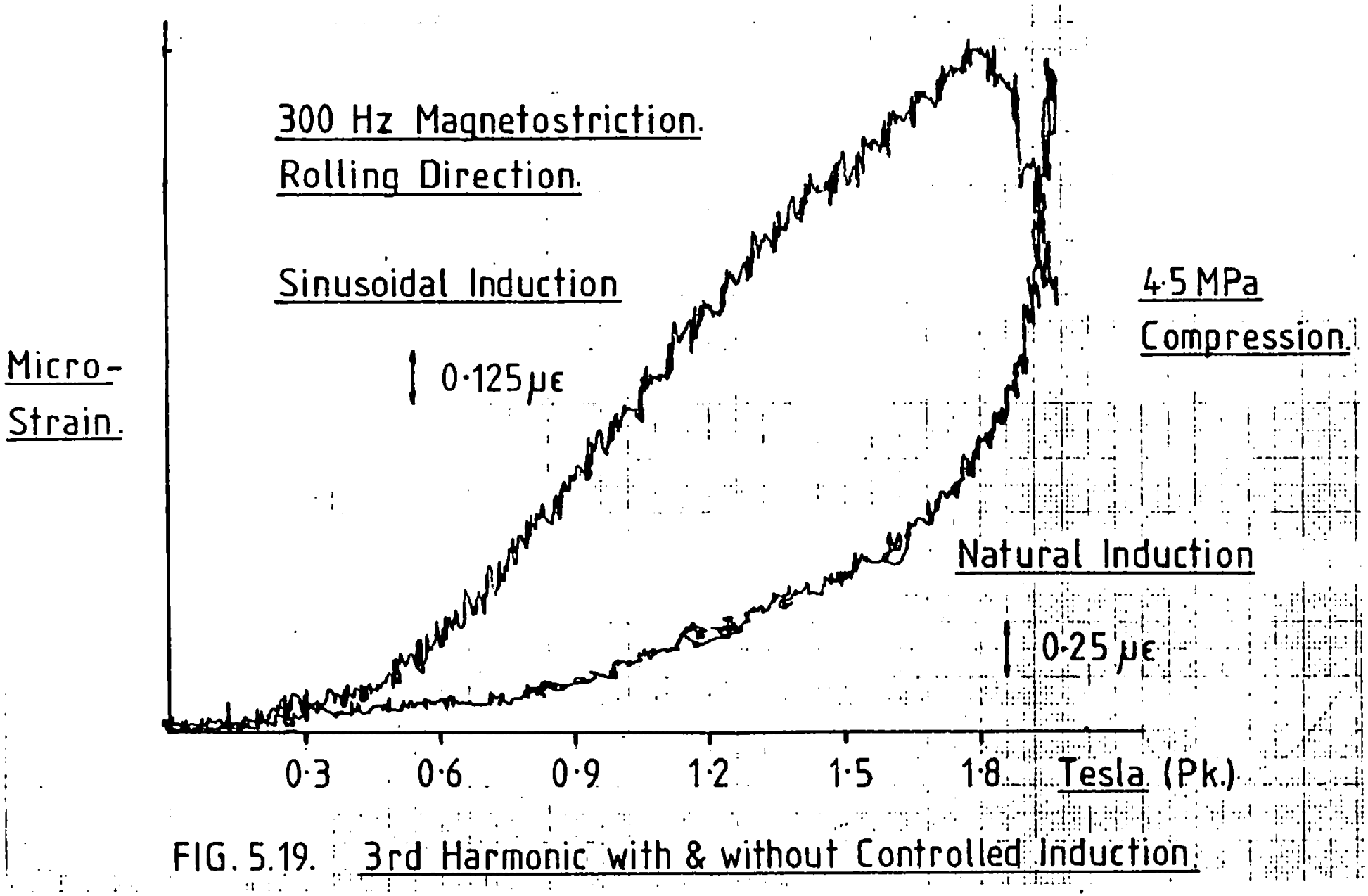

FIG. 5.19. 3rd Harmonic with & without Controlled Induction.

curves are typical of the effect and only one stress level is shown for brevity.

Examination of these curves reveals a surprising result, since the values for natural induction (when that induction will contain a higher harmonic content) are lower than the values with controlled, sinusoidal induction.

A possible explanation of this phenomena can be obtained if the variation of flux harmonics with peak flux density are examined. The variations in the 3rd and 5th harmonics of flux density were measured over the range of stress levels for peak inductions up to saturation. The values were recorded on the X - Y plotter by the means described in Chapter Four, Section 4.4.3. The results for the case of zero stress and 0.76 MPa are shown in Fig. 5.20, and for a stress of 4.5 MPa in Fig 5.21.

For the higher stress case of Fig. 5.21 it will be noticed that a minimum occurs in the 3rd harmonic of induction at around 1.8T. Simultaneous observation of the flux waveforms during the measurements revealed a phase change in the 3rd harmonic with respect to the fundamental at around the same induction.

An experiment was therefore conducted to measure the phase relationship beween the fundamental and 3rd harmonic of induction. This was conducted at a stress level of 4.5 MPa, and the phase shift measured by setting up Lissajou figures on the X - Y oscilloscope included in the Apparatus. The peak induction was increased from the demagnetized state in increments up to saturation, and the phase angle and its sense with respect to the fundamental recorded at each increment. The result obtained is shown in Fig 5.22, wherein the phase lag is seen to be about 130^{o} up to around 1.8T, then changes rapidly to 10^{o} lag as the induction is increased to saturation.

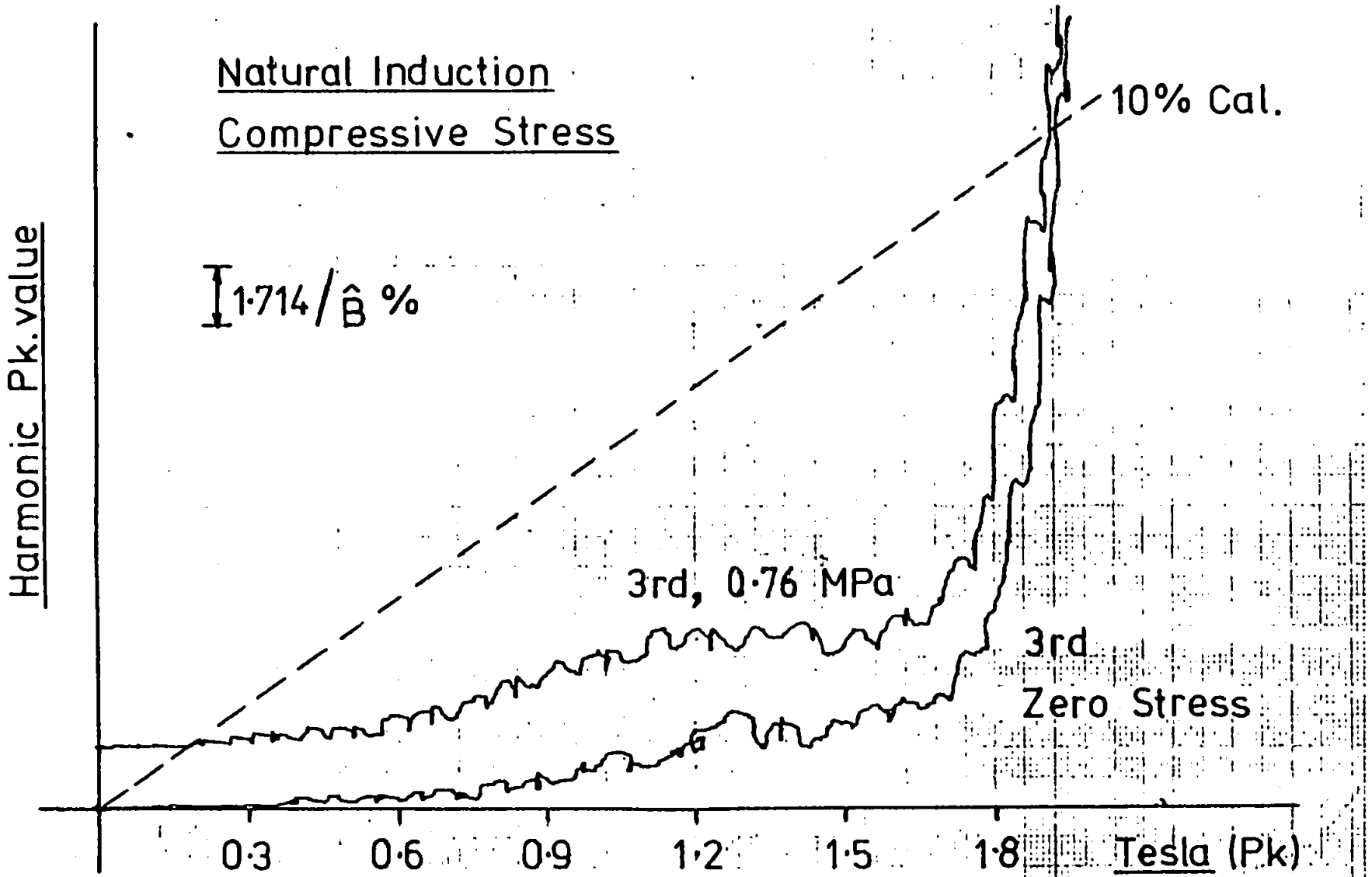

FIG:5.20. Variation of Induction Harmonics

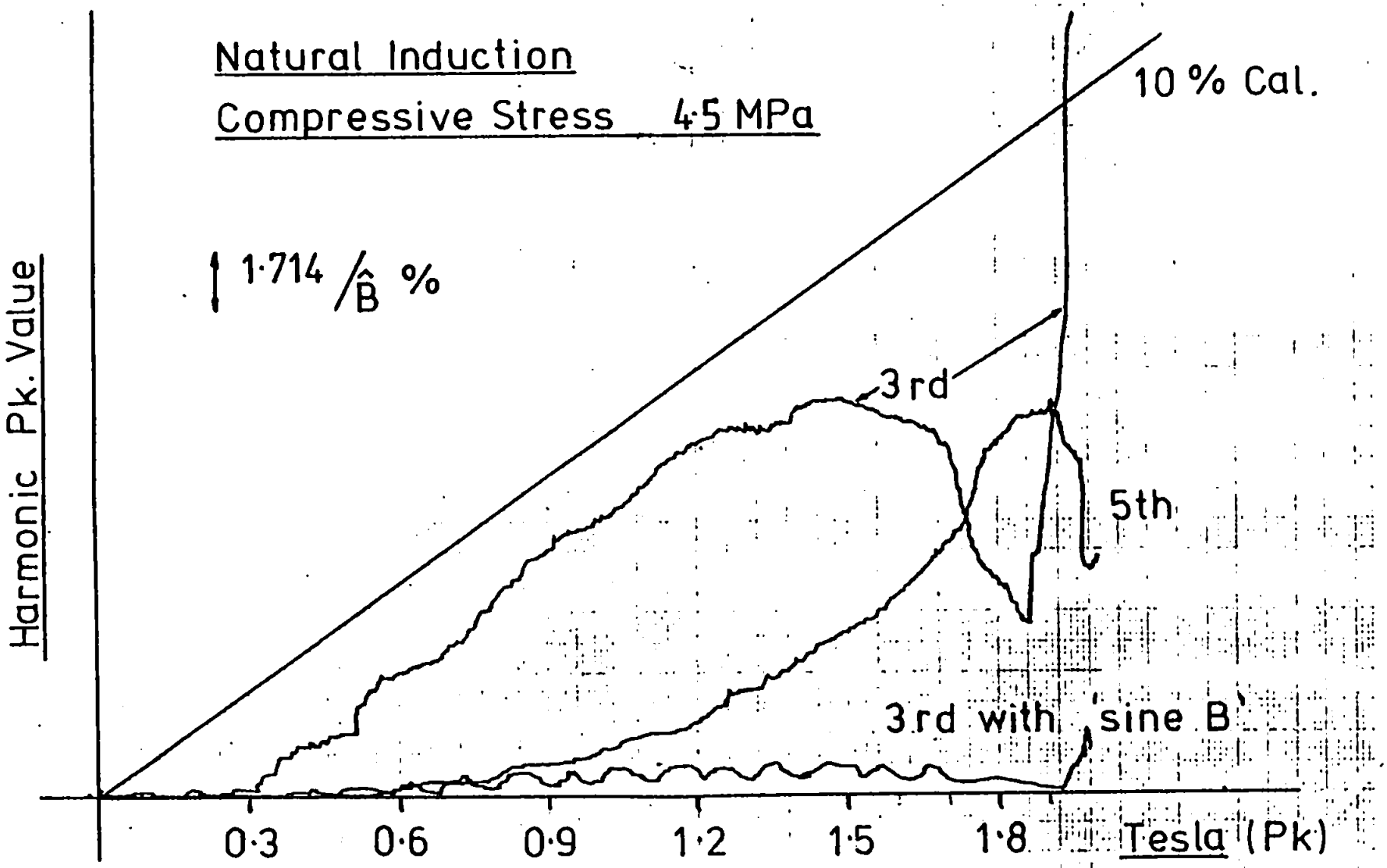

FIG: 5.21. Variation of Induction Harmonics

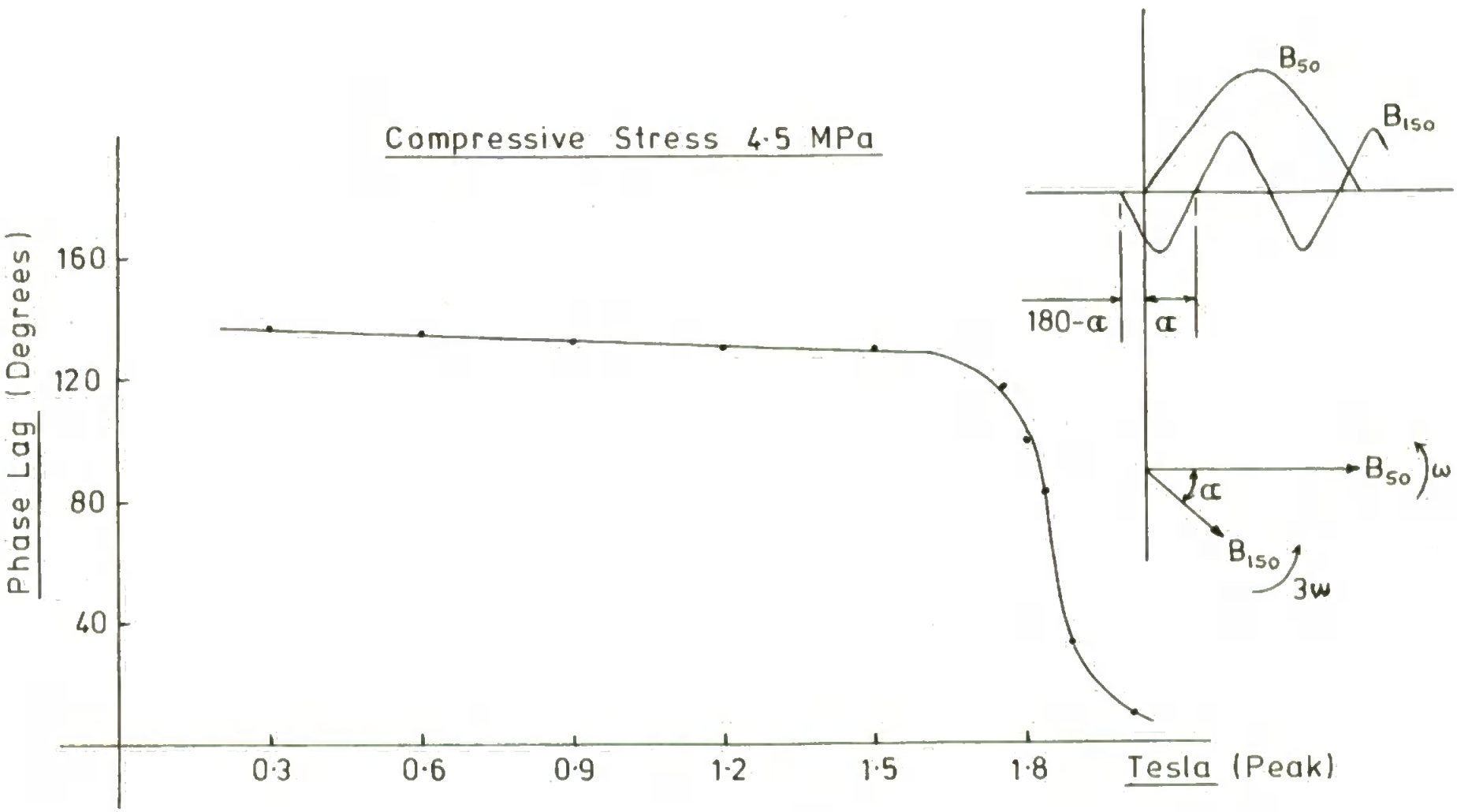

FIG. 5.22. Phase Angle Variation of Induction Third Harmonic.

Reference to the Theory developed in Chapter Three, Section 3.3.4, shows how such a phase change in the flux harmonic can explain the phenomena revealed in Figs. 5.18 and 5.19. A summary graph of the results of this theory is shown again in Fig. 5.23, wherein it will be seen that a cross-over exists between the conditions of controlled (p=o) and uncontrolled (p>o) flux waveforms at phase shifts between 80^{o} and 130^{o} lag. In particular, for the above measured results at a stress of 4.5 MPa, when from Fig 5.21 the flux is seen to contain a maximum 3rd harmonic of about 9%, and approximating the magnetostriction hysteresis to a value $\alpha = 10^{o}$, a crossover will occur at between 60^{o} and 70^{o}. Above this angle the theory predicts that the uncontrolled flux waveshape condition will lead to lower magnetostriction harmonics than for the controlled condition.

When the rapid phase change occurs around 1.8T the theory predicts a large increase in harmonic content when the phase angle approaches zero, as shown in Fig 5.23. This is indeed the case, and explains the experimental curves of Figs. 5.18 and 5.19.

The reason for the phase change in the 3rd harmonic of flux can be explained with reference to the changes in the shape of the B-H loop caused by (a) stress-induced distortion, and (b) saturation. Below the knee of the curve stress-induced distortion exists alone and produces harmonics, as shown by the example of the 3rd harmonic produced from a stress-distorted B-H loop in the photographs of Figs. 5.24 and 5.25. Increasing stress will increase the distortion and increase the flux harmonic content as previously shown by the curves of Figs 5.20 and 5.21. It will be seen in the photograph of Fig 5.25 that the phase of the 3rd harmonic produces a "peaky" flux waveform, the phase angle approaching 180^{o} lag.

With the onset of saturation another, separate, source of distortion occurs, as shown in the photographs of

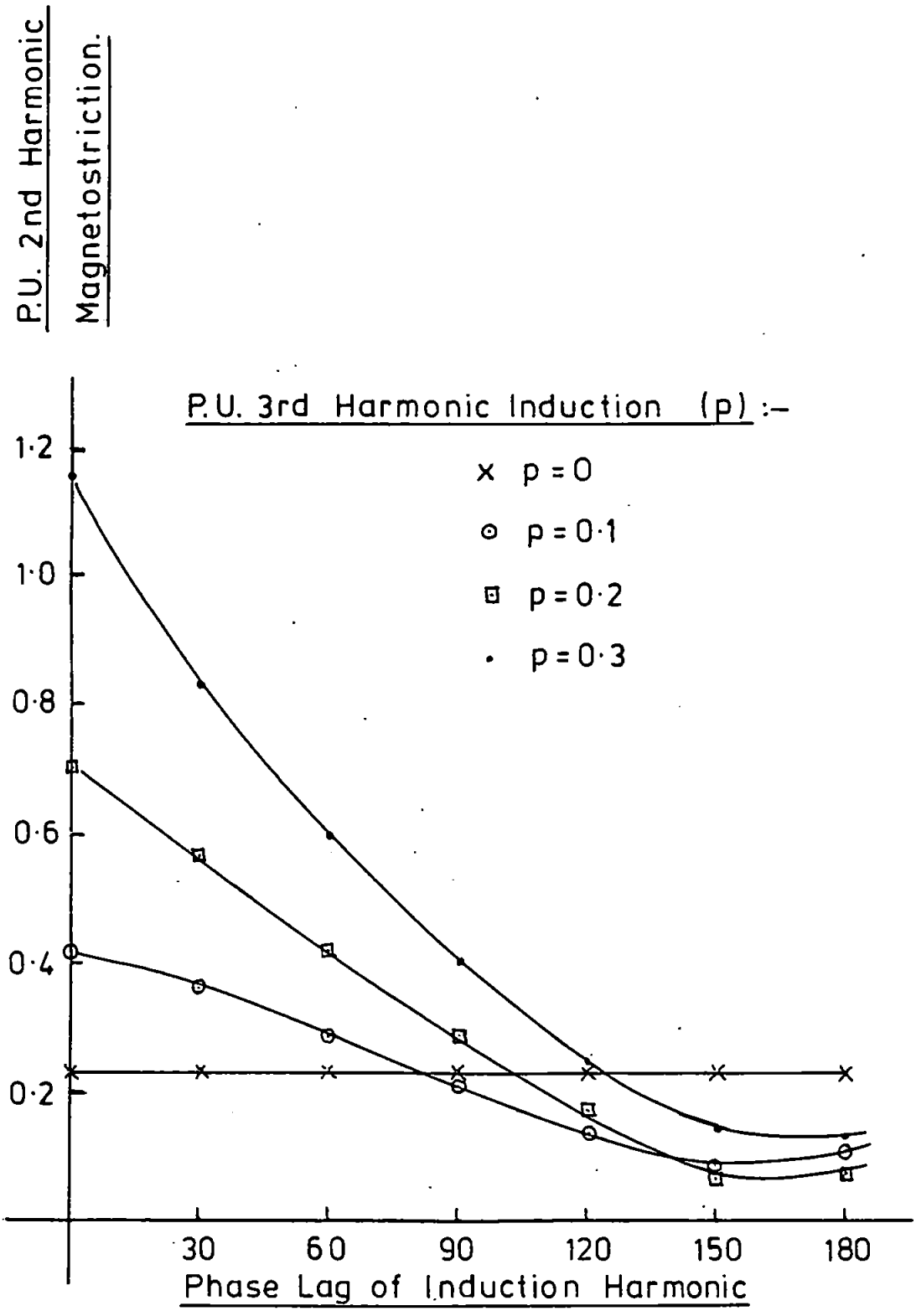

FIG. 5.23. P.U. 2nd Harmonic Magnetostriction :- Dependence on 3rd Harmonic of Induction.

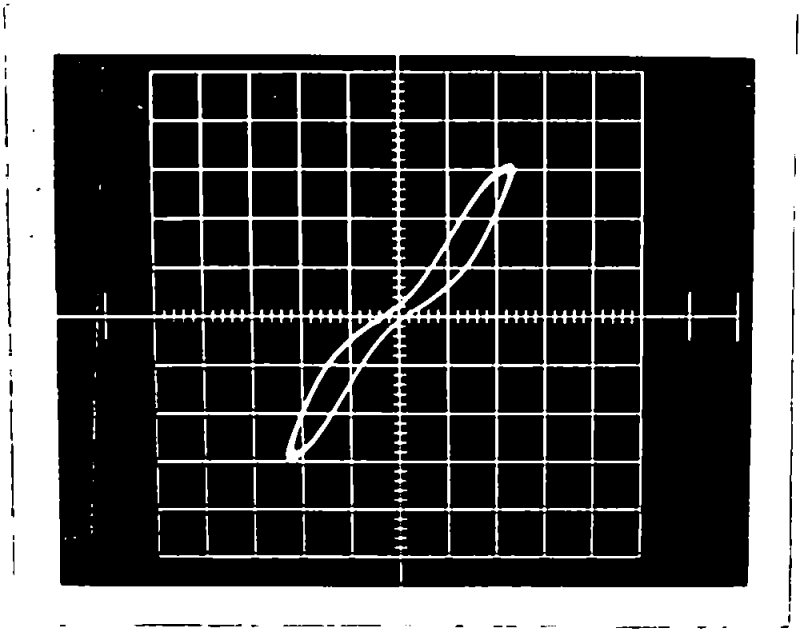

FIG. 5.24. Typical B - H loop showing Stress Induced Distortion.

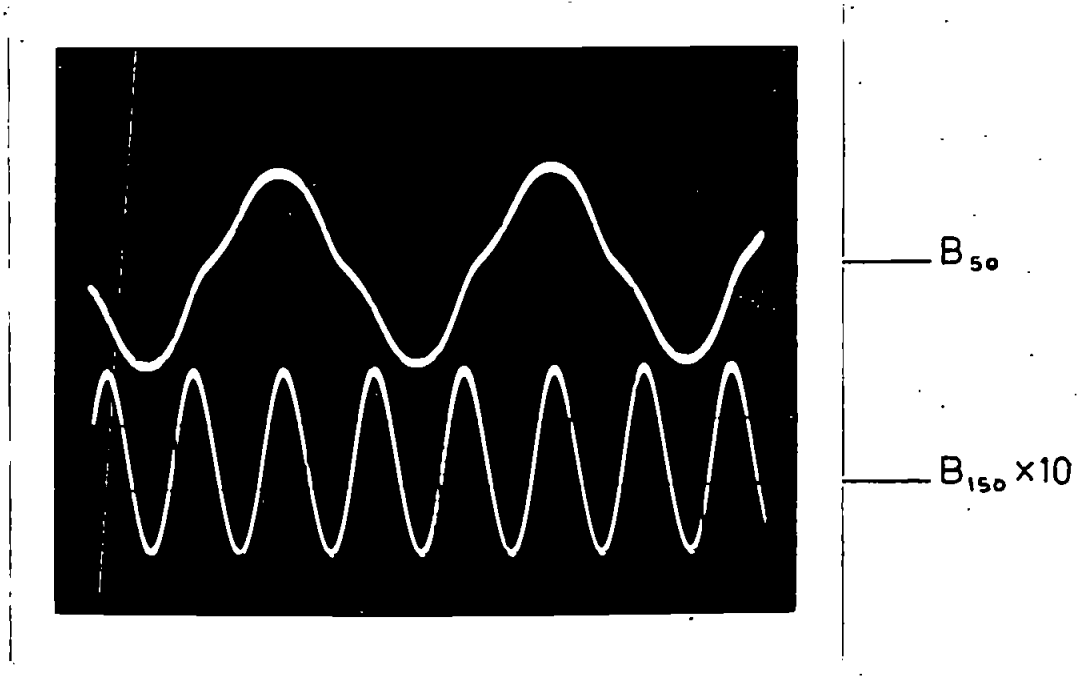

FIG. 5.25. Typical Flux Waveshape and Third Harmonic of Flux produced by the Stress Distortion of FIG.5.24.

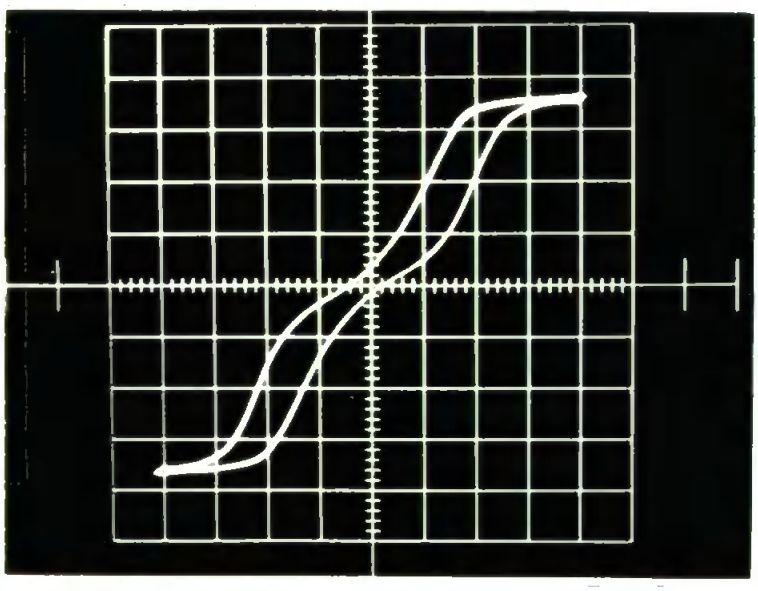

FIG 5.26 Typical B - H loop showing the Saturation Condition under stress.

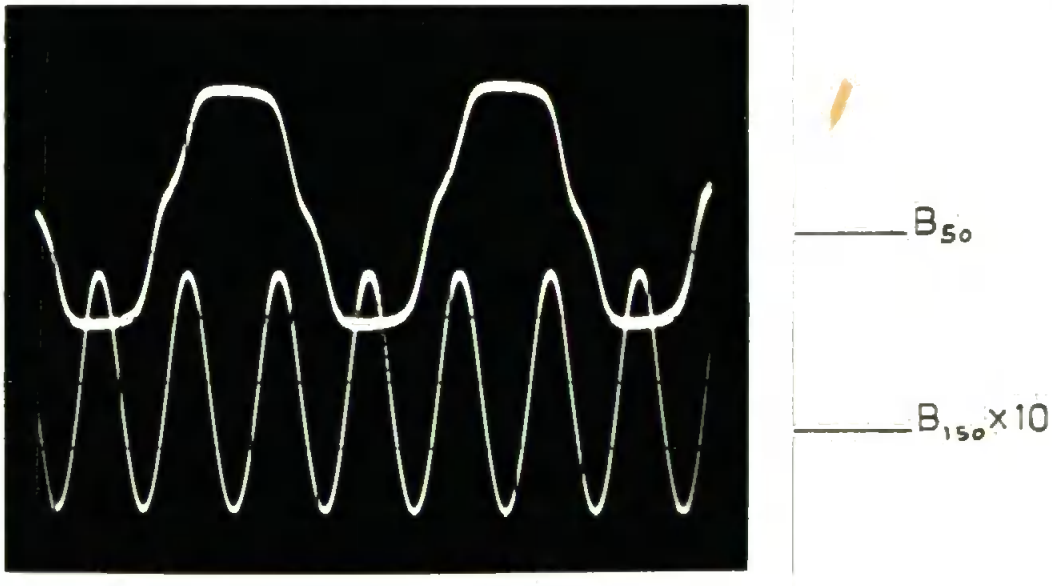

FIG 5.27 Typical Flux Waveshape and Third Harmonic of Flux produced by the Saturation Condition of FIG. 5.26.

Figs. 5.26 and 5.27, producing a "flat-top" flux waveform with a harmonic phase angle approaching zero degrees.

When the two cases are combined, as the induction increases, the effective addition of the two, separate 3rd harmonics produces an amplitude change and a phase change, appearing as a sideways shift along the time axis. This is exactly the effect shown in the phase angle variation of Fig 5.22.

Thus there is a large 3rd harmonic phase shift for flux densities below the knee of the magnetization curve, and, from the Theory of Chapter Three, Section 3.3.4, this will cause a reduction in the 2nd and 3rd harmonics of magnetostriction. Above the knee the phase shift approaches zero and produces a large increase in both magnetostriction harmonics.

5.3.4. The Effect of Tensile Stress

Due to re-orientation of supplementary domain structure from the $\pm$ [100] and $\pm$ [010] directions into the [001] direction nearest to the rolling direction under the application of tensile stress in that direction, it will be expected to observe very small values of magnetostriction. This is the prediction of theory and is the experimental conclusion of other workers (7,8).

A measurement of longitudinal magnetostriction harmonics was made at a tensile stress of 3 MPa and the results are shown in Fig 5.28. A maximum level of 0.9 μe is observed at saturation for the fundamental strain, approximately 5% of that for the case of compressive stress.

The curves of Fig. 5.28 also indicate the noise level in the measuring equipment, equivalent to a strain of about 0.05 μe at 300 Hz. They also reveal the level of sensitivity (resolution) obtained; thus at 100 Hz it is possible to resolve changes in the order of 0.025 μe,

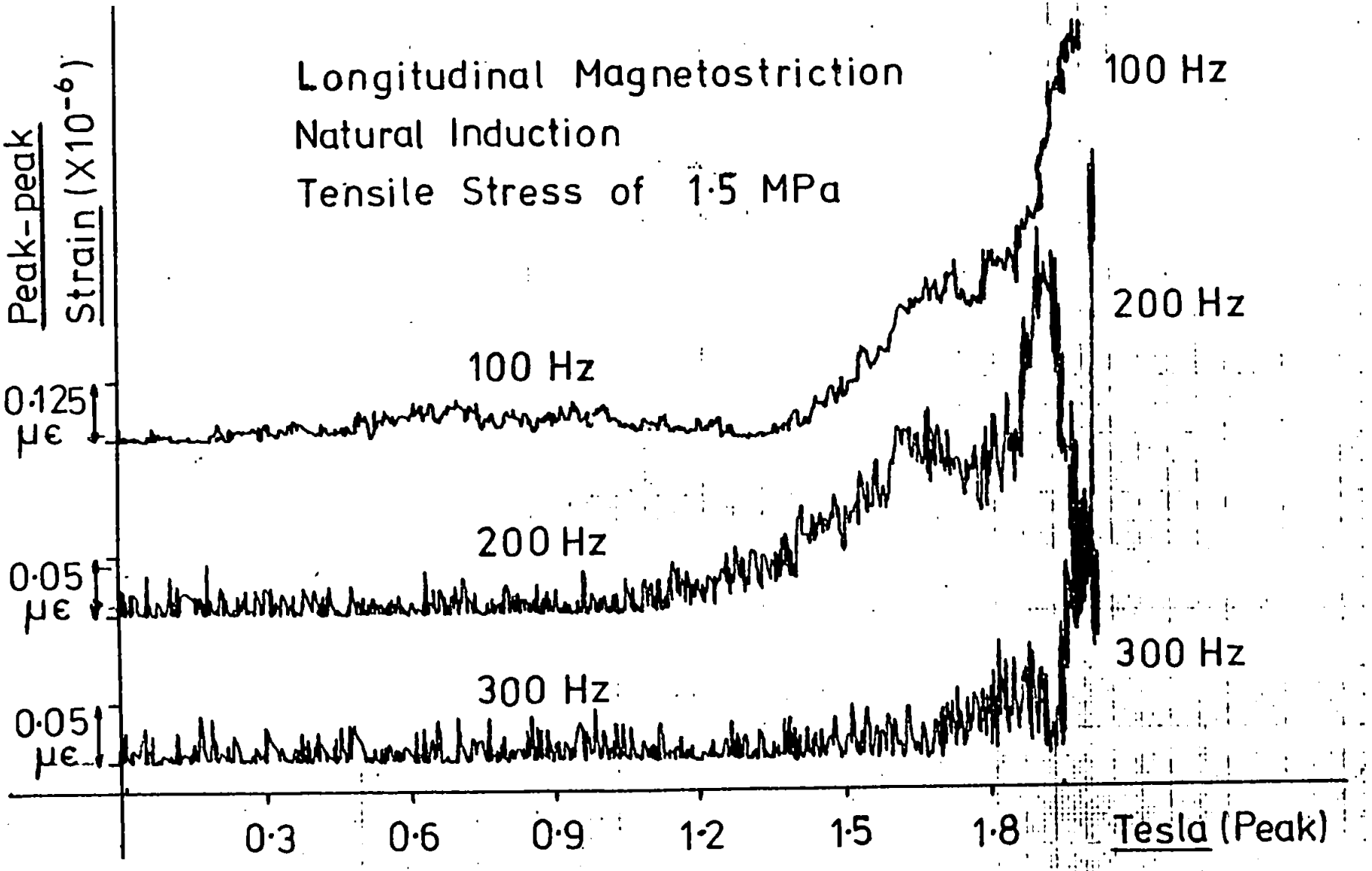

FIG: 5.28: Magnetostriction Variation – Tensile Stress

equivalent to 2 Å at 8 mm transducer separation.

5.4 Magnetostriction Measurements Transverse to the Rolling Direction.

These measurements were made for the same range of stresses and induction as before, but with the transducers rotated through 90° about the central, longitudinal axis of the grain.

5.4.1. Sinusoidal (Controlled) Flux Waveshape.

The flux waveshape control was identical to that previously employed for Section 5.3.1. The results for the first three magnetostriction harmonics versus peak flux density in the grain are shown in Figs. 5.29, 5.30 and 5.31.

The derived curves for magnetostriction versus compressive stress are shown in Figs 5.32 and 5.33.

The shapes of these curves are similar to those for the longitudinal magnetostriction but at a reduced level. Those at 100 Hz are similar to reported values by other workers, but the 2nd and 3rd harmonics are new results, showing similarities to the fundamental. As before, the increase in strain during the onset of Stress Pattern I is apparent.

5.4.2. Natural (Uncontrolled) Flux Waveshape.

The results of Section 5.4.1. are repeated but with no feedback control of the specimen excitation, as in Section 5.3.2. The results are shown in Figs 5.34, 5.35 and 5.36 with the derived curves of magnetostriction harmonics versus compressive stress shown in Figs 5.37 and 5.38.

The same comments may be made regarding the

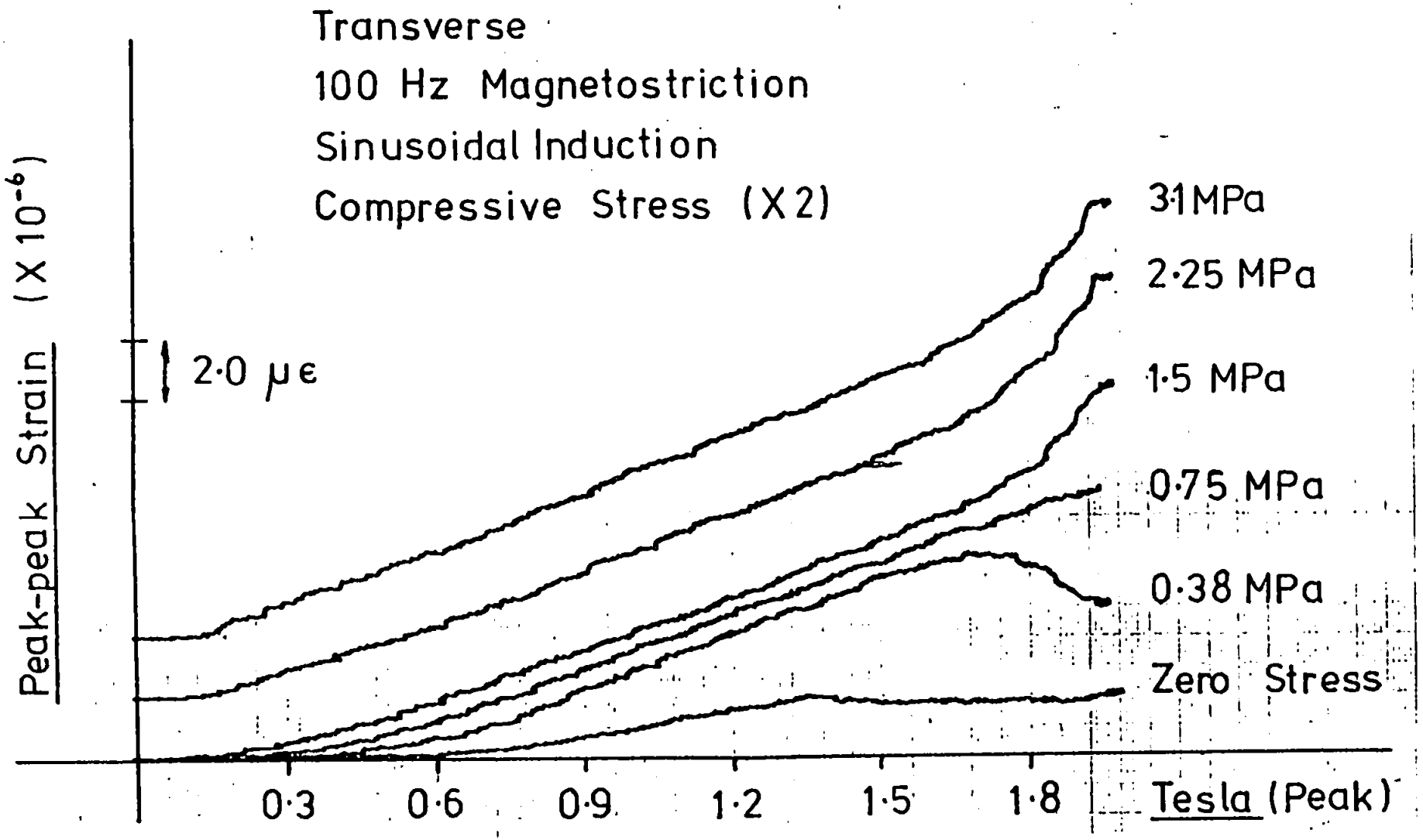

FIG:5.29. Variation of 1st Harmonic Magnetostriction

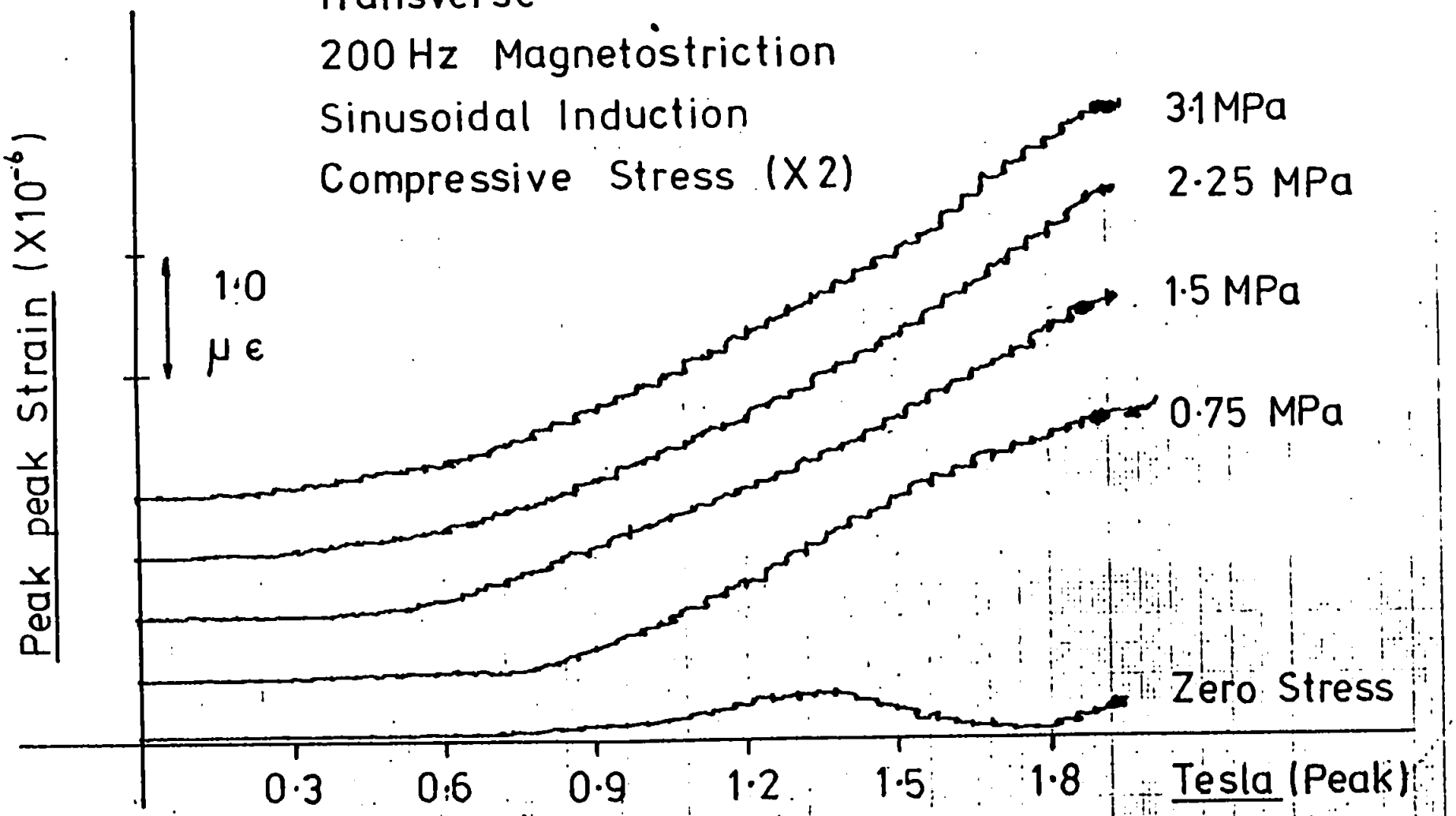

FIG. 5.30 Variation of 2nd Harmonic Magnetostriction

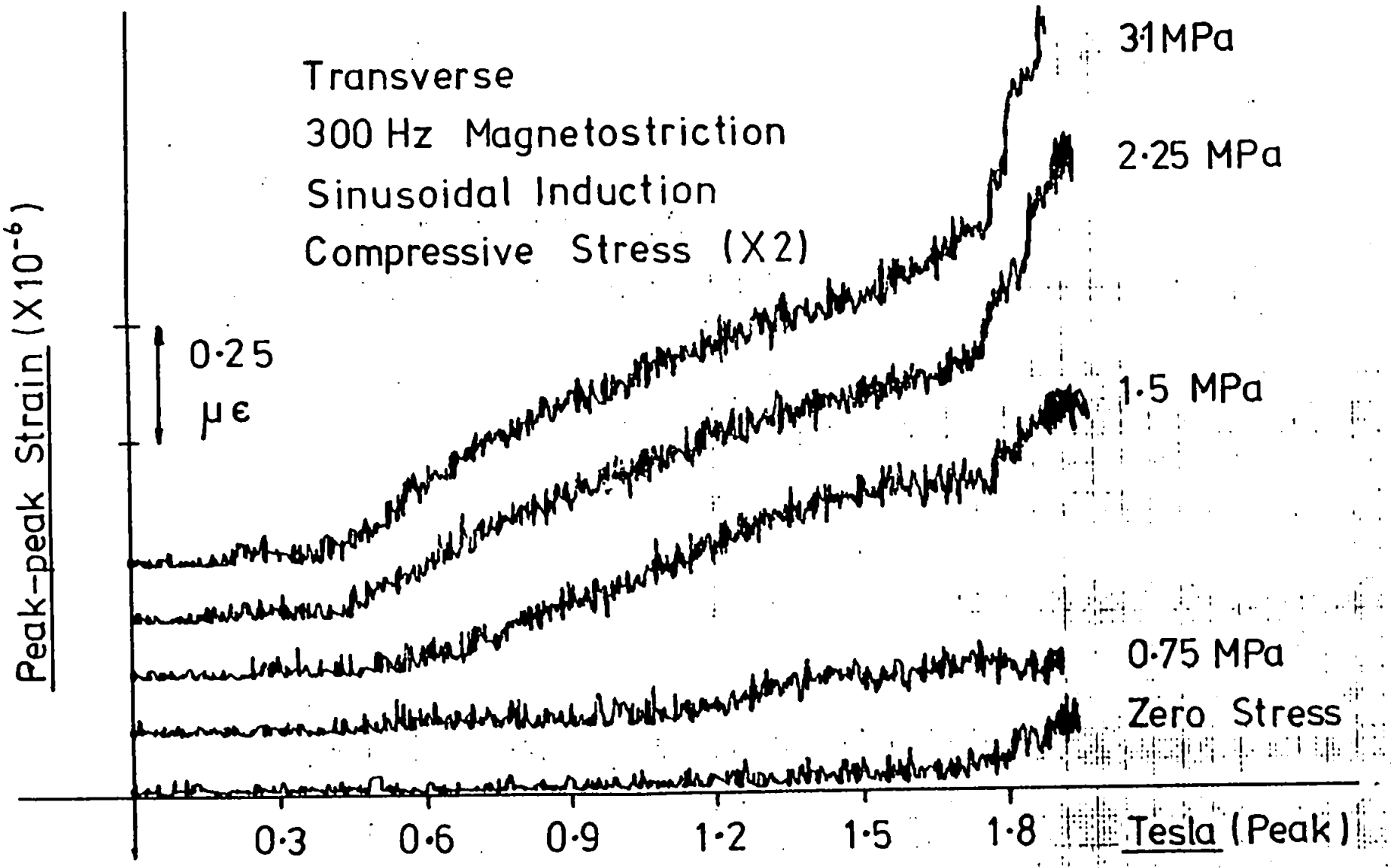

FIG:5.31: Variation of 3rd Harmonic Magnetostriction

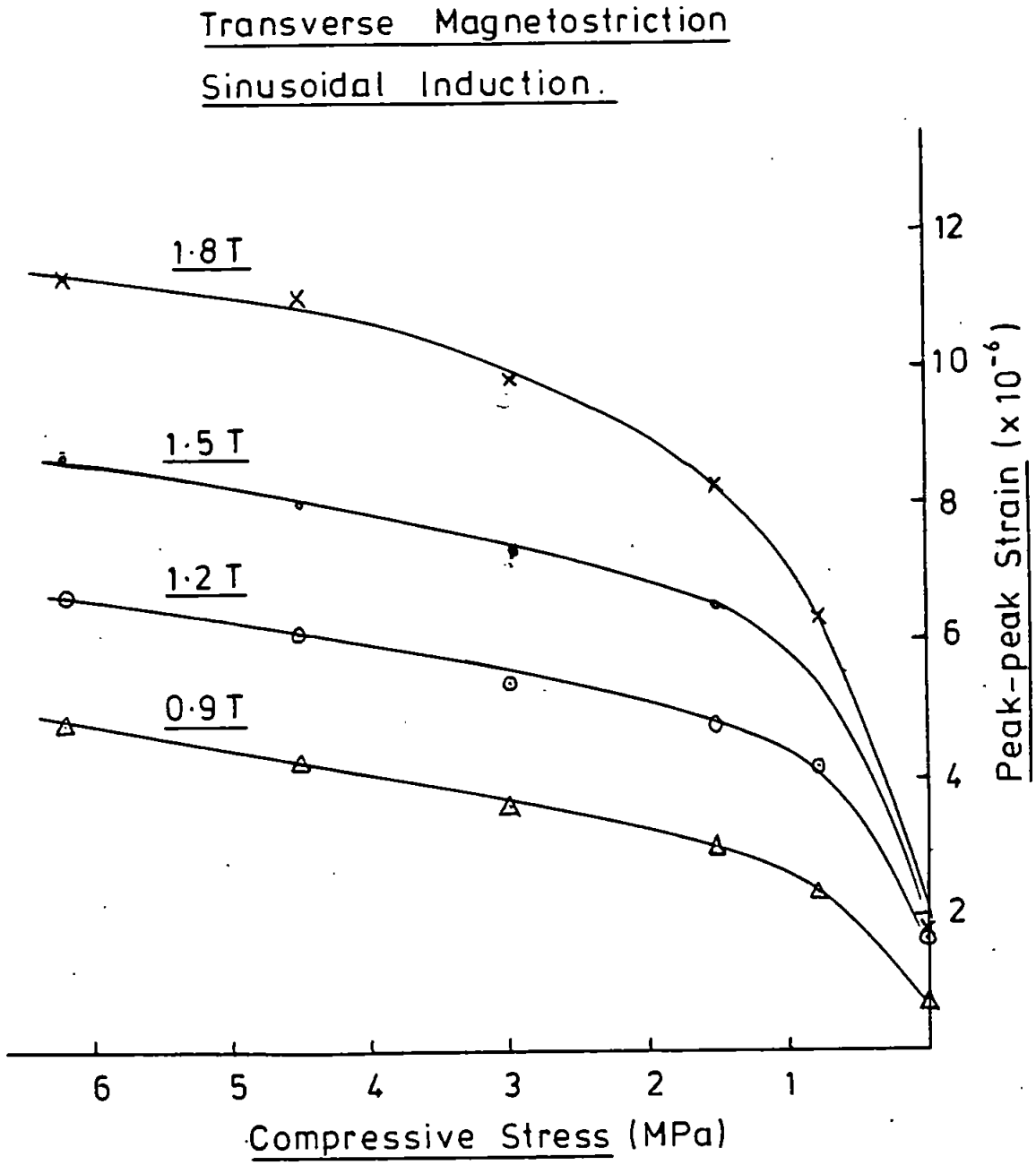

FIG. 5.32. First Harmonic (100 Hz) Stress Sensitivity.

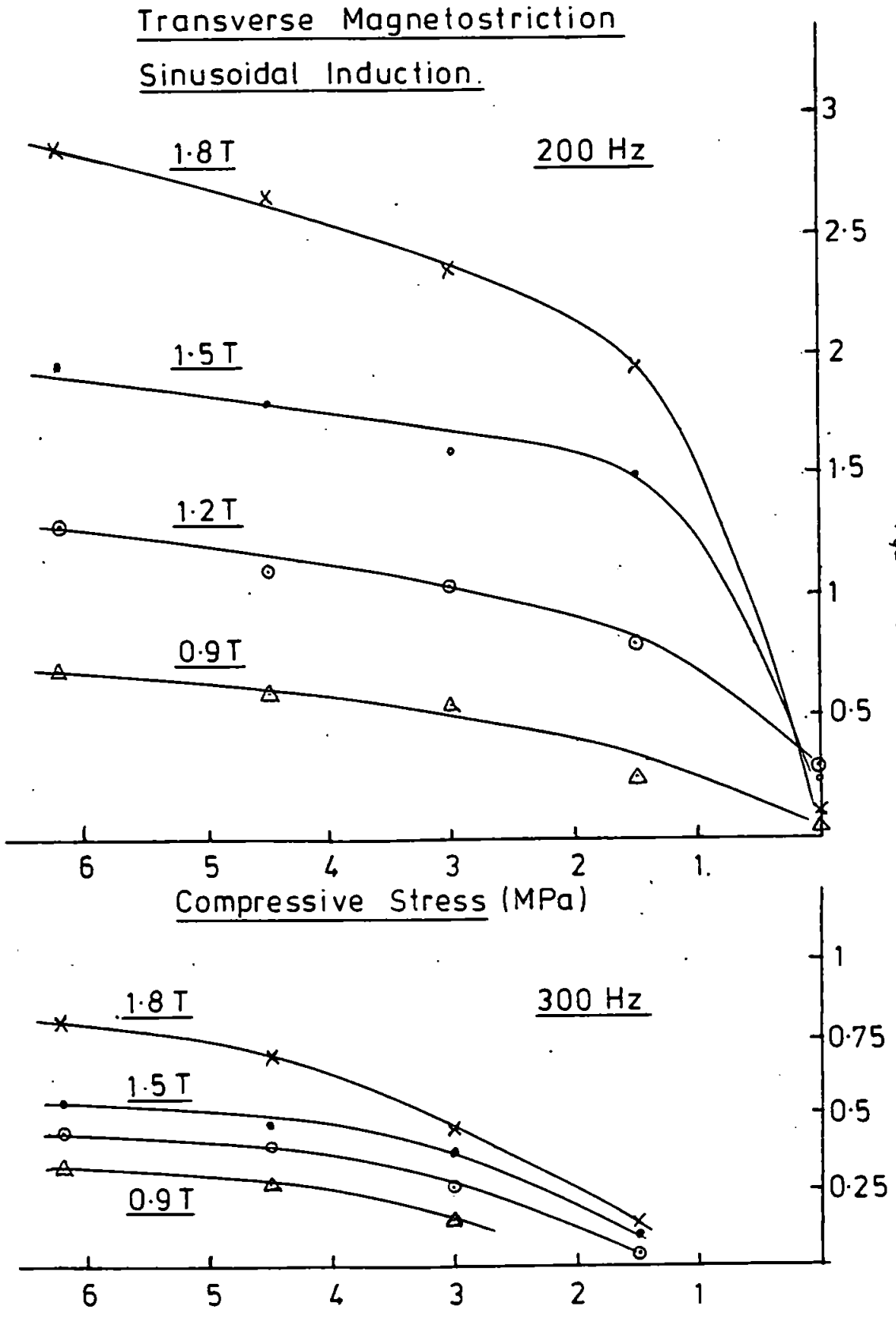

FIG. 5.33. Second (200 Hz) & Third (300 Hz) Harmonic Stress Sensitivities.

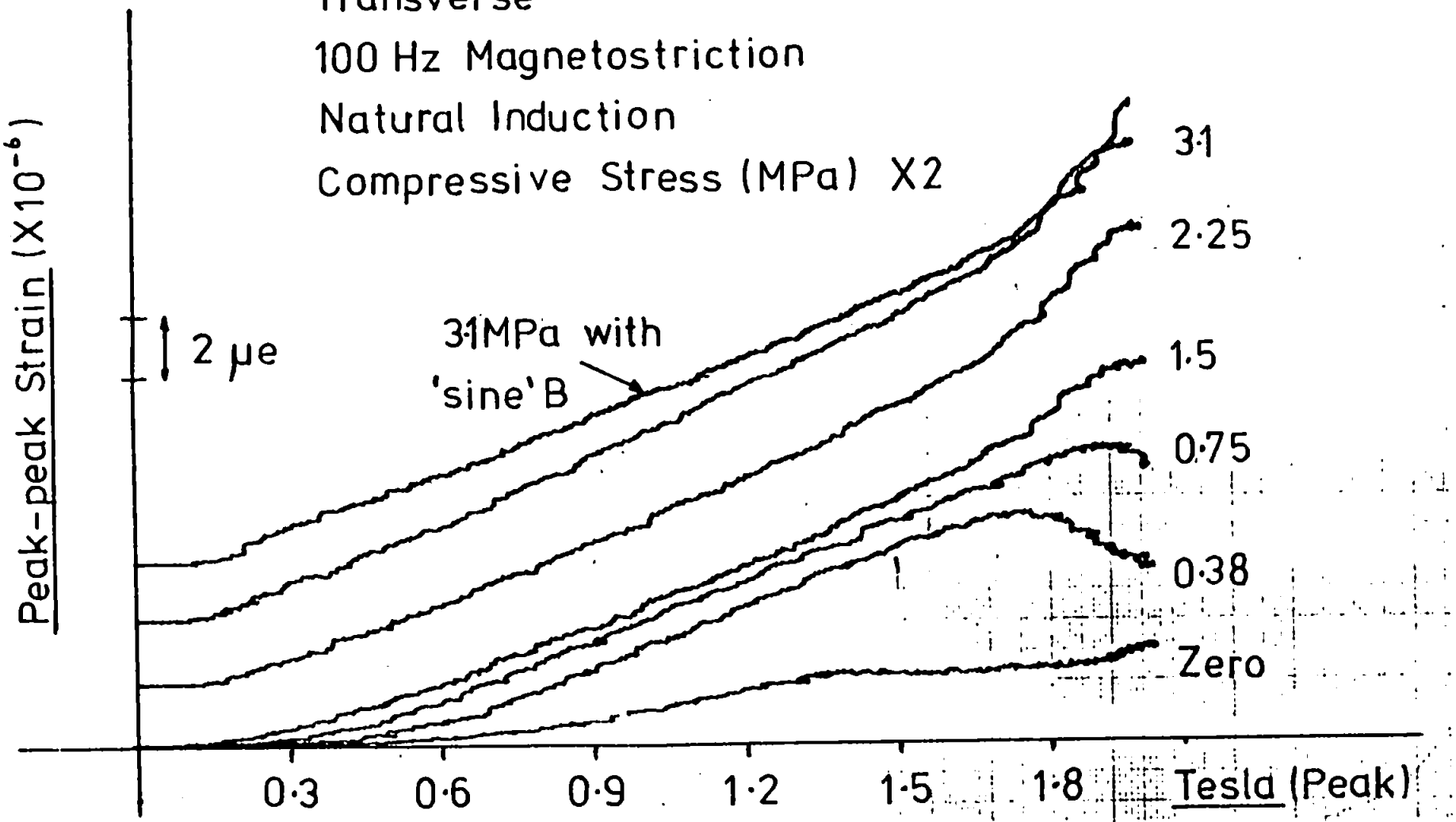

FIG: 5.34. Variation of 1st Harmonic Magnetostriction

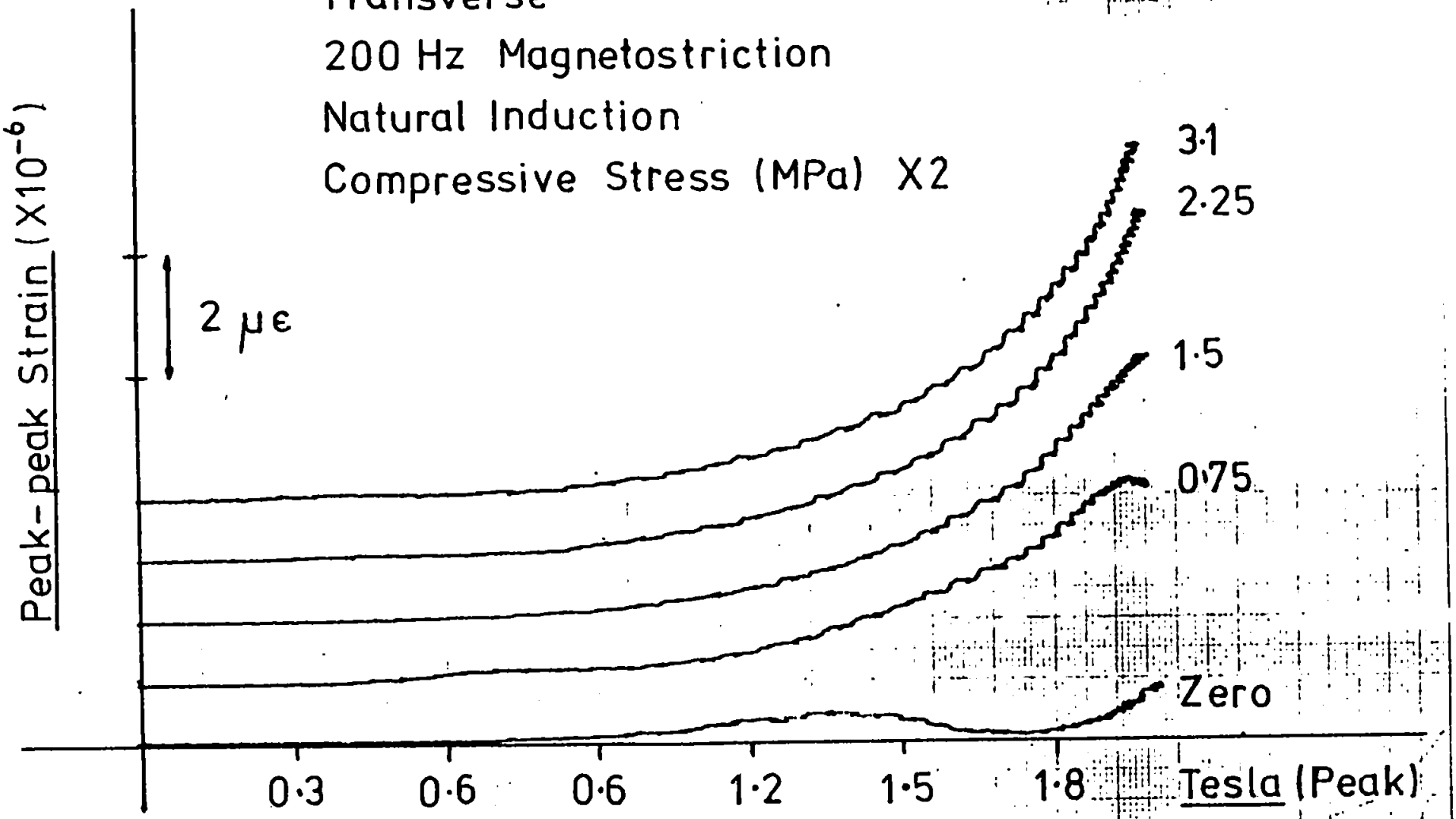

FIG : 5.35. Variation of 2nd Harmonic Magnetostriction

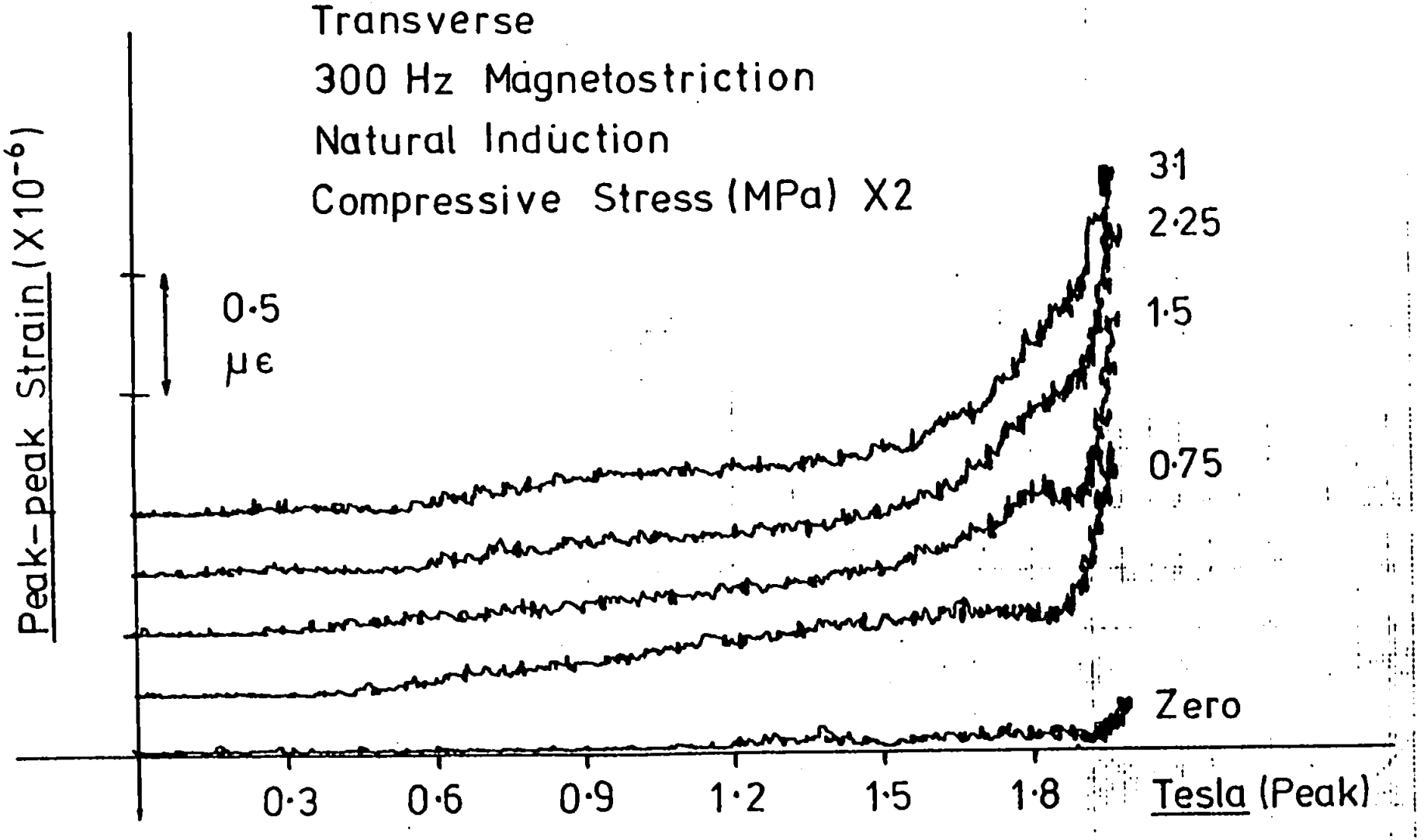

FIG: 5.36. Variation of 3rd Harmonic Magnetostriction

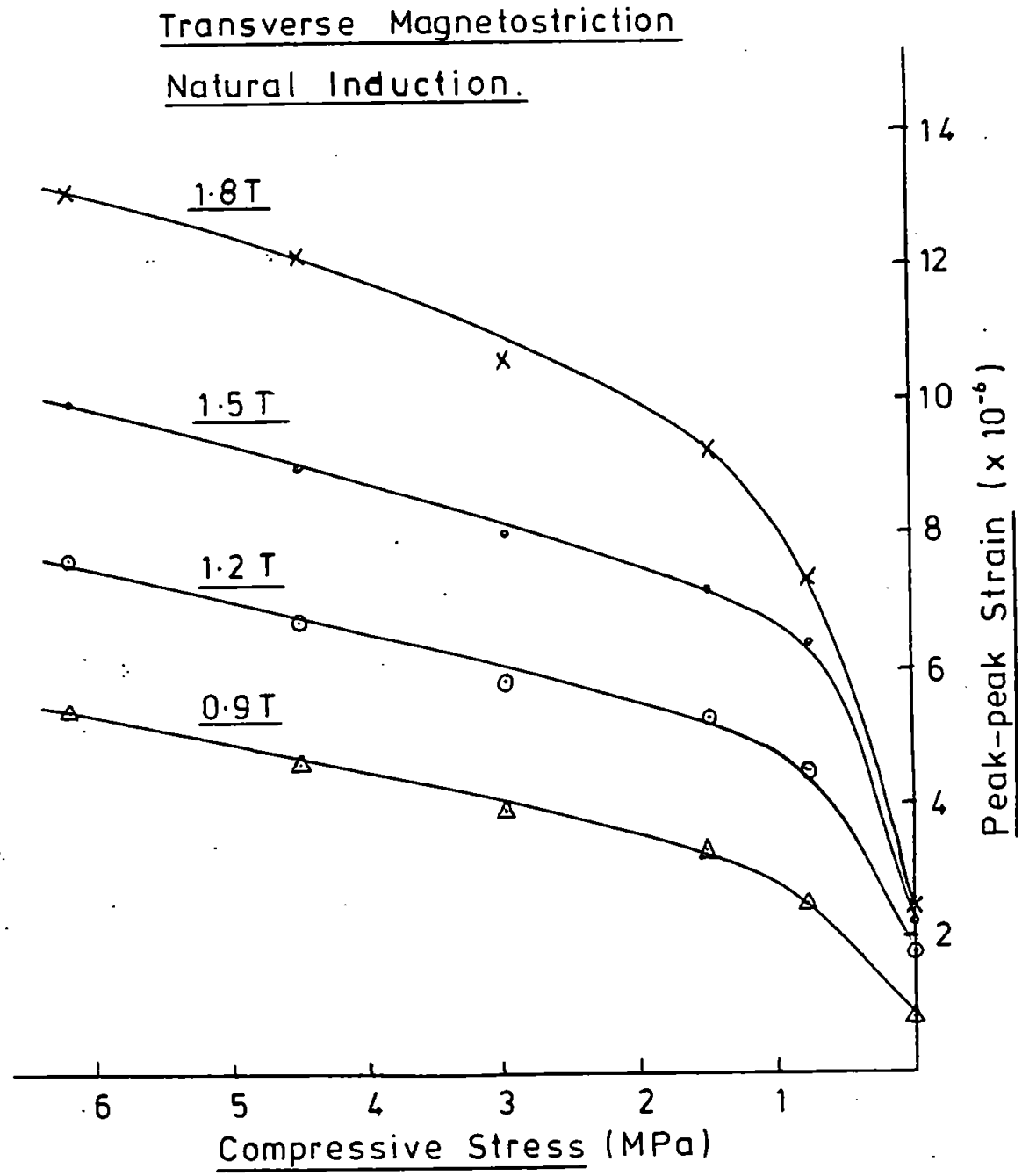

FIG. 5.37. First Harmonic (100 Hz) Stress Sensitivity.

Transverse Magnetostriction

Natural Induction.

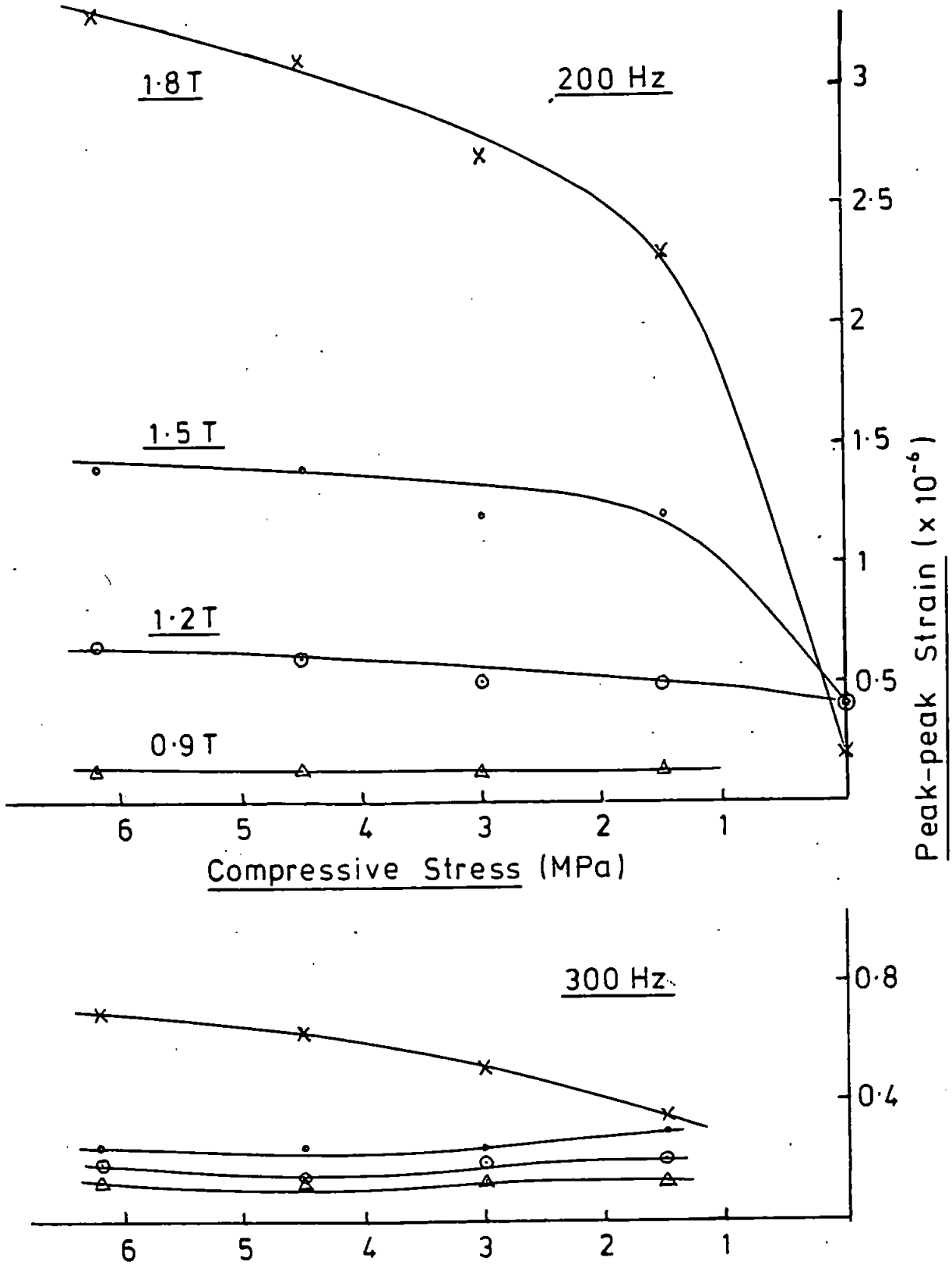

FIG. 5.38. Second (200 Hz) & Third (300 Hz) Harmonic Stress Sensitivities.

general shape of the curves as for all previous measurements, and, as before, the higher harmonics show lower values below about 1.8T when the induction is uncontrolled as compared to the controlled (sinusoidal) condition.

5.4.3 Comparison of Results for Transverse Magnetostriction.

The consequences of a comparison between the results of Section 5.4.1. and Section 5.4.2 and the subsequent explanation are essentially the same as those given in Section 5.3.3. for magnetostriction harmonics measured paralled to the rolling direction. The noteworthy differences between the 2nd and 3rd harmonics for the conditions of controlled and uncontrolled induction are again apparent, and are explained by cancellation of flux third harmonics and the resultant phase shift near to saturation.

Curves are not included in the interests of brevity but can be derived from Figs 5.29 to 5.38.

5.5 Relationships between Longitudinal and Transverse Magnetostriction Harmonics.

The theory of the origins of magnetostriction presented in Chapter Three, Section 3.3.2, suggests that a simple 2:1 relationship exists between stresses applied in tension, transverse to the rolling direction and stresses applied in compression, paralled to the rolling direction, which will provide the same longitudinal magnetostriction, during the existence of the Stress Induced Pattern I. (6).

An alternative theory for the case when transverse and longitudinal magnetostriction levels are compared for compressive stress in the rolling direction only can be developed as follows.

It has been shown in Chapter Three, Section

3.3.2 that the increase in magnetoelastic energy in a cubic crystal under stress is given by

$$E_\lambda = -\sigma\lambda \qquad \text{---------- 5.1}$$

where the stress (σ) is positive for tension or negative for compression, and where λ is given by equation 3.7 of Chapter Three. Combining these equations gives

$$E_\lambda = -\sigma\left[\frac{3}{2}\lambda_{100}\left(l_1^2m_1^2 + l_2^2m_2^2 + l_3^2m_3^2 - \frac{1}{3}\right) + 3\lambda_{111}\left(l_1l_2m_1m_2 + l_1l_3m_1m_3 + l_2l_3m_2m_3\right)\right] \qquad \text{--- 5.2}$$

where l_1 l_2 l_3 are the direction cosines of the measurement directions for λ, m_1 m_2 m_3 are the direction cosines of the domain saturation magnetization (M_s), with respect to the direction in which the stress is applied.

For a compressive stress along the rolling direction, and with λ measured in the same direction, then $l_1 = m_1 = \cos 0^\circ = 1$, $l_2 = m_2 = l_3 = m_3 = \cos 90^\circ = 0$ Therefore

$$E_\lambda = +\sigma\frac{3}{2}\lambda_{100}\left(1 - \frac{1}{3}\right)$$

$$= +\sigma\lambda_{100} \qquad \text{---------- 5.3}$$

However, if λ is now measured in the transverse direction at right angles to the direction of compressive stress, then $l_1 = l_2 = l_3 = \cos 90^\circ = 0$, $m_1 = 1$, $m_2 = m_3 = \cos 90^\circ = 0$.

Therefore

$$E_\lambda = + \sigma \frac{3}{2} \lambda_{100} \left\{ 0 - \frac{1}{3} \right\}$$

$$= - \frac{1}{2} \sigma \lambda_{100} \quad \text{---------- 5.4}$$

Comparison of equation 5.3 and 5.4 shows that a compressive stress of twice the magnitude will need to be applied in the rolling direction in order to produce the same effect on the magnetostriction measured in the transverse direction as compared to when it was measured in the rolling direction.

The negative sign arises since any longitudinal extension will be accompanied by a transverse contraction or vice-versa, the Poisson Effect.

Equally, for the same level of compressive stress the magnetostriction measured in the transverse direction will be half that value measured in the longitudinal or rolling direction.

To test this theory, values of the first three magnetostriction harmonics reported in Sections 5.3.1. and 5.3.2. for the case of measurements parallel to the rolling direction have been plotted against those values reported in Section 5.4.1 and 5.4.2 for the case of transverse measurements.

These experimentally derived results are shown in Figs 5.39, 5.40 and 5.41 for the first, second and third magnetostriction harmonics respectively.

Examination of these results shows a good correlation with the 2:1 ratio predicted by the theory, not

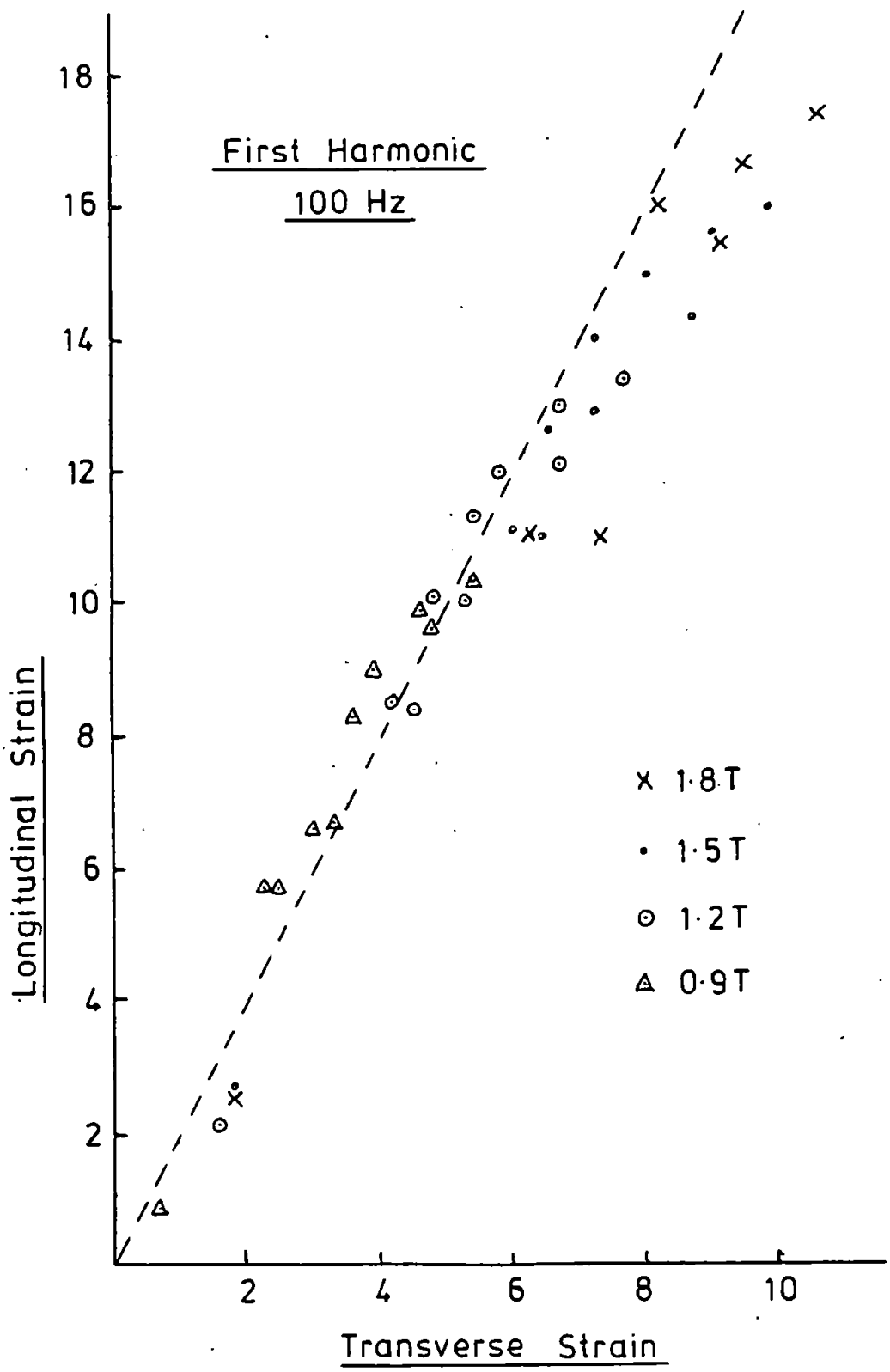

FIG. 5.39. Longitudinal–Transverse Magnetostriction Relations.

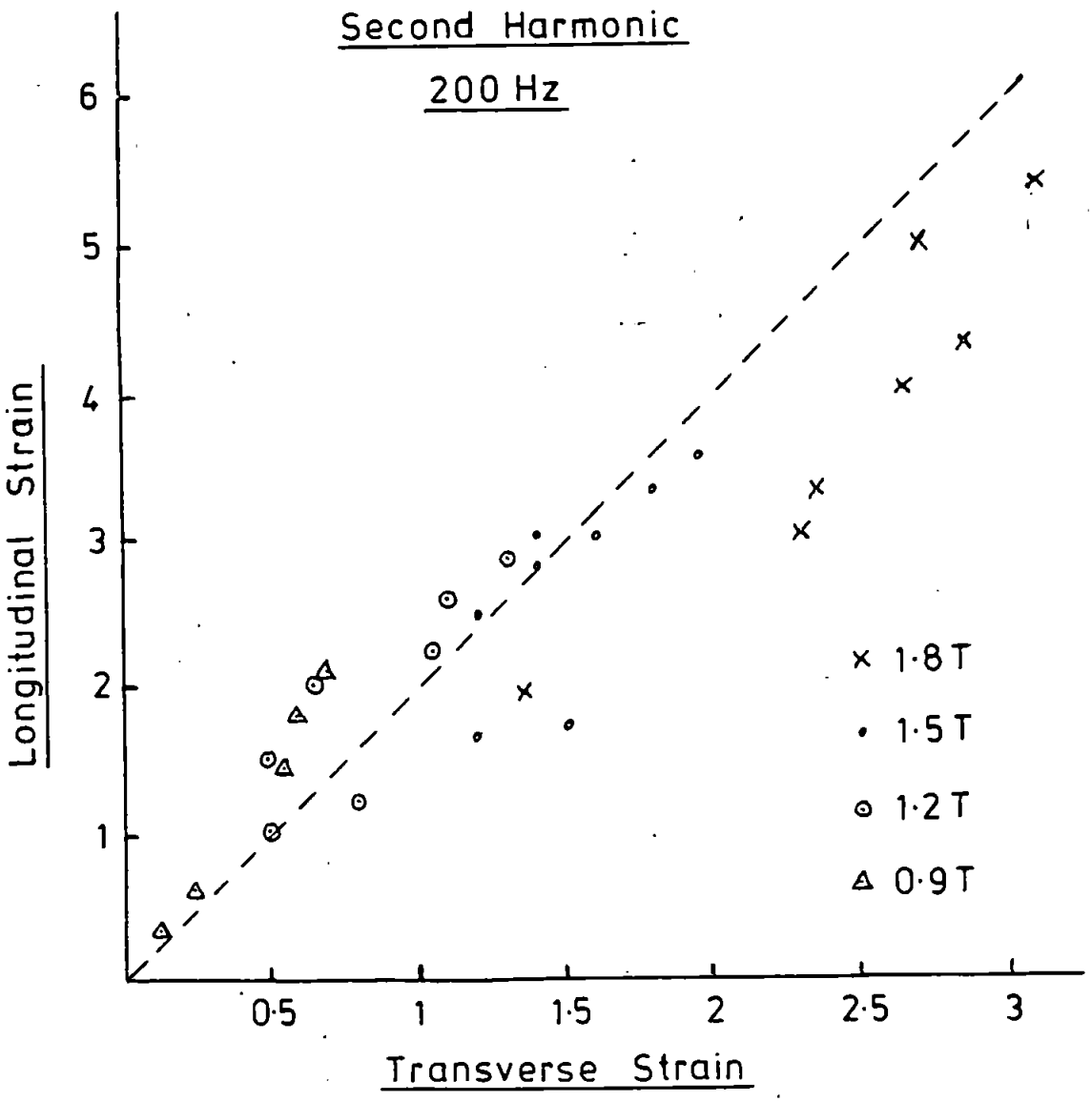

FIG. 5.40. Longitudinal-Transverse Magnetostriction Relations.

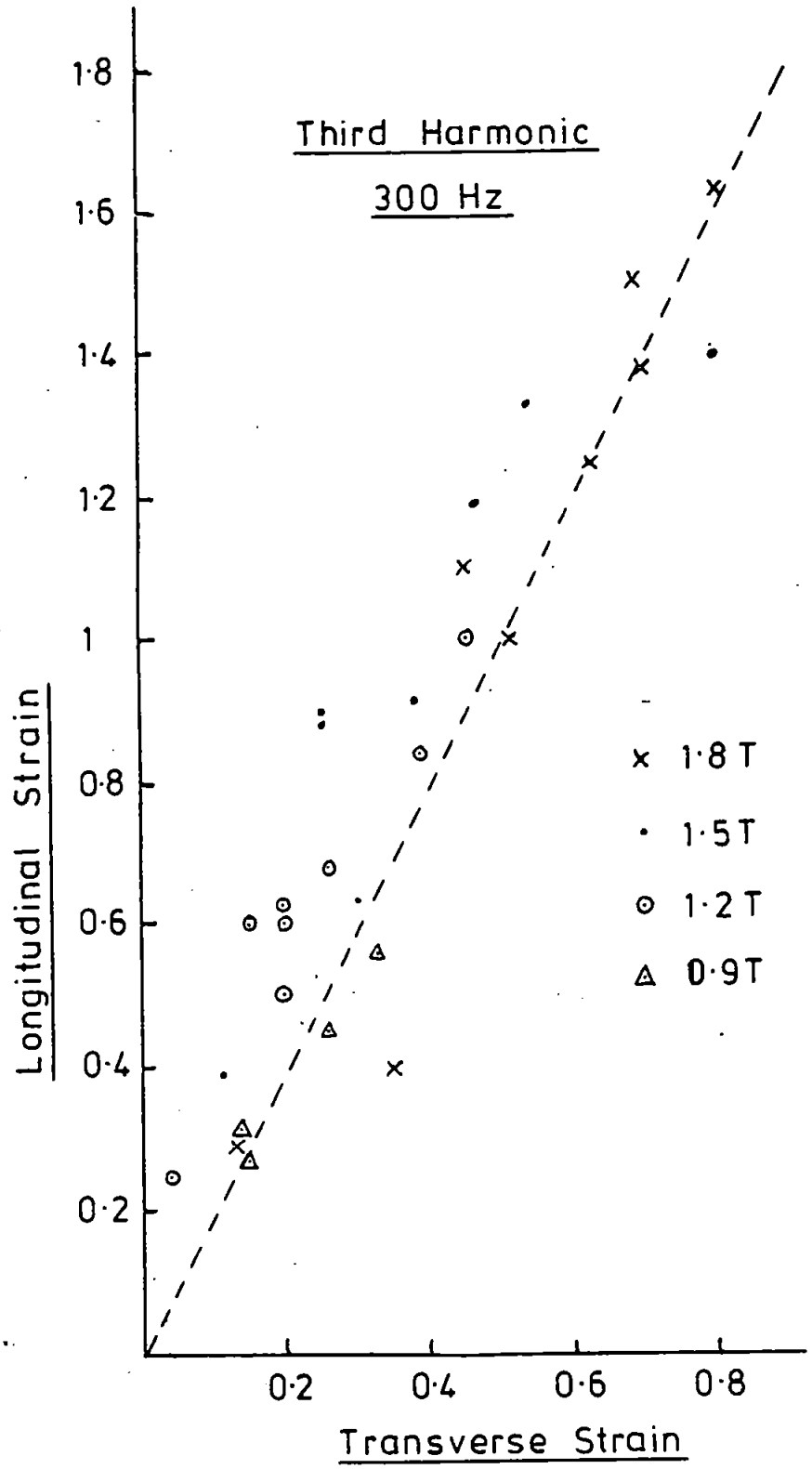

FIG. 5.41. Longitudinal–Transverse Magnetostriction Relations.

just for the fundamental magnetostriction but also for the 2nd and 3rd harmonics. Departures from the theory appear at high induction (1.8T) and at the higher stress levels involved in the measurements. At high inductions around the knee of the curve it is possible that domain rotations away from the easy directions of magnetization parallel to the cube edges are starting to occur. For this case the theory would not be applicable as it assumes that the Ms Vectors lie along the easy directions. At higher stress levels the Stress Induced Pattern I (on which the original theory of Corner and Mason was based) may be altering to the more complex Pattern II or Maze Pattern for which no predictable theories or underlying domain structures have been satisfactorily produced.

In general, however, within the limits of the theory, the above experimental results seem to confirm a 2:1 ratio between magnetostriction harmonics as measured longitudinally and transversely for the same longitudinal compressive stress.

5.6 Variation of Percentage Magnetostriction Harmonics

The theoretical presentation of Chapter 3, Section 3.3.4 demonstrated a possible dependence between the magnitude and phasor relationships of induction harmonics and the percentage harmonics in the magnetostriction, when the higher harmonics are expressed as p.u. values with respect to the fundamental (100 Hz) strain.

In order to test this hypothesis, the results obtained for magnetostriction harmonics reported in earlier sections of this Chapter have been expressed as p.u. values, and plotted against longitudinal compressive stress at various levels of induction.

The p.u. values of induction 3rd harmonic, when the induction is not controlled, have also been plotted for comparative purposes, and the results are shown in

Fig 5.42, at peak inductions of 0.9, 1.2, 1.5, 1.7 and 1.8T. It will be seen that as the induction increases above about 1.2T the level of p.u. harmonic falls. This is consistent with the theory outlined in Section 5.3.3, which explained the phase - shift phenomenon of the 3rd harmonic. It will also be noticed that for stresses above about 3 MPa the p.u. harmonic becomes nearly constant.

5.6.1 Percentage Magnetostriction Measurements

For the case when magnetostriction was measured parallel to the rolling direction, in the same direction as the applied compressive stress, the derived values of p.u. 2nd and 3rd harmonics are shown in Figs 5.43 and 5.44 respectively. Each graph shows the result for the two conditions of controlled (sinusoidal) induction and uncontrolled (natural) induction.

Similarly, for the case when measurements were made transverse to the rolling direction, the derived results are shown in Figs 5.45 and 5.46 respectively.

Examination of these curves enables three general conclusions to be reached:-

(1) When the induction is controlled, both higher harmonics show little variation as the induction changes.

(2) When the induction is not controlled, both higher harmonics show a pronounced variation as the induction changes, being less than the controlled induction case below about 1.5T and greater for inductions of 1.8T.

(3) For either condition of induction, the p.u. harmonics appear to vary with stress, showing a well defined dip at about 1 MPa before rising and starting to level at about 3 MPa.

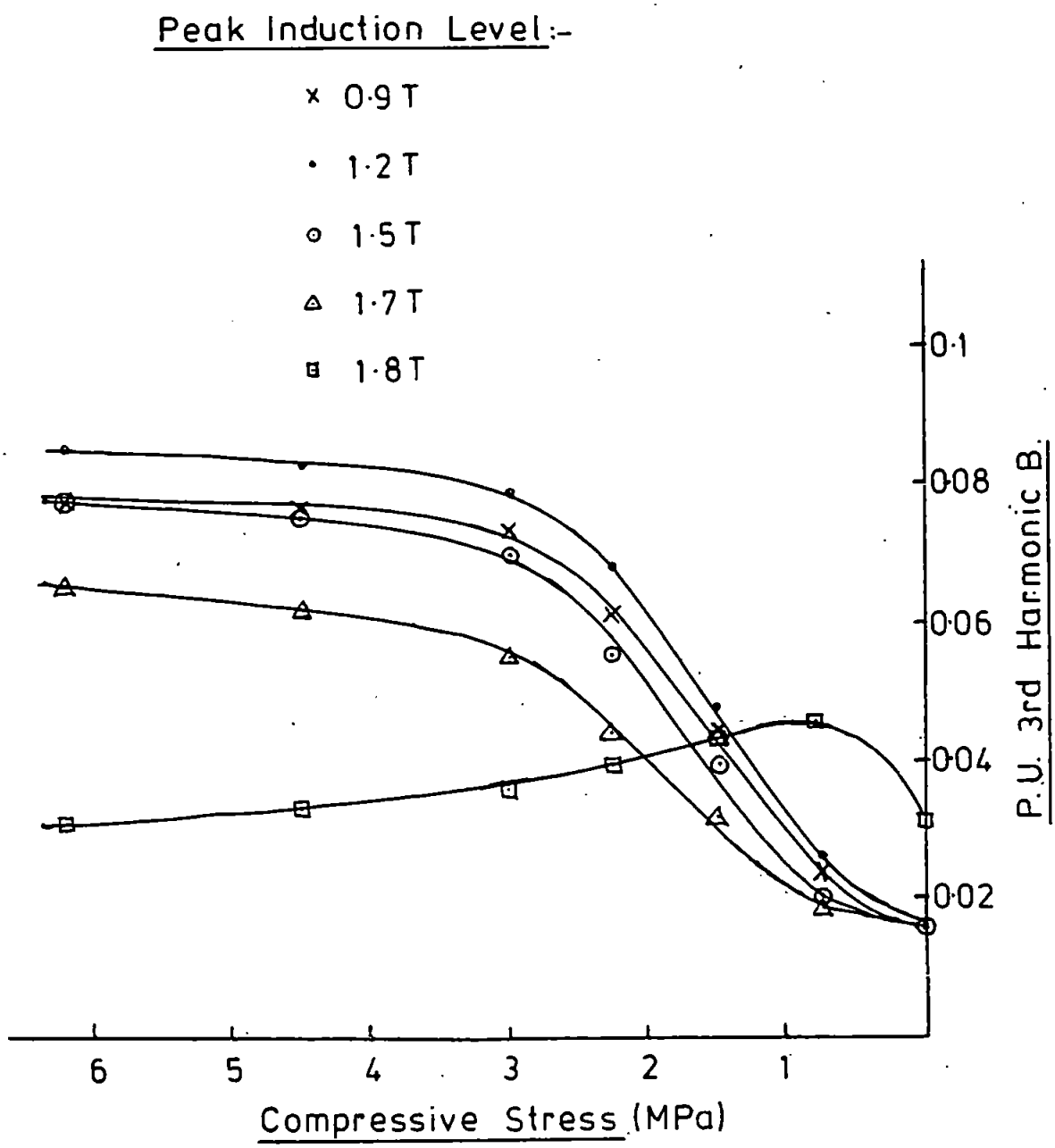

FIG. 5.42: Variation of Induction Per Unit Third Harmonic.

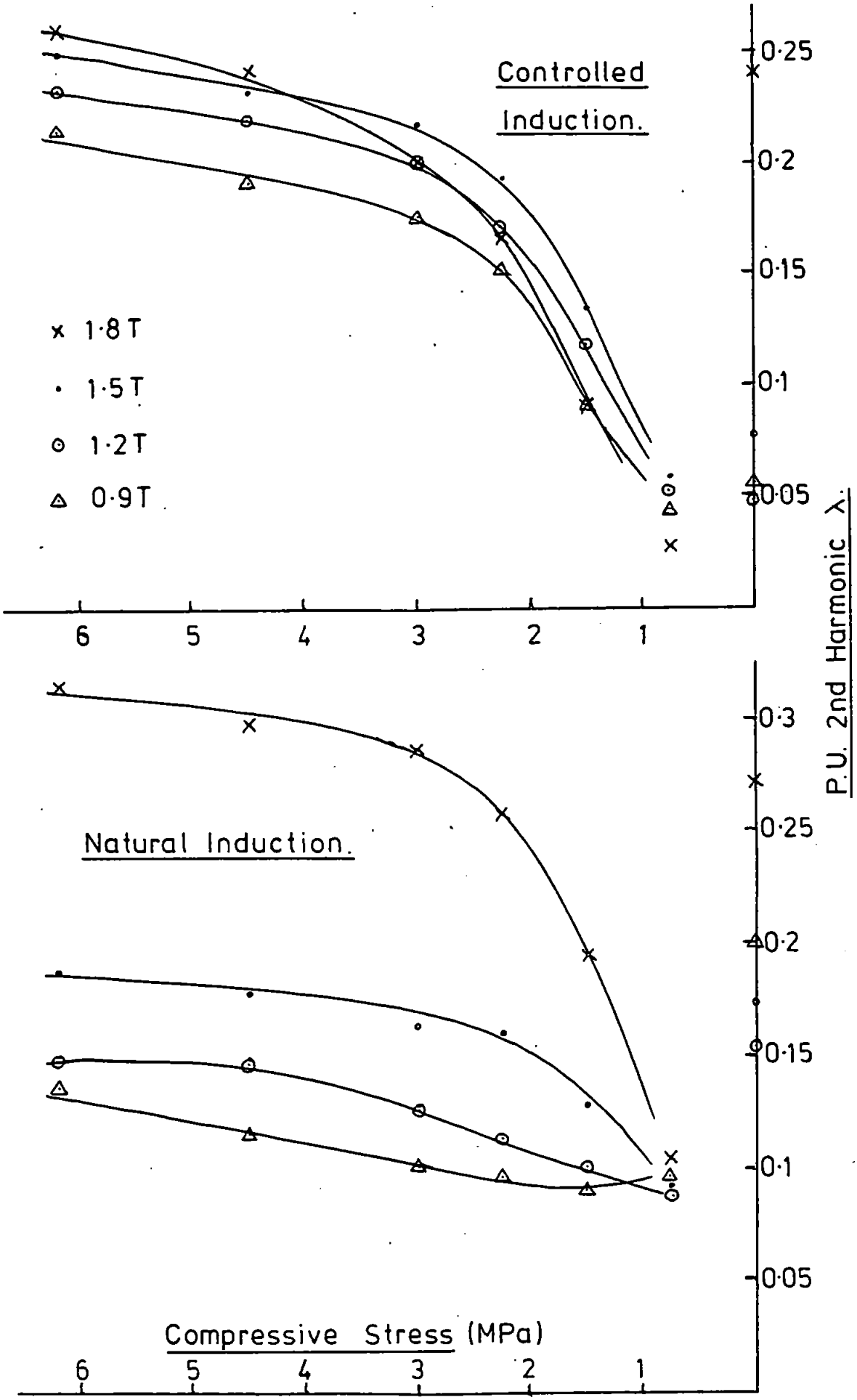

FIG. 5.43. Variation of Magnetostriction Per Unit Second Harmonic.

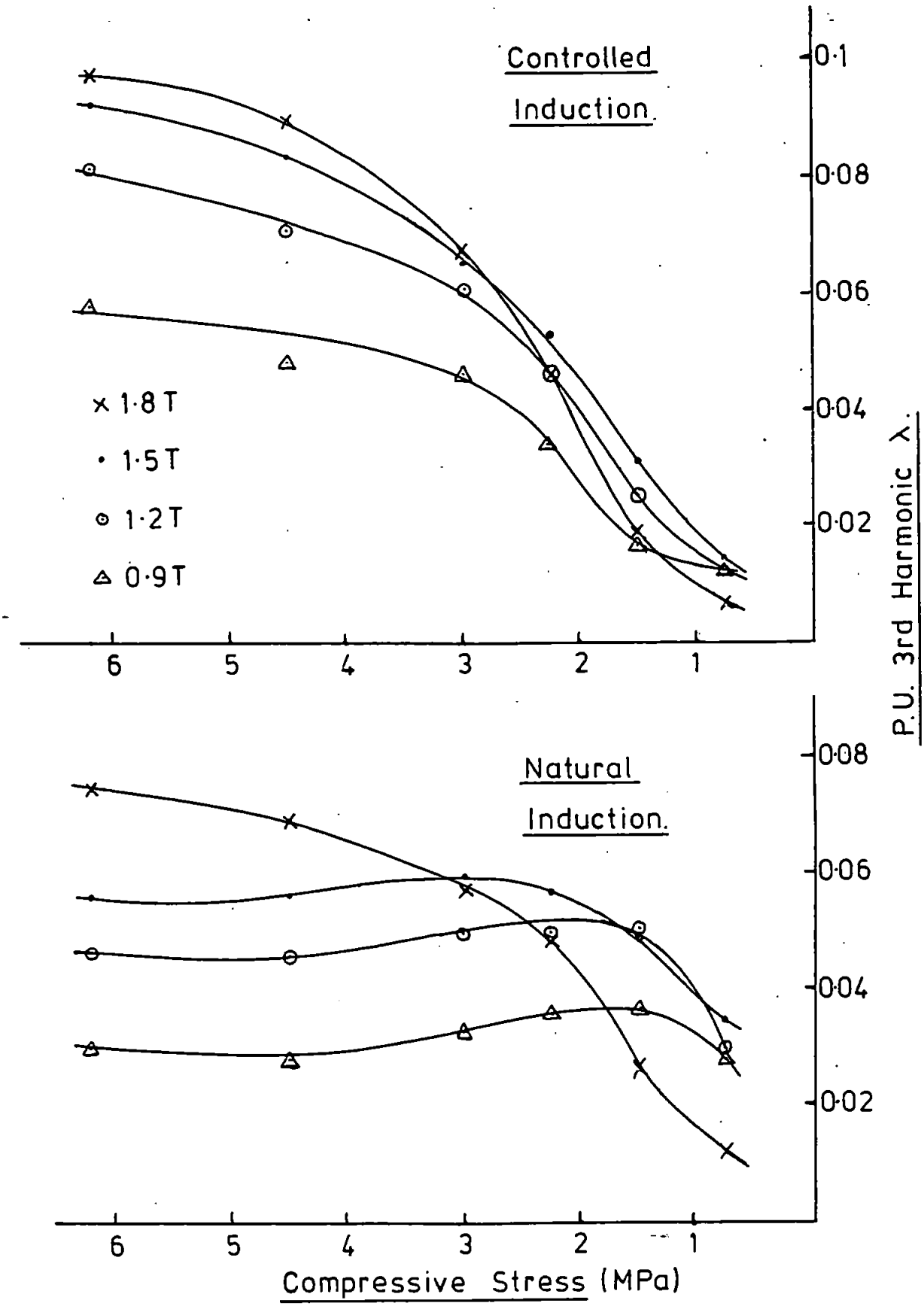

FIG. 5.44. Variation of Magnetostriction P.U. Third Harmonic.

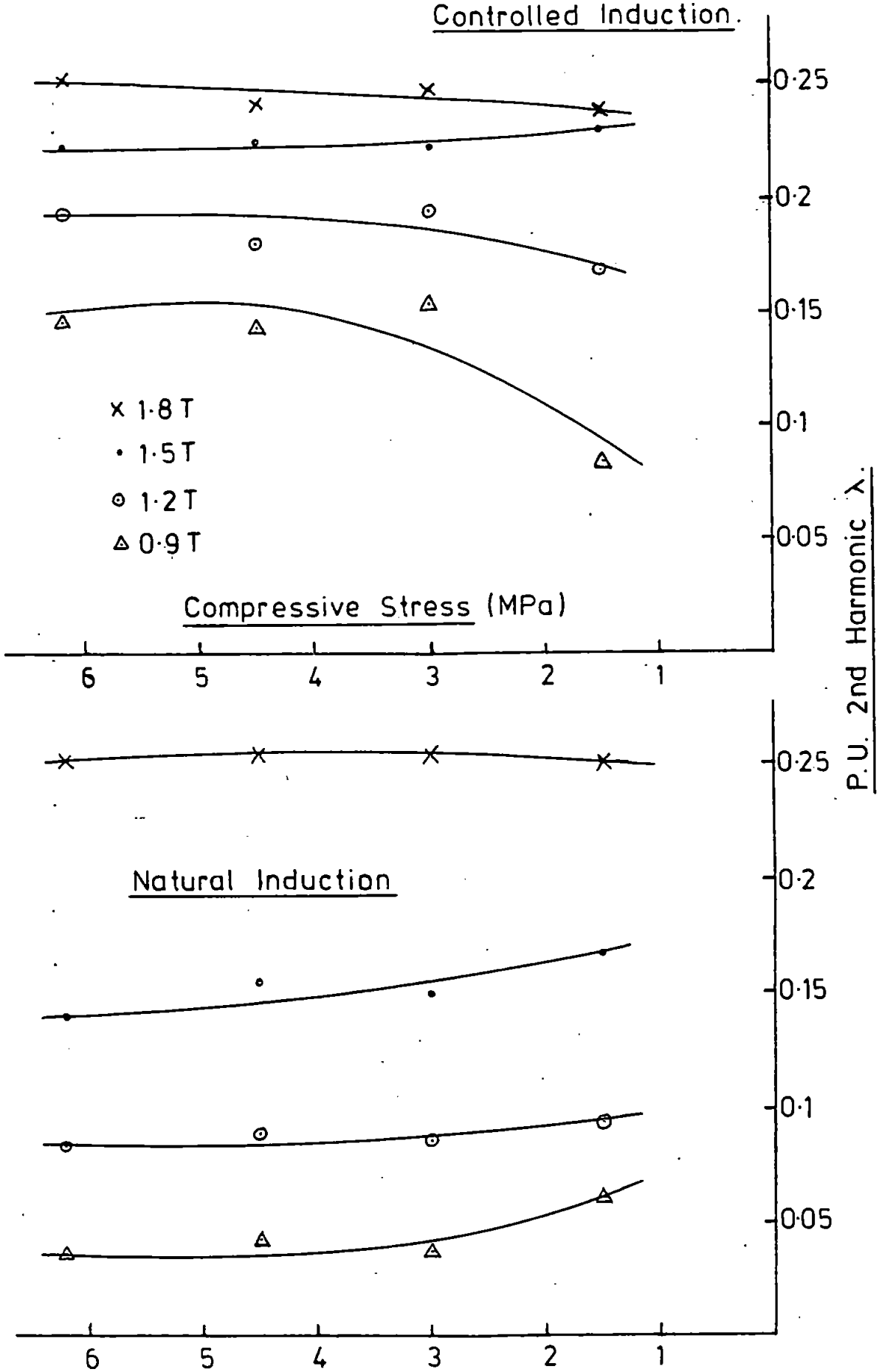

FIG. 5.45. Variation of Transverse Magnetostriction Per Unit Second Harmonic.

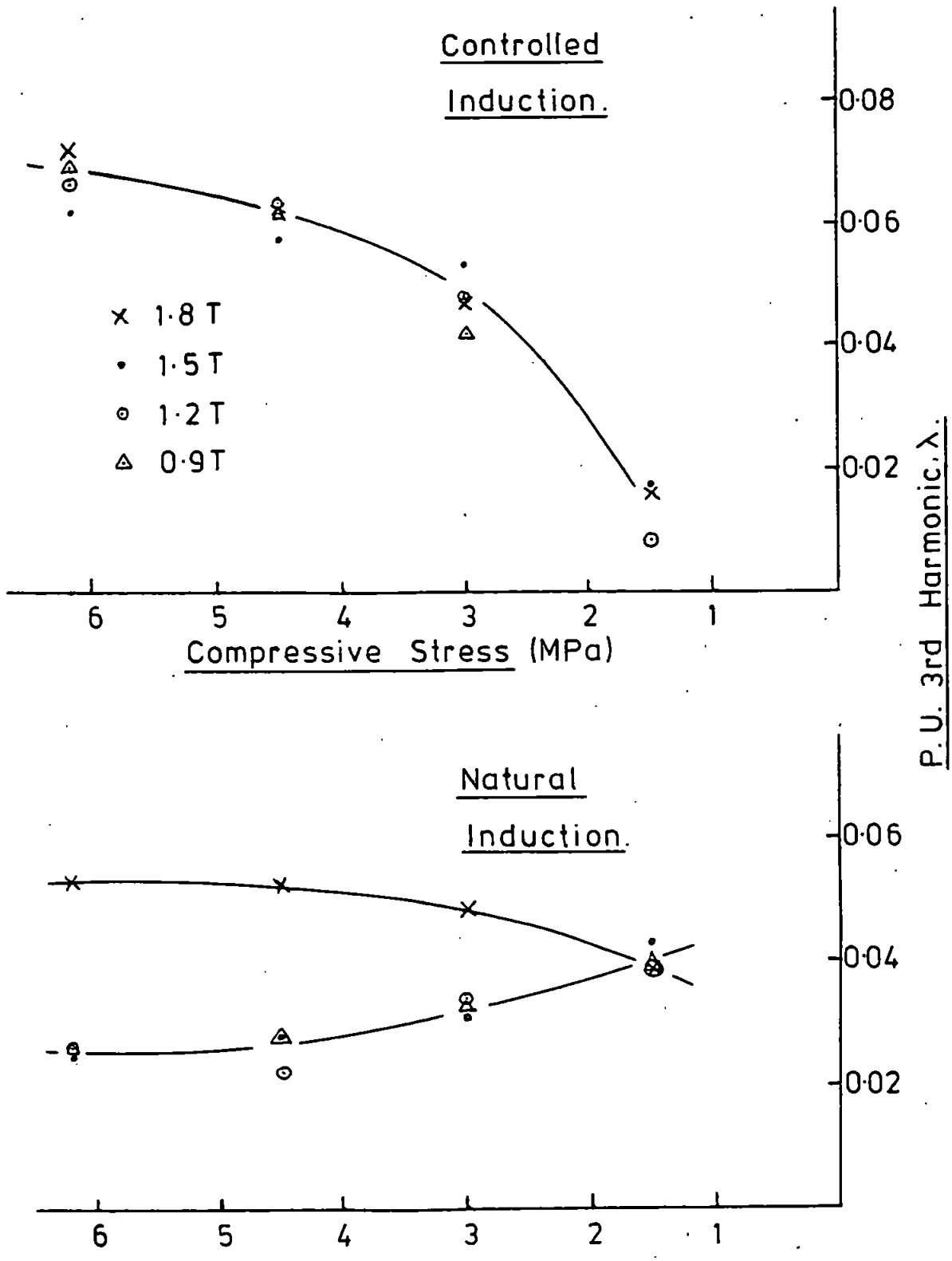

FIG. 5.46. Variation of Transverse Magnetostriction Per Unit Third Harmonic.

5.6.2 Theoretical Analysis of Percentage Harmonics

An explanation of the above results may be obtained by recourse to the original theoretical treatment of Chapter Three.

The equations developed for the fundamental and 2nd harmonic of magnetostriction are reproduced below:-

$$\lambda_1 = \frac{4K\hat{B}}{\pi}\left[\frac{3}{5}p\cos(\alpha \pm \gamma) - \frac{1}{3}\cos\alpha\right]\cos 2wt$$

$$+ \frac{4K\hat{B}}{\pi}\left[\frac{2}{3}\sin\alpha - \frac{2}{5}p\sin(\alpha \pm \gamma)\right]\sin 2wt.$$

$$\lambda_2 = \frac{4K\hat{B}}{\pi}\left[\frac{3}{7}p\cos(\alpha \pm \gamma) + \frac{1}{15}\cos\alpha\right]\cos 4wt$$

$$+ \frac{4K\hat{B}}{\pi}\left[\frac{4}{15}\sin\alpha + \frac{4}{7}p\sin(\alpha \pm \gamma)\right]\sin 4wt..$$

Where K is some constant embracing grain misorientation (ϕ) the magnetostriction constant λ_{100} and dimensional properties of the material; p is the p.u. magnitude of 3rd harmonic induction; γ is the phase angle between the 3rd harmonic induction and its fundamental; α represents the angle of lag between the magnetostriction and the induction due to any hysteresis.

If p=o when the controlled induction contains no harmonics, and assuming that α is small so that $\cos\alpha \gg \sin\alpha$, then the p.u. second harmonic of magnetostriction will be

$$\frac{|\lambda_2|}{|\lambda_1|} = \frac{3}{15} = 0{\cdot}2 \text{ p.u.}$$

Similarly from the equation for λ_3 developed in Section 3.3.4.

$$\frac{|\lambda_3|}{|\lambda_1|} = \frac{3}{35} = 0{\cdot}086 \text{ p.u.}$$

Thus the percentage 2nd and 3rd harmonics in λ will be constant and independent of the level of induction.

If $p > o$ when the natural induction will contain a 3rd harmonic, then the conclusions of Section 3.3.4 will apply. These have been examined earlier in this Chapter in Section 5.3.3, where it was shown that below the knee of the B-H curve, the higher magnetostriction harmonics (and hence the p.u. values) will be less than for the case when p=o. When the induction increases the higher harmonics will increase rapidly due to the effective phase change in the phase angle (γ) between the induction 3rd harmonic and its fundamental.

The above analysis was made by consideration of two specific cases of domain structure. These were :-

(1) the unstressed state of a well aligned grain when only bar-type surface closure structures were present, due to the grain being in the plane of the sheet (angle of dip, ϕ, zero) or because sufficient tensile stress had been applied to remove any supplementary structure caused by $\phi > o$;

(2) a grain under sufficient compressive stress to create a well defined Stress Pattern I as defined in Chapter 3.

Between these two states of stress there will exist a changeover period, the onset of Stress Pattern I, for which no simple domain structures can be postulated to enable prediction of volume weighted sums of domains along the easy directions of magnetization, a process required by the theorectical analysis of Chapter Three.

Hence, for either case of induction with or without harmonics, the p.u. magnetostriction harmonics will have a value of about 20% for the 2nd and 9% for the third at zero stress. When the stress is increased until the formation of a well defined Stress Pattern I the higher harmonics will again have the values given above for the case when the induction is sinusoidal and will be independent of induction level. If the induction contains harmonics then the p.u. magnetostriction harmonics will be dependent on induction level, being lower than before up towards the knee of the B-H loop and greater than before for higher inductions.

Between the two states of stress, no predictions have been made regarding the magnetostriction harmonics.

5.6.3 Discussion of Results.

Examination of Figs 5.43 to 5.46 confirm in general the theoretical observations made above. For example, at 4.5 MPa stress and with sinusoidal induction, the 2nd p.u. harmonic has a value of 0.22 $\pm$ 0.020 p.u. over the induction range 0.9 to 1.8T, when measured parallel to the rolling direction. The equivalent figure for the 3rd harmonic is 0.08 $\pm$ 0.010 p.u. over the induction range 1.2 to 1.8T.

A summary of the results obtained for each set of measurement conditions is shown in the Table of Fig 5.47, for the condition of 4.5 MPa compressive stress.

At zero stress the results are not conclusive, particularly for the 2nd harmonic with controlled induction, and for the 3rd harmonic. In the latter case the levels of magnetostriction being measured were less than 0.1 μe up to 1.8T induction, and, despite the care taken with the apparatus, it is felt that such small measurements were not accurately accomplished. They have, therefore, not been included in Figs 5.44 and 5.46.

In general, however, it is considered that the above experimental results confirm the theoretical predictions made for the p.u. higher magnetostriction harmonics when the harmonic content of the induction is taken into account.

		P.U. 2nd λ			P.U. 3rd λ		
	Tesla	1·2	1·5	1·8	1·2	1·5	1·8
Longitudinal λ	Sine B	0·218	0·232	0·24	0·071	0·084	0·09
4·5 MPa	Nat.B	0·142	0·179	0·298	0·046	0·056	0·069
Transverse λ	Sine B	0·18	0·225	0·241	0·064	0·058	0·063
4·5 MPa	Nat. B	0·09	0·156	0·256	0·022	0·028	0·052
Longitudinal λ	Sine B	0·048	0·077	0·24	All Strains < 0·1μe		
Zero stress	Nat. B	0·154	0·175	0·273			
Transverse λ	Sine B	0·188	0·139	0·056			
Zero stress	Nat. B	0·22	0·182	0·083			

FIG. 5.47. PER UNIT MAGNETOSTRICTION HARMONIC VARIATION WITH INDUCTION.

REFERENCES TO CHAPTER FIVE

1. R. Carey, E.D. Isaac, 'Magnetic Domains and Techniques for their observation, E.U.P., London, 1966.

2. W. S. Paxton, T.G. Nilan, J Appl. Phys., Vol. 26, No 8, August 1955.

3. P. J. Banks, E Rawlinson, Proc. I.E.E., Vol. 114, No 10, October 1967.

4. G. H. Simmons, J. E. Thompson, Proc. I.E.E., Vol. 118, No 9, September 1971.

5. A. J. Moses, P.S. Phillips, I.E.E.E. Trans. Mag., Vol. Mag. 14, No 5, September 1978.

6. W. D. Corner, J. J. Mason, Brit. J. Appl. Phys., Vol. 15, 1964.

7. A. J. Moses, I.E.E.E. Trans. Magn, Vol Mag. 10, No. 2, June 1974.

8. P. Allia et. al., I.E.E.E. Trans Magn., Vol Mag. 14, No 5, September 1978.

CHAPTER SIX

CONCLUSIONS TO THE INVESTIGATION

For dynamic, power frequency magnetostriction measured parallel to the rolling direction and transverse to that direction within a grain of polycrystalline 3.25% Si-Fe, and with compressive stress applied along the rolling direction, the following conclusion may be made regarding the first three harmonics of the magnetostriction :-

(1) They exhibit a stress sensitivity similar in nature to the already well known sensitivity of the overall, total magnetostriction.

(2) Each harmonic shows a 2:1 ratio in magnitude between values in the rolling direction compared to those in the transverse direction, which agrees with a theoretical prediction of such a relationship.

(3) Both the 2nd and 3rd harmonics of magnetostriction are dependent on the level of 3rd harmonic in the flux waveshape.

(4) This dependence is modified by the phase relationship between the 3rd harmonic of flux and its fundamental. At inductions below the knee of the magnetization curve an increase in flux 3rd harmonic due to compressive stresses results in a reduction in magnetostriction harmonics. At the knee a phase change in the flux harmonic occurs which leads to a large increase in magnetostriction harmonics.

(5) Each percentage higher harmonic will be approximately constant and independent of induction level when the induction in the grain is controlled to be sinusoidal, for a well defined Stress Pattern I. When the induction contains harmonics, the percentage higher magnetostriction harmonics will be modified in line with Conclusion (4). These conclusions agree with a theoretical prediction of such relationships.

ACKNOWLEDGEMENTS

Thanks are extended to:-

1. Devon County Council for the provision of a Research Assistantship and facilities for the research project at the Department of Electrical and Electronic Engineering, Plymouth Polytechnic.

2. Dr. D.J. Mapps, Director of Studies for this research, whose advice and encouragement made it all possible.

3. The British Steel Corporation for the provision of silicon-iron specimens.

4. Dr. A.J. Moses and his co-workers at the Wolfson Centre, Cardiff, for technical advice and assistance in specimen preparation.

5. Miss A. Sloman for the typing of this Thesis.